Vol. 51 ■ No. 3 ■ September 2023

JNMT
Journal of Nuclear Medicine Technology

## FEATURED IMAGE

Patient Preparation with Esomeprazole Is Comparable to Ranitidine in Meckel Diverticulum Scintigraphy. Tessa Ververs et al. See page 211.

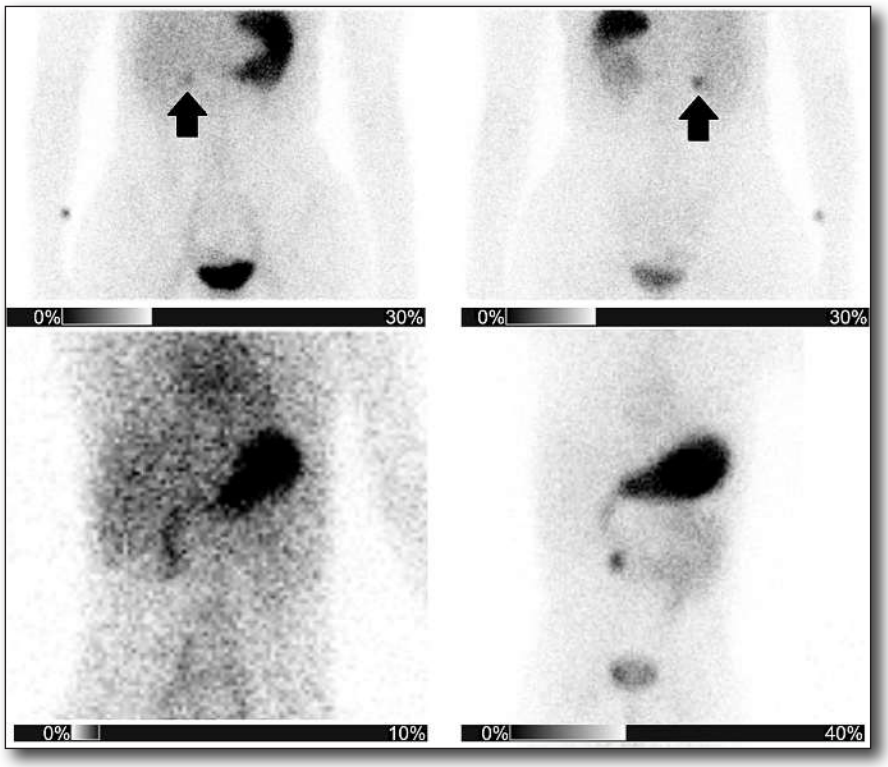


SNMMI Value Initiative
SOCIETY OF NUCLEAR MEDICINE & MOLECULAR IMAGING

# SNMMI and IAC

## Collaborate on New Program for Radiopharmaceutical Therapy

*Radiopharmaceutical therapy is a powerful technique for treating cancer that is now being used to great benefit in patients with prostate and other cancers. It is essential that patients receiving radiopharmaceutical therapy be confident that their providers meet high standards of training and experience. The new SNMMI-IAC Radiopharmaceutical Therapy accreditation helps assure that sites delivering radiopharmaceutical therapy are qualified and experienced, have appropriate facilities and equipment, and can offer safe and reliable radiopharmaceutical therapy.*

**Richard L. Wahl, MD, PhD, FASE**
*SNMMI Immediate Past President,*
*Member of IAC Nuclear/PET Board of Directors*

*SNMMI is excited about this accreditation program because it builds upon both the SNMMI Radiopharmaceutical Therapy Centers of Excellence and the IAC nuclear medicine accreditation programs.*

**Munir Ghesani, MD, FACNM, FACR**
*SNMMI President*

*IAC and SNMMI have worked together for many years, as SNMMI is a founding sponsoring organization of the IAC Nuclear/PET accreditation program. The creation of the new Radiopharmaceutical Therapy accreditation offering is possible through our collaboration and leverages both organizations' strengths toward our aligned missions focused on quality and safe patient care. Through a multi-specialty approach, the SNMMI representatives along with our other sponsoring organizations, have contributed greatly to the development of standards for radiopharmaceutical therapy, ensuring that they are reflective of SNMMI guidelines and current best practices that lead to improved patient care.*

**Howard Lewin, MD, FACC, FASNC**
*President of the IAC Nuclear/PET Board of Directors*

**In partnership with the Society of Nuclear Medicine and Molecular Imaging (SNMMI), the IAC is proud to announce a new accreditation program for Radiopharmaceutical Therapy.**

### Radiopharmaceutical Therapy Accreditation Program

SNMMI SOCIETY OF NUCLEAR MEDICINE & MOLECULAR IMAGING | IAC INTERSOCIETAL ACCREDITATION COMMISSION

The new program offers facilities a mechanism for demonstrating their commitment to quality and patient safety in radiopharmaceutical therapy and will join the existing IAC accreditation areas:

**Nuclear Cardiology, General Nuclear Medicine** and **Positron Emission Tomography (PET)**.

**Learn more today at intersocietal.org/nuclear.**

IAC
*Improving health care through accreditation®*
**intersocietal.org** | 800.838.2110

**IAC Offering 20% Reduction on Base Application Fees for 2023**

To learn more or access our Online Fee Estimator, scan the QR code to the left or visit our website at ***intersocietal.org/iac/2023fees***.

# Pass the NMTCB CT Exam. We *GUARANTEE* It!

Because **MIC** is all about ***outcomes***.

Over 30 Years!

**We guarantee you'll pass the NMTCB CT Exam or *your money back!***

- Technologists must complete 35 hours of didactic education related to CT during the 3 year period prior to applying for the CT Exam.
- NMTCB has approved **MIC**'s **CT Registry Review Program** along with **Sectional Anatomy & Imaging Strategies** to ***completely satisfy that 35-hour CT didactic requirement!***
- Excellent companion for technologists in hybrid imaging.

There's no better time to participate in

**MIC's Self-Study CE**

- Prepare for **CT certification**
- Satisfy NMTCB's **prerequisite**
- Ensure the **highest standards**

**Ask for the CNMT discount when you enroll in both courses!**

Technologists and their managers agree:
**"MIC's courses really work!"**

## Sectional Anatomy & Imaging Strategies™

### Learn the essentials of sectional imaging in a convenient self-study format!

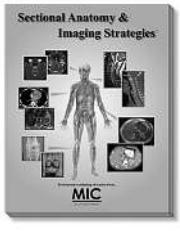


- Patient positioning, artifact reduction, image orientation, slice thickness, etc., for each clinical area.
- Explains sectional imaging with over 1,000 images and figures. The perfect companion to **The CT Registry Review Program**.
- 26 Credits
- 6 StudyModules

## The CT Registry Review Program™

### Pass the CT Exam after completing this course or we will refund your entire tuition!

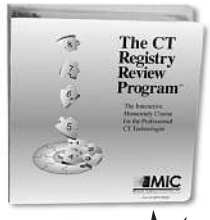


5th Ed!

- Learn **essential** and **advanced** topics on the NMTCB and ARRT CT Exam.
- Prior training in CT is recommended.
- Pass the NMTCB or ARRT Exam in CT or your money back!
- 25 Credits
- 8 StudyModules

***"Over 30 years of helping technologists achieve their educational goals!"***

A Proud Member of...
SNMMI

Call today for your
**Free Info Kit**
**800-589-5685**
**or visit www.MIC*info*.com**

MIC®
Medical Imaging Consultants, Inc.
1037 US Highway 46, Suite G2 • Clifton, NJ 07013 • 800-589-5685
...for *your* perfect image.

JNMT09/23

# Empowering Better, Safer Diagnosis and Treatment

As part of Mirion Medical, we enhance safety and efficiency for technologists and physicists through top-quality nuclear medicine and molecular imaging solutions.

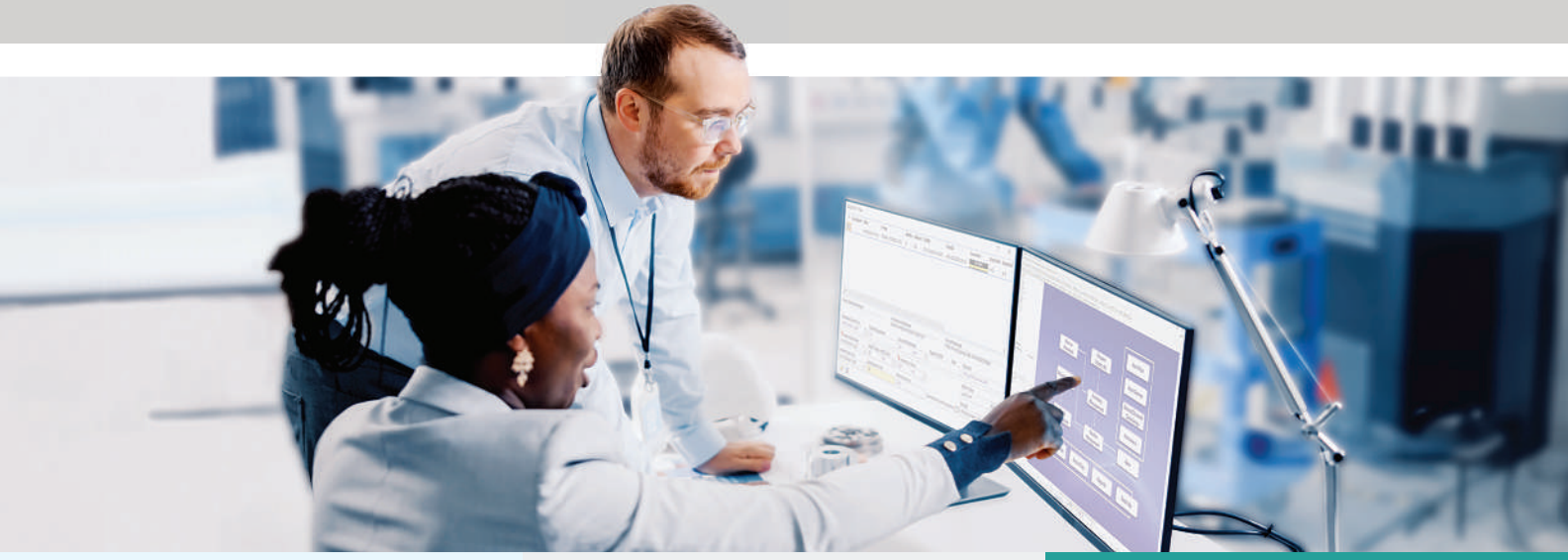


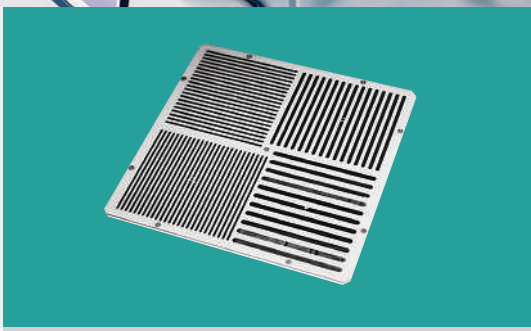

**Delivery, Detection and Diagnosis**
Dose Calibrators, Lung Ventilation and Thyroid Uptake Systems with intuitive software

**Lab Supplies**
Safe, modular, secure Lead-Lined Cabinetry and Accessories

**Quality Assurance**
Reliable, time-tested Phantoms for PET, PET-CT, SPECT and more

CAPINTEC
A MIRION MEDICAL COMPANY



OPS-5980 - 08/2023

Learn more at
**capintec.com**

# JNMT

Volume 51, Number 3 • September 2023

# JNMT Journal of NUCLEAR MEDICINE TECHNOLOGY

The Official Publication of **SNMMI-TS**





The *JOURNAL OF NUCLEAR MEDICINE TECHNOLOGY* (ISSN 0091-4916 [print]; ISSN 1535-5675 [online]) is published quarterly by the SNMMI, 1850 Samuel Morse Dr., Reston, VA 20190-5316; phone: (703) 708-9000; fax: (703) 708-9018. Periodicals postage paid at Reston, VA, and at additional mailing offi ces.

**POSTMASTER:** Send address changes to the *Journal of Nuclear Medicine Technology*, 1850 Samuel Morse Dr., Reston, VA 20190-5316.

**EDITORIAL COMMUNICATIONS** should be sent to the editor, Kathy S. Thomas, MHA, CNMT, PET, FSNMMI-TS, JNMT Office, SNMMI, 1850 Samuel Morse Dr., Reston, VA 20190-5316; phone: (703) 326-1185; fax: (703) 708-9018. To submit a manuscript, go to http://submit-tech.snmjournals.org.

**BUSINESS COMMUNICATIONS** concerning permission requests should be sent to the publisher, SNMMI, 1850 Samuel Morse Dr., Reston, VA 20190-5316; phone: (703) 708-9000; home page address: http://tech.snmjournals.org. Subscription requests, address changes, and missed issue claims should be sent to Membership Department, SNMMI, at the address above. Notify the Society of change of address and telephone number at least 30 days before date of issue by sending both the old and new addresses. Claims for copies lost in the mail are allowed within 90 days of the date of issue. Claims are not allowed for issues lost as a result of insufficient notice of change of address. For information on advertising, contact Team SNMMI (Kevin Dunn, Rich Devanna, and Charlie Meitner; (201) 767-4170; fax: (201) 767-8065; TeamSNMMI@cunnasso.com). Advertisements are subject to editorial approval and are restricted to products or services pertinent to nuclear medicine. Closing date is the 25th of the second month preceding the date of issue.

**INDIVIDUAL SUBSCRIPTION RATES** for the 2023 calendar year are $261 within the United States and Canada; $278 elsewhere. CPC IPM Sales Agreement No. 1415131. Sales of individual back copies are available for $60 at http://www.snmmi.org/subscribe (subscriptions@snmmi.org; fax: (703) 667-5134). Individual articles are available for sale online at http://tech.snmjournals.org.

**MISSION:** SNMMI-TS is dedicated to the advancement of molecular and nuclear medicine technologists by providing education, advocating for the profession, and supporting research to achieve clinical excellence and optimal patient outcomes. **VISION:** To be recognized as the leader in molecular imaging and therapy. To be dedicated to the advancement of the profession through adoption of emerging technologies.

JNMT Journal of NUCLEAR MEDICINE TECHNOLOGY

# Moving into 2024 and Our Future

Dmitry D. Beyder, MPA, CNMT

What an incredible time for nuclear medicine and molecular imaging, with nuclear medicine imaging seeing a resurgence, PET growing at a stratospheric pace, and theranostics being adopted and used for various patient treatments internationally. Thank you, members and nuclear medicine professionals, for voting for me to be your president during this exciting time! I am eager to work with the SNMMI leadership team, committee members, SNMMI staff, and all of you to deliver on my promises and set up nuclear medicine technologists for future success.

In 2023, with Krystle Glasgow as Technologist Section president, we started working on a significant part of the platform I ran under in 2022: empowering the nuclear medicine technologist (NMT) to play a pivotal role in all components of theranostics. With Krystle's work, we are working to launch an NMT Therapy Boot Camp in early 2024 that will allow practicing NMTs to gain more therapy skills to support authorized users in radiopharmaceutical therapy practice.

As I was sworn in as the SNMMI Technologist Section president in June, my additional goals for the next 12 months included establishing formal theranostics education; continuing to put energy, resources, and ingenuity into developing the NMT workforce pipeline; and increasing our global collaboration with other NMT professional associations worldwide.

#### Theranostics Education

With eyes on the resurgence of the Nuclear Medicine Advanced Associate (NMAA) program in 2025, our goal is to provide NMTs with formal and complete training in theranostics. This includes working up patients for treatment, collecting and addressing their vitals, understanding their therapy history, and making therapy decisions with that in mind. It includes working and charting appropriately within the electronic medical record, ordering labs, and evaluating lab work and other diagnostic testing. It also includes working closely with an authorized user to administer the therapy radiopharmaceutical along with appropriate adjunctive medications such as amino acids.

#### NMT Workforce Pipeline

During the past year, we embarked on a thorough and professional evaluation of practicing and certified NMTs throughout the United States. Based on various data that we evaluated, with a forecasted increase in demand for theranostics services and traditional nuclear medicine over the next 5 years, we could see a 15%–25% shortfall in the number of professional NMTs available to take care of our patients; this is a problem that we are working hard to address. We collected and are now analyzing survey data that will allow us to fine-tune our plan to put support and financial resources in place that will stimulate the development of new NMTs. We will continue to support NMT educational programs throughout the United States. During the 2023 SNMMI Annual Meeting in Chicago, we launched our first-ever Student Leadership Academy and our first-ever program to stimulate interest in nuclear medicine technology among high school students; both of these events were huge successes! We will continue to build on those successes and to increase both the quantity and quality of new technologists entering our field.

Dmitry Beyder, MPA, CNMT

#### Global Collaboration

We will also continue to focus attention on international collaboration throughout the world, including Europe, Australia, Africa, and beyond. We are working on defining and establishing a global role in therapy for the NMT, which will help us move the NMT profession forward on a global scale.

Our 2023 Strategic Plan specifically calls for collaborative work among physicians, scientists, and technologists. In continuous collaboration with Dr. Helen Nadel, current president of SNMMI, and with our other SNMMI partners, we will advance the profession as a whole, working together to accomplish many priorities and initiatives and taking care of the entire SNMMI membership.

The SNMMI Technologist Section elected leadership have a full slate of initiatives in place for the coming year. Julie Bolin, president-elect, and Krystle, immediate past president, will join me in exploring and implementing innovative ideas to position our membership for a wonderful and bright future. Thank you for your help and support!

# The Gathering

Kathy S. Thomas, MHA, CNMT, PET, FSNMMI-TS

Editor, *JNMT*

The Annual Meeting of the Society of Nuclear Medicine and Molecular Imaging in Chicago was fantastic! Gathering with nuclear medicine professionals from around the world to share new ideas, technologies, and information is always an exhilarating experience, and this year was no exception. Although the haze and smoke from the Canadian fires darkened the city skies, nothing could darken the mood of those attending the meeting, either virtually or in person. There was something for everyone, including the festive opening ceremony, the very competitive knowledge bowl, the packed educational opportunities, the many social events, the informative and educational exhibit hall, and the new 'virtual' poster hall, not to mention the many networking opportunities! A great social and educational time was had by all!

During the educational program, Mary Beth Farrell, *JNMT*'s CE Editor, presented "How to Write a Manuscript" to students and attending nuclear medicine professionals, designed to provide and encourage future authors with the tools to write successfully. *JNMT* is always looking for new content and new authors! I followed with a very brief summary of the publication process once the manuscript is submitted. For authors new to the publication process, we stressed the fact that help is available and emphasized that, aside from the prestige and bragging rights of being published, there also may be financial rewards associated with being published! For those not quite ready to put pen to paper, ok, so I'm "old school"—how about fingers to the keyboard—we encouraged becoming a reviewer. Every nuclear medicine professional is an expert in some aspect of nuclear medicine. Why not consider becoming a reviewer of manuscripts specific to that expertise? The process is easy and begins by creating an account on the SNMMI publication portal at JNM Manuscript Processing System (snmjournals.org).

Turning to this issue, a diverse collection of continuing education articles is offered. Dual-energy x-ray absorptiometry (DXA) units replaced dual-energy photon absorptiometry (DPA) units in the late 1980s; however, many nuclear medicine departments continue to perform DXA procedures today. Banks et al. present Part 1 of a two-part series that summarizes bone physiology, osteoporosis etiology, and the principles and technical aspects of DXA (*1*). Part 2 will follow in the December issue with a review of DXA interpretation as well as potential scanning pitfalls and techniques to improve image quality. Practice guidelines support best practice in the clinical setting. The Society of Nuclear Medicine and Molecular Imaging (SNMMI) and the European Association of Nuclear Medicine (EANM) routinely review and update guidelines for imaging and therapeutic nuclear medicine procedures to improve the quality of service for patients worldwide. The updated practice guideline for the treatment of palliation of bone pain provides the latest information on the therapeutic use of available radiopharmaceuticals to treat osteoblastic metastases (*2*). Finally, an in-depth discussion is presented on the appropriate use of $^{18}$F-fluoroestradiol (Cerianna) to identify estrogen receptor plus tumor cells throughout the body (*3*). The Practical Protocol Tip that follows the Cerianna article provides a detailed protocol on Cerianna whole-body imaging that can be clipped and incorporated into a department's procedure manual (*4*).

**Kathy S. Thomas, MHA, CNMT, PET, FSNMMI-TS**

Although the negative clinical impact associated with the COVID-19 pandemic has stabilized, its influence on current clinical practice continues. A survey performed by the Nuclear Medicine Technology Certification Board (NMTCB) to assess data used to determine the current appropriateness of the entry-level certification exam offers some interesting thoughts and insights regarding current practice and ongoing consequences of the pandemic (*5*).

Meckel's imaging is used to identify unexplained gastrointestinal bleeding associated with ectopic gastric mucosa. Pretreatment with an H2 inhibitor enhances the scan's sensitivity by reducing washout activity in the intestinal lumen. Ververs et al. explore the effectiveness of the proton pump inhibitor (PPI) esomeprazole as an ideal substitute for the H2 histamine blocker ranitidine (*6*).

In the Educators' Forum, Currie introduces ChatGPT, an artificial intelligence algorithm that has been described as an immediate threat to academic and scientific writing as well as a potential benefit in supporting and enhancing student learning (*7,8*).

When time allows, don't miss the additional clinical discussions, radiation safety topics, and teaching case studies included in this issue.

With your support, *JNMT* continues to offer content relevant to your professional growth. Please contact me if you are interested in becoming an author or reviewer and, most importantly, please contact me at ksthomas0412@msn.com with your ideas and suggestions to enhance *JNMT* content.

## REFERENCES


1. Banks KP, Farrell MB, Gunther RS, et al. Improving DXA quality by avoiding common technical and diagnostic pitfalls: Part 1. *J Nucl Med Technol.* 2023;51:167–175.
2. Pantel AR, Eiber M, Beyder DD, et al. SNMMI procedure standard/EANM practice guideline for palliative nuclear medicine therapies of bone metastases. *J Nucl Med Technol.* 2023;51:176–187.
3. Grabher BJ. $^{18}$F-FES whole-body imaging protocol for evaluating tumor estrogen receptor status in patients with recurrent or metastatic breast cancer. *J Nucl Med Technol.* 2023;51:188–193.
4. Grabher BJ. $^{18}$F-fluroroestradiol whole-body imaging. *J Nucl Med Technol.* 2023;51:194–195.
5. Youngblood SN, Johnson SL. The impact of covid on the clinical environment. *J Nucl Med Technol.* 2023;51:196–203.
6. Ververs TF, Lobbezzo A-FH, Hobbelink MG, Braat AJ. Patient preparation with esomeprazole is comparable to ranitidine in Meckel diverticulum scintigraphy. *J Nucl Med Technol.* 2023;51:211–214.
7. Currie GM and Barry K. ChatGPT in nuclear medicine education. *J Nucl Med Technol.* 2023;51:247–254.
8. Currie GM. A conversation with ChatGPT. *J Nucl Med Technol.* 2023;51:255–260.

# Improving DXA Quality by Avoiding Common Technical and Diagnostic Pitfalls: Part 1

Kevin P. Banks[1,2], Mary Beth Farrell[3], Rutger S. Gunther[1], Nathan E. McWhorter[1,2], Doug W. Byerly[1,2], and Justin G. Peacock[1,2]

*[1]Department of Radiology, Brooke Army Medical Center, San Antonio, Texas; [2]Department of Radiology, Uniformed Services University, Bethesda, Maryland; and [3]Intersocietal Accreditation Commission, Ellicott City, Maryland*

**CE credit:** For CE credit, you can access the test for this article, as well as additional JNMT CE tests, online at https://www.snmmilearningcenter.org. Complete the test online no later than September 2026. Your online test will be scored immediately. You may make 3 attempts to pass the test and must answer 80% of the questions correctly to receive 1.0 CEH (Continuing Education Hour) credit. SNMMI members will have their CEH credit added to their VOICE transcript automatically; nonmembers will be able to print out a CE certificate upon successfully completing the test. The online test is free to SNMMI members; nonmembers must pay $15.00 by credit card when logging onto the website to take the test.

Dual-energy x-ray absorptiometry (DXA) is an accurate means to assess bone mineral density, determine the risk of a fragility fracture, and monitor response to therapy. Despite its seemingly straightforward nature—the review of 2-to-3 nondiagnostic images and a few automatically generated numbers—the proper performance and interpretation of DXA can often be complex. It is complex because it is highly dependent on many factors, such as image acquisition, processing, analysis, and subsequent examination interpretation. Each step is subject to potential errors, artifacts, and diagnostic pitfalls; hence, meticulous attention must be paid to the technique by both the technologist and the interpreting physician to provide high-quality results and, in turn, maximize the examination's clinical utility. This article is part 1 of a 2-part series. Part 1 will begin with a review of bone physiology and osteoporosis etiology, followed by a discussion of the principles underlying DXA and the technical procedure. Part 2 will focus on DXA interpretation and discuss scanning pitfalls and clues to recognizing issues and improving scan quality.

**Key Words:** dual-energy x-ray absorptiometry; DXA; DEXA; bone mineral density; osteoporosis; osteopenia

**J Nucl Med Technol 2023; 51:167–175**
DOI: 10.2967/jnmt.122.264885

Osteoporosis is a skeletal disorder of weakened bone strength resulting in elevated fracture risk. A common but silent disease until a fracture occurs, an estimated one half of women and one fifth of men over age 50 y will experience an osteoporosis-related fracture (*1*). These fractures are referred to as fragility fractures because they result from low-energy trauma, equal to or less than a fall from standing height. The most common fracture sites are the spine, pelvis, hip, and distal radius. These fractures commonly result in long-term disability, diminished quality of life, and increased mortality, particularly with hip fractures, which almost always require hospitalization and have a 20% mortality rate and 50% permanent disability rate (*2*). With one-third of people in the United States aged 50 y or older, the prevention, detection, and treatment of this prevalent disease are critical to the well-being of a substantial portion of the population (*3*).

Bone strength and, consequently, fracture risk are a function of bone quality and bone mineral density (BMD). Bone quality comprises approximately 30% of bone strength, whereas BMD comprises the remaining 70%. Bone quality refers to a constellation of factors influencing how well a bone resists fracturing. These factors include osseous architecture, accumulated microscopic damage, mineral crystal size, collagen structure, and bone turnover rate (*4*). BMD is simply the bone mass per area ($g/cm^2$) (*5*).

Bone quality cannot be directly measured in the clinical setting. Bone density, however, can easily be measured via dual-energy x-ray absorptiometry (DXA), a quick, inexpensive, and readily available radiologic procedure. This article is part 1 of a 2-part series. Part 1 will begin with a review of bone physiology and osteoporosis etiology, followed by a discussion of the principles underlying DXA and the technical procedure. Part 2 will focus on DXA interpretation and discuss scanning pitfalls and clues to recognizing issues and improving scan quality.

## BONE PHYSIOLOGY AND OSTEOPOROSIS

### Bone Physiology

Normal bone physiology is a process of formation and remodeling (*6*). Bones grow in both the longitudinal and the radial directions, with continuous remodeling throughout life in reaction to microtrauma. It is estimated that most of an adult's skeleton is replaced every 10 y. Bone remodeling is essential because it replenishes bone strength and mineral content, thus averting the accumulation of damaged bone.

There are 2 types of bone: cortical and trabecular. Cortical bone, also known as compact bone, is the hard outer layer of

Received Sep. 6, 2022; revision accepted Sep. 23, 2022.
For correspondence or reprints, contact Mary Beth Farrell (farrell@intersocietal.org).
Published online Oct. 4, 2022.

strong, dense bone. Trabecular bone, also called cancellous bone, is the lighter, less dense, spongy inner network of trabeculae (meshlike layer of holes connected by thin rods and plates filled with red bone marrow) (*7*). Approximately 3% of cortical bone is resorbed and replaced each year, compared with 25% of trabecular bone.

Although cortical bone and trabecular bone differ in their structure, they have a similar molecular composition (*6*). Both have an extracellular matrix, and the composition and arrangement of the extracellular matrix determine a bone's mechanical characteristics. Bone strength is influenced by collagenous proteins (tensile strength) and mineralized osteoid (compressive strength).

*Bone Cells.* Three predominant bone cells include osteocytes, osteoclasts, and osteoblasts. Osteocytes account for 90%–95% of total bone cells (*8*). The adult body has approximately 42 billion. They have a lifespan of up to 25 y. They are often described as terminally differentiated osteoblasts embedded in a mineralized osteoid matrix of calcium and phosphate (hydroxyapatite).

Osteoclasts are responsible for bone resorption, whereas osteoblasts are responsible for bone formation. Their function depends on each other and is linked in regard to bone remodeling. For resorption, osteoclasts secret acid and enzymes that digest bone minerals and bone matrix. Osteoblasts secrete and mineralize osteoid bone and control osteoclast resorption. Osteoblasts differentiated into osteocytes appear to control the timing and location of remodeling in response to environmental stress or mechanical strain. Osteoclast resorption of bone, at the microscopic scale, takes weeks, whereas osteoblast formation of new bone takes 4–6 mo. Thus, any condition that increases the rate of bone remodeling causes net bone loss over time.

*Bone Remodeling Phases.* Peak bone mass, representing the greatest amount of bone a person can reach or the bony tissue present at the end of skeletal maturation, occurs between 20 and 30 y of age for men and women, with men typically reaching a higher peak (Fig. 1) (*6*). In men, bone mass gradually declines over time until old age. In women, bone mass plateaus until menopause, and then there is an accelerated period of bone loss for several years. After peak bone mass is attained, bone mass and structural integrity are determined by remodeling for the remainder of a person's life.

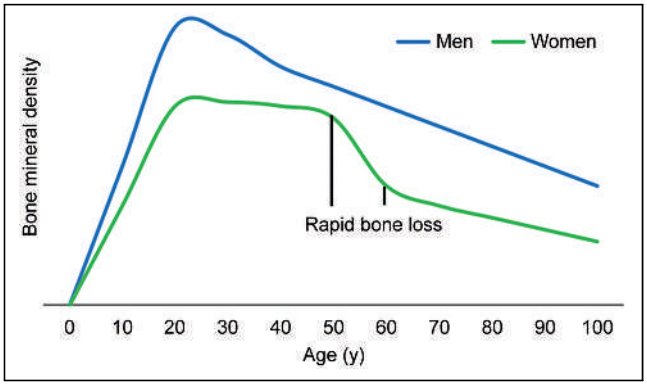


**FIGURE 1.** Normal bone loss over time for men and women. For both men and women, bone mass peaks at 20–30 y old. Men then begin to lose bone mass over time gradually. Bone mass in women plateaus until menopause, and then there is rapid bone loss for several years.

During remodeling, old bone tissue is replaced by new bone tissue through coupling of bone formation and resorption. There are 4 sequential phases: quiescence/activation, resorption, reversal, and formation. During quiescence/activation, cytokines and growth factors stimulate preosteoclasts, which differentiate into mature osteoclasts, which digest old bone during the resorption phase. During reversal, the resorption of the mineral matrix ends, and the osteoclasts signal preosteoblasts to initiate bone formation. During the bone formation phase, osteoblasts synthesize new bone by producing an organic matrix of protein and polysaccharides (osteoid) that become bone after mineralization. At the end of formation, the osteoblasts become quiescent and line the newly formed bone surface.

## Osteoporosis

*Osteoporosis Etiology.* Osteoporosis is defined as low bone mass and microstructural weakening of bone tissue leading to increased bone fragility (*6*). The reduction in bone mass is caused by a decoupling of bone resorption and bone formation. Normally, bone resorption and formation are fairly equally balanced. However, a decrease in bone formation or an increase in bone resorption can result in osteoporosis. In osteoporosis, the coupling mechanism between osteoclasts and osteoblasts does not keep pace with the continuous microtrauma of the trabecular bone. The cause of the imbalance is multifactorial based on genetic, intrinsic, exogenous, and lifestyle factors.

Osteoporosis can be categorized as primary or secondary (Fig. 2). Primary, or idiopathic, osteoporosis, the most common type, can be further divided into postmenopausal (type I) and age-associated or senile (type II) osteoporosis. A decrease in estrogen is the main cause of postmenopausal osteoporosis. Senile osteoporosis is caused by decreased calcium and an aging skeleton. Secondary osteoporosis is caused by disease processes (e.g., renal hypercalciuria or Cushing syndrome), dietary deficiency (e.g., alcoholism or anorexia), or medications (e.g., glucocorticoid, proton pump inhibitors, or selective serotonin reuptake inhibitors).

The primary risk factor for osteoporosis is advanced age. However, there are many other identified risk factors, such as being female, having white or Asian ethnicity, or having a family history of osteoporosis (Table 1).

*Osteoporosis Treatment.* Although there is no cure for osteoporosis, the prognosis is good if it is detected early and properly treated. Thus, prevention and recognition of the causes are the primary steps to lessen the impact and halt progression of the disease (*6*). Treatment includes lifestyle modifications such as increased exercise, smoking cessation, and limiting of alcohol consumption. Calcium and vitamin D are also usually prescribed.

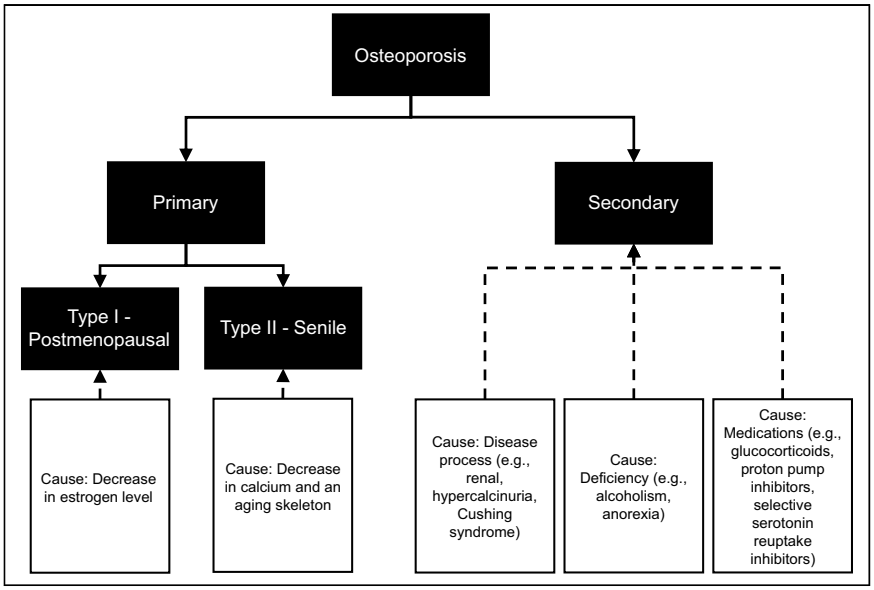


**FIGURE 2.** Osteoporosis types. Osteoporosis can be categorized as primary or secondary. Primary osteoporosis consists of type 1 (postmenopausal) and type II (also called senile). Type I is caused by decreases in estrogen levels, whereas type II is caused by decreased calcium and skeletal aging. Secondary osteoporosis is caused by other diseases, diet, or medications.

Some medications may be helpful, depending on the underlying cause of osteoporosis (Table 2). These include antiresorptive agents such as bisphosphonates (e.g., alendronate [Fosamax; Merck], risedronate [Actonel; Allergan Pharma], or zoledronic acid [ReClast; Novartis]), which reduce osteoclast function; selective estrogen receptor modulators (e.g., raloxifene [Evista; Eli Lilly] and bazedoxifene [Duavee, Duavive, Pfizer, Inc.]), which act on estrogen receptors to downmodulate osteoclast activity; RANK (receptor activator of nuclear factor κ B) ligand inhibitors such as denosumab (e.g., Prolia [Amgen] and Xgeva [Amgen]), which block osteoclast maturation; and anabolic agents (e.g., abaloparatide (Tymlos [Radius Health, Inc.]) and teriparatide (Forteo [Eli Lilly]), which promote new bone formation (*9–12*).

**TABLE 1**
Osteoporosis Risk Factors

| Category | Risk factor |
|---|---|
| Nonmodifiable | ≥50 y old |
| | Female |
| | Asian or white ethnicity |
| | Family history |
| | Thin physique or low weight (<57.6 kg [127 lb]) |
| | Androgen or estrogen deficiency |
| | Hypogonadism |
| | Amenorrhea |
| | Late menarche |
| | Early menopause |
| | Postmenopausal |
| | Immobility |
| | Certain medications (e.g., anticonvulsants, steroids, thyroid drugs, heparin, chemotherapy, insulin) |
| | Dowager hump (focal kyphosis of upper thoracic spine) |
| Modifiable | Physical inactivity |
| | Smoking |
| | Excessive alcohol consumption |
| | Low calcium or vitamin D |

## DXA PRINCIPLES

Newer nuclear medicine technologists may not realize that DXA began as a nuclear medicine procedure, and DXA is still performed in many nuclear medicine departments today. The systems used in the 1970s to measure BMD were dual-energy photon absorptiometry systems that measured the attenuation of monochromatic emissions from the radioisotope $^{153}$Gd (*13*). In 1987, the first DXA scanners became commercially available. DXA uses polychromatic x-ray spectra at different energy levels. Using x-rays shortened the examination time because of the higher photon flux from the x-ray tube, resulting in better resolution and precision.

DXA is based on the variable absorption of x-ray photons by different tissues in the body. An x-ray source below the patient produces alternating high-energy (140 kVp) and low-energy (70–100 kVp) pulses. The use of 2 distinct energy levels enables bone to be measured separately from soft tissue (*14*). A detector above the patient measures the transmitted low- and high-energy photons and calculates bone density based on the difference between soft-tissue and bone attenuation. Although density typically represents mass per unit volume, DXA results are obtained from a planar (2-dimensional) image, and consequently, depth cannot be determined (*13*). Therefore, density, or more accurately areal density, is reported as mass per unit area (g/cm$^2$), unlike CT, for which traditional density is reported as mass per volume (g/cm$^3$).

The calculated BMD results are compared with a reference-subject database. The SD (how much the result varies from the average mean) is reported as a T-score or a Z-score. The scores indicate the relationship between peak bone mass and subsequent bone loss. The results may vary somewhat between manufacturers depending on the database used and differences in the technology.

The T-score, as defined by the World Health Organization, represents how a patient's measured BMD differs from that of a healthy 30-y-old adult woman (presumed peak bone mass) (*15*). The T-score is used to assess BMD

**TABLE 2**
Osteoporosis Medications

| Type | Function | Example |
|---|---|---|
| Antiresorptive agents | Reduce osteoclast function | Bisphosphonates: alendronate, risedronate, zoledronic acid |
| Selective estrogen receptor modulators | Act on estrogen receptors to downmodulate osteoclast activity | Raloxifene, bazedoxifene (FRAX) |
| RANK ligand inhibitors | Block osteoclast maturation | Denosumab |
| Anabolic agents | Promote new bone formation | Abaloparatide teriparatide |

in postmenopausal women and men aged 50 y and older. In contrast, younger patients, particularly children, are assessed using a Z-score, which also considers age, sex, and ethnicity.

The T-score, not to be confused with the "t" in the commonly used Student *t* test, is determined by taking the difference between the patient's measured BMD and the mean BMD of healthy 30-y-old adults, which is then divided by the 30-y-old adult SD (*16*).

$$\text{T-score} = \frac{\text{patient BMD} - \text{mean healthy 30-y-old adult BMD}}{\text{healthy 30-y-old adult SD}}$$

A T-score of −1.0 (SD) or greater is considered normal BMD, and a T-score of −2.5 or less is diagnostic of osteoporosis (*15*). T-scores of less than −1.0 but greater than −2.5 are classified as osteopenia, with *low bone density* also an acceptable term (Table 3).

Z-scores are calculated similarly to T-scores; however, Z-scores use the mean age-, sex-, and ethnicity-matched (population-specific) score.

$$\text{Z-score} = \frac{\text{patient BMD} - \text{mean population-specific (matched) BMD}}{\text{population-specific SD}}$$

Z-scores of greater than −2.0 are considered normal, whereas scores of −2.0 or less are considered low bone density for age. Note, Z-scores are not used to formally diagnose osteoporosis; instead, the score serves as a clue to look for a cause of secondary osteoporosis.

**TABLE 3**
World Health Organization Osteoporosis T-Score Classification*

| T-score | Classification |
|---|---|
| ≥−1 | Normal |
| Between −1.0 and −2.5 | Osteopenia |
| ≤−2.5 or lower | Osteoporosis |
| ≤−2.5 (with fragility fracture) | Severe or established osteoporosis |

*Compared with mean bone density of young adult women.

## DXA ALTERNATIVES

DXA is the preferred technique to measure BMD because of its high precision and accuracy (1%–2% margin of error) (*17*). Precision refers to the reproducibility of a measurement, whereas accuracy refers to how close a measurement is to the true value. DXA measurements also can be quickly obtained at a relatively low radiation dose. However, other methods are available, including quantitative CT (QCT) and quantitative ultrasound (QUS).

QCT of the lumbar spine, or central QCT, is performed on a standard CT machine using specialized protocols. QCT of the forearm, also called peripheral QCT, can be measured using smaller, less sophisticated equipment; however, the measurements correlate poorly with central measures (*16*). QCT is a 3-dimensional technique that calculates the true volume and volumetric bone density ($g/cm^3$) (*13*). The geometry of the vertebra can be assessed. QCT also allows for differentiation between cortical and trabecular bone (*18*). However, one drawback to QCT is the higher radiation dose than DXA. Another drawback is the lack of validated diagnostic criteria.

QUS can assess the BMD of the peripheral skeleton, usually the calcaneus. QUS uses ultrasound attenuation instead of x-ray attenuation and the speed of sound. The advantages of QUS are that it is relatively inexpensive compared with QCT and DXA and that the equipment can be portable. The disadvantage of QUS is that it is less accurate than QCT and DXA.

## DXA PROCEDURE

### Indications/Contraindications

The practice parameters of the American College of Radiology, Society for Pediatric Radiology, and Society for Skeletal Radiology provide a long list of clinical indications for DXA (*23*). Essentially, DXA is used to diagnose abnormalities of BMD, estimate the risk of fractures, monitor changes in density over time, and assess response to treatment.

There are no absolute contraindications for DXA (*14*). However, several conditions may result in scans of limited value: recent administration of gastrointestinal contrast media or radiopharmaceuticals, severe degenerative changes in the measurement area, fracture, implants or devices in the measurement area, patient's inability to be positioned or remain motionless during the scan, and extremely low or high body mass. Pregnancy is a relative contraindication, and the risks

**TABLE 4**
Patient Medical History Screening

| Category | Condition |
|---|---|
| Bone marrow disorders | Multiple myeloma |
| | Myelodysplasia |
| | Systemic mastocytosis |
| | Thalassemia |
| Endocrine or metabolic diseases | Acromegaly |
| | Anorexia nervosa |
| | Cushing syndrome |
| | Diabetes mellitus type 1 |
| | Hypercalcemia |
| | Hyperparathyroidism |
| | Hyperprolactinemia |
| | Hyperthyroidism |
| | Hypopituitarism |
| Other conditions | Chronic kidney disease |
| | History of organ transplantation |
| | Hypercalciuria |
| | Immobilization (e.g., paraplegia, quadriplegia, or muscular dystrophy) |
| | Inadequate calcium uptake |
| | Malabsorption (e.g., celiac disease) |
| | Rheumatoid arthritis |
| | Secondary hyperparathyroidism due to renal disease |
| | Vitamin D deficiency |

**TABLE 5**
Medications Causing Bone Loss or Increased Fracture Risk

| Parameter | Medication |
|---|---|
| Bone loss | Anticonvulsants (e.g., phenobarbital, phenytoin) |
| | Aromatase inhibitors |
| | Cytotoxic agents |
| | Glucocorticoids > 3 mo |
| | Gonadotropin-releasing hormone agonists or antagonists (e.g., androgen deprivation therapy, Lupron [AbbVie]) |
| | Immunosuppressive agents (e.g., cyclosporine) |
| | Intramuscular medroxyprogesterone (Depo-Provera [AbbVie]) |
| | Thyroid hormone excess |
| Increased fracture risk | Benzodiazepines/Z-drugs, insulin with hypoglycemia, opioids, thiazolidinediones, selective norepinephrine reuptake inhibitors, selective serotonin reuptake inhibitors, SGLT-2 inhibitors |

Z-drugs = eszopiclone (Lunesta; Sunovion Medical); zaleplon (Sonata; Pfizer); and zolpidem (Ambien; Sanofi-Aventis LLC); SGLT-2 = sodium-glucose co-transporter 2.

and benefits of DXA should be discussed with the referring physician.

### Patient Preparation

Patients should be prescreened to ensure that they can lie on their back for up to 10 min. They should have received no barium or gadolinium oral contrast medium within 2 wk beforehand, and they should have taken no calcium tablets within 24 h before the scan (*18*). They should be wearing loose-fitting clothing without metal. Finally, if they underwent DXA previously, they should have brought a copy of the results for comparison.

A detailed patient history is required to perform and interpret DXA correctly. The history should include risk factors, prior surgery that could affect the accuracy of measurements, previous fractures, endocrine or metabolic diseases, bone marrow–related disorders, and other associated conditions (Table 4) (*19*). Patients should also be screened for medications associated with bone loss or increased fracture risk (Table 5). The International Society of Clinical Densitometry (www.iscd.org) provides patient history questionnaires.

In addition, the World Health Organization fracture risk algorithm can be used to calculate a score from the patient history that can be used to correlate with DXA findings. The FRAX estimates the 10-y probability of fracture due to osteoporosis in postmenopausal women and men over 50 y old. It evaluates risk factors including age, sex, low body weight, height, previous fracture, parent history of hip fracture, smoking, glucocorticoid use, history of rheumatoid arthritis, menopausal state, and excess alcohol intake (*19*). The FRAX tool is helpful for risk-stratifying osteopenic individuals to identify those who are most likely to benefit from therapy.

### Acquisition

*Equipment.* Several manufacturers produce DXA scanners, and the equipment can be full-table systems that can measure multiple sites, such as the spine or hip, or peripheral systems that measure the wrist or ankle (*20*). Full-table systems offer the most options and are the preferred osteoporosis assessment and management method.

The first-generation DXA scanners used pencil-beam geometry and a single detector that scanned across the area of interest in a raster pattern (*21*). Current scanners use fan-beam technology with multiple detectors that sweep the measurement area. One advantage of fan-beam over pencil-beam technology is shorter scan times of 30 s for the hip and spine compared with 3–10 min for pencil-beam technology (*13*). The disadvantages of fan-beam scanners include slight image distortion due to magnification of the tissue and increased scanner cost. Another disadvantage of fan-beam scanners is increased scatter.

*Quality Control.* The accuracy of BMD measurement depends on the consistency of the scanner (*22*). Quality control procedures vary by manufacturer but usually require scanning a dedicated phantom and automatic analysis that checks and calibrates mechanical function, radiation quality, and the absorption coefficient of tissue-equivalent materials. The procedure is performed daily before use and at least

3 times a week (*13*). If the results fall outside the acceptable limits, the scanner should be evaluated by a field service engineer.

Cross-calibration procedures are necessary for precise longitudinal assessment when replacing scanners (the same model is usually preferred) or validating measurements between systems (*22*). Cross calibration entails scanning the phantom 10 times on each scanner. The measures should be within 1%.

*Areas of Study.* For routine DXA, the lumbar spine and hip are assessed, with measurement of either or both hips considered acceptable. Assessment of both hips provides information on the hip with the lowest BMD and allows for longitudinal evaluation even if one hip is fractured or undergoes surgery in the future (*23*). In addition, the nondominant forearm BMD should be included in all patients with hyperparathyroidism. The forearm should also be measured when the hip or spine cannot be measured or correctly interpreted because of hardware or other confounding factors. The final diagnosis is made using the lowest score among the measured skeletal sites.

The patient must remove all objects from their pockets or body in the scan field, such as wallets, cell phones, underwire bras, watches, and bracelets.

*Positioning.* Correct patient positioning is essential to obtaining reliable and reproducible BMD measurements. Incorrect positioning is one of the most common reasons for errors.

*Spine.* For the spine, posteroanterior images are obtained of L1–L4 with the patient lying supine on the DXA table (*24*). The lower back should be aligned in the middle of the table with the spine straight compared with the table's long axis and not rotated (Fig. 3). A tip to ensure that the spine is straight is to stand at the patient's head, gently reach under the underarms, and pull the patient upward. The legs should be elevated using a foam block—placed under the patient's lower legs so the thighs are as close to a 90° angle to the body as possible—to minimize lordosis and increase intervertebral spacing. The patient should rest the arms and hands comfortably at the sides.

The scan field of view extends superiorly to include a portion of the lowest thoracic vertebra (confirmed by the presence of ribs) and inferiorly to show the iliac crests (about the level of the L4–L5 interspace). Usually, proper patient positioning can be achieved by locating the patient's iliac crest and starting the scan 5 cm (2 in) below. Most scanners begin the acquisition inferiorly and move superiorly.

As the scan is acquired, the technologist monitors the emerging planar image to ensure that the entire spine is centered and straight. There should be equal amounts of soft tissue on both sides of the spine, and a small part of the iliac crest should be visible in the lower corners of the screen. If the patient is not positioned correctly, the technologist should stop the scan, reposition, and restart the acquisition. The scan can be terminated when the ribs attached to the 12th thoracic vertebra (T12) are visualized.

*Hip.* The hip images must include the entire femoral head, the greater trochanter, and 2.5 cm (1 in) or more of the femoral shaft below the lesser trochanter (Fig. 4). The technologist must first locate the patient's greater trochanter to ensure that the hip is correctly positioned in the field of view. The greater trochanter can be identified by holding the patient's ankle and rotating inward and outward while pressing firmly on the thigh with the other hand. The greater trochanter will roll back and forth under the fingertips. An alternative method is to ask the patient to bend at the knee and lift the leg. The crease formed at the top of the leg is approximately in line with the greater trochanter.

A hip-positioning device is placed under the patient's lower legs at the midline of the patient's body. The long axis of the femur should be parallel to the long axis of the table.

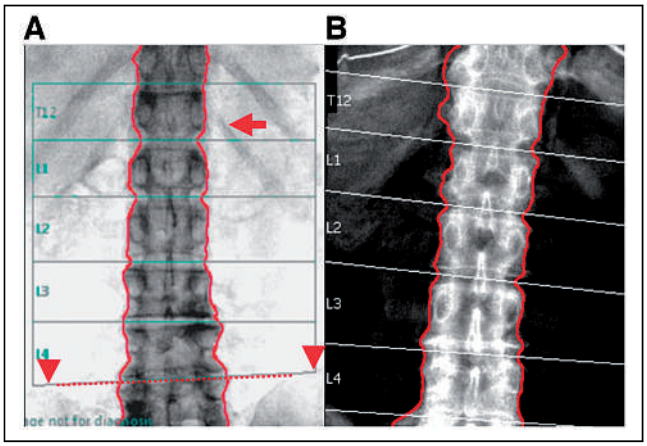


**FIGURE 3.** (A) Properly positioned posteroanterior view of lumbar spine with appropriate field of view. Spinous processes should be centered straight (midline) and include part of iliac crest (arrowheads) and part of vertebra with ribs (arrow). Iliac crests provide helpful landmark. Dashed line connecting this will typically bisect L4–5 disk space. (B) Incorrectly positioned posteroanterior view of lumbar spine in which spine is angled and left iliac crest is not visible.

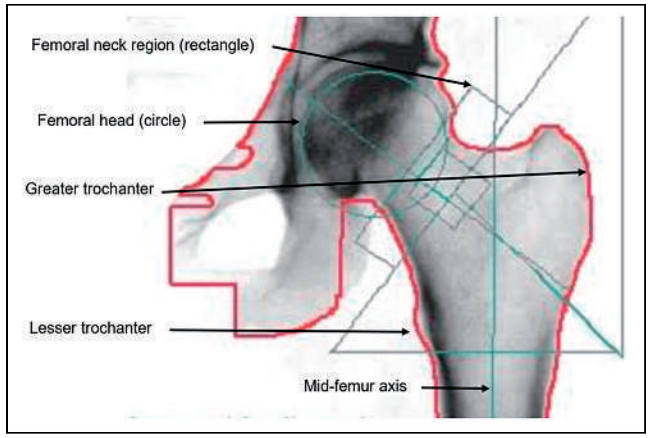


**FIGURE 4.** Essential hip anatomy for proper positioning includes femoral head, femoral neck, greater trochanter, lesser trochanter, and mid-femur axis.

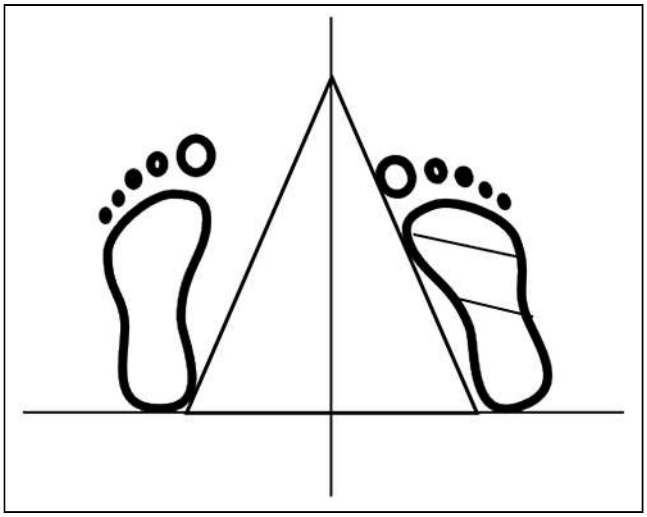

**FIGURE 5.** Hip positioning device. To properly align axis of femoral neck, leg must be rotated 15°–25° inward and strapped to hip-positioning device.

The leg of the hip to be measured is rotated inward and strapped against the positioning device, abducting or internally rotating 15°–25° to position the femoral neck axis parallel to the table plane and ensure precise measurement (Fig. 5). When rotating the leg, the technologist should place one hand above the knee and the other hand below the knee and gently turn the entire leg, not just the lower portion.

Incorrect leg rotation causes foreshortening of the femoral neck, presenting a smaller cross-sectional area, possibly resulting in a falsely elevated BMD (*25*). An excess of internal or external rotation of as low as 10° can lead to significant changes in measured BMD in approximately 10% of patients (Fig. 6).

The patient can rest the arms on the chest or outside the scan field. The scan begins at a position 5 cm (2 in) below the level of the greater trochanter. A horizontal laser line can ensure that the femoral shaft is parallel.

On scan completion, the technologist should verify correct hip positioning. The lesser trochanter will be barely visible on a properly aligned and rotated hip, and the shaft of the femur will be straight.

*Forearm.* When the forearm is being imaged, the patient sits next to the table, with the nondominant forearm, wrist, and hand laid flat, palm side down, and secured to a positioning board with a restraining strap (*26*). The ulnar and radial shafts should be aligned with the long axis of the table, with the carpal bones in the top third of the image (Fig. 7). This position ensures inclusion of the radius 33% (also known as one-third radius), consisting of a 20-mm length of the radial shaft located one third of the distance between the ulnar styloid and the olecranon. The radius 33% is the recommended forearm site when either the lumbar spine or the hip cannot be assessed or in cases of hyperparathyroidism.

### Analysis

The first step in analyzing the DXA image is to confirm positioning and the absence of patient motion on the planar image (*27*). The image must also be reviewed for artifacts such as metal, overlying hardware, or barium.

*Spine.* Most DXA scanners use automated region-of-interest (ROI) placement. However, the technologist must manually adjust the ROI to ensure appropriate intervertebral designations (*13*). Correct identification and numbering of the lumbar vertebrae are critical. Staron et al. found that incorrect intervertebral disk space ROI placement was the most common analysis error (*28*).

The spine measurement region includes L1 through L4, with the box placed at the top of L1 and the bottom of L4 (*13*). The intervertebral lines should be moved and angled as appropriate to ensure proper numbering of the vertebrae. A line drawn from the highest point of one iliac crest to the other iliac crest most commonly traverses the L4–L5 intervertebral disk space and is used as a landmark (*29*). In addition, there must be adequate soft tissue on both sides of the spine; insufficient soft tissue results in underestimation of the BMD.

*Hip.* The hip ROI includes the femoral neck, trochanter, and total hip. Although the Ward triangle (not a true anatomic area but a calculated area of the lowest BMD in the femoral head) and the intertrochanteric region are often

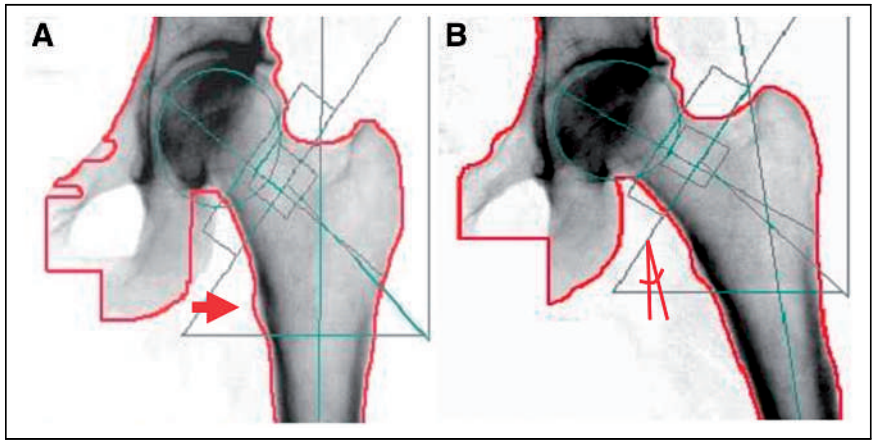


**FIGURE 6.** (A) Properly positioned hip. Femur shaft is aligned with craniocaudal axis. Appropriate internal rotation is demonstrated by minimal visualization of lesser trochanter (arrow). Field of view is centered correctly with greater trochanter at midway craniocaudal point. (B) Improperly positioned hip with femoral shaft off axis, in 20° of abduction (angle). Incorrect rotation or alignment causes foreshortening of femoral neck, which presents smaller cross-sectional area, possibly resulting in falsely elevated BMD. Excess internal or external rotation of as low as 10° can lead to significant changes in measured BMD in approximately 10% of patients (*25*). Additionally, this incorrect positioning is often not reproduced on follow-up, potentially propagating error by calculation of spurious interval change.

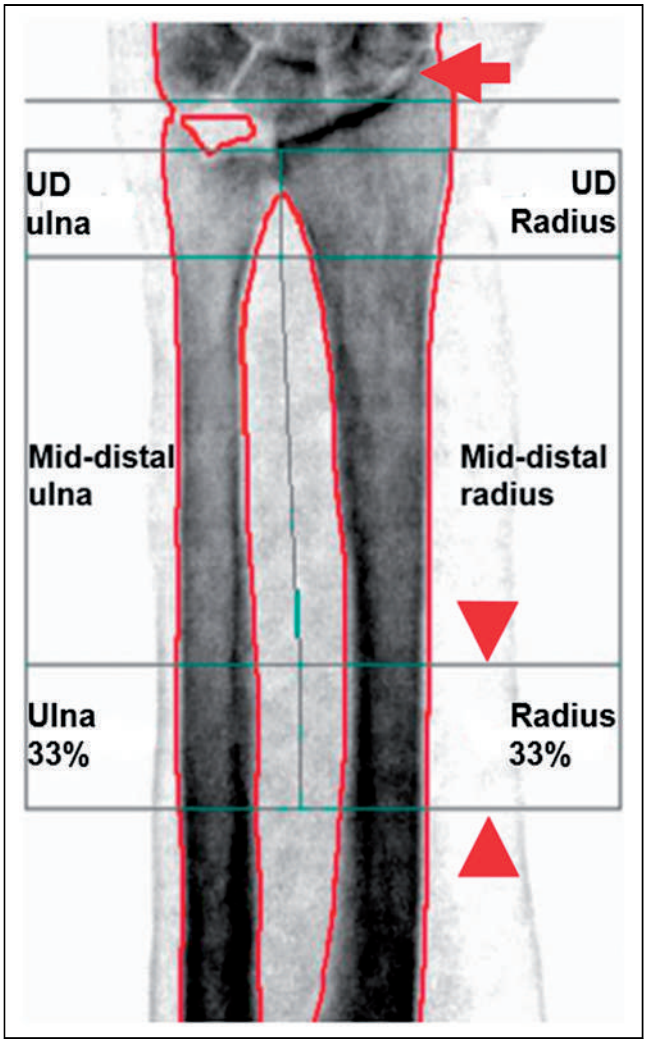


**FIGURE 7.** Appropriately positioned nondominant forearm. Ulnar and radial shafts are aligned with long axis of table, with carpal bones (arrow) in top third of image. This position ensures inclusion of radius 33%, also known as one-third radius, consisting of 20-mm length of radial shaft located one third of distance between ulnar styloid and olecranon (arrowheads). UD = ultradistal.

included in manufacturers' hip BMD results, these regions are not relevant and not reported (*30*). The first step in the hip analysis is to ensure that the line midline and parallel through the hip is correctly placed. All other ROIs depend on correct placement of this line. The femoral neck ROI is usually placed halfway between the femoral head and trochanter or on the distal portion of the femoral neck, depending on the DXA manufacturer.

*Forearm.* The ROI for the forearm must be manually positioned. The 3 regions of the distal radius must be defined: the ultradistal region (a 15-mm section from the endplate of the radius); the proximal region, also called the one-third distal (a 20-mm section one third of the distance between the ulnar styloid and the olecranon); and the intermediate or mid-distal radius (the remaining section between the 2 other regions) (*26*).

### Longitudinal Measurement Note

Currently available DXA systems use various filters, collimators, detectors, and analysis algorithms (*18*). Thus, it is advisable to perform longitudinal measurements or follow-up scans on the same piece of equipment as earlier scans. When scans are performed on the same stationary equipment, accuracy is high, with a margin of error of 1%–2% (*17*). In addition, the same skeletal site, ROI, and area size should be used if quantitative comparisons are performed (*23*). Only qualitative comparisons can be made if follow-up scans are done on a different device.

### Radiation Dose

The radiation dose from DXA is relatively low (*18*). The average dose for spine-plus-hip DXA ranges from 1 to 15 μSv, depending on the equipment (*31*). The dose from pencil-beam systems is usually less, at about 1 μSv, whereas fan-beam systems may be up to 15 μSv. For comparison, the average effective dose from a chest radiograph ranges from 20 to 50 μSv, and the average dose from natural background radiation is about 10 μSv per day. The low radiation doses from DXA make serial imaging acceptable if the initial results are abnormal.

## CONCLUSION

Osteoporosis is a common skeletal disorder of weakened bone strength, leading to increased bone fragility and elevated fracture risk. Therefore, preventing, detecting, and treating this disease is critical to the well-being of a substantial portion of the U.S. population. Bone strength and, thus, fracture risk can be assessed from measurement of BMD via DXA.

The precision and accuracy of DXA results depend on the procedure's proper performance and interpretation. Therefore, correct patient positioning, acquisition, and analysis are essential. This article, part 1 of a 2-part series, has laid a foundation for performing DXA by, first, reviewing bone anatomy and physiology along with osteoporosis etiology and treatment. Next, the article explained the principles underlying DXA and the scanner features. Finally, the article detailed the DXA acquisition protocol, including the indications, contraindications, patient preparation, positioning, acquisition, and analysis. Part 2 of the series will review DXA interpretation, use of DXA for monitoring changes in BMD, and pitfalls and clues for quality DXA results.

## DISCLOSURE

No potential conflict of interest relevant to this article was reported.

## REFERENCES

1. Sözen T, Ozısık L, Başaran NC. An overview and management of osteoporosis. *Eur J Rheumatol.* 2017;4:46–56.
2. Osteoporosis: assessing the risk of fragility fracture. National Institute for Health and Care Excellence website. https://www.nice.org.uk/guidance/cg146. Published August 8, 2012. Updated February 7, 2017. Accessed November 7, 2022.

3. Housing America's older adults 2019. Harvard University website. https://www.jchs.harvard.edu/housing-americas-older-adults-2019/. Published 2019. Accessed November 7, 2022.
4. NIH Consensus Development Panel on Osteoporosis Prevention, Diagnosis, and Therapy. Osteoporosis prevention, diagnosis, and therapy. *JAMA.* 2001;285:785–795.
5. Ammann P, Rizzoli R. Bone strength and its determinants. *Osteoporos Int.* 2003;14(suppl 3):S13–S18.
6. Elam REW, Jackson NN, Machua W, Carbone LD. Osteoporosis. Medscape website. https://emedicine.medscape.com/article/330598-overview. Updated January 20, 2021. Accessed November 7, 2022.
7. Ott SM. Cortical or trabecular bone: what's the difference? *Am J Nephrol.* 2018;47:373–375.
8. Florencio-Silva R, Sasso GR, Sasso-Cerri E, Simões MJ, Cerri PS. Biology of bone tissue: structure, function, and factors that influence bone cells. *BioMed Res Int.* 2015;2015:421746.
9. An KC. Selective estrogen receptor modulators. *Asian Spine J.* 2016;10:787–791.
10. Leder BZ. Optimizing sequential and combined anabolic and antiresorptive osteoporosis therapy. *JBMR Plus.* 2018;2:62–68.
11. Hanley DA, Adachi JD, Bell A, Brown V. Denosumab: mechanism of action and clinical outcomes. *Int J Clin Pract.* 2012;66:1139–1146.
12. Lewiecki EM. Bisphosphonates for the treatment of osteoporosis: insights for clinicians. *Ther Adv Chronic Dis.* 2010;1:115–128.
13. *IAEA Human Health Series No. 15: Dual-Energy X-Ray Absorptiometry for Bone Mineral Density and Body Composition Assessment*. International Atomic Energy Agency; 2010:31–67.
14. Krugh M, Dual energy x-ray absorptiometry. StatPearls website. https://www.statpearls.com/physician/cme/activity/22242/?specialty=Public%20and%20Preventive%20Medicine&deg=MD. Updated January 1, 2021. Accessed November 7, 2022.
15. Kanis JA, Glüer CC. An update on the diagnosis and assessment of osteoporosis with densitometry. Committee of Scientific Advisors, International Osteoporosis Foundation. *Osteoporos Int.* 2000;11:192–202.
16. Blake GM, Fogelman I. The role of DXA bone density scans in the diagnosis and treatment of osteoporosis. *Postgrad Med J.* 2007;83:509–517.
17. Albanese CV, Diessel E, Genant H. Clinical applications of body composition measurements using DXA. *J Clin Densitom.* 2003;6:75–85.
18. Lorente Ramos RM, Azpeitia Arman J, Arevalo Galeano N, Munoz Hernandex A, Garcia Gomez J, Gredilla Molinero J. Dual-energy x-ray absorptiometry: fundamentals, methodology, and clinical applications. *Radiologia.* 2012;54:410–423.
19. Osteoporosis screening, diagnosis, and treatment guideline. Kaiser Permanente website. https://wa.kaiserpermanente.org/static/pdf/public/guidelines/osteoporosis.pdf. Published March 2022. Accessed November 7, 2022.
20. El Maghraoui A, Roux C. DXA scanning in clinical practice. *QJM.* 2008;101:605–617.
21. Koo WW, Hammami M, Hockman E. Interchangeability of pencil-beam and fan-beam dual-energy x-ray absorptiometry measurements in piglets and infants. *Am J Clin Nutr.* 2003;78:236–240.
22. Kim HS, Yang SO. Quality control of DXA system and precision test of radiotechnologists. *J Bone Metab.* 2014;21:2–7.
23. ACR-SPR-SSR practice parameter for the performance of dual energy x-ray absorptiometry (DXA). American College of Radiology website. https://www.acr.org/-/media/ACR/Files/Practice-Parameters/DXA.pdf. Revised 2018. Accessed November 7, 2022.
24. National Health and Nutrition Examination Survey (NHANES): dual energy x-ray absorptiometry (DXA) procedures manual. Center for Disease Control and Prevention website. https://www.cdc.gov/nchs/data/nhanes/nhanes_07_08/manual_dexa.pdf. Published January 2007 Accessed November 7, 2022.
25. Lekamwasam S, Lenora R. Effect of leg rotation on hip bone mineral density measurements. *J Clin Densitom.* 2003;6:331–336.
26. Miyamura S, Kuriyama K, Ebina K, et al. Utility of distal forearm DXA as a screening tool for primary osteoporotic fragility fractures of the distal radius: a case-control study. *JBJS Open Access.* 2020;5:e0036.
27. Jacobson JA, Jamadar D, Hayes C. Dual x-ray absorptiometry: recognizing image artifact and pathology. *AJR.* 2000;174:1699–1706.
28. Staron RB, Greenspan R, Miller T, Bilezikian J, Shane E, Haramati N. Computerized bone densitometric analysis: operator-dependent errors. *Radiology.* 1999;211:467–470.
29. Render CA. The reproducibility of the iliac crest as a marker of lumbar spine level. *Anaesthesia.* 1996;51:1070–1071.
30. Doroudinia A, Colletti P. Bone mineral measurements. *Clin Nucl Med.* 2015;40:647–657.
31. Radiation protection of patients during DEXA. IAEA website. https://www.iaea.org/resources/rpop/health-professionals/other-specialities-and-imaging-modalities/dxa-bone-mineral-densitometry/patients#1. Accessed November 7, 2022.

# SNMMI Procedure Standard/EANM Practice Guideline for Palliative Nuclear Medicine Therapies of Bone Metastases

Austin R. Pantel[1], Matthias Eiber[2], Dmitry D. Beyder, CNMT[3], A. Tuba Kendi[4], Richard Laforest[5], Isabel Rauscher[6], Edward B. Silberstein[7], and Matthew P. Thorpe[4]

[1]*University of Pennsylvania, Department of Radiology;* [2]*School of Medicine, Department of Nuclear Medicine, Technische Universität München, Munich, Germany;* [3]*Barnes-Jewish Hospital, Department of Radiology;* [4]*Mayo Clinic Rochester, Department of Radiology;* [5]*Washington University, Department of Radiology, St. Louis;* [6]*Technical University of Munich, Department of Nuclear Medicine; and* [7]*University of Cincinnati Medical Center, Cincinnati*

## PREAMBLE

The Society of Nuclear Medicine and Molecular Imaging (SNMMI) is an international scientific and professional organization founded in 1954 to promote the science, technology, and practical application of nuclear medicine. The European Association of Nuclear Medicine (EANM) is a professional nonprofit medical association that facilitates communication worldwide between individuals pursuing clinical and research excellence in nuclear medicine. The EANM was founded in 1985. SNMMI and EANM members are physicians, technologists, and scientists specializing in the research and practice of nuclear medicine.

The SNMMI and EANM will periodically define new guidelines for nuclear medicine practice to help advance the science of nuclear medicine and to improve the quality of service for patients throughout the world. Existing practice guidelines will be reviewed for revision or renewal, as appropriate, on their fifth anniversary or sooner, if indicated.

Each practice guideline, representing a policy statement by the SNMMI/EANM, has undergone a thorough consensus process in which it has been subjected to extensive review. The SNMMI/EANM recognizes that the safe and effective use of diagnostic nuclear medicine imaging requires specific training, skills, and techniques, as described in each document. Reproduction or modification of the published practice guideline by those entities not providing these services is not authorized.

These guidelines are an educational tool designed to assist practitioners in providing appropriate care for patients. They are not inflexible rules or requirements of practice and are not intended, nor should they be used, to establish a legal standard of care. For these reasons and those set forth below, both the SNMMI and the EANM caution against the use of these guidelines in litigation in which the clinical decisions of a practitioner are called into question.

The ultimate judgment regarding the propriety of any specific procedure or course of action must be made by the physician or medical physicist in light of all the circumstances presented. Thus, there is no implication that an approach differing from the guidelines, standing alone, is below the standard of care. To the contrary, a conscientious practitioner may responsibly adopt a course of action different from that set forth in the guidelines when, in the reasonable judgment of the practitioner, such course of action is indicated by the condition of the patient, limitations of available resources, or advances in knowledge or technology subsequent to publication of the guidelines.

The practice of medicine includes both the art and the science of the prevention, diagnosis, alleviation, and treatment of disease. The variety and complexity of human conditions make it impossible to always reach the most appropriate diagnosis or to predict with certainty a particular response to treatment. Therefore, it should be recognized that adherence to these guidelines will not ensure an accurate diagnosis or a successful outcome. All that should be expected is that the practitioner will follow a reasonable course of action on the basis of current knowledge, available resources, and the needs of the patient to deliver effective and safe medical care. The sole purpose of these guidelines is to assist practitioners in achieving this objective.

## I. PURPOSE

The purpose of this guideline is to assist nuclear medicine practitioners in treating patients with $^{89}$Sr-chloride, $^{153}$Sm-lexidronam ($^{153}$Sm-EDTMP), or $^{223}$Ra-dichloride ($^{223}$Ra-$Cl_2$) for palliation of bone pain secondary to osteoblastic metastases. These guidelines provide information on (*1*) evaluating patients who might be candidates for radiopharmaceutical treatment, (*2*) performing these treatments, and (*3*) understanding the sequelae of therapy.

Received Apr. 24, 2023; accepted Apr. 24, 2023.
For correspondence or reprints, contact Austin R. Pantel (austin.pantel@pennmedicine.upenn.edu).
Published online Jun. 14, 2023.

**TABLE 1**
Summary of Indications, Radiophysical Data, and Administered Activity

| Agent | Indication | Emission(s) | Physical half-life | Administered activity |
|---|---|---|---|---|
| $^{89}$Sr-chloride | Relief of bone pain caused by osseous metastases | β, rare γ | 50.5 days | 148 MBq (4.0 mCi) is recommended; alternative weight-based activity of 1.5-2.2 MBq/kg (40-60 μCi/kg) may be used |
| $^{153}$Sm-lexidronam | Pain relief in patients with osteoblastic metastases seen on radionuclide bone scan | β, γ | 1.9 days | Weight-based activity of 37 MBq (1.0 mCi) per kg |
| $^{223}$Ra-dichloride | Treatment of patients with castration-resistant prostate cancer with symptomatic osseous metastases and no known visceral metastatic disease | Predominantly α, with additional β and γ | 11.4 days | Weight-based activity of 55 kBq (1.49 μCi) per kg |

## II. DEFINITIONS AND BACKGROUND INFORMATION

Please see Table 1 for a summary of indications, radiophysical data, and administered activity.

### A. Definitions

1. $^{89}$Sr-chloride

   $^{89}$Sr-chloride is a radiopharmaceutical indicated for relief of bone pain in patients with painful osseous metastases. Currently marketed as Strontium89, $^{89}$Sr-chloride was previously marketed as Metastron. It decays through beta emissions with a maximum energy of 1.46 MeV, a mean energy of 0.58 MeV, and an average soft tissue range of 2.4 mm. $^{89}$Sr-chloride has a rare gamma emission (0.01%) with an energy of 0.91 MeV (*1*). Gamma camera images may be obtained by imaging bremsstrahlung emission following administration of $^{89}$Sr-chloride (*2,3*). Its physical half-life is 50.5 days (*4*). $^{89}$Sr-chloride is given through an intravenous injection. A fixed activity of 148 MBq (4 mCi) is recommended, but an alternative weight-based scaling of injected activity of 1.5-2.2 MBq/kg (40-60 μCi/kg) may be used (*5*). Radiation dosimetry is provided in Table 2. $^{89}$Sr-chloride is not commonly used today.

2. $^{153}$Sm-lexidronam ($^{153}$Sm-EDTMP)

   A radiopharmaceutical for pain relief in patients with osteoblastic metastases, $^{153}$Sm-EDTMP consists of radioactive $^{153}$Sm complexed to a chelator, ethylenediaminetetramethylenephosphonic acid (EDTMP). $^{153}$Sm-EDTMP emits multiple beta (β) particles with a maximum energy of 0.81 MeV and an average energy 0.23 MeV (*1*). The average and maximum beta particle range in water are 0.5 mm and 3.0 mm, respectively. A gamma (γ) emission with 29% abundance and an energy of 103 keV allows concomitant imaging. $^{153}$Sm-EDTMP has a 1.93-day physical half-life. $^{153}$Sm-EDTMP therapy is given through an intravenous injection as a weight-based scaling of activity of 37 MBq/kg (1.0 mCi/kg) (*6*). Radiation dosimetry is provided in Table 3. $^{153}$Sm-EDTMP is marketed as Quadramet and is not commonly used today.

3. $^{223}$Ra-dichloride ($^{223}$Ra-$Cl_2$)

   $^{223}$Ra-$Cl_2$ is a radiopharmaceutical for the treatment of patients with castration-resistant prostate cancer (CRPC) with symptomatic osseous metastases and no known visceral metastatic disease (*7*). $^{223}$Ra-$Cl_2$ is chemically similar to calcium (-chloride), with the Ra ion behaving similarly to the Ca ion, and is concentrated in the calcium-dense osteoblastic metastases of prostate cancer (*8*). Here, it delivers alpha (α) particles to neighboring cancer cells within the bone matrix with high linear energy transfer (*9,10*). $^{223}$Ra-$Cl_2$ decays through a complex decay series with alpha emission predominating. Additional beta and gamma emissions result in a total energy emitted of 28.2 MeV (*7,11*). Alpha emission energy for Ra-223 and its progeny ranges from 5 to 7.5 MeV (*11*). A soft tissue range of less than 100 μm for alpha particles limits toxicity to nontarget adjacent tissues. $^{223}$Ra-$Cl_2$ has a 11.4-day physical half-life (*7*). Imaging can be performed by gamma camera (either

**TABLE 2**
$^{89}$Sr-Chloride Radiation Absorbed Doses (*1*)

| Organ | mGy/MBq | rad/mCi |
|---|---|---|
| Bone surface | 17.0 | 63.0 |
| Red bone marrow | 11.0 | 40.7 |
| Lower bowel wall | 4.7 | 17.4 |
| Bladder wall | 1.3 | 4.8 |
| Testes | 0.8 | 2.9 |
| Ovaries | 0.8 | 2.9 |
| Uterine wall | 0.8 | 2.9 |
| Kidneys | 0.8 | 2.9 |

**TABLE 3**
$^{153}$Sm-Lexidronam Radiation Absorbed Doses (*6,34*)

| Organ | mGy/MBq | rad/mCi |
|---|---|---|
| Bone surface | 6.8 | 25.0 |
| Red bone marrow | 1.5 | 5.7 |
| Lower bowel wall | 0.01 | 0.04 |
| Bladder wall | 1.0 | 3.60 |
| Testes | 0.01 | 0.02 |
| Ovaries | 0.01 | 0.03 |
| Kidneys | 0.02 | 0.07 |

planar or single-photon emission computed tomography) through the detection of the ~84 keV X-rays (~40%), 154 keV gamma (5.79%), and 270 keV gamma (14%) from the parent $^{223}$Ra (*12*), although this is rarely performed. $^{223}$Ra-$Cl_2$ is administered through an intravenous injection as a weight-based scaling of injected activity of 55 kBq/kg (1.49 μCi/kg). $^{223}$Ra-$Cl_2$ is marketed as Xofigo and is usually given at 4-week intervals for 6 total injections, as tolerated (*11*). Radiation dosimetry is provided in Table 4.

4. Osteoblastic metastases

   Osteoblastic metastases are sites of increased radiotracer uptake demonstrated with bone scintigraphy secondary to active bone formation (*13*). Bone scintigraphy can detect an increase in focal osteoblastic activity caused by a metastasis to bone before it can be seen with anatomic imaging studies such as plain radiography or computed tomography (CT) (*14*).

5. Visceral metastases

   Visceral metastases are those to organs, such as the liver or lung, excluding osseous and lymph node metastases.

### B. Osseous Metastases

For all cancers, bone is the third most common site of metastasis, only outnumbered by lung and liver metastases. Breast and prostate cancer have a particular propensity to develop osseous metastases, in part owing to the indolent clinical course of some subtypes of these malignancies (*15*). The incidence of osseous metastases in prostate cancer increases with time, approaching 30% at 10 years (*16*). In the 10%-20% of patients who develop CRPC, ≥ 84% have osseous metastases at the time of diagnosis (*17*). Bone is also the most common site of metastasis in breast cancer (*18*), and the incidence of osseous metastases increases over time, with over 8% of patients developing osseous disease in 10 years (*16*). Nevertheless, osseous disease portends a poor prognosis and the associated pain affects quality of life (*19*).

Bone metastases are rarely solitary and prefer the axial to the appendicular skeleton, likely reflecting the distribution of hematopoietic red marrow (*15*). The development of metastases requires breaking of intercellular cohesion and tissue boundaries, circulation in blood or lymph, evasion of tumor-suppressing immune response, manipulation of the cellular microenvironment of the metastatic site, and angiogenesis to promote growth. Neoplastic cells migrating to the bone may remain dormant or quiescent for years, evading detection thresholds and treatment, only to activate and grow much later (*20*).

Osteoblastic metastases alter the regulation of the coupling of bone formation and reabsorption, allowing reactive bone mineral deposition to outpace lysis in the normal cycle of bone turnover. This process is not well understood and may vary in different cancer types (*21,22*). Osteoblastic metastases are typical of prostate cancer and can be seen in breast cancer (*15,22,23*).

Osteolytic metastases are typical of myeloma, renal cell carcinoma, non-small cell lung cancer, thyroid cancer, and non-Hodgkin lymphoma, among others (*15*). Although not a simple one-factor process, osteolysis is primarily due to misregulated osteoclast activity rather than direct destruction by growing tumor (*24*). Currently available radionuclide therapy agents target osteoblastic metastases, leaving purely osteolytic metastases outside the practice scope of this guideline.

Mixed blastic and lytic osseous metastases may be seen in gastrointestinal and squamous cell cancers, as well as in some breast cancers (*15*). Radionuclide therapy may be used for mixed blastic/lytic metastases, depending on symptoms, treatment alternatives, and the preponderance of a blastic over a lytic component. Technetium 99m-methylene diphosphonate ($^{99m}$Tc-MDP) or technetium 99m-hydroxymethylene diphosphonate ($^{99m}$Tc-HDP) bone scintigraphy should be used as a surrogate for the presence of osteoblastic uptake of bone-seeking therapeutic agents.

### C. Targeted Radionuclide Therapy of Osseous Metastases

Intravenous injection of $^{89}$Sr-chloride, $^{153}$Sm-EDTMP, and $^{223}$Ra-$Cl_2$ have been approved by the U.S. Food and Drug Administration (FDA) and the European Medicines Agency (EMA) for the treatment of bone pain resulting from osseous metastases. $^{89}$Sr-chloride and $^{153}$Sm-EDTMP are indicated for pain relief from bone metastases regardless of the primary malignancy (*5,6*); on-label use of $^{223}$Ra-$Cl_2$ is currently limited to patients with CRPC (*11*). Physicians involved in treating such patients should understand radiation safety, the pathophysiology and natural history of the disease process, the rationale for radionuclide therapy, and the limitations of radionuclide therapy. Treating physicians should collaborate closely with the other physicians and healthcare personnel involved in the overall management of metastatic disease.

The administration of these agents in the United States falls under the guidelines of the Nuclear Regulatory Commission (NRC), Title 10 CFR Part 35.300, or Agreement State Institutional License. Institutional licenses must specifically list individuals licensed to use Section 35.300 materials. In Europe, clinicians involved in treatment with radionuclide therapy must be aware of and compliant with all national and local legislation and regulations.

$^{32}$P-sodium phosphate was discussed in the prior version of this guideline; however, this treatment is not currently available in the United States. The discussion of $^{32}$P-sodium therapy for bone metastases has therefore been eliminated. $^{32}$P-sodium phosphate proved effective in treating pain from

**TABLE 4**
$^{223}$Ra-Dichloride Radiation Absorbed Doses (*11*)

| Organ | mGy/MBq | rad/mCi |
|---|---|---|
| Osteogenic cells | 1152 | 4263 |
| Red bone marrow | 139 | 514 |
| Lower large intestine wall | 46 | 172 |
| Colon | 38 | 142 |
| Upper large intestine wall | 32 | 120 |
| Urinary bladder wall | 4.0 | 15 |
| Kidneys | 3.2 | 12 |
| Testes | 0.08 | 0.31 |
| Ovaries | 0.49 | 1.8 |

osteoblastic metastases (*25*) and had several production advantages (*26*). However, bone marrow suppression from high-energy β-emission hampered widespread clinical acceptance (*26*), and commercial manufacturing was discontinued in 2009 (*27*).

Additional radiopharmaceuticals will be added to the guideline when they are approved by the FDA for the palliative treatment of painful bone metastases. Several radiopharmaceuticals approved in countries outside of the United States (e.g., $^{186}$Re-etidronate) are not discussed in this guideline. If new indications are added to the radionuclide therapies included here, these new indications will likewise be added to the discussion.

## III. INDICATIONS AND CLINICAL TRIAL EXPERIENCE

### A. $^{89}$Sr-chloride

$^{89}$Sr-chloride is a beta-emitting, bone-seeking radiopharmaceutical that localizes to foci of osteoblastic activity in a manner similar to calcium (*28*). $^{89}$Sr-chloride is indicated for relief of bone pain from osseous metastases (*29*). It is used for palliation of bone pain caused by osteoblastic or mixed osteoblastic lesions from any tumor that has abnormally increased focal osteoblastic activity as seen on bone scan.

A systematic review in 2005 of clinical trials of $^{89}$Sr-chloride reported a range of efficacy for relief of pain, with a mean overall response rate of 76% (32% of patients had a complete response and 44% had some response). A decrease in analgesic use was also seen. Efficacy has been demonstrated with repeat dosing. Pain relief with $^{89}$Sr-chloride began between 3 days and 4 weeks after administration, with relief lasting up to 15 months (*30*). Delayed and variable onset of relief limits the utility of $^{89}$Sr-chloride in patients with a short life expectancy and those in need of rapid relief.

A transient increase in pain or "flare" after therapy, usually within 72 hours (*1*), has been reported in up to 25% of patients. Although speculation exists that this may predict good clinical response, the available data do not demonstrate an association of flare with response (*31,32*). Transient variable hematologic side effects are the most common adverse event, with platelet count decreasing by ~30% and white cell count by up to 65%; these effects generally recover without intervention (*30*). $^{89}$Sr-chloride is not recommended in the presence of compromised bone marrow reserve. Bone scintigraphy may help assess the extent of marrow involvement; extensive osteoblastic activity may suggest compromised marrow reserve, necessitating careful attention to blood counts preceding and following therapy.

A phase II study of prostate cancer showed a survival benefit with the addition of $^{89}$Sr-chloride to doxorubicin compared with doxorubicin alone in patients with androgen-independent prostate cancer (*33*). No other data are available to support a potential survival advantage.

### B. $^{153}$Sm-lexidronam ($^{153}$Sm-EDTMP)

$^{153}$Sm-EDTMP is a beta-emitting radiopharmaceutical that localizes to bone and bony metastases in a manner similar to $^{99m}$Tc-MDP (*34*). $^{153}$Sm-EDTMP is indicated for pain relief in patients with osteoblastic metastases that demonstrate uptake on radionuclide bone scan (*6,29*).

Numerous clinical trials of $^{153}$Sm-EDTMP have demonstrated efficacy in relieving the pain of osseous metastases. Patients with prostate cancer have been most extensively studied, followed by patients with breast cancer and other cancers. Pain relief has been assessed through a variety of metrics, including patient and physician assessment and decreased opiate use. Response rates have varied, but consistently over 50% of patients have received some benefit (*35–38*). Relief was attained as early as 1 week with sustained responses seen at up to 4 months (*30*). A minority of patients (variable, but reported to be up to 31%-38%) had a marked response to therapy, including resolution of pain (*36,38*). Transient marrow toxicity, generally mild, was noted with a nadir at approximately 1 month and recovery by 2 months. No grade 4 toxicities or irreversible toxicities were observed (*35–38*).

A transient increase in pain after treatment, deemed "flare phenomenon," is seen in a small percentage of patients (up to 8% in the 1 mCi/kg group (*35,36*)). In a study of 152 men with prostate cancer, the same percentage of patients, 6%, experienced flare in the $^{153}$Sm-EDTMP treatment group as in the placebo groups (*38*).

Previously, concern was raised that combining bone-targeted therapies may decrease the effectiveness of pain palliation (*1*). However, more recent studies suggest possible synergy (*39*) in which $^{153}$Sm-EDTMP may be safely combined with bisphosphonate therapy. Bisphosphonates do not decrease uptake of $^{153}$Sm-EDTMP (*40–42*). A small study demonstrated a shorter time to pain relief after $^{153}$Sm-EDTMP when zoledronic acid was given 2 to 3 days prior to $^{153}$Sm-EDTMP compared with a week before or after therapy (*43*).

There is no convincing evidence of a survival benefit with $^{153}$Sm-EDTMP.

### C. $^{223}$Radium dichloride ($^{223}$Ra-$Cl_2$)

$^{223}$Ra-$Cl_2$ is an alpha particle-emitting calcium mimetic approved by the FDA and EMA, both in 2013, for CRPC with symptomatic bone metastases and no known visceral metastatic disease (*11*).

The phase III randomized, placebo-controlled Alpharadin in Symptomatic Prostate Cancer (ALSYMPCA) trial demonstrated a survival benefit of 3.6 months (median survival 14.9 months in the treatment arm compared with 11.3 months in the placebo arm in an updated analysis), independent of concurrent bisphosphonate use or prior docetaxel therapy. Moreover, the time to first symptomatic skeletal events was significantly longer in the treatment group than in the control group (15.6 vs. 9.8 months), and subjects in the treatment group had improved quality-of-life scores (*44,45*). Patients with a good baseline performance status and more than 6 osseous metastases, but without extensive confluent osteoblastic metastases (often called a "superscan") on pretreatment imaging, were more likely to achieve a survival benefit (*44*).

Although the ALSYMPCA trial excluded patients with lymph node metastases measuring greater than 3 cm in the short axis, and $^{223}Ra\text{-}Cl_2$ has not been validated in that population, such lymphadenopathy is not a contraindication on the FDA label. Similarly, although residual primary prostate malignancy is not an absolute contraindication to $^{223}Ra\text{-}Cl_2$, a trial of 44 $^{223}Ra\text{-}Cl_2$ patients observed a higher death rate in those with intact primary prostate masses than in those with radical prostatectomy (*46*). For both of these populations, we consider the occasional use of $^{223}Ra\text{-}Cl_2$ for palliation of painful bony metastases with the caveat that these patients may not achieve a survival benefit. In addition, although the label indication emphasizes palliation of bone pain and deemphasizes survival benefit, a recent trial of $^{223}Ra\text{-}Cl_2$ demonstrated that asymptomatic patients were more likely to complete treatment and had better overall survival, time to progression, and time to symptomatic skeletal event than did symptomatic patients (*47*), suggesting a beneficial role among asymptomatic patients and those with a smaller tumor burden.

The 2019 National Comprehensive Cancer Network (NCCN) guidelines for management of prostate cancer include $^{223}Ra\text{-}Cl_2$ among the options for systemic therapy for patients with symptomatic bone metastases and no visceral metastases, with category 1 or high-quality evidence supporting its use.

According to the NCCN guideline, $^{223}Ra\text{-}Cl_2$ may be considered as first-, second-, or subsequent-line therapy in this population (*48*). The optimal timing of $^{223}Ra\text{-}Cl_2$ relative to alternative therapies is not known. Within the heavily pretreated population of Expanded Access Programs (EAPs), patients with more advanced disease and pain tended to discontinue treatment early and had a shortened life expectancy (*49*). Conversely, $^{223}Ra\text{-}Cl_2$ in patients with fewer cycles of prior systemic therapy was associated with prolonged survival (*50*). It is unclear whether this indicates greater efficacy of $^{223}Ra\text{-}Cl_2$ earlier in the therapeutic algorithm, or that patients with progression through multiple systemic therapies simply have more advanced disease.

A group of practicing urologists and medical oncologists has argued that, as bone metastases most often precede visceral metastases in CRPC cases, there may be a window of eligibility for $^{223}Ra\text{-}Cl_2$ that favors use earlier in the disease course, perhaps as second-line therapy following advanced anti-androgen therapy, rather than as salvage therapy (*49*). For example, use of $^{223}Ra\text{-}Cl_2$ as second-line therapy following advanced anti-androgen therapy, rather than as salvage therapy, may capitalize on the window of opportunity; however, no trials have studied this directly. In ALSYMPCA, the survival benefit of $^{223}Ra\text{-}Cl_2$ was similar among those with or without prior docetaxel therapy (*51*). A secondary analysis of ALSYMPCA patients that evaluated outcomes of chemotherapy after $^{223}Ra\text{-}Cl_2$ (docetaxel in 70% of cases) found no difference in adverse effects or survival from the start of chemotherapy among $^{223}Ra\text{-}Cl_2$ vs. placebo arms (*52*). Patients receiving $^{223}Ra\text{-}Cl_2$ did initiate subsequent chemotherapy later than those receiving placebo, 3.8 vs. 2.6 months after completion of study treatment, in keeping with a possible progression-free survival benefit of $^{223}Ra\text{-}Cl_2$; however, the statistical significance of this 1.2-month difference was not reported. Overall survival following docetaxel therapy was similar by prior treatment with $^{223}Ra\text{-}Cl_2$ (16 months) vs. placebo (15.8 months)

Taken together, the available data indicate that $^{223}Ra\text{-}Cl_2$ is safe and effective either preceding or subsequent to systemic chemotherapy. Whether either timeline offers superior survival is unclear; however, earlier use of $^{223}Ra\text{-}Cl_2$ likely reduces the risk of losing eligibility because of the development of visceral metastases.

Whether $^{223}Ra\text{-}Cl_2$ can or should be used in combination with anti-androgen or chemotherapy is also unclear. Single-arm studies through EAPs suggested that combination therapy with abiraterone, enzalutamide, or denosumab was safe and may increase survival benefit by about 3 months over $^{223}Ra\text{-}Cl_2$ alone (*50,53*). However, the blinded, randomized, placebo-controlled ERA 223 trial of combination $^{223}Ra\text{-}Cl_2$ with abiraterone and prednisone/prednisolone raised doubts about the safety of combination therapy. The trial was unblinded prematurely because of an increased rate of fractures in the treatment arm and a nonsignificant trend for poorer survival in the treatment arm vs. the placebo arm (*54*). This prompted the EMA in 2018 to issue a formal warning, contraindicating the use of $^{223}Ra\text{-}Cl_2$ in combination with abiraterone plus these steroids (*55*). In addition, it has restricted the use of $^{223}Ra\text{-}Cl_2$ to metastatic CRPC (mCRPC), to be used only after 2 previous mCRPC treatments or when other treatments cannot be taken. Moreover, the FDA does not recommend $^{223}Ra\text{-}Cl_2$ in combination with abiraterone plus prednisone/prednisolone, citing increased fractures and mortality (*11*).

Notably, there was no appreciable difference in pathological fracture rates or progression of osseous metastases in ERA 223. The excess fractures were primarily fragility fractures at sites uninvolved by metastases. Accordingly, some experts have concluded that the excess fractures were not secondary to the combination of $^{223}Ra\text{-}Cl_2$ and abiraterone per se, but to the concomitant steroid course required to offset abiraterone's inhibition of glucocorticoid synthesis and maintain homeostasis in the adrenocorticotropic hormone-mineralocorticoid axis (*56*). Prednisone/prednisolone alters bone turnover and suppresses osteoblast differentiation and activity (*57*), and it may have an interactive effect with $^{223}Ra\text{-}Cl_2$, which suppresses alkaline phosphatase, a marker of osteoblast activity (*58,59*). Future trials may investigate the use of smaller steroid doses or alternative combinations not requiring steroids; for the time being, no combination therapy involving $^{223}Ra\text{-}Cl_2$ is proven safe or superior to monotherapy.

Currently, retreatment following completion of $^{223}Ra\text{-}Cl_2$ is not routine. A single-arm trial of repeat treatment of up to 6 additional injections of $^{223}Ra\text{-}Cl_2$ demonstrated no new

safety concerns or serious adverse events over up to 2 years of follow-up (*60*). Median overall survival was 24.4 months; no control arm was implemented to establish whether survival was prolonged by retreatment.

The approved indication for $^{223}Ra\text{-}Cl_2$ includes patients with prostate cancer only. $^{223}Ra\text{-}Cl_2$ has been studied in other malignancies in which investigators noted that the radiopharmaceutical localized to areas of bone turnover, not to the tumor itself. $^{223}Ra\text{-}Cl_2$ has been studied in breast cancer with several case reports (*61,62*) and early clinical trials in a variety of settings with encouraging results (*63,64*); additional trials are planned. Trials in different disease states in a variety of settings, including renal cell carcinoma, have also been reported (*65,66*)

*Summary.* In the United States, $^{223}Ra\text{-}Cl_2$ is indicated as first-, second-, or third-line/salvage treatment for patients with CRPC with osseous metastases and bone pain, but no visceral metastases. In Europe, the EMA has limited its approval to patients with mCRPC after 2 previous lines of treatment. $^{223}Ra\text{-}Cl_2$ confers a survival benefit of approximately 3 months in select populations. Current expert consensus regarding the timing of $^{223}Ra\text{-}Cl_2$ is that it should be used after progression through advanced anti-androgen therapy, but ideally early in the treatment course, as the prevalence of visceral metastases increases over time and would preclude $^{223}Ra\text{-}Cl_2$. Although studies are ongoing, there is no current role for combination therapy or retreatment with $^{223}Ra\text{-}Cl_2$. Residual primary disease and lymph node metastases $> 3$ cm do not absolutely contraindicate palliative use for symptomatic bone metastases, but likely reduce the survival benefit of $^{223}Ra\text{-}Cl_2$. Given the demonstrable survival benefit, and favorable effects on symptomatic skeletal events, $^{223}Ra\text{-}Cl_2$ should be considered a treatment of choice in select men with prostate cancer.

## IV. PROCEDURE

### A. Qualifications and Responsibilities of the Facility and Personnel

1. $^{89}$Sr-chloride, $^{153}$Sm-EDTMP, and $^{223}Ra\text{-}Cl_2$ may be administered only in a facility with a valid radioactive materials license incorporating NRC Section 35.300 or comparable Agreement State license in the United States, or an equivalent license in the European Union.
2. All administering physicians/staff (both the physician writing the prescription and the physician/staff injecting the therapy) must be listed on the NRC or Agreement State license or specifically designated under a broad license. A written directive must be signed by an authorized user prior to administration.
3. Patients should be seen in consultation with the administering/treating physician in collaboration with the physician assuming overall patient management. The physician directing the administration of the radionuclide therapy should participate in the care of the patient as part of the patient management team. Discussion with the patient regarding radiation safety after administration must be completed prior to administration (outpatient instructions covered below). Written informed consent should be obtained by the treating physician following a risk-benefit discussion with the patient.
4. Physicians should be aware of the wide variations that occur between jurisdictions with respect to who may administer radioisotope therapy (e.g., technologist vs. physician/authorized user).
5. The facility in which the treatment is performed must have proper radiation safety procedures, including waste disposal, handling of contamination of personal belongings, understanding what to do in case of a spill or variations during administration, etc.
6. Printed documentation regarding radiation safety should be available to patients at the time of therapy and discussed prior to therapy administration.

### B. Patient Preparation

1. Prior to administration of $^{89}$Sr-chloride, $^{153}$Sm-EDTMP, or $^{223}Ra\text{-}Cl_2$, the patient should have a recent radionuclide bone scan to demonstrate osteoblastic metastases (within 3 months is preferred, though a longer interval may be suitable in specific patient circumstances). In particular, radiotracer uptake at sites of painful metastases is important for expectation of pain relief. A bone scan must be used to verify that sclerotic lesions seen on radiograph or CT have increased radiotracer uptake, given the mechanism of radionuclide localization as discussed earlier; quiescent, treated metastases may remain sclerotic indefinitely. Similarly, osteolytic metastases seen on anatomic imaging should be further characterized with a bone scan, as increased uptake at such sites suggests utility in treating with $^{89}$Sr-chloride, $^{153}$Sm-EDTMP, or $^{223}Ra\text{-}Cl_2$. For $^{223}Ra\text{-}Cl_2$, CT of the thorax, abdomen, and pelvis should be obtained to exclude visceral disease, as discussed previously.
2. Bone scintigraphic abnormalities should be correlated with appropriate physical examination and anatomic imaging studies to evaluate for abnormalities that require attention prior to radionuclide treatment (e.g., lesions that may cause nerve/cord compression, lesions prone to pathologic fracture). In these cases, radionuclide therapies should be pursued only in conjunction with targeted therapy (local radiation or surgical treatment). Radionuclide therapies have no role in the treatment of acute presentations of these entities.
3. The presence of concomitant non-osseous abnormalities or other causes of pain may limit the extent of symptomatic relief of painful lesions from radionuclide therapy. Prior to therapy, clinicians should consider other sources of pain indicated by the patient's clinical history and physical examination.
4. Given the potential treatment myelotoxicity, clinicians should discontinue myelosuppressive chemotherapy in anticipation of $^{89}$Sr-chloride, $^{153}$Sm-EDTMP, or $^{223}Ra\text{-}Cl_2$ treatment (6-8 weeks for long-acting myelosuppressive chemotherapy and $\sim$4 weeks for other myelosuppressive chemotherapy), although there is a paucity of data in this area.
5. Concomitant treatment with $^{89}$Sr-chloride, $^{153}$Sm-EDTMP, or $^{223}Ra\text{-}Cl_2$ in patients being treated with external beam hemibody radiation should be considered with caution as data describing combined adverse effects are lacking. The potential for overlapping myelotoxicity from these treatments should be considered. In general, withholding external beam radiation for 2-4 weeks prior to radionuclide therapy is recommended. Following radionuclide therapy, withholding hemi-body radiation until blood counts have stabilized is advised.

6. Complete blood counts should be performed within 2 weeks prior to starting $^{89}$Sr-chloride, $^{153}$Sm-EDTMP, or $^{223}$Ra-$Cl_2$ therapy and for subsequent treatments with $^{223}$Ra-$Cl_2$.
   a. $^{89}$Sr
      Low blood counts are a relative contraindication. A complete blood count (CBC) should be obtained within 2 weeks prior to the start of therapy. The following thresholds should be considered prior to initiating therapy: hemoglobin (Hb) > 9 g/dL, white blood cell (WBC) count > 3,500/μL, platelet count > 100,000/μL. According to EANM guidelines, in select cases, more liberal thresholds of a platelet count > 60,000/μL and WBC count > 2,400/μL may be considered, provided coagulation tests exclude disseminated intravascular coagulation (DIC). Blood counts typically recover within months of treatment, either partially or completely, and should be monitored (*5,67*).
   b. $^{153}$Sm-EDTMP
      CBC should be obtained within 2 weeks prior to the start of therapy. The following thresholds should be considered prior to initiating therapy: platelet count > 60,000/μL (preferably >100,000/μL), WBC count > 2,400/μL (preferably >5,000/μL), absolute neutrophil count (ANC) > 2000/μL, Hb > 10 g/dL (*1*). Blood counts typically recover after treatment and should be monitored.
   c. $^{223}$Ra-$Cl_2$
      1. CBC should be obtained within 2 weeks prior to start of therapy. The following thresholds should be considered prior to initiating therapy: ANC ≥ 1.5 x $10^9$/L, platelet count ≥ 100 x $10^9$/L, Hb ≥ 10 g/dL.
      2. Prior to subsequent treatments, ANC should be confirmed as ≥ 1 x $10^9$/L and platelet count ≥ 50 x $10^9$/L (*11*).
7. Treatment with $^{223}$Ra-$Cl_2$ concomitantly with abiraterone plus steroids is contraindicated in the treatment of prostate cancer as described earlier, and the patient's medication list should be screened for such agents. There are no known contraindications to combining hormone therapy with $^{153}$Sm-EDTMP at this time. The patient's medication list may also be screened for bone health agents (e.g., denosumab or zoledronic acid) and referral may be made for consideration of such agents.
8. The approved indications for $^{89}$Sr-chloride, $^{153}$Sm-EDTMP, or $^{223}$Ra-$Cl_2$ stipulate symptomatic/painful bone metastases. $^{89}$Sr, $^{153}$Sm-EDTMP, and $^{223}$Ra-$Cl_2$ have demonstrated benefit in decreasing pain, with only $^{223}$Ra-$Cl_2$ having a survival benefit (*44*).
9. Active DIC may be a risk factor for severe thrombocytopenia after therapy (*68*). Appropriate testing for this condition is important if there is any doubt as to the cause of thrombocytopenia. Moreover, if laboratory values are thought to be in flux, repeat blood work should be performed to confirm adequate counts prior to treatment.
10. Renal excretion of $^{89}$Sr-chloride and $^{153}$Sm-EDTMP suggests caution in dosing patients with renal dysfunction. Hence, severe renal dysfunction (glomerular filtration rate < 30 mL/min) should preclude treatment with $^{89}$Sr-chloride or $^{153}$Sm-EDTMP (*6,69*). $^{223}$Ra-$Cl_2$ has only limited renal excretion. Dose adjustment is not necessary in patients with mild to moderate renal impairment (creatinine clearance < 60 mL/min). Limited data are available for patients with severe renal dysfunction (creatinine clearance < 30 mL/min) (*11*), although adequate renal function was an eligibility criterion for the ALSYMPCA trial (*44*).
11. Patients should remain well hydrated before, during, and after treatment, as $^{89}$Sr-chloride and $^{153}$Sm-EDTMP are renally excreted. Dehydration has also been observed in 3% of patients treated with $^{223}$Ra-$Cl_2$ (*11*). Patients do not need to fast before or after therapy.
12. $^{89}$Sr-chloride, $^{153}$Sm-EDTMP, and $^{223}$Ra-$Cl_2$ should be administered by slow intravenous injection over 1 minute. An indwelling catheter should be placed for radiopharmaceutical administration and patency should be assessed through visualization of blood return and flushing. A running intravenous line may help avoid subcutaneous infiltration. A 3-way stopcock may be used to flush the syringe containing the radiopharmaceutical.
13. Patients should not be treated as inpatients.
14. Pain relief from radionuclide therapy may begin within 1 to 4 weeks of treatment, with maximum response achieved later (*38,70*). A patient with a life expectancy of less than a month is unlikely to achieve full benefit of treatment. Given the survival benefit of $^{223}$Ra-$Cl_2$, a life expectancy of 6 months or longer is preferred prior to treatment. In addition, certain precautions at autopsy may be necessary with patients recently treated (reviewed in reference (*71*)). Cremation may also be affected.
15. Patients may be retreated with $^{89}$Sr-chloride and $^{153}$Sm-EDTMP if blood counts recover appropriately. $^{153}$Sm-EDTMP has been readministered as soon as 8 weeks after the preceding treatment (up to 3 total administrations) without an increase in adverse events and with continued palliative benefit (*72*). Data on the efficacy of repeated treatments are sparse, but cumulative toxicity has not been apparent (*73*). Potential retreatment with $^{223}$Ra-$Cl_2$, as discussed earlier, is not currently approved.

### C. Information Pertinent to Performing the Procedure

1. Patient demographics (age, sex, weight, diagnosis).
2. Indications for therapy.
3. Current medications, especially hormonal or chemotherapy, or those affecting coagulation.
4. Extent of disease on bone scan obtained prior to initial therapy.
5. CBC and basic metabolic panel within 1-2 weeks prior to therapy.
6. Relevant radiographs or magnetic resonance imaging (MRI) of painful sites to exclude cord compression or lesions with an increased risk of pathologic fracture should be considered prior to initial treatment. CT imaging should be obtained prior to initial $^{223}$Ra-$Cl_2$ therapy to evaluate for extraosseous metastases.
7. Life expectancy estimate.
8. Performance and pain status.
9. Pregnancy and breastfeeding are absolute contraindications to therapy with bone-seeking radionuclides.

### D. Instructions for Patients

1. The following information should be discussed with patients prior to $^{89}$Sr-chloride treatment:
   a. $^{89}$Sr-chloride has a greater than 50% probability of achieving some element of pain relief. The chance of relieving pain completely for some period of time is real (*30*).
   b. $^{89}$Sr-chloride is not a curative treatment for cancer, but a palliative treatment to relieve pain. No survival benefit has been demonstrated. Radionuclide therapy could theoretically cause a secondary cancer to develop; however, this is

very unlikely for patients receiving $^{89}$Sr-chloride for metastatic prostate cancer.

c. Mild and transient/reversible side effects include the following (*30*):
   i. Pain flare (~15%) 1 to 5 days after treatment, lasting up to 4 days. Pain relief may be obtained by increasing analgesia dose, if required.
   ii. Variable decrease in platelet and WBC counts, which most often normalize without intervention. A decrease in platelet and WBC counts can increase the risk of bleeding and infection, respectively. If unusual bleeding is noted, or there are signs of infection such as fever, patients should contact their doctor immediately.

d. For 2 weeks, patients should follow radiation safety precautions:
   i. Urinate while sitting and flush twice. Spilled urine should be cleaned up.
   ii. Wash hands thoroughly with soap and water after using the toilet.
   iii. Don gown and gloves when cleaning spilled body waste.
   iv. Wash soiled sheets and clothing immediately and separately from other clothes.
   v. For incontinent patients, urinary catheterization should be performed.

e. Pregnancy should be avoided for 6 months following treatment (*67*).

2. The following information should be discussed with patients prior to $^{153}$Sm-EDTMP treatment:
   a. $^{153}$Sm-EDTMP has a greater than 50% probability of achieving some element of pain relief. The chance of relieving pain completely for some period of time is real (*30,69*). Pain reduction is not immediate, and a "flare" is possible (*30*).
   b. This is not a curative treatment for cancer, but a treatment to palliate pain and no survival benefit has been demonstrated.
   c. The following are potential side effects:
      i. Nausea/vomiting (~33% estimate) (*69*).
      ii. Weakness, constipation, anorexia (≤10%) (*69*).
      iii. Pain flare (12%-20%, depending on the study (*30*)), most often within 72 hours of injection (*6*). Pain relief may be obtained by increasing analgesia dose, if required.
      iv. Transient myelosuppression is common, with platelet and WBC counts attaining a nadir at approximately 1 month after administration. The vast majority of blood counts recover to baseline values (*69*). A decrease in platelet and WBC counts can increase the risk of bleeding and infection, respectively. If unusual bleeding is noted, or there are signs of infection such as fever, patients should contact their doctor immediately.
      v. Radionuclide therapy could theoretically cause a secondary cancer to develop.
   d. For 2 days after therapy, the following radiation safety precautions should be followed. $^{153}$Sm-EDTMP can be excreted in the urine for up to 12 hours after therapy.
      i. Urinate while sitting and flush twice. Spilled urine should be cleaned up.
      ii. Wash hands thoroughly with soap and water after using the toilet.
      iii. Don gown and gloves when cleaning spilled body waste.
      iv. Do not have sexual intercourse for 2 days. An effective method of contraception should be used after receiving $^{153}$Sm-EDTMP (*6*). Pregnancy should be avoided for 6 months following treatment (*67*).
      v. Wash soiled sheets separately from other clothes or store for 1-2 weeks to allow for radioactive decay.
      vi. For incontinent patients, urinary catheterization should be performed.

3. The following information should be discussed with patients prior to $^{223}$Ra-$Cl_2$ treatment.
   a. Patients receiving $^{223}$Ra-$Cl_2$ have an approximately 60% chance of pain reduction (*74,75*) and may benefit from an extension of life expectancy by approximately 3-4 months (*44*). Patients may also see a delay in bone-related complications such as pathologic fracture.
   b. Early side effects may include the following:
      i. Nausea (38%)
      ii. Diarrhea (27%)
      iii. Vomiting (21%)
      iv. Peripheral edema (15%)
      v. Renal impairment (4%)
      vi. Dehydration (3%)
      vii. Injection site reactions (1%)
      viii. These are usually mild and self-limited but may be more severe in <5% of patients.
   c. Late side effects include the following:
      i. Anemia is common, and affected 90% or more of patients receiving $^{223}$Ra-$Cl_2$ and their control group receiving placebo in the largest clinical trial. This was usually mild and self-limited, but more severe in 6% of both treatment and placebo groups. Anemia may cause light-headedness, racing heartbeat, or fatigue and is most likely due to disease progression.
      ii. Lymphocytopenia affected up to 92% of treated patients in a trial and was moderate to severe in 20%. Neutropenia affected 20%. These conditions were usually self-limited, and although they could increase infection risk, the rate of infections was not different between treatment and placebo groups in the ALSYMPCA trial.
      iii. Low platelets affected 34% of patients, increasing the risk of bleeding. This was usually mild and self-limited.
      iv. Bone marrow failure resulting in pancytopenia is estimated to affect 2% of patients.
      v. Radionuclide therapy could theoretically cause a secondary cancer to develop. Available data are insufficient to estimate this risk precisely; it is likely less than 1% and usually takes years to occur. This is unlikely to affect the length or quality of life of patients with mCRPC.
   d. Radiation safety precautions include the following:
      i. For 2 days, use a separate bathroom when possible. Wipe yourself dry to avoid contaminating clothing. Wipe toilet seat with dampened toilet paper after use and throw in toilet to dispose.
      ii. For 1 week after each treatment, sit when voiding and avoid using a urinal. Flush the toilet twice and close the lid prior to flushing.
      iii. Follow good hygiene practices and wash hands thoroughly after voiding while receiving treatment and for 1 week after final treatment. Use of your own towel is advised. If you are incontinent, gloves should be worn when handling pads; hands should be washed thoroughly afterward.

iv. Clothing soiled with urine or fecal material should be washed promptly and separately from other clothing.
v. Your caregivers should use universal precautions when handling bodily fluids or handling materials contaminated with bodily fluids. This includes use of disposable gloves and barrier gowns. Caregivers should wash their hands thoroughly with soap and water after providing care.
vi. If sexually active, a condom should be used while receiving treatment and for 1 month after the last treatment. Do not father a child while receiving treatment or for at least 6 months after the last treatment. A female partner who can have children must use highly effective birth control.

e. Patients should stay well-hydrated while undergoing therapy. For 2 days, drinking 8 glasses of water or other nonalcoholic beverage per day is advised.

4. The following instructions pertain to $^{89}$Sr, $^{153}$Sm-EDTMP, and $^{223}$Ra-$Cl_2$ treatment.
   a. A written consent form is strongly suggested and should include indications, expected outcomes, risks (including infection, bleeding, and death), and alternatives to treatment. Local hospital policies and state regulations should be followed.
   b. All questions should be answered prior to therapy.
   c. Expected follow-up should be reiterated to patients, including laboratory tests and clinic visits. A contact phone number should be given in the event that patients need to discuss their care with a treating physician.
   d. Patients should be provided with written outpatient instructions.
   e. Patients may continue a normal diet.
   f. Patients should be advised to contact their health care provider if they have any of the following signs or symptoms: temperature 100.4°F (38°F) or higher; chills; difficulty urinating; diarrhea, nausea, or vomiting; pain not relieved by medication; bruising; blood in urine, semen, or stool; shortness of breath; lethargy; swelling of extremities.

#### E. Precautions

1. The degree of leukopenia and thrombocytopenia present should not be severe, as noted earlier. CBCs should be obtained as detailed earlier. Disseminated, confluent disease in the bones as seen on a bone scan (often referred to as a "superscan") indicates higher risk of bone marrow involvement.
2. Renal failure may require a reduction in the activity injected; no definite guidelines are available for specific recommendations.
3. Previous (especially recent) chemotherapy or wide-field radiation may decrease marrow reserve and possibly lead to treatment-induced leukopenia or thrombocytopenia.
4. Exclude spinal cord compression or soft-tissue tumor as the cause of the pain that is being treated. Lesions with a Mirel's score $\geq 8$ may be referred for orthopedic evaluation for appropriateness of prophylactic fixation prior to therapy (*76*).
5. A careful injection technique must be used to avoid infiltration. No specific therapy is available if infiltration occurs, but local heat may increase the rate of reabsorption and therefore decrease the local radiation dose.
6. DIC should be excluded prior to treatment.
7. In women of childbearing potential, a pregnancy test within 2 days prior to treatment must have a negative result.
8. Patient and caregivers should be educated on radiation safety precautions and how to minimize contamination. Written instructions should also be provided.

#### F. Radiopharmaceuticals

1. $^{89}$Sr-chloride
   Recommended activity of 148 MBq. Alternatively, 1.5-2.2 MBq/kg body weight (*5*).
2. $^{153}$Sm-EDTMP
   Recommended activity of 37 MBq/kg (1.0 mCi/kg).
3. $^{223}$Ra-$Cl_2$
   Recommended activity of 55 kBq/kg body weight administered every 4 weeks for 6 total injections.

#### G. Guidelines for Measuring the Activity

Both $^{153}$Sm-EDTMP and $^{223}$Ra-$Cl_2$ should be measured in a properly calibrated radioisotope dose calibrator (activity calibrator). The residual activity in the syringe must be measured to know the precise activity administered.

#### H. Interventions

Not applicable.

#### I. Processing

Not applicable.

#### J. Interpretation Criteria

$^{153}$Sm-EDTMP and $^{223}$Ra-$Cl_2$ are not routinely imaged after treatment, but both have gamma emissions that could be imaged. Some centers acquire images regularly and dosimetry applications have been proposed and published for $^{153}$Sm-EDTMP and $^{223}$Ra-$Cl_2$ (*77–81*).

#### K. Reporting

After treatment, a report should be generated that includes the following items:

1. History and indication.
2. Correlative imaging (e.g., bone scan, radiographs, CT, positron emission tomography (PET)/CT) that was reviewed.
3. That informed consent was obtained and the patient was aware of the major associated risks, including leukopenia and thrombocytopenia. Pretherapy blood counts and date may be mentioned. The need for blood monitoring should be mentioned, as described earlier. The delay in pain reduction (1-3 weeks) and possibility of a pain flare may also be mentioned.
4. A sentence stating that all patient questions were answered to the patient's apparent satisfaction prior to therapy.
5. A record of the activity administered.
6. The status of the patient prior to leaving the department (e.g., the patient left the department in stable condition).
7. For multiple treatments, the number of the current treatment and total planned treatments should be mentioned (e.g., This was the $X^{th}$ of 6 planned $^{223}$Ra-$Cl_2$ treatments).

#### L. Follow-up

1. Follow-up can be performed either by the treating nuclear medicine physician (preferred) or the referring physician (e.g., urologist, oncologist). If the nuclear medicine physician will not be following the patient, it should be confirmed that the patient

will receive adequate follow-up elsewhere before leaving the treating facility.

2. $^{89}$Sr

   Monitor blood counts at least bimonthly, continuing until recovery, noting the recovery may take greater than 3 months (*82*).

3. $^{153}$Sm-EDTMP

   Weekly CBC starting 2 weeks after therapy and continuing for 8 weeks or until recovery from nadir is achieved.

4. $^{223}$Ra-$Cl_2$

   a. CBC should be repeated within 2 weeks prior to the next scheduled treatment. Treatment may continue if the following laboratory values are met: ANC $\geq 1 \times 10^9$/L and platelet count $\geq 50 \times 10^9$/L. If these laboratory values do not normalize within 6-8 weeks, future treatments are generally discontinued. Blood counts should be monitored after completion of therapy until recovery as well. Supportive care—including colony-stimulating factor administration—may be considered if clinically indicated.

   b. If the patient's general condition deteriorates significantly (decrease in Karnofsky index to <50% or increase in Eastern Clinical Oncology Group [ECOG] performance status to > 2), additional imaging may be appropriate (e.g., bone scan, PET/CT, CT, MRI). In the event of clear progression (appearance of new metastases), treatment should be continued only after careful risk-benefit assessment.

   c. Monitoring of common biomarkers (e.g., prostate-specific antigen [PSA], lactate dehydrogenase, C-reactive protein, alkaline phosphatase) after several cycles (e.g., before the fourth therapy cycle) is preferable. However, fluctuations of biomarkers are not uncommon during therapy. Increasing biomarkers do not necessarily represent a lack of therapy response. There is growing evidence that alkaline phosphatase can better predict response compared with PSA (*74*). A comparison with findings from imaging (e.g., bone scan, PET/CT, CT, MRI) is advisable in order to objectify increasing biomarkers. In the event of clear disease progression (appearance of new metastases), the treatment should be continued only after careful risk-benefit assessment.

   d. Continued monitoring of common biomarkers after therapy should depend on the duration of the disease, tumor biology, and previous course (if biomarkers were increased pretherapeutically). Common intervals are 3 to 6 months at the beginning and yearly thereafter.

   e. Timing of follow-up imaging (e.g., bone scan, PET/CT, PET/MRI) should depend on symptoms, duration of illness, and tumor biology. Imaging should be performed 3-6 months after the last treatment, or earlier as symptoms dictate. Patients should be advised that anatomic improvement on imaging takes time and that reactive osseous remodeling may lead to new sclerosis on CT.

#### M. Quality Control

1. The Institutional Quality Management Program mandated by the NRC should be followed. In Europe, similar programs are required for implementation by the EU Basic Safety Standards Directive.
2. Close communication and coordination between the referring physicians and treating physicians is recommended in all aspects of patient workup, treatment, and follow-up. Multidisciplinary conferences may be used to facilitate in-depth discussion.
3. Relevant patient information should be reviewed prior to treatment.

#### N. Sources of Error

1. Improper use of the dose calibrator: The activity must be measured in a geometry and a container consistent with previous calibration of the dose calibrator.
2. The radiopharmaceutical should be injected though an intravenous line, as described, with proper radiation precautions and with adequate flushing of the administered activity.

#### O. Future Outlook

Treatment of bone pain with radionuclide therapy has the potential to improve the quality of life of patients with osseous metastases. Treatment with $^{89}$Sr-chrloride, $^{153}$Sm-EDTMP, and $^{223}$Ra-$Cl_2$ has a proven role for patients, the latter approved only for metastatic prostate cancer and the only agent with a demonstrable but small survival benefit. The integration of these therapies into clinical care should continue to evolve as experience and research efforts continue. New agents will also become available in the future. Most notably, $^{177}$Lu-prostate-specific membrane antigen radionuclide therapy for mCRPC has demonstrated encouraging results for efficacy and partly for bone pain palliation with a favorable safety profile (*83,84*). This agent has recently been granted FDA approval. Compared with the bone-seeking agents described herein, new oncotropic therapies with specific tumor targeting may offer greater benefit in patients with bone metastases. New agents and expanded indications for current agents should continue to improve and expand the treatment armamentarium.

## V. LIABILITY STATEMENT

This guideline summarizes the views of the EANM Bone & Joint Committee, the EANM Dosimetry Committee, the EANM Radiation Protection Committee, and the SNMMI. It reflects recommendations for which the EANM cannot be held responsible. The recommendations should be taken in the context of good practice of nuclear medicine and do not substitute for national and international legal or regulatory provisions.

## VI. DISCLOSURE

ARP reports consulting activities for GE, Blue Earth Diagnostics Ltd., and Progenics and institutional research support from Progenics – all outside the submitted work. ME reports prior consulting activities for Blue Earth Diagnostics Ltd., Novartis, Telix, Progenics, Bayer, Point Biopharma, and Janssen and a patent application for rhPSMA – all outside the submitted work. DDB has no conflicts of interest to disclose. ATK has no conflicts of interest to disclose. RL has no conflicts of interest to disclose. IR has no conflicts of interest to disclose. EBS has no conflicts of interest to disclose. MPT has no conflicts of interest to disclose.

## VII. ACKNOWLEDGEMENTS

The guidelines were brought to the attention of the relevant EANM Committees and the National Societies of Nuclear Medicine. The comments and suggestions from the EANM Bone & Joint Committee, the EANM Dosimetry Committee, the EANM Radiation Protection Committee, and the SNMMI are highly appreciated and have been considered for this guideline.

## REFERENCES

1. Silberstein EB, Buscombe JR, McEwan A, Taylor A Jr. Society of Nuclear Medicine procedure guideline for palliative treatment of painful bone metastases. *Society of Nuclear Medicine Procedure Guidelines Manual.* 2003;3:147-153.
2. Cipriani C, Atzei G, Argiro G, et al. Gamma camera imaging of osseous metastatic lesions by strontium-89 bremsstrahlung. *Eur J Nucl Med.* 1997;24:1356-1361.
3. Narita H, Hirase K, Uchiyama M, Fukushi M. New knowledge about the bremsstrahlung image of strontium-89 with the scintillation camera. *Ann Nucl Med.* 2012;26:603-607.
4. Goyal J, Antonarakis ES. Bone-targeting radiopharmaceuticals for the treatment of prostate cancer with bone metastases. *Cancer Lett.* 2012;323:135-146.
5. Strontium chloride Sr-89 injection, USP. Package insert. Q BioMed; January 2020. Accessed April 16, 2020. https://strontium89.wpengine.com/wp-content/uploads/2021/02/Sr89-Chloride-Injection-Packaging-Insert_021120.pdf
6. Quadramet (samarium-153 lexidronam). Package insert. Lantheus Medical Imaging. U.S. Food and Drug Administration website. Revised September 2017. Accessed October 9, 2019. https://www.accessdata.fda.gov/drugsatfda_docs/label/2017/020570s008lbl.pdf
7. Dauer LT, Williamson MJ, Humm J, et al. Radiation safety considerations for the use of 223RaCl2 DE in men with castration-resistant prostate cancer. *Health Phys.* 2014;106:494.
8. Deshayes E, Roumiguie M, Thibault C, et al. Radium 223 dichloride for prostate cancer treatment. *Drug Des Devel Ther.* 2017;11:2643-2651.
9. Henriksen G, Breistol K, Bruland OS, Fodstad O, Larsen RH. Significant antitumor effect from bone-seeking, alpha-particle-emitting (223)Ra demonstrated in an experimental skeletal metastases model. *Cancer Res.* 2002;62:3120-3125.
10. Henriksen G, Fisher DR, Roeske JC, Bruland OS, Larsen RH. Targeting of osseous sites with alpha-emitting 223Ra: comparison with the beta-emitter 89Sr in mice. *J Nucl Med.* 2003;44:252-259.
11. Xofigo (radium Ra 223 dichloride). Package insert. Bayer Healthcare. U.S. Food and Drug Administration website. Revised December 2019. Accessed November 9, 2021. https://www.accessdata.fda.gov/drugsatfda_docs/label/2019/203971s016lbl.pdf
12. Benabdallah N, Bernardini M, Bianciardi M, de Labriolle-Vaylet C, Franck D, Desbrée A. $^{223}$Ra-dichloride therapy of bone metastasis: optimization of SPECT images for quantification. *EJNMMI Res.* 2019;9:20.
13. Roodman GD. Mechanisms of bone metastasis. *N Engl J Med.* 2004;350:1655-1664.
14. Love C, Din AS, Tomas MB, Kalapparambath TP, Palestro CJ. Radionuclide bone imaging: an illustrative review. *Radiographics.* 2003;23:341-358.
15. Macedo F, Ladeira K, Pinho F, et al. Bone metastases: an overview. *Oncol Rev.* 2017;11:321.
16. Hernandez RK, Wade SW, Reich A, Pirolli M, Liede A, Lyman GH. Incidence of bone metastases in patients with solid tumors: analysis of oncology electronic medical records in the United States. *BMC Cancer.* 2018;18:44.
17. Kirby M, Hirst C, Crawford ED. Characterising the castration-resistant prostate cancer population: a systematic review. *Int J Clin Pract.* 2011;65:1180-1192.
18. Solomayer EF, Diel IJ, Meyberg GC, Gollan C, Bastert G. Metastatic breast cancer: clinical course, prognosis and therapy related to the first site of metastasis. *Breast Cancer Res Treat.* 2000;59:271-278.
19. Selvaggi G, Scagliotti GV. Management of bone metastases in cancer: a review. *Crit Rev Oncol Hematol.* 2005;56:365-378.
20. Chambers AF, Naumov GN, Varghese HJ, Nadkarni KV, MacDonald IC, Groom AC. Critical steps in hematogenous metastasis: an overview. *Surg Oncol Clin N Am.* 2001;10:243-255, vii.
21. Coleman RE. Metastatic bone disease: clinical features, pathophysiology and treatment strategies. *Cancer Treat Rev.* 2001;27:165-176.
22. Keller ET, Zhang J, Cooper CR, et al. Prostate carcinoma skeletal metastases: cross-talk between tumor and bone. *Cancer Metastasis Rev.* 2001;20:333-349.
23. Cook GJ, Houston S, Rubens R, Maisey MN, Fogelman I. Detection of bone metastases in breast cancer by 18FDG PET: differing metabolic activity in osteoblastic and osteolytic lesions. *J Clin Oncol.* 1998;16:3375-3379.
24. Taube T, Elomaa I, Blomqvist C, Beneton MN, Kanis JA. Histomorphometric evidence for osteoclast-mediated bone resorption in metastatic breast cancer. *Bone.* 1994;15:161-166.
25. Silberstein EB. The treatment of painful osseous metastases with phosphorus-32-labeled phosphates. *Semin Oncol.* 1993;20:10-21.
26. Das T, Banerjee S. Radiopharmaceuticals for metastatic bone pain palliation: available options in the clinical domain and their comparisons. *Clin Exp Metastasis.* 2017;34:1-10.
27. Haynes E. Phosphocol P 32 chromic phosphate and sodium phosphate P 32 solution product discontinuations. Written communication. 2009. http://www.radiopharmaceuticals.info/uploads/7/6/8/7/76874929/p-32_discontinuation_letter.pdf
28. Robinson RG, Blake GM, Preston DF, et al. Strontium-89: treatment results and kinetics in patients with painful metastatic prostate and breast cancer in bone. *Radiographics.* 1989;9:271-281.
29. Autio KA, Scher HI, Morris MJ. Therapeutic strategies for bone metastases and their clinical sequelae in prostate cancer. *Curr Treat Options Oncol.* 2012;13:174-188.
30. Finlay IG, Mason MD, Shelley M. Radioisotopes for the palliation of metastatic bone cancer: a systematic review. *Lancet Oncol.* 2005;6:392-400.
31. Kraeber-Bodere F, Campion L, Rousseau C, Bourdin S, Chatal JF, Resche I. Treatment of bone metastases of prostate cancer with strontium-89 chloride: efficacy in relation to the degree of bone involvement. *Eur J Nucl Med.* 2000;27:1487-1493.
32. Zenda S, Nakagami Y, Toshima M, et al. Strontium-89 (Sr-89) chloride in the treatment of various cancer patients with multiple bone metastases. *Int J Clin Oncol.* 2014;19:739-743.
33. Tu SM, Millikan RE, Mengistu B, et al. Bone-targeted therapy for advanced androgen-independent carcinoma of the prostate: a randomised phase II trial. *Lancet.* 2001;357:336-341.
34. Eary JF, Collins C, Stabin M, et al. Samarium-153-EDTMP biodistribution and dosimetry estimation. *J Nucl Med.* 1993;34:1031-1036.
35. Resche I, Chatal J-F, Pecking A, et al. A dose-controlled study of 153Sm-ethylenediaminetetramethylenephosphonate (EDTMP) in the treatment of patients with painful bone metastases. *Eur J Cancer.* 1997;33:1583-1591.
36. Serafini AN, Houston SJ, Resche I, et al. Palliation of pain associated with metastatic bone cancer using samarium-153 lexidronam: a double-blind placebo-controlled clinical trial. *J Clin Oncol.* 1998;16:1574-1581.
37. Tian J-h, Zhang J-m, Hou Q-t, et al. Multicentre trial on the efficacy and toxicity of single-dose samarium-153-ethylene diamine tetramethylene phosphonate as a palliative treatment for painful skeletal metastases in China. *Eur J Nucl Med.* 1999;26:2-7.
38. Sartor O, Reid RH, Hoskin PJ, et al. Samarium-153-Lexidronam complex for treatment of painful bone metastases in hormone-refractory prostate cancer. *Urology.* 2004;63:940-945.
39. Vassiliou V, Bruland O, Janjan N, Lutz S, Kardamakis D, Hoskin P. Combining systemic bisphosphonates with palliative external beam radiotherapy or bone-targeted radionuclide therapy: interactions and effectiveness. *Clin Oncol (R Coll Radiol).* 2009;21:665-667.
40. Lam MG, Dahmane A, Stevens WH, van Rijk PP, de Klerk JM, Zonnenberg BA. Combined use of zoledronic acid and 153Sm-EDTMP in hormone-refractory prostate cancer patients with bone metastases. *Eur J Nucl Med Mol Imaging.* 2008;35:756-765.
41. Waldert M, Klatte T, Remzi M, Sinzinger H, Kratzik C. Is $^{153}$-Samarium-ethylenediamine-tetramethyl-phosphonate (EDTMP) bone uptake influenced by bisphosphonates in patients with castration-resistant prostate cancer? *World J Urol.* 2012;30:233-237.
42. Marcus CS, Saeed S, Mlikotic A, et al. Lack of effect of a bisphosphonate (pamidronate disodium) infusion on subsequent skeletal uptake of Sm-153 EDTMP. *Clin Nucl Med.* 2002;27:427-430.
43. Rasulova N, Lyubshin V, Arybzhanov D, Sagdullaev S, Krylov V, Khodjibekov M. Optimal timing of bisphosphonate administration in combination with samarium-153 oxabifore in the treatment of painful metastatic bone disease. *World J Nucl Med.* 2013;12:14-18.
44. Parker C, Nilsson S, Heinrich D, et al. Alpha emitter radium-223 and survival in metastatic prostate cancer. *N Engl J Med.* 2013;369:213-223.
45. Sartor O, Coleman R, Nilsson S, et al. Effect of radium-223 dichloride on symptomatic skeletal events in patients with castration-resistant prostate cancer and bone metastases: results from a phase 3, double-blind, randomised trial. *Lancet Oncol.* 2014;15:738-746.
46. Serretta V, Valerio MR, Costa R, et al. Radium-223 treatment in castration resistant bone metastatic prostate cancer. Should be the primary tumor always treated? *Urol Oncol.* 2019;37:964-969.
47. Heidenreich A, Gillessen S, Heinrich D, et al. Radium-223 in asymptomatic patients with castration-resistant prostate cancer and bone metastases treated in an international early access program. *BMC Cancer.* 2019;19:12.

48. Mohler JL, Antonarakis ES, Armstrong AJ, et al. Prostate cancer, Version 2.2019, NCCN clinical practice guidelines in oncology. *J Natl Compr Canc Netw.* 2019; 17:479-505.
49. Heinrich D, Bektic J, Bergman AM, et al. The contemporary use of radium-223 in metastatic castration-resistant prostate cancer. *Clin Genitourin Cancer.* 2018;16: E223-231.
50. Sartor O, Vogelzang NJ, Sweeney C, et al. Radium-223 safety, efficacy, and concurrent use with abiraterone or enzalutamide: first U.S. experience from an expanded access program. *Oncologist.* 2018;23:193-202.
51. Hoskin P, Sartor O, O'Sullivan JM, et al. Efficacy and safety of radium-223 dichloride in patients with castration-resistant prostate cancer and symptomatic bone metastases, with or without previous docetaxel use: a prespecified subgroup analysis from the randomised, double-blind, phase 3 ALSYMPCA trial. *Lancet Oncol.* 2014;15:1397-1406.
52. Sartor O, Hoskin P, Coleman RE, et al. Chemotherapy following radium-223 dichloride treatment in ALSYMPCA. *Prostate.* 2016;76:905-916.
53. Saad F, Carles J, Gillessen S, et al. Radium-223 and concomitant therapies in patients with metastatic castration-resistant prostate cancer: an international, early access, open-label, single-arm phase 3b trial. *Lancet Oncol.* 2016;17:1306-1316.
54. Smith M, Parker C, Saad F, et al. Addition of radium-223 to abiraterone acetate and prednisone or prednisolone in patients with castration-resistant prostate cancer and bone metastases (ERA 223): a randomised, double-blind, placebo-controlled, phase 3 trial. *Lancet Oncol.* 2019;20:408-419.
55. Gourd E. EMA guidance on radium-223 dichloride in prostate cancer. *Lancet Oncol.* 2018;19:e190.
56. Dalla Volta A, Formenti AM, Berruti A. Higher risk of fragility fractures in prostate cancer patients treated with combined radium-223 and abiraterone: prednisone may be the culprit. *Eur Urol.* 2019;75:894-895.
57. Hardy RS, Zhou H, Seibel MJ, Cooper MS. Glucocorticoids and bone: consequences of endogenous and exogenous excess and replacement therapy. *Endocr Rev.* 2018;39:519-548.
58. Parker CC, Pascoe S, Chodacki A, et al. A randomized, double-blind, dose-finding, multicenter, phase 2 study of radium chloride (Ra 223) in patients with bone metastases and castration-resistant prostate cancer. *Eur Urol.* 2013;63:189-197.
59. Nilsson S, Franzen L, Parker C, et al. Bone-targeted radium-223 in symptomatic, hormone-refractory prostate cancer: a randomised, multicentre, placebo-controlled phase II study. *Lancet Oncol.* 2007;8:587-594.
60. Sartor O, Heinrich D, Mariados N, et al. Re-treatment with radium-223: 2-year follow-up from an international, open-label, phase 1/2 study in patients with castration-resistant prostate cancer and bone metastases. *Prostate.* 2019;79: 1683-1691.
61. Takalkar A, Paryani B, Adams S, Subbiah V. Radium-223 dichloride therapy in breast cancer with osseous metastases. *BMJ Case Rep.* 2015;2015:bcr2015211152.
62. Costa RP, Tripoli V, Princiotta A, et al. Therapeutic effect of RA223 in the management of breast cancer bone metastases. *Clin Ter.* 2019;170:e1-e3.
63. Coleman R, Aksnes AK, Naume B, et al. A phase IIa, nonrandomized study of radium-223 dichloride in advanced breast cancer patients with bone-dominant disease. *Breast Cancer Res Treat.* 2014;145:411-418.
64. Ueno NT, Tahara RK, Saigal B, et al. Phase II study of Ra-223 combined with hormonal therapy and denosumab for treatment of hormone receptor-positive breast cancer with bone-dominant metastasis. *J Clin Oncol.* 2018;36:1065-1065.
65. McKay RR, Bosse D, Gray KP, et al. Radium-223 dichloride in combination with vascular endothelial growth factor-targeting therapy in advanced renal cell carcinoma with bone metastases. *Clin Cancer Res.* 2018;24:4081-4088.
66. Geva R, Lopez J, Danson S, et al. Radium-223 in combination with paclitaxel in cancer patients with bone metastases: safety results from an open-label, multicenter phase Ib study. *Eur J Nucl Med Mol Imaging.* 2019;46:1092-1101.
67. Handkiewicz-Junak D, Poeppel TD, Bodei L, et al. EANM guidelines for radionuclide therapy of bone metastases with beta-emitting radionuclides. *Eur J Nucl Med Mol Imaging.* 2018;45:846-859.
68. Leong C, McKenzie MR, Coupland DB, Gascoyne RD. Disseminated intravascular coagulation in a patient with metastatic prostate cancer: fatal outcome following strontium-89 therapy. *J Nucl Med.* 1994;35:1662-1664.
69. Sartor O. Overview of samarium Sm 153 lexidronam in the treatment of painful metastatic bone disease. *Rev Urol.* 2004;6(suppl 10):S3-S12.
70. Nilsson S, Strang P, Aksnes AK, et al. A randomized, dose-response, multicenter phase II study of radium-223 chloride for the palliation of painful bone metastases in patients with castration-resistant prostate cancer. *Eur J Cancer.* 2012;48: 678-686.
71. Gaynor L. Radiation protection considerations in the case death of radionuclide therapy patients. *Physica Medica.* 2016;32:952.
72. Sartor O, Reid RH, Bushnell DL, Quick DP, Ell PJ. Safety and efficacy of repeat administration of samarium Sm-153 lexidronam to patients with metastatic bone pain. *Cancer.* 2007;109:637-643.
73. Menda Y, Bushnell DL, Williams RD, Miller S, Thomas MO. Efficacy and safety of repeated samarium-153 lexidronam treatment in a patient with prostate cancer and metastatic bone pain. *Clin Nucl Med.* 2000;25:698-700.
74. Prelaj A, Rebuzzi SE, Buzzacchino F, et al. Radium-223 in patients with metastatic castration-resistant prostate cancer: efficacy and safety in clinical practice. *Oncol Lett.* 2019;17:1467-1476.
75. Zhang I, Gilbo P, Kohn N, Cox B. Clinical response to radium-223 dichloride in men with metastatic castrate-resistant prostate cancer. *Pract Radiat Oncol.* 2018;8: 452-457.
76. Mirels H. Metastatic disease in long bones: a proposed scoring system for diagnosing impending pathologic fractures. *Clin Orthop Relat Res.* 1989:256-264.
77. Flux GD. Imaging and dosimetry for radium-223: the potential for personalized treatment. *Br J Radiol.* 2017;90:20160748.
78. Pacilio M, Ventroni G, Basile C, Ialongo P, Becci D, Mango L. Improving the dose-myelotoxicity correlation in radiometabolic therapy of bone metastases with 153Sm-EDTMP. *Eur J Nucl Med Mol Imaging.* 2014;41:238-252.
79. Pacilio M, Ventroni G, De Vincentis G, et al. Dosimetry of bone metastases in targeted radionuclide therapy with alpha-emitting (223)Ra-dichloride. *Eur J Nucl Med Mol Imaging.* 2016;43:21-33.
80. Murray I, Chittenden SJ, Denis-Bacelar AM, et al. The potential of $^{223}$Ra and $^{18}$F-fluoride imaging to predict bone lesion response to treatment with $^{223}$Ra-dichloride in castration-resistant prostate cancer. *Eur J Nucl Med Mol Imaging.* 2017;44: 1832-1844.
81. Mínguez P, Rodeño E, Fernández I, Esteban A, Martínez-Indart L, Gómez de Iturriaga A. A retrospective study on the potential of (99m) Tc-HDP imaging before therapy for individualizing treatments with (223) Ra-Cl(2) for metastatic castration resistant prostate cancer. *Med Phys.* 2021;48:1395-1403.
82. Robinson RG, Preston DF, Schiefelbein M, Baxter KG. Strontium 89 therapy for the palliation of pain due to osseous metastases. *JAMA.* 1995;274:420-424.
83. Yadav MP, Ballal S, Sahoo RK, Dwivedi SN, Bal C. Radioligand therapy with (177)Lu-PSMA for metastatic castration-resistant prostate cancer: a systematic review and meta-analysis. *AJR Am J Roentgenol.* 2019;213:275-285.
84. Sartor O, de Bono J, Chi KN, et al. Lutetium-177-PSMA-617 for metastatic castration-resistant prostate cancer. *N Engl J Med.* 2021.

# $^{18}$F-FES Whole-Body Imaging Protocol for Evaluating Tumor Estrogen Receptor Status in Patients with Recurrent or Metastatic Breast Cancer

Barbara J. Grabher, CNMT, RT(N), NCT FSNMMI-TS

*Grabher Consulting & Specialty Services, Forest Hill, Maryland*

**CE credit:** For CE credit, you can access the test for this article, as well as additional *JNMT* CE tests, online at https://www.snmmilearningcenter.org. Complete the test online no later than September 2026. Your online test will be scored immediately. You may make 3 attempts to pass the test and must answer 80% of the questions correctly to receive 1.0 CEH (Continuing Education Hour) credit. SNMMI members will have their CEH credit added to their VOICE transcript automatically; nonmembers will be able to print out a CE certificate upon successfully completing the test. The online test is free to SNMMI members; nonmembers must pay $15.00 by credit card when logging onto the website to take the test.

In September 2020, the *Journal of Nuclear Medicine and Technology* published a continuing education article, "Breast Cancer: Evaluating Tumor Estrogen Receptor Status with Molecular Imaging to Increase Response to Therapy and Improve Patient Outcomes," that reviewed a promising new PET tracer, 16α-$^{18}$F-fluoro-17β-fluoroestradiol ($^{18}$F-FES). This tracer had the potential to be a valuable tool for medical oncologists and breast surgeons in noninvasively evaluating the estrogen receptor site status of their patients' recurrent tumor and secondary metastatic lesions. In May 2020, $^{18}$F-FES received Food and Drug Administration approval and began being marketed by Zionexa using the trade name Cerianna and manufactured by PETNET. In May 2021, GE Healthcare acquired Zionexa, and Cerianna and is now being marketed by GE Healthcare and is still being manufactured by PETNET. This article will review the $^{18}$F-FES package insert information and imaging protocol, as well as important guidelines for imaging with $^{18}$F-FES.

**Key Words:** breast cancer; estrogen receptor imaging; $^{18}$F-fluoroestradiol; Cerianna; $^{18}$F-fluoroestradiol; patient outcomes

**J Nucl Med Technol 2023; 51:188–193**
DOI: 10.2967/jnmt.122.265272

Sometimes breast cancer patients present their medical oncologist or breast surgeon with a clinical dilemma on how their particular type of cancer should be treated, especially when standard treatment options fail. An accurate diagnosis and treatment plan remain essential for patient survival and longevity. Some breast cancer tumors respond to treatment, whereas others do not. Knowing the type of breast tumor, its estrogen receptor (ER) site status, and how it might respond to therapy is vital to effective and successful treatment, ultimately improving patient outcomes and overall survival rates.

An accurate and high-quality 16α-$^{18}$F-fluoro-17β-fluoroestradiol ($^{18}$F-FES) (Cerianna; Zionexa) whole-body (WB) scan can be a key piece of the diagnostic workup for the physician. ER-positive (ER+) tumors are the most prevalent breast tumor type, representing approximately 75%–80% of all breast tumors (*1*), making $^{18}$F-FES WB imaging a diagnostic tool that can help accurately identify ER+ tumor cells throughout the body. $^{18}$F-FES WB imaging noninvasively evaluates the ER status of patients with recurrent or metastatic breast cancer. It is essential to be aware of the $^{18}$F-FES package insert (PI) and contraindications and follow the correct preparation for the scan to ensure the highest-quality images possible.

## MECHANISM OF ACTION, PHARMACODYNAMICS, AND PHARMACOKINETICS

$^{18}$F-FES has a 60%–100% relative binding affinity for the ER, making it an excellent tracer to image ERs throughout the body (*2*). The pharmacodynamics of $^{18}$F-FES uptake are directly proportional to tumor ER expression measured by in vitro assays: the higher the ER+ expression, the greater the uptake, and vice versa (*3*). According to the $^{18}$F-FES PI, the relationship between plasma concentrations and image interpretation has not been studied (*3*).

$^{18}$F-FES is rapidly metabolized in the liver, and at 20 min after injection, approximately 20% of circulating radioactivity in the plasma is in the form of nonmetabolized $^{18}$F-FES. At 120 min after injection, less than 5% of the injected dose remains unmetabolized (*3*).

According to section 12.3 of the PI, 95% of $^{18}$F-FES is bound to plasma proteins after intravenous injection, and the tracer distributes primarily within the hepatobiliary system but also within the small and large intestines, heart wall, blood, kidney, uterus, and bladder. The critical organ is the liver, which receives 0.126 mGy/MBq (*3*). $^{18}$F-FES is also distributed systemically, with high physiologic uptake in the

Received Nov. 30, 2022; revision accepted Apr. 25, 2023.
For correspondence or reprints, contact Barbara J. Grabher (barbara.grabher@gmail.com).
Published online Jul. 11, 2023.

uterus and ovaries (*2*). The effective radiation dose resulting from an administration of 222 MBq (6 mCi) to an adult weighing 70 kg is estimated to be 4.9 mSv (*3*). Excretion is biliary and urinary (*3*).

## PATIENT SELECTION

Physicians must keep several things in mind when selecting the right treatment options. The hormone receptor status in the primary tumor does not necessarily predict the hormone receptor status of metastatic lesions. A primary tumor may be heterotypical, having both ER+ and ER-negative receptors within the lesion instead of a single ER status type. Hormone receptor genes may be downregulated or lost in metastatic lesions (*4*), complicating accurate treatment decision-making. So, one treatment option might work for the ER+ primary tumor but not for a metastatic lesion whose receptor has become downregulated or lost and is now ER-negative. Lindstrom et al. noted that in about a third of patients, ER status can change after disease recurrence or progression and that a change to ER-negative was associated with a 48% increase in mortality (*4*). The ability to predict therapeutic response in distant lesions is critical to planning the approach to treating patients with metastatic disease, and $^{18}$F-FES ER imaging is like getting a noninvasive WB biopsy in which all ER+ lesions throughout the body can be visualized on the scan. Most importantly, $^{18}$F-FES ER imaging correlates well with immunohistochemistry results and may be able to predict response to endocrine therapy (*5,6*). Patients initially diagnosed with lobular breast cancer who are being worked up for recurrent or metastatic breast cancer are perfect candidates for $^{18}$F-FES WB imaging because lobular breast cancer tumors have a low affinity for $^{18}$F-FDG but a high affinity for $^{18}$F-FES. Figures 1 and 2 illustrate 2 patients with lobular breast cancer. $^{18}$F-FDG scans showed uptake in some tumors, but when patients 1 and 2 were scanned with $^{18}$F-FES at 1 d and 1 mo, respectively, after $^{18}$F-FDG PET, the $^{18}$F-FES scans showed multiple lesions not seen on the $^{18}$F-FDG PET scans.

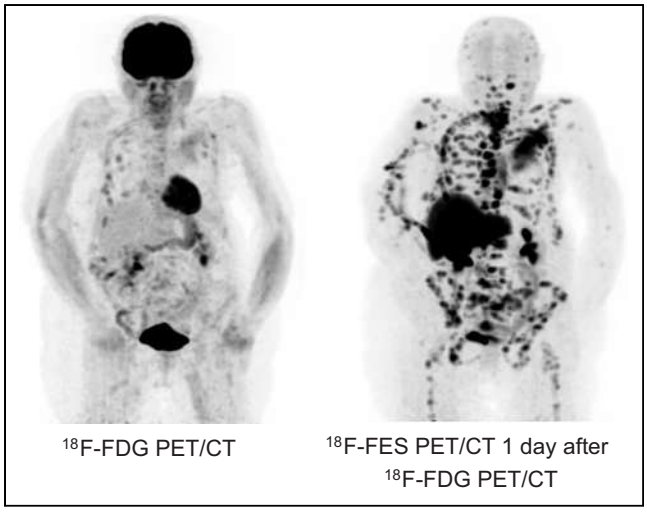


**FIGURE 1.** Patient 1. History: ER+, HER2-negative, T2N0M0 left breast lobular carcinoma treated with neoadjuvant chemotherapy, surgery, adjuvant chemotherapy, radiation therapy, and 5 y of hormone therapy (tamoxifen). Eight years after treatment completion, T10 and T12 fractures emerged, and cancer antigen 15-3 was 3,500 U/mL (reference level, <25 U/mL). Outcome: all lesions expressed ERs on $^{18}$F-FES PET/CT. Accumulation was higher for $^{18}$F-FES than for $^{18}$F-FDG, probably because of lobular histology. Some lesions were barely seen with $^{18}$F-FDG. Treatment: aromatase inhibitor (exemestane), with lesion stabilization and cancer antigen 15-3 reduction from 3,500 to 1,50 U/mL 2 y after treatment began. (Reprinted from (*10*).)

## APPROPRIATE-USE CRITERIA FOR ER-TARGETED PET

In October 2022, the appropriate-use criteria for ER-targeted PET imaging with $^{18}$F-FES were created to help medical oncologists, breast surgeons, and interpreting physicians know when to order or not order ER-targeted PET imaging. The working group of experts determined that ordering $^{18}$F-FES PET imaging is appropriate in 3 instances: to assess for ER functionality when endocrine therapy is considered either at initial diagnosis of metastatic breast cancer or after progression of disease on endocrine therapy, to assess the ER status of lesions that are difficult or dangerous to biopsy, and to assess the ER status of lesions when other tests are inconclusive (*7*).

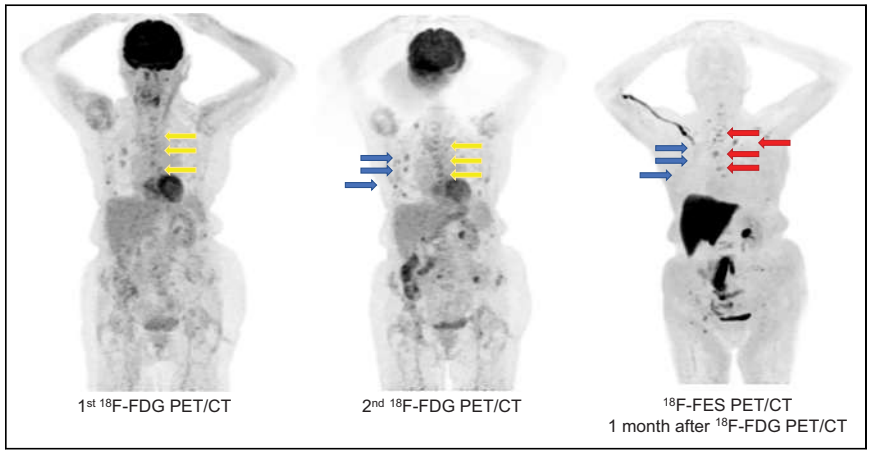


**FIGURE 2.** Patient 2. History: ER+, progesterone receptor–negative, HER2-negative lobular carcinoma with initial bone metastases. Outcome: lesion heterogeneity ($^{18}$F-FES PET/CT scan showing both $^{18}$F-FES–positive lesions [red arrows] and $^{18}$F-FES–negative lesions [blue arrows]). No uptake was seen on $^{18}$F-FES PET/CT scan for lesions that showed uptake on second $^{18}$F-FDG PET/CT scan (blue arrows). $^{18}$F-FES–positive lesions corresponded to progressive lesions seen with $^{18}$F-FDG (yellow arrows), potentially explaining progression with hormone therapy. Treatment: aromatase inhibitor (blocks ERs), which resulted in reduction or disappearance of $^{18}$F-FES PET signal; radiation therapy on T9 and left iliac bone; and exemestane, resulting in bone progression on L5 and left iliac bone. (Reprinted from (*10*).)

**TABLE 1**
Appropriate-Use Guidelines for 14 Clinical Scenarios (*7*) in Which $^{18}$F-FES PET Might Be Used

| Scenario | Appropriateness of use | Score |
|---|---|---|
| | Appropriate (scores of 7–9) | |
| 8 | For assessing ER status when lesions are difficult to biopsy or biopsy is nondiagnostic | 8 |
| 9 | For considering second line of endocrine therapy after progression of metastatic disease | 8 |
| 10 | For considering endocrine therapy at initial diagnosis of metastatic disease | 8 |
| 14 | For detecting ER status when findings of other imaging tests are equivocal or suggestive | 8 |
| | May be appropriate (scores of 4–6) | |
| 2 | For diagnosing malignancy of unknown primary when biopsy is nonfeasible or nondiagnostic | 5 |
| 5 | For routine staging of extraaxillary nodes and distant metastases | 5 |
| 6 | For staging invasive lobular carcinoma and low-grade invasive ductal carcinoma | 5 |
| 7 | For assessing ER status, in lieu of biopsy, in lesions that are easily accessible for biopsy | 5 |
| 13 | For detecting lesions in suspected or known recurrent or metastatic breast cancer | 5 |
| | Rarely appropriate (scores of 1–3) | |
| 1 | For diagnosing primary breast cancer | 2 |
| 3 | For routine staging of primary tumor (T staging) | 1 |
| 4 | For routine staging of axillary nodes | 3 |
| 11 | For considering endocrine therapy at initial diagnosis of primary breast cancer | 1 |
| 12 | For measuring response to therapy | 1 |

Inappropriate-use criteria must also be reviewed to make sure physicians are not ordering scans for patients who will not benefit. Ordering a $^{18}$F-FES scan inappropriately results in unnecessary radiation exposure to the patient, increased out-of-pocket costs to the patient, and unnecessary costs to the patient's insurance company. The working group came up with 14 clinical scenarios in which $^{18}$F-FES PET imaging could be used, grouping the scenarios as "appropriate," "may be appropriate," or "rarely appropriate" on a scale from 1 to 9. Scores of 7–9 indicate that the procedure is appropriate for the scenario and is generally considered acceptable. Scores of 4–6 indicate that the procedure may be appropriate for the scenario; this implies that more evidence is needed to classify the scenario definitively. Scores of 1–3 indicate that the procedure is rarely appropriate for the scenario and is generally not considered acceptable (*7*). Table 1 outlines the scenarios and their scores.

## CLINICAL INDICATION AND LIMITATIONS OF USE

$^{18}$F-FES PET is indicated for detecting ER+ lesions as an adjunct to biopsy in patients with recurrent or metastatic breast cancer (*3*). The $^{18}$F-FES limitations of use state that "Tissue biopsy should be used to confirm recurrence of breast cancer and to verify ER status by pathology. CERIANNA is not useful for imaging other receptors, such as human epidermal growth factor receptor 2 (HER2) and the progesterone receptor (PR)" (*3*).

## PATIENT PREPARATION

The patient should be well hydrated before being injected. If a patient is of childbearing age, it is recommended that pregnancy status be checked per instruction guidelines. The $^{18}$F-FES PI states that "Certain classes of systemic endocrine therapies, including ER modulators and ER downregulators, block ER, reduce the uptake of fluoroestradiol F 18, and may reduce detection of ER-positive lesions after administration of CERIANNA. Drugs from these classes such as tamoxifen and fulvestrant may block ER for up to 8 and 28 weeks, respectively. Do not delay indicated therapy to administer CERIANNA. Administer CERIANNA prior to starting systemic endocrine therapies that block ER" (*3*).

**TABLE 2**
$^{18}$F-FES Acquisition Parameters

| Acquisition parameter | Specification | Standard/preferred/optional |
|---|---|---|
| PET scanner type | 2 or 3 dimensional | Standard |
| Energy peak | 511 keV | Standard |
| Energy window | $^{18}$F-fluorine | Standard |
| Patient position | Supine with arms above head, if possible | Standard |
| Injection-to-scan time | 20–80 min after injection | Standard |
| | 80 min | Preferred |
| Acquisition area | WB (thighs to vertex) | Standard |
| Acquisition time | 20–30 min | Standard |
| Number of bed positions | 6–8 | Standard |
| Time per bed position | 3–4 min | Standard |

Additional information to keep in mind when imaging with $^{18}$F-FES is that lower estrogen levels will result in no or low uptake of $^{18}$F-FES (*8*). Aromatase inhibitors and the hormone therapy medication mentioned above block ERs and may reduce or eliminate the $^{18}$F-FES PET signal (*8*).

There are no contraindications before performing a $^{18}$F-FES scan (*3*); however, knowing when other recent nuclear medicine studies have been performed (radiopharmaceutical-dependent) can be helpful to ensure the highest-quality $^{18}$F-FES PET scan with no interference from any other radiopharmaceutical.

## DOSE AND ADMINISTRATION

The recommended dose of $^{18}$F-FES is 222 MBq (6 mCi), with an acceptable dose range of 111–222 MBq (3–6 mCi). $^{18}$F-FES is intravenously injected over a 1- to 2-min time frame followed by a 0.9% sodium chloride flush to ensure proper dose delivery (*2*). It is preferred that $^{18}$F-FES be injected in an arm contralateral to the primary tumor site (*2*). The $^{18}$F-FES user guide "Seeing ClearER+" states, "Administering Cerianna through a central port is not contraindicated but is dissuaded" (*2*). $^{18}$F-FES may be diluted with 0.9% sodium chloride injection (*3*). Because $^{18}$F-FES imaging can begin anywhere from 20 to 80 min after injection (*3*), PET imaging departments can pick a postinjection scan time that best fits the department's workflow. If most scans in the department are done at 45 min or 60 min after injection, then acquiring a $^{18}$F-FES scan at 45 or 60 min after injection is fine and is still follows the PI guidelines for imaging; however, scanning 80 min after injection is preferred (*3*).

Because $^{18}$F-FES is not glucose-dependent, light, noise, and sound will not affect uptake after tracer injection. Physical activity before a $^{18}$F-FES injection does not need to be avoided as it does for $^{18}$F-FDG. After $^{18}$F-FES is injected, as with all PET procedures, hydration and frequent voiding by the patient are suggested to help decrease radiation exposure. Physical activity is permitted after $^{18}$F-FES injection (*2*). Sedation can be given if needed before imaging, but patients should not be allowed to drive themselves home afterward.

## ACQUISITION AND PROCESSING PARAMETERS

The acquisition and processing parameters for $^{18}$F-FES WB PET are fairly simple. The standard WB $^{18}$F-FDG acquisition protocol can be used for acquiring a WB $^{18}$F-FES scan. The first steps include cloning the existing $^{18}$F-FDG protocol and adding $^{18}$F-FES to the isotope inventory. Once $^{18}$F-FES is loaded into the isotope inventory, it is selected from the available isotopes and the imaging protocol is resaved as $^{18}$F-FES WB PET. With older PET scanners, it is important to increase the time per bed position by 30% (i.e., 3 min to 4 min or 5 min to 6.5 min) to acquire an adequate number of counts per bed position and ensure a good-quality scan. For PET/CT protocols, the manufacturer's recommendations for CT acquisition parameters should be followed (*2,3*). Table 2 outlines other important acquisition settings, including PET scanner type, energy peak and energy window, preferred patient positioning, injection-to-scan time, and acquisition area. Preferred acquisition times, number of bed positions, and time per bed position are also listed.

Other important acquisition steps for a $^{18}$F-FES WB PET scan are to have the patient void before scanning, to position the patient supine on the imaging table with arms above head if possible, and to scan from vertex to mid thigh or knees (*2*). Once the scan is complete, it is also important to review the raw data for image quality and motion or any other defects that may require additional follow-up. If significant motion is detected, making a scan unreadable, the scan should be repeated.

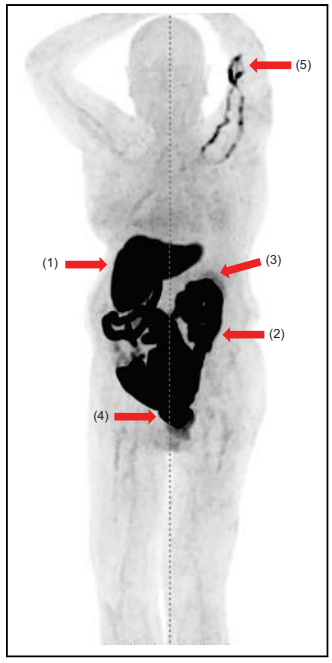


**FIGURE 3.** Normal increased uptake of $^{18}$F-FES in liver (1), gastrointestinal tract (2), kidneys (3), urinary bladder (4), and injected vessel (5). Uptake in injected vessel, seen in most patients, is probably due to sticking of tracer to vessel wall or endothelial cells (*2*). (Courtesy of DRA Imaging.)

It is recommended that processing of $^{18}$F-FES WB PET scans follow the Society of Nuclear Medicine and Molecular Imaging procedure standards for $^{18}$F-FDG PET/CT (*2*).

## $^{18}$F-FES TRACER DISTRIBUTION PATTERNS

Normal uptake of $^{18}$F-FES can be seen in the liver, gastrointestinal tract, kidneys, and urinary bladder (Fig. 3) (*2*). Increased uptake may also be seen in the injected vessel in most patients; the cause is unknown but is probably due to sticking of the tracer to the vessel wall or endothelial cells. If the uptake appears abnormal or questionable, the interpreting physician should be informed and should determine whether additional images are needed (e.g., a skull image illustrating 2 metastatic brain lesions is shown in Fig. 4).

## IMAGE INTERPRETATION

Although training is not required for $^{18}$F-FES interpreters, it is strongly suggested. Information on training can be obtained through a Cerianna sales representative or the GE Healthcare website (https://landing1.gehealthcare.com/PDX-US-Cerianna-InterpreterTraining.html).

According to the $^{18}$F-FES user's guide, in interpretation of an $^{18}$F-FES WB scan, "Detection of ER+ tumors should be based on comparison with tissue background outside of organs with high physiologic uptake and regions with high

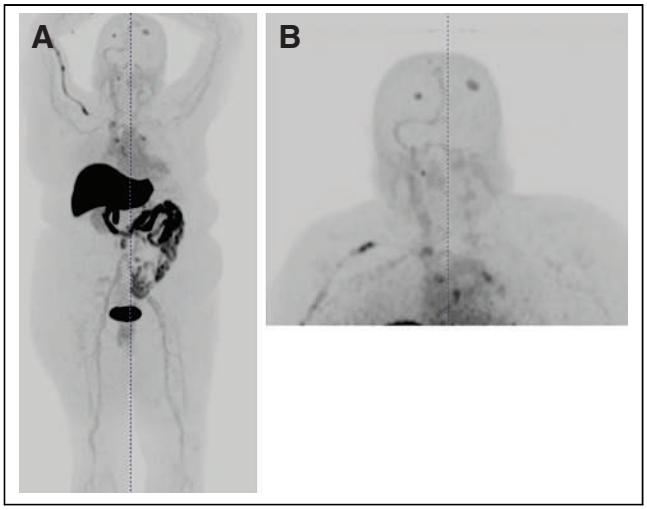


**FIGURE 4.** Abnormal uptake of $^{18}$F-FES. Although $^{18}$F-FDG WB imaging is not helpful in visualizing brain metastasis, $^{18}$F-FES WB imaging is. (A) WB $^{18}$F-FES image from vertex to mid thighs, with increased uptake in chest and brain. (B) Extra image of skull that clearly illustrates the 2 brain metastatic lesions (*2*). (Courtesy of DRA Imaging.)

activity due to hepatobiliary and urinary excretion. As a general rule, all lesions with fluoroestradiol F 18 uptake greater than background (e.g., physiological liver uptake) are considered ER+". Assessing ER expression in regions with normally high physiologic activity (e.g., liver) is not advised (*2*).

## WARNINGS, PRECAUTIONS, AND ADVERSE REACTIONS

Several sections of the $^{18}$F-FES PI should be reviewed carefully, including the warnings and precautions (section 5) and the adverse reactions (section 6). The former includes a risk of misdiagnosis regarding inadequate tumor characterization and other ER+ pathology, stating, "Breast cancer may be heterogeneous within patients and across time. CERIANNA images ER and is not useful for imaging other receptors such as HER2 and PR. The uptake of fluoroestradiol F 18 is not specific for breast cancer and may occur in a variety of ER-positive tumors that arise outside of the breast, including from the uterus and ovaries. Do not use CERIANNA in lieu of biopsy when biopsy is indicated in patients with recurrent or metastatic breast cancer" (*3*). Another risk of misdiagnosis regards false-negative $^{18}$F-FES findings. Negative $^{18}$F-FES findings do not rule out ER+ breast cancer. Pathology or clinical characteristics that suggest a patient may benefit from systemic hormone therapy should take precedence over discordantly negative $^{18}$F-FES findings (*3*).

Regarding adverse reactions, the most common in over 1,200 injections during clinical trials were injection-site pain and dysgeusia (distortion of taste), occurring in less than 1% of patients (*3*).

## USE IN SPECIAL PATIENT POPULATIONS

Use of $^{18}$F-FES in specific patient populations is also important to review. According to the PI (*3*), pregnant woman should be advised of the potential risks of fetal exposure to radiation doses, and lactating women should be advised to avoid breastfeeding for 4 h after administration. Regarding geriatric use, clinical studies did not reveal any difference in pharmacokinetics or biodistribution in patients aged 65 y or over.

## BENEFITS OF $^{18}$F-FES ER IMAGING

There are many benefits to imaging with $^{18}$F-FES; WB imaging can be used when lesions are inaccessible or challenging to biopsy or when lesions are insufficiently suggestive to justify an invasive procedure. $^{18}$F-FES imaging is also beneficial when the tumor pathology is aggressive or a patient refuses biopsy. $^{18}$F-FES imaging can also evaluate potential disease heterogeneity. A study by Yang et al. showed that 37.5% of patients with metastatic breast cancer had a heterogeneous pattern of both ER+ and ER-negative lesions (*6*). Evaluating all lesions for their ER status is a critical step in determining the appropriate treatment option, helping improve the overall response to therapy, the patient's outcome, and the patient's ultimate survival. Breast imaging with $^{18}$F-FES can complement a patient's biopsy and can noninvasively evaluate multiple areas of the body, including organs such as the brain, which standard $^{18}$F-FDG WB imaging cannot do.

Although $^{18}$F-FES imaging has many benefits, it does have some limitations. It has a limited ability to detect liver metastases because it has increased uptake in the liver due

**TABLE 3**
$^{18}$F-FES Access Support

| Category | Reimbursement service |
|---|---|
| Investigation of benefits | Aid in determining patient's health insurance coverage |
| Billing and coding assistance | Provide guidance for billing and coding requirements |
| Claims assistance | Help in navigating through claims process |
| Preservice and postservice appeals | Aid in assisting with and expediting these appeals |
| Prior-authorization support and status monitoring | Help with initiating and monitoring prior-authorization requests from insurance companies (prefill request on your behalf) |
| Medical necessity support | Provide support to establish medical necessity |
| Peer-to-peer preparation | Provide one-on-one collaborative training and strategies to assist health-care provider in seeking $^{18}$F-FES insurance coverage |

to increased hepatic metabolism (*5*). Considerable enterohepatic circulation can also complicate abdominal imaging when using $^{18}$F-FES (*5*). $^{18}$F-FES is not useful for imaging other receptors, such as human epidermal growth factor receptor 2 and the progesterone receptor.

From a sensitivity and specificity perspective, $^{18}$F-FES has a high accuracy for the detection of ER+ lesions, with proven concordance when compared with biopsy immunohistochemistry for determining ER status in metastatic breast cancer. The sensitivity of $^{18}$F-FES is 78% (95% CR, 65.0%–88.0%), and its specificity is 98% (95% CR, 65.0%–100%) (*2*). When evaluated for efficacy for assessing the ER status of non–primary breast cancer lesions, $^{18}$F-FES WB PET/CT interpretation and biopsy resulted in a 76.6% positive agreement (95% CR, 62.0%–87.7%; $P = 0.0018$) and a 100% negative agreement (95% CR, 90.8%–100%; $P = 0.00053$) (*2*).

## SUPPORT WITH $^{18}$F-FES ACCESS

Sometimes when a radiopharmaceutical is newly approved by the Food and Drug Administration, it can be challenging to make sure an imaging facility gets reimbursed properly by Medicare and private insurance companies. When first imaging with $^{18}$F-FES, an imaging center and its billing department must confirm that they have all the billing and coding information, prior-authorization information, and any other information needed for insurance companies to correctly process the claim.

To help, GE Healthcare has created a network of reimbursement services and support ranging from benefits investigation support (determining a patient's insurance coverage) to medical necessity support (Table 3). Requesting support requires submission of a Cerianna Support Provider Consent Form signed by the physician or provider (available by calling 833-946-6392 or visiting www.cerianna.com/reimbursement) (*9*).

## CONCLUSION

Since the Food and Drug Administration approved $^{18}$F-FES in May 2020, ER imaging with $^{18}$F-FES is now a viable option to obtain valuable information on the ER status of all tumors in the body. A single noninvasive scan can simultaneously evaluate both the primary breast tumor and any metastatic lesions—like performing a WB biopsy regarding ER status. A patient's ER status can change after metastasis occurs, resulting in a treatment option that works for the primary tumor but not for the metastases. Knowing the ER status of all tumors is vital to the success of treatment selection, especially when standard treatment options fail. Physicians need to consider the appropriate-use criteria for $^{18}$F-FES to ensure that the right patient is scanned for the right reason at the right time, and PET imaging departments need to follow the PI and imaging protocol to ensure the highest-quality $^{18}$F-FES WB scans possible.

## DISCLOSURE

No potential conflict of interest relevant to this article was reported.


## ACKNOWLEDGMENTS

I thank Deepak Behera, MD, and Darcy Phillips for helping me with the manuscript, and I thank Ula Thompsett from DRA Imaging, Poughkeepsie, NY, for providing $^{18}$F-FES images for this article.


## REFERENCES


1. Breast cancer facts & figures 2017-2018. American Cancer Society website. https://www.cancer.org/content/dam/cancer-org/research/cancer-facts-and-statistics/breast-cancer-facts-and-figures/breast-cancer-facts-and-figures-2017-2018.pdf. Published 2017. Accessed May 5, 2023.
2. Seeing ClearER+. Cerianna user's guide. GE Healthcare; October 2022.
3. CERIANNA™ (fluoroestradiol F 18) injection. Package insert. Zionexa US Corp.; March 2022.
4. Lindstrom LS, Karlsson E, Wilking UM, et al. Clinically used breast cancer markers such as estrogen receptor, progesterone receptor, and human epidermal growth factor receptor 2 are unstable throughout tumor progression. *J Clin Oncol.* 2012; 30:2601–2608.
5. Liao GJ, Clark AS, Schubert EK, Mankoff DAF. $^{18}$-Fluoroestradiol PET: current status and potential future clinical applications. *J Nucl Med.* 2016;57:1269–1275.
6. Yang Z, Sun Y, Zhang Y, et al. Can fluorine-18 fluoroestradiol positron emission tomography-computed tomography demonstrate the heterogeneity of breast cancer in vivo? *ClinBreast Cancer.* 2013;13:359–363.
7. Appropriate use criteria for estrogen receptor-targeted PET imaging with 16α-$^{18}$F-fluoro-17β-fluoroestradiol. Society of Nuclear Medicine and Molecular Imaging website. https://www.snmmi.org/ClinicalPractice/content.aspx?ItemNumber=42023. Accessed May 5, 2023.
8. Linden HM, Kurland BF, Peterson LM, et al. Fluoroestradiol positron emission tomography reveals differences in pharmacodynamics of aromatase inhibitors, tamoxifen, and fulvestrant in patients with metastatic breast cancer. *Clin Cancer Res.* 2011;17:4799–4805.
9. Cerianna is now available in your area. Brochure. GE Healthcare; April 2022.
10. Grabher BJ. Breast cancer: evaluating tumor estrogen receptor status with molecular imaging to increase response to therapy and improve patient outcomes. *J Nucl Med Technol.* 2020;48:191–201.

# $^{18}$F-Fluoroestradiol Whole-Body Imaging

Barbara J. Grabher, CNMT, RT(N), NCT FSNMMI-TS

## RATIONALE

Treating and managing metastatic breast cancer can be challenging for breast oncologists and their patients. Estrogen receptors (ERs) in a patient's primary tumor can be either estrogen-positive or estrogen-negative to varying degrees or absent on initial biopsy, but this can change if the primary tumor starts to metastasize elsewhere in the body, making treatment decisions difficult. Whole-body imaging with $^{18}$F-fluoroestradiol (Cerianna; GE Healthcare) is like performing a whole-body biopsy on the patient, helping to localize ER-positive tumors anywhere in the body (*1,2*). Knowing where and how many ER-positive tumors are in the body can help breast oncologists and their patients make more accurate management decisions, potentially leading to better outcomes.

## CLINICAL INDICATIONS

- $^{18}$F-fluoroestradiol injection is a radioactive diagnostic agent indicated for use with PET imaging for the detection of ER-positive lesions as an adjunct to biopsy in patients with recurrent or metastatic breast cancer.

## CONTRAINDICATIONS

- There are no contraindications. However, knowing when other recent nuclear medicine studies have been performed (radiopharmaceutical-dependent) can be helpful to ensure the highest-quality $^{18}$F-fluoroestradiol PET scan with no interference from any other radiopharmaceutical.

## PATIENT PREPARATION AND EDUCATION

- If the patient is of childbearing age, a pregnancy test should be performed.

**TABLE 1**
Medication to Withhold Before $^{18}$F-Fluoroestradiol Imaging

| Drug | Time frame for withholding |
|---|---|
| Tamoxifen (ER modulator) | 8 wk |
| Fulvestrant (ER downregulator) | 28 wk |

- The patient should be instructed to drink water to ensure adequate hydration before administration of $^{18}$F-fluoroestradiol.
- The patient should be instructed not to take drugs that block the ER or reduce the uptake of $^{18}$F-fluoroestradiol (Table 1). Indicated therapy should not be delayed in order to administer $^{18}$F-fluoroestradiol.
- Patients should be imaged with $^{18}$F-fluoroestradiol before starting systemic endocrine therapies that block the ER (e.g., ER modulators and ER downregulators).
- A through patient history should be obtained, to include …
  - Current medications and when taken last.
  - Recent imaging procedures (e.g., CT, MRI, PET, and SPECT).
- Patient education should include a careful explanation of the procedure, including imaging time, the initial uptake period, and the importance of remaining still during image acquisition. If the patient has severe anxiety or may have difficulty lying still for the procedure, sedation may be used and administered per institutional guidelines.

## PROTOCOL/ACQUISITION INSTRUCTIONS

- The patient is interviewed, an intravenous catheter is placed, and the $^{18}$F-fluoroestradiol dose is injected (111–222 MBq [3–6 mCi]) over 1–2 min followed by a 10-mL saline flush to ensure proper dose delivery.

**TABLE 2**
Radiopharmaceutical, Recommended Dose, Uptake Time, and PET Scanner Acquisition Time

| Radiopharmaceutical | Recommended dose | Uptake time | Acquisition time |
|---|---|---|---|
| $^{18}$F-fluoroestradiol | 222 MBq (6 mCi) (range, 111–222 MBq [3–6 mCi] administered as intravenous injection over 1 to 2 min) | 80 min (range, 20–80 min after drug administration) | 20–30 min |


DOI: 10.2967/jnmt.122.265271

**TABLE 3**
Acquisition Parameters

| Parameter | Description | Standard/preferred/optional |
|---|---|---|
| PET scanner type | 2- or 3-dimensional | Standard |
| Energy peak | 511 keV | Standard |
| Energy window | $^{18}$F-fluorine | Standard |
| Patient position | Supine with arms above head, if possible | Standard |
| Injection-to-scan time | 20–80 min after injection | Standard |
| | 80 min | Preferred |
| Acquisition area | Whole body (thighs to vertex) | Standard |
| Acquisition time | 20–30 min | Standard |
| Number of bed positions | 6–8 | Standard |
| Time per bed position | 3–4 min/bed | Standard |

For older scanners, increase time per bed position by 30% (i.e., 3 min to 4 min or 5 min to 6.5 min). Standard $^{18}$F-FDG whole-body acquisition protocol can be used for WB $^{18}$F-fluoroestradiol scan. For PET/CT protocols, refer to manufacturer's recommendations for CT acquisition parameters.

It is preferred that $^{18}$F-fluoroestradiol be injected in the arm contralateral to the primary tumor site. $^{18}$F-fluoroestradiol may be diluted with a 0.9% sodium chloride injection. After the injection, the catheter is removed, and the patient is instructed to return for imaging 20–80 min later. The patient may eat and should be encouraged to hydrate and void the urinary bladder frequently during the first hours after administration to reduce radiation exposure. Table 2 outlines the radiopharmaceutical, recommended dose, uptake time, and PET scanner acquisition time.

- After the uptake period, the patient is instructed to void the urinary bladder and then is positioned supine on the imaging table with the arms above the head if possible. The use of a body strap, knee cushion, and blanket is recommended to increase patient comfort. Table 3 summarizes the acquisition parameters.

## IMAGE PROCESSING

- The raw data are reviewed for image quality and motion. If significant motion is detected, making the scan unreadable, a repeat scan is acquired.
- The basic processing parameters should follow the $^{18}$F-FDG PET/CT procedure standards of the Society of Nuclear Medicine and Molecular Imaging.

## WARNINGS AND PRECAUTIONS

- Limitations of use: tissue biopsy should be used to confirm recurrence of breast cancer and to verify ER status by pathology. $^{18}$F-fluoroestradiol is not useful for imaging other receptors, such as human epidermal growth factor receptor 2 and the progesterone receptor.
- Risk of misdiagnosis
  - Tumor characterization may be inadequate, and there may be other ER-positive pathology. Breast cancer may be heterogeneous within patients and across time. $^{18}$F-fluoroestradiol images ERs and is not useful for imaging other receptors such as human epidermal growth factor receptor 2 and progesterone receptor.
  - Uptake of $^{18}$F-fluoroestradiol is not specific for breast cancer and may occur in a variety of ER-positive tumors that arise outside the breast, including from the uterus and ovaries.
  - $^{18}$F-fluoroestradiol should not be used in lieu of biopsy when biopsy is indicated in patients with recurrent or metastatic breast cancer.
  - A negative $^{18}$F-fluoroestradiol scan may be false-negative and does not rule out ER-positive breast cancer. Pathology or clinical characteristics that suggest a patient may benefit from systemic hormone therapy should take precedence over a discordant negative $^{18}$F-fluoroestradiol scan.
- Use in specific populations
  - Pregnancy: a pregnant woman should be advised of the potential risks of fetal exposure to radiation doses with $^{18}$F-fluoroestradiol.
  - Lactation: a lactating woman should be advised to avoid breastfeeding for 4 h after $^{18}$F-fluoroestradiol administration.
  - Geriatric use: clinical studies with $^{18}$F-fluoroestradiol did not reveal any difference in pharmacokinetics or biodistribution in patients aged 65 y or over.
- The most common adverse reactions are injection-site pain and dysgeusia.
- If sedation is used and the patient traveled to the appointment by car, an accompanying adult should drive the patient home.

## REFERENCES


1. Cerianna injection. Package insert. Zionexa US Corp.; March 2022.
2. User's guide: Cerianna™ (fluoroestradiol F 18) injection. Cerianna website. https://www.cerianna.com/wp-content/uploads/2020/07/Cerianna-users-guide.pdf. Accessed March 6, 2023.

# The Impact of the Coronavirus Disease 2019 Pandemic on the Clinical Environment

Shannon N. Youngblood[1] and Sara L. Johnson[2]

[1]*University of Arkansas for Medical Sciences, Little Rock, Arkansas, and Ochsner Medical Center, Baton Rouge, Louisiana; and*
[2]*Nuclear Medicine Technology Certification Board, Tucker, Georgia, and AdventHealth University, Orlando, Florida*

The Nuclear Medicine Technology Certification Board performed an impact survey on the coronavirus disease 2019 pandemic to better assess the current state of nuclear medicine practice within the United States, as well as the perceptions and experiences of technologists working during the pandemic. **Methods:** A web-based automation platform was used to create, collect, and analyze the survey data. **Results:** The survey revealed many department protocol variations during the pandemic, a decrease in patient volume, and several other concerns and issues. Experiences regarding staffing and wage changes were varied. **Conclusion:** This research showed significant inconsistencies in practice and stresses to nuclear medicine technology during the pandemic, as well as concerns for the workforce pipeline. NMTCB decided to delay the JTA process and conduct additional research regarding the workforce.

**Key Words:** CNMT; research methods; statistical analysis; COVID-19; job task analysis; staffing

**J Nucl Med Technol 2023; 51:196–203**
DOI: 10.2967/jnmt.123.265808

Recent studies have shown that nuclear medicine professionals have been directly impacted by the coronavirus disease 2019 (COVID-19) pandemic. Several global studies were performed in the spring and summer of 2020 showing a widespread reduction in nuclear medicine procedures (*1–3*). Early surveys showed disruptions to the supply chain, including the availability of radiopharmaceuticals and the $^{99}$Mo/$^{99m}$Tc generator supply (*2*). Freudenberg et al. conducted a global survey including 72 countries and found an average 54% decline in nuclear medicine imaging procedures, including a 60% overall decline in myocardial perfusion imaging and a 67% decrease in thyroid uptake and scan procedures (*2*). The decline in procedures occurred primarily because nuclear medicine departments were postponing routine and elective scans or had concerns over infection prevention (*3*). Czernin et al. also reported that patient volume was reduced to accommodate staffing shortages that were due to staff illness (*4*). Nuclear medicine therapies were also significantly reduced (*5*).

Received Dec. 31, 2022; revision accepted Jul. 6, 2023.
For correspondence or reprints, contact Sara L. Johnson (sjohnson@nmtcb.org).


Image prioritization was recommended and may have contributed to the reduction in studies performed. The International Atomic Energy Agency released technical guidance for nuclear medicine departments, including a detailed chart to help departments prioritize procedures (*6*). The chart showed prioritization for oncologic procedures, especially PET imaging, as well as emergent procedures such as gastrointestinal bleeding or ventilation/perfusion (V/Q) lung scans. Several general imaging studies were deprioritized or deemed nonessential, such as parathyroid imaging and bone scans performed for nononcologic indications (*6*).

Nuclear medicine departments also modified procedures to maximize infection prevention efforts. Changes to daily functions included the development of new infection control and prevention protocols specific to nuclear medicine, longer time slots for patients to allow for room sanitization, and increased use of personal protective equipment (*7*). Imaging protocols were also modified. Myocardial perfusion imaging protocols in some cases were modified to pharmacologic-only or stress-first protocols (*8*). In some institutions, patients were switched to cardiac PET protocols. One-day imaging was preferred for all studies that would typically take multiple days to perform. V/Q lung scans were greatly modified over concerns about infection prevention in staff and COVID-19–related conditions (*7,9,10*). Modifications to V/Q lung scan protocols included switching to Technegas (Cyclomedica Australia) for ventilation, performing the scan as perfusion only, and switching the protocol to SPECT or SPECT/CT (*7,10*). Perfusion-only lung SPECT/CT is a useful tool for detecting COVID-19–related lung disease in addition to detecting pulmonary embolism (*10*).

Supply shortages and supply chain issues greatly disrupted daily operations during the pandemic (*4,5*). Shortages of personal protective equipment, radioisotopes, cold kits, and generators were reported (*5*). Procurement and allocation of personal protective equipment were a concern for many nuclear medicine departments (*7*). It became critical, yet challenging, for department leadership to advocate for the proper allocation of personal protective equipment to nuclear medicine personnel who face the same infection risk yet are less visible to management than other health-care workers, such as nurses (*7*). Shortages for various radiopharmaceuticals have been ongoing and include mebrofenin, sulfur colloid, mertiatide, methylene diphosphonate, pyrophosphate,

and sestamibi (*11*). $^{177}$Lu and $^{131}$I shortages due to reactor and supply issues were also reported (*5,11*).

Lastly, staffing issues have remained a concern and a challenge for employers, as well as a cause of stress for many nuclear medicine technologists (NMTs) (*4,5*). Modifications to staffing in nuclear medicine departments include reducing staff, reassigning staff to assist in other areas, reducing hours due to decreased volume, extending shifts to longer hours to accommodate sick staff, and developing A and B teams (*12*). Some staff were furloughed or laid off. Some received decreased pay for decreased hours, whereas others received crisis pay (*12*). Staffing shortages exist in nuclear medicine and other imaging modalities, with concerns over safety due to the pandemic and lack of support compared with other health professions being cited as contributing factors (*13*).

The Nuclear Medicine Technology Certification Board (NMTCB) routinely analyzes the current status of the field and uses these data to ensure that the board's entry-level examination remains reflective of current nuclear medicine practices. This is one way the NMTCB ensures that applicants are being tested on the knowledge, skills, and competencies needed to enter the workforce. The NMTCB conducts a job task analysis (JTA) every 5 y to examine current practices as a way to ensure that the certified NMT (CNMT) examination remains relevant to current practices (*14*). As part of the JTA, an extensive literature review is performed to create a draft list of tasks and procedures performed by NMTs. A survey is then sent to participating NMTCB-CNMTs, who determine the importance and level of competency required for entry into the workforce. The NMTCB's last JTA process was in 2017, and the next began in 2022.

On the basis of previous pandemic research and other feedback from the nuclear medicine community, the NMTCB board of directors and staff have had concerns that the ongoing pandemic may still be impacting nuclear medicine. Research from the pandemic showed several modifications to current nuclear medicine practices and protocols, supply chain issues, and significant job-related stressors for technologists. Conducting a JTA while nuclear medicine is still experiencing pandemic changes, shortages, protocol modifications, and a decreased volume for some procedures would impact the results of a JTA. If certain imaging and therapy procedures are not being performed or the frequency of certain procedures is still being altered because of the pandemic, the data from the JTA would likely be inaccurate, potentially resulting in unnecessary changes to examinations and certification processes. Therefore, the NMTCB performed a COVID-19 impact survey to better assess the current state of nuclear medicine practice within the United States, as well as the perceptions and experiences of technologists working during the pandemic. The results of this survey have been used to make data-driven decisions within the NMTCB, including determining whether it was necessary to delay the JTA process, as well as providing more insight into the experiences of working NMTs.

## MATERIALS AND METHODS

The NMTCB review board approved this study as exempt under section 45CFR46.104, and the requirement to obtain informed consent was waived. All participants were provided full disclosure regarding the purpose of the survey and voluntarily indicated informed consent when selecting to open, participate, and conclude the survey. A mixed-study single-group analysis was used to survey CNMTs in the NMTCB e-mail database. The survey consisted of 19 multiple-choice answers with an option for open-ended responses after each question (all questions and answers are available at the end of this article, as well as online as Supplemental Data at http://jnmt.snmjournals.org). Survey instructions included a disclaimer that the survey was voluntary, that it should require less than 5 min to complete, and that results would be anonymous and confidential. A survey invitation was sent to active holders of a CNMT credential who live within the United States and have an e-mail address on file with the NMTCB. The invitation was sent via e-mail on August 20, 2021. Two reminder emails were sent: one on August 30, 2021, and the other on September 7, 2021. The survey was closed on September 14, 2021.

Mailchimp, a web-based automation platform, was used to create, collect, and analyze the survey data. The survey was sent via e-mail to 19,379 NMTs. In total, 7,466 participants opened the survey. Of these, 3,600 completed it fully. Incomplete responses were excluded from the data analysis. Respondents were provided the opportunity to submit individual comments for each question. Analysis of response data was based on the frequency of responses. Survey comments were open-coded and compared for themes.

## RESULTS

The survey was sent via e-mail to 19,379 NMTs and received 7,466 open notifications and 3,600 completed responses, for an 18.57% completion rate. Most respondents were full-time NMTs (74.9%) (question 1). A relatively even distribution of department size was reported, with 27.9% of departments employing 1–2 NMTs; 25%, 3–4; 21.4%, 5–7; and 16%, more than 10 (question 2). Most respondents were employed in hospital-based settings (65%) (question 3). Additional respondent workplace employment included outpatient imaging centers (12.5%), cardiac centers (11%), and PET facilities (5%). Respondents were geographically distributed, with responses representing 11 states.

### Staffing

When asked if working hours increased or decreased during the pandemic, responses were varied (question 4). Work hours increased by 10%–25% for 8% of respondents, whereas 22.7% of respondents stated their hours decreased by 10%–25%. Another 9.1% of respondents stated their hours were drastically reduced by 26%–50%. Although the reduction of work hours may invoke trepidation, 45% of respondents stated their normal work hours did not change. Most respondents also did not change employers during the pandemic (question 5).

Many respondents entered open-text comments regarding working hours during the pandemic. One respondent wrote, "At the beginning, March to December 2020, we went from 80 h biweekly to 72 h then down to 60 h. All outpatient

scans were canceled because of the COVID-19 patients in the hospital. We lost some members of staff to COVID-19, some were laid off, and we are now fully operational back to 80 h biweekly plus overtime. The hospital has hired 2 new nuclear medicine techs, and most of the department has now cross-trained in diagnostic CT." Another commented that working hours "both increased and reduced by 10%–25% over the last 18 mo depending on the current events surrounding COVID-19 (i.e., reduced surgery volumes impacting productivity or reduced staff)." Overall feedback from responses and comments indicated that early in the pandemic, many NMTs experienced reductions in hours and pay or were furloughed. However, as of summer 2021, most had returned to normal working hours or were getting overtime hours due to staffing shortages.

#### Wages

When asked if they experienced a change in wages or salary in the past 18 mo, 33% of respondents reported an increase (question 6). No change was reported by 54.3% of respondents. The comments revealed that some NMTs received bonus hazard pay and others received cost-of-living adjustments or annual increases. Many others reported that no raises were given to anyone in the radiology department or hospitalwide. Wages decreased for 9.9% of respondents, for reasons such as having their position eliminated, being furloughed, or having a pay decrease due to a decrease in hours worked.

#### Patient Volumes

Respondents reported a decrease in volume for all patient types (question 7). When asked about a reduction in patient volume, 47.5% of respondents reported a decrease in outpatients, 20.4% reported a reduction in inpatients, and 11.77% reported a reduction in emergency room patients. Another 15.7% reported a decrease in on-call procedures. The comments indicated that the greatest reductions occurred in 2020 at the beginning of the pandemic, when stay-at-home orders were in place and elective procedures were canceled. One NMT reported, "At the beginning of the pandemic, we didn't get patients, except for emergencies and PET patients." Many respondents commented that volumes are starting to return to prepandemic levels for all procedures.

#### Protocol Variations

Respondents reported many protocol variations and modifications to department protocols during the pandemic (questions 9–11). The most significant change in nuclear medicine protocols due to COVID-19 was in V/Q studies. Many respondents reported an increase in V/Q and myocardial perfusion imaging studies (question 10). A perfusion-only protocol for V/Q studies was implemented in 56.5% of departments regardless of the COVID-19 status of the patient (question 11).

Most respondents (61.8%) reported that their facility required them to perform examinations on COVID-19–positive patients (question 12). Additionally, several protocol variations were made for procedures on COVID-19–positive patients (question 13). For identified COVID-19–positive patients, 50.6% of respondents followed a perfusion-only protocol for V/Q studies. Other affected nuclear medicine protocols included myocardial perfusion imaging studies, with pharmacologic-only stress portions performed by 14.6% of respondents. Nineteen percent of respondents performed studies on COVID-19–positive patients only at the end of the day. Interesting to note is that 29.9% of respondents reported that their department did not modify existing protocols and that 26.8% of respondents reported no modification of any nuclear medicine studies when performed on a COVID-19–positive patient. Respondents reported changes to allow for distancing of patients while waiting for their procedure, an increase in cleaning time between patients, and additional stressors due to COVID-19–related issues.

#### Other Concerns

Through survey questions and open comments, respondents reported several other pandemic-related concerns and issues: low patient volumes (58.9%), supply shortages (45.9%), staffing shortages (35.9%), and reassigned duties (28.85%) (question 14). Fifty-four percent of respondents reported no current changes in wages or salary, and 87% had not changed employers during the previous 18 mo. Regarding the vaccination battle, 57.9% of respondents reported that their institution or employer required either vaccination or a written attestation or request for an exemption (question 15). A large percentage (83.3%) of NMTs reported not having tested positive for COVID-19 during the past 18 mo, with those testing positive stating they acquired the virus occupationally (7.3%) and 6.8% through community transmission (question 16).

Throughout the survey, respondents were given the opportunity to comment freely on their experiences working as an NMT during the pandemic. Comments included an initial reduction in patients during the unexpected shutdown period and employers who did not allow employees to know the COVID-19 status of patients. A frequent concern expressed by the NMTs is what challenges to their livelihood will arise as new variants emerge and what approach will be best for handling current issues, both professionally and personally. Many nuclear medicine educators went from classroom teaching to online teaching, which posed its own hurdles.

Although 67.2% of NMTs reported that they do not plan to retire within the next 5 y, a staggering 28.4% reported that they do plan to retire within the next 5 y (question 17). Respondents reported a desire to leave their existing employer or profession if required to receive the vaccine against their will or if facing stressful working conditions, staffing shortages, health risks, depression, lack of respect for their profession, or lack of leadership from administrators. The staffing shortages that have been noted in other radiologic modalities, such as radiography, CT, and MRI, have shown the value of holding multimodality certifications, as well as the need for more nuclear medicine advanced associate professionals.

## DISCUSSION

This survey was sent on August 20, 2021, when federal vaccine mandates for health-care workers were being created but had not yet been implemented by most employers. On September 9, 2021, President Biden issued a mandate that all employers with more than 100 workers require their employees to be vaccinated or tested for the virus weekly, affecting about 80 million Americans. Workers at health facilities that receive federal Medicare or Medicaid were mandated to be fully vaccinated. This was a controversial topic, and many NMTs who had medical or religious exemptions for other vaccines were at risk of losing their job. The comments submitted in our survey revealed that many NMTs were unhappy about the mandate and feared being fired. Many also expressed that they did not feel comfortable with the efficacy and safety of the vaccine but would agree to receive it if forced by their employer. The timing of the vaccine mandate, which was enacted during the active survey collection period, may have caused respondents to alter their original opinion.

The NMTCB used the data from this survey to drive decisions about the JTA and how to further assess the current state of nuclear medicine technology. Temporary reductions or avoidance of some procedures, along with protocol modifications, may negatively impact the validity and reliability of the JTA process. Because the JTA impacts the content of the entry-level certification examination, it is imperative that temporary changes adopted during the pandemic either be returned to previous practices or be converted into permanent practices. As a result of this survey, the NMTCB delayed the JTA process by 1 y to allow staffing, patient volumes, and protocol modifications to stabilize.

Comments about a desire to retire or leave the field were a cause for concern. A question was added to the annual NMTCB renewal in 2022 to reach every NMTCB certificate holder and attain a more accurate picture of whether the study result was reflective of the overall field: "Do you plan to retire or leave the field of nuclear medicine within the next 5 y?" Approximately 13% stated that they do plan to leave in the next 1–5 y, with 87% stating that they have no plans to leave in the near future. Although this provides a more accurate picture of workforce attrition and is less concerning than the COVID-19 impact survey showed, it still incites some concern over the workforce pipeline and the potential for future staffing shortages.

## CONCLUSION

To project what the future will hold for our profession, additional research is warranted encompassing the long-term effects of the pandemic on the field of nuclear medicine. We must adapt to challenges and changes as they arise. It is encouraging that exciting and innovative radiopharmaceuticals, safety measures, and theranostics are on the horizon. The demand for nuclear medicine professionals with multimodality certifications and skills, as well as the need for more nuclear medicine advanced associates, has risen exponentially because of the effects of COVID-19 and the surge in theranostics. However, an increase in new technologists entering the field is needed to meet the staffing demands caused by retiring technologists and expansions of the field. The JTA, which was initially delayed because of the results of this survey, will be conducted throughout 2023 and the results implemented in 2024. The NMTCB also recently conducted a salary survey, the results of which are forthcoming. As we look toward the future, the NMTCB is committed to continuous support and guidance of the nuclear medicine profession by providing resources such as this survey and the salary survey and by offering additional certifications in CT, PET, radiation safety, and nuclear cardiology, as well as the opportunity to earn certification as a nuclear medicine advanced associate.

## DISCLOSURE

No potential conflict of interest relevant to this article was reported.

### KEY POINTS

**QUESTION:** How has the COVID-19 pandemic impacted nuclear medicine technology?

**PERTINENT FINDINGS:** COVID-19 greatly impacted the clinical environment for NMTs. Changes to clinical practice may impact the NMTCB's JTA and examination development process. The results of this survey also created concerns over workforce retention.

**IMPLICATIONS FOR PATIENT CARE:** Care of patients during future pandemics may be improved by the planning that surveys such as ours enables.

## REFERENCES


1. Annunziata S, Bauckneht M, Albano D, et al. Impact of the COVID-19 pandemic in nuclear medicine departments: preliminary report of the first international survey. *Eur J Nucl Med Mol Imaging.* 2020;47:2090–2099.
2. Freudenberg LS, Paez D, Giammarile F, et al. Global impact of COVID-19 on nuclear medicine departments: an international survey in April 2020. *J Nucl Med.* 2020;61:1278–1283.
3. Gnanasegaran G, Williams J, Huang HL, Bomanji JB. Coronavirus (COVID-19) pandemic: what the nuclear medicine departments should know. *J Nucl Med Technol.* 2020;48:89–97.
4. Czernin J, Fanti S, Meyer PT, et al. Nuclear medicine operations in the times of COVID-19: strategies, precautions, and experiences. *J Nucl Med.* 2020;61:626–629.
5. Annunziata S, Albano D, Laudicella R, Bauckneht M. Surveys on COVID-19 in nuclear medicine: what happened and what we learned. *Clin Transl Imaging.* 2020; 8:303–305.
6. *COVID-19 Pandemic: Technical Guidance for Nuclear Medicine Departments.* International Atomic Energy Agency; 2020.
7. McFarland GA, Johnson SG. Nuclear medicine clinical practice in the United States during the COVID-19 era and beyond. *J Nucl Med Technol.* 2020;48: 218–226.
8. Skali H, Murthy VL, Paez D, et al. Guidance and best practices for reestablishment of non-emergent care in nuclear cardiology laboratories during the coronavirus disease 2019 (COVID-19) pandemic: an information statement from ASNC, IAEA, and SNMMI. *J Nucl Med.* 2020;61:1534–1539.

9. SNMMI statement: COVID-19 and ventilation/perfusion (V/Q) lung studies. Society of Nuclear Medicine and Molecular Imaging website. http://www.snmmi.org/NewsPublications/NewsDetail.aspx?ItemNumber=36714. Published September 22, 2021. Accessed August 1, 2023.
10. Kumar A, Moadel RM, Haramati LB, Ye K, Freeman LM, Zuckier LS. Experience with a perfusion-only screening protocol for evaluation of pulmonary embolism during the COVID-19 pandemic surge. *J Nucl Med.* 2022;63:598–601.
11. Radiopharmaceutical Tc99m kit supply update. Society of Nuclear Medicine and Molecular Imaging website. https://www.snmmi.org/IssuesAdvocacy/content.aspx?ItemNumber=29602. Published February 8, 2022. Accessed August 1, 2023.
12. Beyder DD, Crosthwaite MH, Crowley J, et al. From one technologist to another—COVID-19 questions answered. *J Nucl Med Technol.* 2020;48:102–105.
13. Fleishon HB. The radiology labor shortage. American College of Radiology website. https://www.acr.org/Practice-Management-Quality-Informatics/ACR-Bulletin/Articles/March-2022/The-Radiology-Labor-Shortage. Published February 10, 2022. Accessed August 1, 2023.
14. The Nuclear Medicine Technology Certification Board certified nuclear medicine technologist job analysis report. Nuclear Medicine Technology Certification Board website. https://nmtcb.org/documents/publications/NMTCB-CNMT-Job-Task-Analysis-Report-2017_Final-8-25-2017.pdf. Published August 2017. Accessed August 1, 2023.

## APPENDIX

Question 1 has 3,605 answers.

"Are you currently employed as a nuclear medicine technologist?"

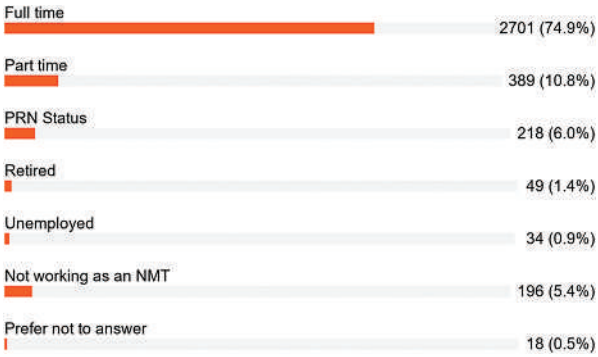


Question 2 has 3,555 answers.

"How many total NMTs are currently employed by your institution? You may include administrators, educators, and contract (agency) NMTs who maintain their NMT certification."

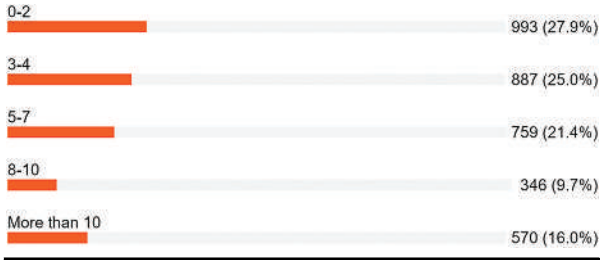


Question 3 has 3,581 answers.

"Which of the following best describes your workplace setting?"

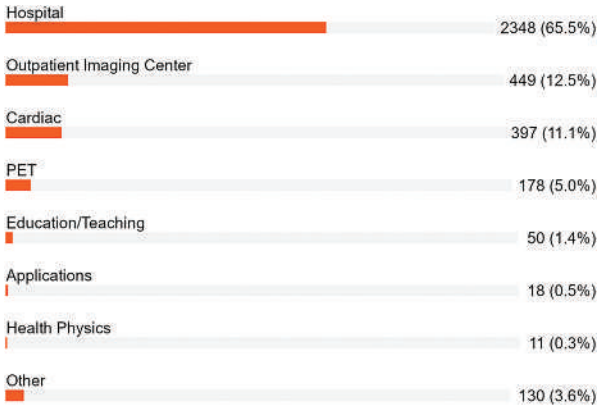


Question 4 has 3,577 answers.

"Have your hours working in Nuclear Medicine been REDUCED or INCREASED in the past 18 months due to the impact of Covid-19?"

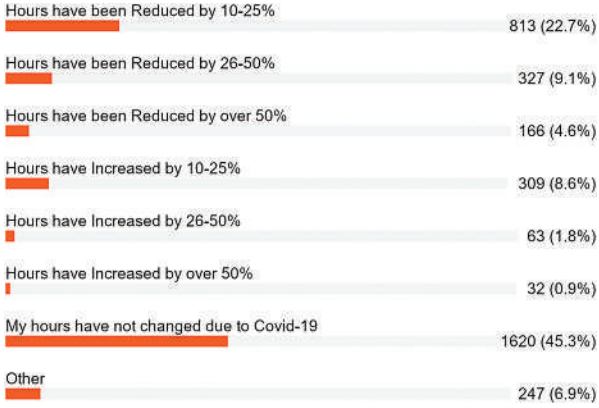


Notable responses:

- "A roller coaster of increase/decrease due to our NM patients and also helping out in other departments."
- "…most of the department has now cross trained in diagnostic CT".
- "Most of the techs are now multi-modality, doing Nuclear, PET/CT and diagnostic CT".
- "Before I retired hours were decreased, the suddenly increased".
- "Drastic fluctuations. Sometimes weeks with not much then a wave passes and everyone wants to get everything done."
- "I was never able to pick up hours due to decrease of full time techs hours. They finally let prn staff go."

Question 5 has 3,584 answers.

"Have you changed employers during the past 18 months?"


Question 6 has 3,569 answers.

"Have you experienced a change in wages/salary in the past 18 months?"


Notable responses:

- "From March 2020 – June 2020 hours AND pay reduced by 50%."
- "All raises were put on hold."
- "As a front line worker, nurses are being offered higher pay, but we are getting these patients right from the ER and exposed everyday."
- "There has been no restitution for any of us, just keep coming in grinding the pavement and come back tomorrow. We are providing the best care to Covid patients, and they cut our hours or don't want to pay what we should be getting, it's very sad oh and then try to make us work extra shifts in other areas of hospital and not pay extra".
- "Didn't get a regular raise, they stopped contributing to retirement, kept the bonuses for the company."
- "Everyone's salary was decreased by 20% For the same period above. We were not allowed to work over 32 hours per week."
- "Used up all PTO due to slow down."

Question 7 has 3,302 answers.

"If you work in a hospital setting, have you experienced a REDUCTION in the following patient types due to the COVID pandemic?"


Question 8 has 3,051 answers.

"If you work in a hospital setting, have you experienced an INCREASE in the following patient types due to the COVID pandemic?"


Question 9 has 2,900 answers.

"Which nuclear medicine studies and procedures do you feel have had the most volume REDUCTION due to Covid-19 at your institution? Pick all that apply:"

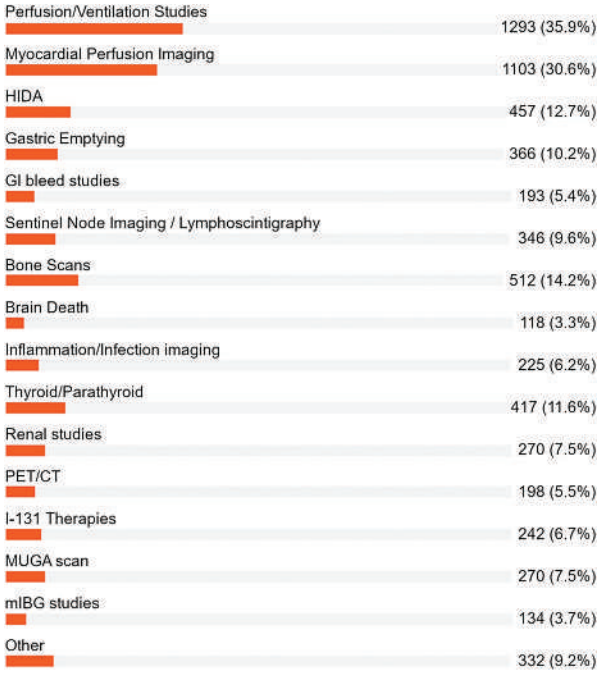

Question 10 has 2,541 answers.

"Which nuclear medicine studies and procedures do you feel have had the most volume INCREASE due to Covid-19 at your institution? Pick all that apply."

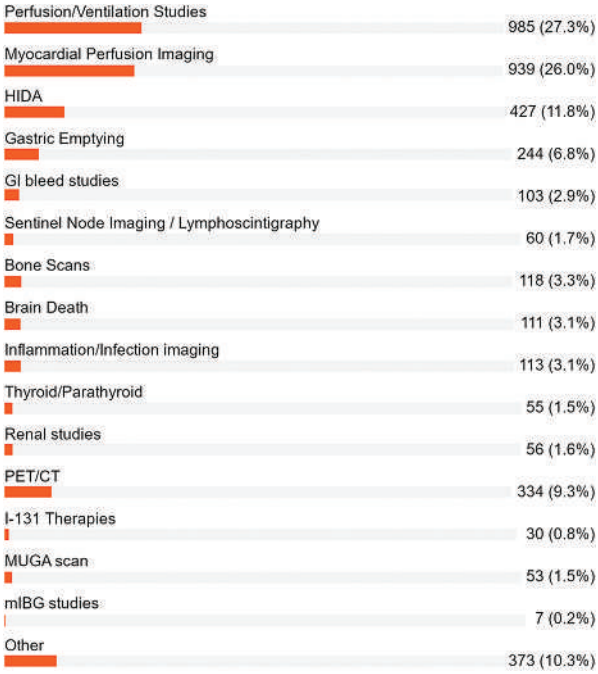


Question 11 has 3,382 answers.

"Which of the following modifications has your department made due to COVID-19? Pick all that apply."

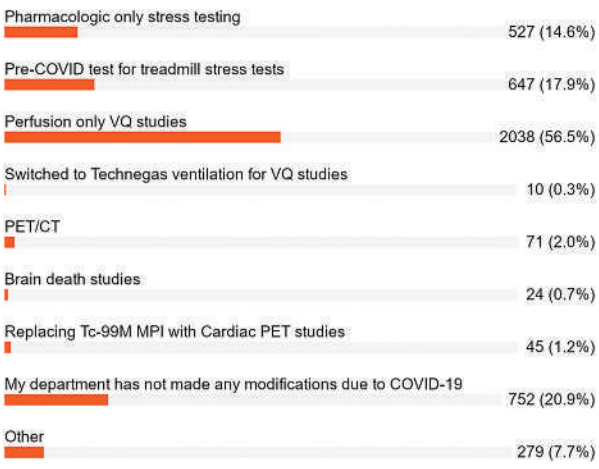


Question 12 has 3,490 answers.

"Does your facility require you to perform exams on COVID positive patients?"

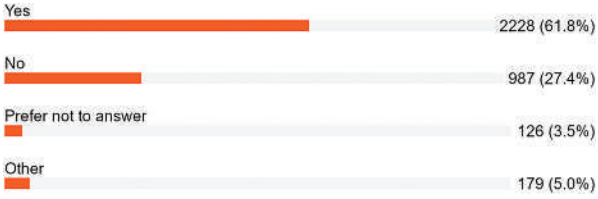


Question 13 has 3,233 answers.

"Have you modified any exams when imaging known COVID positive patients?"

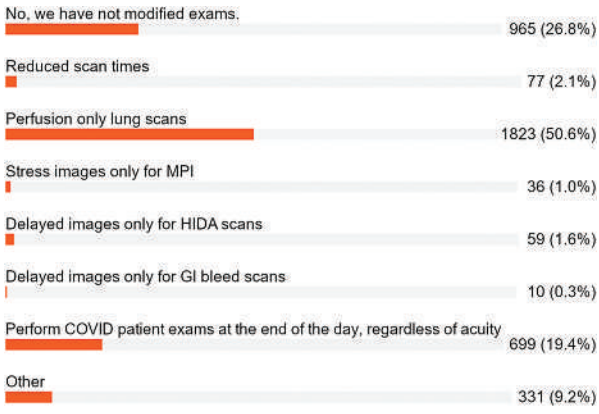


Question 14 has 3,480 answers.

"Which of the following issues has your department faced during the pandemic?"

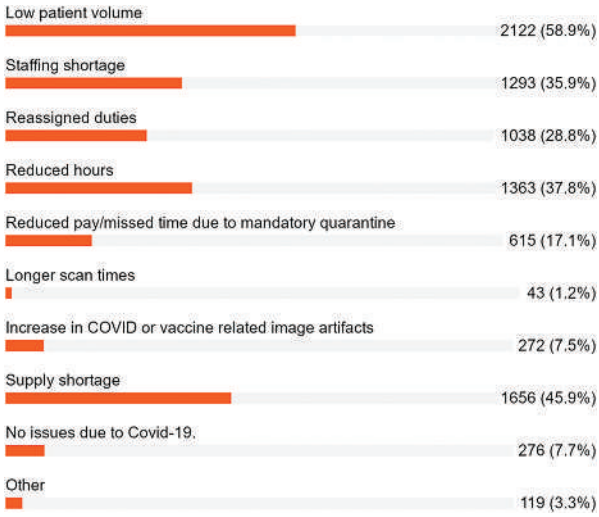


Notable responses:

- "A great many issues as an educator – virtual classrooms, delayed clinical experiences, trying to graduate students on time, recruiting efforts especially international students."
- "I was told by a text 'no patients, no work, you and your coworker figure out who will work one day next week.' Not fired. 'Good luck', when asked to work again I carried a lot of anger and apprehension. I don't want to with doctors anymore, they were not caring toward me or my colleges."
- "More responsibilities, cleaning, sanitizing, more stress and increased demand."
- "Reduced pay/missed time due to mandatory quarantine."

Question 15 has 3,554 answers.

"Is your institution or employer requiring you to be vaccinated against Covid-19 or provide written attestation that you have been vaccinated?"

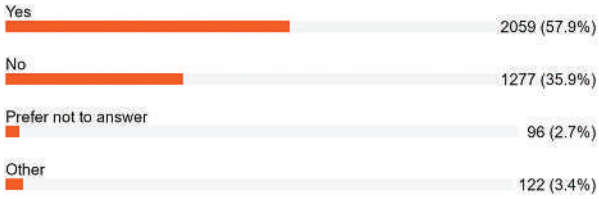

Question 16 has 3,571 answers.

"In the past 18 months have you tested positive for COVID-19?

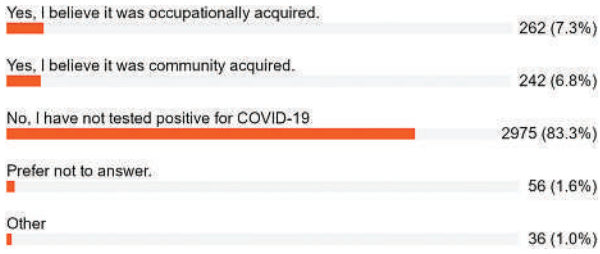


Question 17 has 3,571 answers.

"Do you plan to retire from your current position within the next five years?"


Notable responses:

- "Already retired to much stress to deal with, no help from administration."
- "Can't retire in 5 years but would like to change fields."
- "I have been not employed as an NMT for approximately one month. I am changing professions …. I no longer desire to work in healthcare or a hospital setting."
- "I plan to leave my current position due to the pandemic and lack of protocols to ensure staff safety."
- "… I'm finding this whole process not really worth my time for what I'm paid in relation to the daily stress of all the unknowns of this whole Covid-19 thing; the daily tussles with my co-workers just because we all are so exhausted and so over all the highs/lows … "
- "I use to love my job; but the risks of exposure that I take on the daily; along with the constant inter-department squabbling that goes on because everyone is just plain exhausted by all of this Covid-19 crap – have me re-thinking my 'why' for showing up each day for work."
- "Making me rethink what else I can do with my certification."
- "Not retiring. Planning to leave the field of nuclear medicine for something better. It is not a profession I would ever recommend to anyone. Abusive hospital systems make this field unbearable. Not to mention most of what we do does not have a significant impact on patient outcomes."
- "… this pandemic took a toll on me. I don't know if I want to stay working in the medical field."
- "… if I find a job outside of the medical field that is enjoyable I will probably not return to NM. Employers have cut staff in nuclear so short that there have been injuries due to transport and lifting of patients in past years. Not worth being crippled due to a lack of management understanding."
- "… Healthcare as burnt me out"

Question 18 has 3,605 answers.

"Which state/location do you work?"

Multiple answers.

Question 19 has 436 answers.

"If you would like to submit additional comments regarding your experience working as a nuclear medicine technologist during the Covid-19 pandemic, please type your feedback here. All individual survey responses are anonymous."

Notable responses:

- "I realize this employer (and medical staff,) in no unclear terms, does not care about its employees. Stress testing resume as soon as patients agreed to come in, professional society recommendations were ignored completely, weren't in the conversation."
- "My decision for retirement was strongly based upon the fact I felt working conditions were too stressful. My underlying risk factors were minimized by my employer and because I worked solo, there was never anyone else to assist in any way. Work on this job for over 19 years."
- "Additional cleaning protocols were put in place without additional time allowed in the schedule to effectively clean between patients."
- "… I am now pursuing a nursing degree."
- "As always, the department is overlooked by administrators."
- "As the pandemic continues I have seen a more nonchalantattitude. This scares me since my state has not taken the pandemic seriously enough."
- "I was forced to use my sick/vaca time and could not get any unemployment. Now I am left with no sick/vaca time. Seems ridiculously unfair, since we were deemed 'essential'."
- "At the beginning of the pandemic, our hours were cut by 50%..."
- "At the start of the pandemic, I was mocked by my manager for requesting to wear a mask. They were of limited supply. There was hoarding of masks and PPET. I don't want to complain, just want to record these facts for posterity!"
- "Attention needs to be made more public that not all front line hospital workers are nurses."
- "… new students have suffered their education has suffered big time and for no reason except for unneeded restrictions. The patient load we are seeing is also from unneeded restrictions people are sick because they neglected their health."
- "Creating a work life balance during a pandemic is difficult than normal – having to blow through PTO for children needing to be quarantined due to daycare exposure etc. staff out for Covid quarantines but not adjusting schedules properly."
- "Most staffing shortages at the nuc med tech level are due to management reacting to volatile metrics and imposing "doing with the least staffing resources possible" philosophies, rather than developing strategic flexibility with smarter staffing margins. We simply need more techs, and more flexible techs hired."
- "… management does not really tend to the safe practices of their employees. Physicians write orders when our radiologist do not understand why this positive COVID patient needs this order. … Sometimes it just seems all about the money just checking the box because there is nothing else to for the patient."
- "Due to shortage of some kits or isotopes, one Doctor said, 'what a perfect way to kill a dying modality'!!"
- "Our biggest challenge now is supply shortages including gloves, IVs, butterflies, meds such as CCK, and radiopharmaceuticals such as Mebrofenin."
- "Even though patient volumes have increased within the past few months, my Nuclear Medicine department will be closing indefinitely."
- "Ever since I have graduated I have not worked in the field much for several years. A significant amount of technologists have stayed in the same positions making it difficult to allow new persons to come in."
- "Everyone seems very overworked and underpaid in general within the healthcare system. Covid simply made everything more stressful."
- "Everything seems to have become a political issue."
- "Feel like some PET patients may have delayed follow-up scans, which resulted in delay treatments."
- "Forced mandates on vaccination and unfair work practices."
- "… have also been tasked with housekeeping and secretarial duties as there's been a shortage in those areas. If we complain about doing these extra duties in addition to our own work we've been told to shut up and be glad that we have jobs!"
- "Our physicians informed us that we're not allowed to. enter their offices or the reading room because they don't want to be exposed to us as we're 'dirty' and everything we touch is 'contaminated'."

# Report on the PET/CT Image–Based Radiation Dosimetry of [$^{18}$F]FDHT in Women, a Validated Imaging Agent with New Applications for Evaluation of Androgen Receptor Status in Women with Metastatic Breast Cancer

Keisha C. McCall[1], Mofei Liu[2], Su-Chun Cheng[2], Amanda Abbott[3], Shipra Dubey[4], Diane Young[5], Mayzie Johnston[5], Annick D. Van den Abbeele[3,6], Beth Overmoyer[7], and Heather Jacene[3,6]

*[1]Department of Radiology, Henry Ford Health, Detroit, Michigan; [2]Division of Biostatistics, Department of Data Science, Dana-Farber Cancer Institute, Boston, Massachusetts; [3]Department of Imaging, Dana-Farber Cancer Institute, Boston, Massachusetts; [4]BiCOR, Brigham and Women's Hospital, Boston, Massachusetts; [5]GTx, Inc., Memphis, Tennessee; [6]Department of Radiology, Mass General Brigham, Boston, Massachusetts; and [7]Susan F. Smith Center for Women's Cancers, Dana-Farber Cancer Institute, Boston, Massachusetts*

In a prospective clinical trial, [$^{18}$F]fluoro-5α-dihydrotestosterone ([$^{18}$F]FDHT), the radiolabeled analog of the androgen dihydrotestosterone, was used as a PET/CT imaging agent for in vivo assessment of metastatic androgen receptor–positive breast cancer in postmenopausal women. To our knowledge, this article presents the first report of PET/CT image–based radiation dosimetry of [$^{18}$F]FDHT in women. **Methods:** [$^{18}$F]FDHT PET/CT imaging was performed on a cohort of 11 women at baseline before the start of therapy and at 2 additional time points during selective androgen receptor modulator (SARM) therapy for androgen receptor–positive breast cancer. Volumes of interest (VOIs) were placed over the whole body and within source organs seen on the PET/CT images, and the time-integrated activity coefficients of [$^{18}$F]FDHT were derived. The time-integrated activity coefficients for the urinary bladder were calculated using the dynamic urinary bladder model in OLINDA/EXM software, with biologic half-life for urinary excretion derived from VOI measurements of the whole body in postvoid PET/CT images. The time-integrated activity coefficients for all other organs were calculated from VOI measurements in the organs and the physical half-life of $^{18}$F. Organ dose and effective dose calculations were then performed using MIRDcalc, version 1.1. **Results:** At baseline before SARM therapy, the effective dose for [$^{18}$F]FDHT in women was calculated as 0.020 ± 0.0005 mSv/MBq, and the urinary bladder was the organ at risk, with an average absorbed dose of 0.074 ± 0.011 mGy/MBq. Statistically significant decreases in liver SUV or uptake of [$^{18}$F]FDHT were found at the 2 additional time points on SARM therapy (linear mixed model, $P < 0.05$). Likewise, absorbed dose to the liver also decreased by a small but statistically significant amount at the 2 additional time points (linear mixed model, $P < 0.05$). Neighboring abdominal organs of the gallbladder wall, stomach, pancreas, and adrenals also showed statistically significant decreases in absorbed dose (linear mixed model, $P < 0.05$). The urinary bladder wall remained the organ at risk at all time points. Absorbed dose to the urinary bladder wall did not show statistically significant changes from baseline at any of the time points (linear mixed model, $P \geq 0.05$). Effective dose also did not show statistically significant changes from baseline (linear mixed model, $P \geq 0.05$). **Conclusion:** Effective dose for [$^{18}$F]FDHT in women before SARM therapy was calculated as 0.020 ± 0.0005 mSv/MBq. The urinary bladder wall was the organ at risk, with an absorbed dose of 0.074 ± 0.011 mGy/MBq.

**Key Words:** FDHT; dosimetry; androgen receptor; breast cancer; PET/CT

**J Nucl Med Technol 2023; 51:204–210**
DOI: 10.2967/jnmt.123.265623

The radiolabeled analog of the androgen dihydrotestosterone, [$^{18}$F]fluoro-5α-dihydrotestosterone ([$^{18}$F]FDHT), has been used as an imaging agent for in vivo assessment of androgen receptor expression (*1,2*). [$^{18}$F]FDHT has been studied in prospective clinical trials as an imaging agent for castration-resistant prostate cancer in men since the early 2000 s (*3–5*). In contrast, prospective clinical trials have recently begun for [$^{18}$F]FDHT imaging of metastatic androgen receptor–positive breast cancer in women (*6,7*).

The androgen receptor is expressed in most estrogen receptor–positive (ER+) breast cancers, and a prospective phase 2 therapeutic clinical trial investigating a novel selective androgen receptor modulator (SARM) in postmenopausal women with ER+ metastatic breast cancer was conducted at the Dana-Farber Cancer Institute (*8,9*). As part of that trial, we performed a prospective imaging substudy exploring the feasibility of [$^{18}$F]FDHT PET/CT as an imaging biomarker for androgen receptor expression and evaluating response to SARM therapy (*7–9*). This article presents the [$^{18}$F]FDHT image–based radiation dosimetry for the cohort of 11 women who participated in the [$^{18}$F]FDHT PET/CT imaging substudy.

Zanzonico et al. published the human dosimetry of [$^{18}$F]FDHT for 7 men with prostate cancer (*10*), and Beattie

Received Jan 3, 2022; revision accepted Mar. 21, 2023.
For correspondence or reprints, contact Keisha C. McCall (kmccall2@hfhs.org).
Published online Jun. 14, 2023.

et al. studied [$^{18}$F]FDHT pharmacokinetics (*11*). However, to our knowledge, there have been no published studies on the biodistribution and radiation dosimetry of [$^{18}$F]FDHT in women.

## MATERIALS AND METHODS

### Patients and Study Design

As part of a prospective phase 2 therapeutic clinical trial investigating a novel SARM, enobosarm (G200802 [GTx, Inc.], NCT02463032), in postmenopausal women with ER+ metastatic breast cancer, 11 women participated in a single-site imaging substudy at Dana-Farber Cancer Institute from March 2017 through February 2018. The trial was conducted in full concordance with the principles of the Declaration of Helsinki and good clinical practice and was approved by the Dana-Farber Cancer Institute review board. All participants gave written informed consent.

Results from the clinical aspects of the imaging substudy (*7*) and the parent therapeutic clinical trial (*8,9*) have been reported. The major eligibility criteria for the phase 2 therapeutic clinical trial were postmenopausal women diagnosed with ER+/HER2-negative metastatic or locally recurrent advanced breast cancer with radiologic or clinical evidence of disease recurrence or progression within 30 d of randomization onto the therapeutic trial, at least 1 prior hormonal treatment but no more than 1 course of chemotherapy in the metastatic setting, tumor tissue from a biopsy or archival tissue available, bone-only nonmeasurable disease or measurable disease by RECIST 1.1, adequate organ function as shown by biomarkers in blood samples, Eastern Cooperative Oncology Group performance status 0 or 1, and no concurrent hormone replacement therapy. Participants were randomized 1:1 to receive 9 or 18 mg of enobosarm orally per day for up to 24 mo. Enobosarm specifically binds androgen receptors to promote agonist activity in ER+ breast cancer. Participants did not receive any hormonal therapy for the treatment of breast cancer other than the study drug on trial.

### [$^{18}$F]FDHT PET/CT Imaging

[$^{18}$F]FDHT PET/CT scans were obtained before the start of SARM therapy (study time-point 0 [S0]) and at 42 ± 7 d (study time-point 1 [S1]) and 84 ± 7 d (study time-point 2 [S2]) after starting SARM therapy.

Whole-body PET/CT images were acquired from the mid-thigh through the vertex of the skull starting at 52 ± 6 min after intravenous administration of 310 ± 29 MBq (8.4 ± 0.8 mCi) of [$^{18}$F]FDHT. [$^{18}$F]FDHT was manufactured at the Brigham and Women's Nuclear Medicine/Biomedical Imaging Research Core under investigational-new-drug application 122,852 using methods previously described (*12,13*). No patient preparation was required before the administration of [$^{18}$F]FDHT. Participants were instructed to void before the start of PET/CT imaging.

All PET/CT images were acquired on GE Healthcare Discovery ST and Discovery MI scanners. PET emission data were acquired for 4 min per bed position in 3-dimensional acquisition mode with 23% overlap between bed positions. The PET images were reconstructed using ordered-subsets expectation maximization (OSEM) iterative reconstruction algorithms with corrections for attenuation, scatter, detector normalization, dead time, and the radioactive decay between the start and end of the PET imaging. PET reconstruction parameters were harmonized between the PET/CT scanners by imaging a phantom containing cylinders 12, 16, and 25 mm in diameter and an activity concentration ratio of 2.5 relative to the phantom background. The reconstruction parameters for each scanner were selected so that the mean pixel value in the background was with ±5% of the activity concentration in the phantom background and the interscanner difference in the mean pixel values in the cylinders was within ±1 SD times the standard deviation measured in the background.

The reconstructed PET image voxel values were converted to SUV, calculated as …

$$\mathrm{SUV} = \frac{[A]}{A_0} \times \text{body weight}_{\text{subject}} \times 1,000, \qquad \text{Eq. 1}$$

where $A_0$ was the administered activity, $[A]$ was activity concentration per gram measured in the image voxels and corrected for the radioactive decay that occurred since the time of administration, body $\text{weight}_{\text{subject}}$ was the weight of the participant in kilograms, and 1,000 was the constant to convert weight in kilograms to grams.

Low-dose CT images were acquired immediately before the PET acquisition on the PET/CT scanner and used for attenuation and scatter corrections and for anatomic localization of the organs in the PET/CT images during image analysis.

### Image Analysis

Organ dose and effective dose calculations were performed using MIRDcalc software, version 1.1 (*14*), with time-integrated activity coefficients derived from [$^{18}$F]FDHT PET/CT images. Time-integrated activity coefficients were calculated using an exponential decay model and the [$^{18}$F]FDHT activity measured in source organs and regions in the PET/CT images (*10,15*). The source organs for [$^{18}$F]FDHT dosimetry were the cerebellum, kidneys, liver, lungs, and spleen, and source regions were the remaining whole body, left ventricle blood pool, and red bone marrow.

The fraction of administered activity retained within organs at the time of imaging was …

$$\frac{A_{\text{organ}}}{A_0} = \frac{[A]_{\text{organ}}}{A_0} \times \text{mass}_{\text{organ}} \times \frac{\text{body weight}_{\text{subject}}}{58}, \qquad \text{Eq. 2}$$

where $[A]_{\text{organ}}$ was mean activity concentration measured in a volume of interest (VOI) within the organ corrected for radioactive decay that occurred since the time of administration, and $\text{mass}_{\text{organ}}$ was the reference organ mass in grams for the reference adult female. The body weight for the reference adult female phantom was 58 kg (*16*). Direct image-based measurements of organ masses were not feasible because of the low contrast resolution of attenuation correction CT. Therefore, masses were estimated by scaling the reference mass of the organ by the ratio of the mass of the participant and the mass of the reference adult female.

The relationship between SUV and activity concentration was shown in Equation 1, and by substituting Equation 1 into Equation 2, the fraction of the administered activity in the organ was calculated as …

$$\frac{A_{\text{organ}}}{A_0} = \frac{\mathrm{SUV}_{\text{organ}}}{1,000} \times \frac{\text{mass}_{\text{organ}}}{58}, \qquad \text{Eq. 3}$$

where $\mathrm{SUV}_{\text{organ}}$ was the $\mathrm{SUV}_{\text{mean}}$ measured in the VOIs within the organ.

The $\mathrm{SUV}_{\text{mean}}$ was measured for VOIs within the whole body, cerebellum, kidneys, liver, lungs, and spleen on the [$^{18}$F]FDHT PET/CT images. The $\mathrm{SUV}_{\text{mean}}$ of heart chamber contents was also measured for a VOI within the left ventricle. The fraction of activity retained in these organs at the time of imaging was then calculated using Equation 3. The diameters of the VOI spheres were

1 cm in the cerebellum, 1.5 cm in the kidneys, 2 cm in the spleen and left ventricle blood pool, and 3 cm in the liver and lungs.

For 10 participants without bone disease, the fraction of activity in the red bone marrow was estimated using quantitative imaging as recommended by the 2010 European Association of Nuclear Medicine Dosimetry Committee (*17*). The fraction of activity in the red marrow was calculated as …

$$\frac{A_{\text{bone marrow}}}{A_0} = \frac{\text{SUV}_{\text{marrow}}}{1,000} \times \frac{\text{mass}_{\text{marrow}}}{58}, \quad \text{Eq. 4}$$

where $\text{SUV}_{\text{marrow}}$ was $\text{SUV}_{\text{mean}}$ in a spheric VOI 2 cm in diameter within a lumbar vertebral body and $\text{mass}_{\text{marrow}}$ was reference mass in grams for red marrow in the reference adult female.

For the participant with bone disease, the fraction of activity in the red bone marrow was estimated using the blood activity method (*17*), assuming no uptake in blood cells and assuming equilibrium between blood plasma and red marrow extracellular space. Therefore, the fraction of activity in the red marrow was calculated as …

$$\frac{A_{\text{bone marrow}}}{A_0} = \frac{\text{SUV}_{\text{blood}}}{1,000} \times \frac{\text{mass}_{\text{marrow}}}{58} \times \frac{\text{RMECFF}}{(1-\text{HCT})}, \quad \text{Eq. 5}$$

where $\text{SUV}_{\text{blood}}$ was $\text{SUV}_{\text{mean}}$ in a cylindric VOI of 1-cm diameter and 5-slice or about 2 cm height within the descending aorta in the thorax. RMECFF was the red marrow extracellular fluid fraction, HCT was the hematocrit, and (1 − HCT) was the proportion of blood volume that was plasma. RMECFF and HCT reference values in women were 0.19 and 0.47, respectively (*17,18*).

For the 10 participants without bone disease, bone marrow activity was also estimated using $\text{SUV}_{\text{blood}}$ and Equation 5 at S0, S1, and S2. Statistical analysis was then performed to test for significant differences in the 28 paired datasets of $\frac{A_{\text{bone marrow}}}{A_0}$ estimated from the blood pool using Equation 5 versus directly measured from the vertebral body using Equation 4.

The fraction of activity retained within the whole body, $\frac{A_{\text{whole body}}}{A_0}$, was determined by substituting reference organ mass in Equation 3 with the reference body weight, 58,000 g, which reduced the calculation to …

$$\frac{A_{\text{whole body}}}{A_0} = \text{SUV}_{\text{whole body}}, \quad \text{Eq. 6}$$

where $\text{SUV}_{\text{whole body}}$ was the $\text{SUV}_{\text{mean}}$ within a VOI around all parts of the body within the image. In Equation 6, whole-body activity, including arms and legs outside the image, was estimated by scaling the mean activity sampled by the VOI to the total mass of the participant.

[$^{18}$F]FDHT activity was removed from the body only through radioactive decay and urinary excretion during the time between radiopharmaceutical administration and PET/CT imaging. Removal of [$^{18}$F]FDHT from the body by urinary excretion was modeled using a monoexponential decay function, $A_{\text{whole body}} = A_0 \times e^{\ln(2)/T_{\text{biol}} \times \Delta t}$. Therefore, the biologic half-life of [$^{18}$F]FDHT, $T_{\text{biol}}$, was calculated as …

$$T_{\text{biol}} = \frac{-\ln(2)}{\ln\left(\frac{A_{\text{whole body}}}{A_0}\right)} \times \Delta t, \quad \text{Eq. 7}$$

where $\frac{A_{\text{whole body}}}{A_0}$ was calculated using Equation 6, and $\Delta t$ was the time between radiopharmaceutical administration and imaging.

The time-integrated activity coefficient in an organ, $\tilde{a}_{\text{organ}}$, represents the cumulative number of $^{18}$F radioactive decays occurring per unit activity of [$^{18}$F]FDHT during the time the activity remains in the organ. For this study, the $\tilde{a}_{\text{organ}}$ values for the cerebellum, left ventricle heart blood pool, kidneys, liver, lungs, and spleen were calculated as …

$$\tilde{a}_{\text{organ}} = \frac{A_{\text{organ}}}{A_0} * \frac{T_{\text{phy}}}{\ln(2)}, \quad \text{Eq. 8}$$

conservatively estimating monoexponential clearance of activity by radioactive decay only, where $T_{\text{phy}}$ was the half-life of physical radioactive decay for $^{18}$F and $\frac{A_{\text{organ}}}{A_0}$ was calculated using Equation 3.

Time-integrated activity coefficient in the red bone marrow, $\tilde{a}_{\text{bone marrow}}$, was calculated using Equation 8 with $\frac{A_{\text{organ}}}{A_0} = \frac{A_{\text{bone marrow}}}{A_0}$, where $\frac{A_{\text{bone marrow}}}{A_0}$ was derived using Equation 4 for the 10 participants without bone disease and Equation 5 for the participant with bone disease.

The time-integrated activity coefficient of urinary bladder contents, $\tilde{a}_{\text{excr}}$, was calculated using the dynamic bladder tool in the OLINDA/EXM software (*19*) with a urinary bladder voiding time of 2 h. For the dynamic bladder model, $T_{\text{biol}}$ values from Equation 7 were the rate constant for urinary elimination, and the fraction of activity excreted via the urinary bladder was estimated as the fraction of activity not in the liver at the time of imaging, $1 - A_{\text{liver}}$.

The time-integrated activity coefficient in the remaining body tissues and organs was calculated as …

$$\tilde{a}_{\text{remainder}} = \left(1 - \sum \frac{A_{\text{organ}}}{A_0}\right) \times \frac{T_{\text{phy}}}{\ln(2)} - \tilde{a}_{\text{excr}}, \quad \text{Eq. 9}$$

where $\sum \frac{A_{\text{organ}}}{A_0}$ was the sum of the fractions of activity calculated using Equation 3 in cerebellum, left ventricle chamber contents, kidneys, liver, lungs, spleen, and Equation 4 or Equation 5 in red bone marrow, and $\tilde{a}_{\text{excr}}$ for urinary bladder contents had been calculated by the dynamic bladder model.

## RESULTS

### [$^{18}$F]FDHT Biodistribution

Eleven women, with a median age 59 y (range, 47–73 y), were enrolled in the [$^{18}$F]FDHT PET/CT imaging substudy. Nine participants were imaged at all 3 time points, whereas 2 participants were imaged only at S0 and S1. PET/CT images in Figure 1 show the typical biodistribution of [$^{18}$F]FDHT, and Table 1 presents averages of $\text{SUV}_{\text{organ}}$ measurements in the 11 participants.

As shown in Figure 1, blood-pool activity within the circulatory system remained higher than in surrounding muscle at 52 ± 6 min after administration of [$^{18}$F]FDHT. Uptake was highest within the liver, spleen, and kidneys and in the gallbladder and urinary bladder, indicating gastrointestinal and urinary excretion of the radiopharmaceutical.

PET/CT images showed no changes in the visual appearance of the [$^{18}$F]FDHT biodistribution at S1 and S2, compared with S0. However, $\text{SUV}_{\text{organ}}$ measurements revealed a statistically significant decrease in liver uptake from S0 to S1 and S2 (linear mixed model, $P < 0.05$), as shown in Figure 2 and Table 1. A statistically significant decrease in SUV was also found for the aorta blood pool at S1 (linear mixed model, $P < 0.05$). Other than liver and aorta blood pool, no other source organs or regions showed significant changes in $\text{SUV}_{\text{organ}}$ measurements at S1 or S2 compared with S0 (linear mixed model, $P \geq 0.05$).

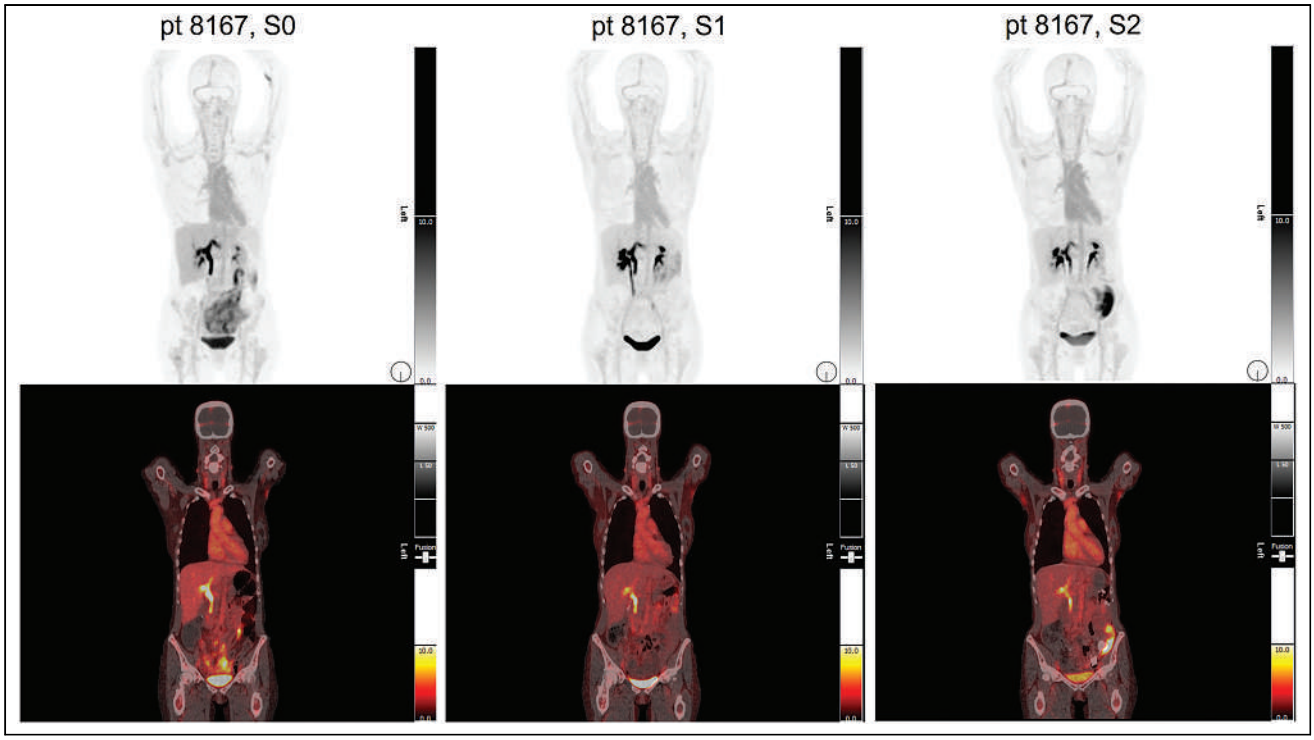


**FIGURE 1.** Biodistribution in typical female participant at 52 ± 6 min after administration of [$^{18}$F]FDHT. Figure shows PET/CT images of participant with breast cancer imaged at S0, S1, and S2. At top are maximum-intensity projection images, and at bottom are coronal PET/CT images at level of gallbladder and bile duct.

Two participants had a prior history of cholecystectomy. Of the 9 participants with gallbladders, gastrointestinal accumulation of radioactivity was seen in the gallbladder and bile ducts at one or more of the imaging time points for 8 participants, whereas 5 participants showed gallbladder uptake at all 3 time points. Gastrointestinal excretion of activity into the large intestines was not yet observed at the time of imaging.

Urinary excretion was seen as activity in the renal pelvis draining into the ureters, and accumulation in the urinary bladder at the time of imaging, for all participants at all 3 time points. Participants were instructed to empty their urinary bladder before the PET/CT imaging. However, the amount of activity remaining within the urinary bladder in the images was visibly much greater than in the blood pool and varied among participants.

### Dosimetry

There was no significant difference among the 28 paired data points of the fraction of activity in the red marrow, estimated from aorta blood-pool VOIs and Equation 5 versus lumbar spine VOIs and Equation 4 (2-tailed paired $t$ test, $P = 0.6$).

Table 1 shows averages of the $SUV_{organ}$ measurements in source organs and regions from the [$^{18}$F]FDHT PET/CT images at each of the 3 time points. Time-integrated activity

**TABLE 1**
Intersubject Averages of $SUV_{organ}$ Measurements from [$^{18}$F]FDHT PET/CT Images in 11 Women with Breast Cancer at S0, S1, and S2

| | S0 | | S1 | | S2 | |
|---|---|---|---|---|---|---|
| Organ | Mean | SD | Mean | SD | Mean | SD |
| Aorta blood pool | 4.8 | 0.7 | 4.4 | 0.4 | 4.6 | 0.5 |
| Lumbar vertebral body | 1.7 | 0.9 | 1.7 | 0.4 | 1.8 | 0.3 |
| Cerebellum | 0.29 | 0.07 | 0.32 | 0.05 | 0.30 | 0.05 |
| Left ventricle blood pool | 4.9 | 0.6 | 4.5 | 0.3 | 4.7 | 0.5 |
| Kidneys | 3.7 | 0.6 | 3.6 | 0.4 | 3.6 | 0.4 |
| Liver | 3.8 | 0.5 | 2.9 | 0.4 | 2.9 | 0.6 |
| Lungs | 0.85 | 0.22 | 0.82 | 0.21 | 0.77 | 0.18 |
| Spleen | 2.3 | 0.3 | 2.2 | 0.2 | 2.3 | 0.3 |
| Whole body | 0.80 | 0.06 | 0.77 | 0.07 | 0.79 | 0.05 |

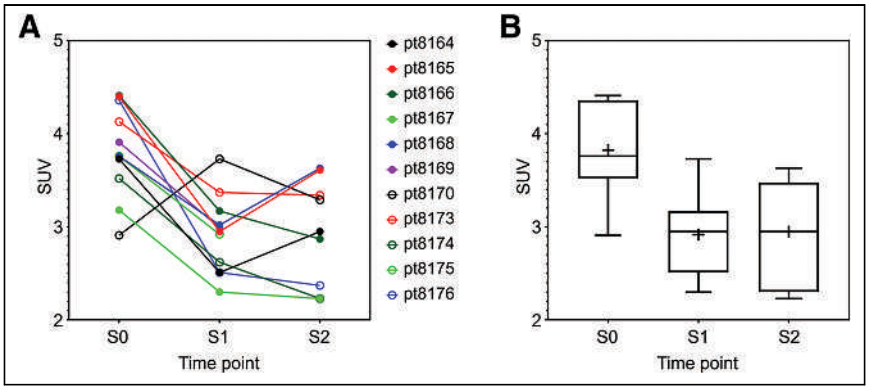


**FIGURE 2.** [$^{18}$F]FDHT $SUV_{organ}$ measurements in liver of women with breast cancer at S0, S1, and S2. (Left) Spaghetti plot showing changes in measurements in individuals across all time points. (Right) Box plot showing median, interquartile range, and mean (+) of measurements over the 11 participants at each time point. Linear mixed model analysis found statistically significant decrease in uptake in individual participants at S1 compared with S0 ($P < 0.05$) and no statistically significant change between S1 and S2 ($P = 0.87$). pt = patient.

coefficients derived from these $SUV_{organ}$ measurements are in the supplemental materials to this article (available at http://jnmt.snmjournals.org). Table 2 shows the resulting absorbed doses to target organs and the effective doses calculated at S0. The results for S1 and S2 are also in the supplemental materials.

Absorbed doses calculated for the liver showed decreases at S1 and S2 compared with S0 that were found to be statistically significant (linear mixed model, $P < 0.05$). There were also statistically significant decreases in absorbed dose at S1 and S2 (linear mixed model, $P < 0.05$) for the gallbladder wall, stomach, pancreas, and adrenals, which are located very close to the liver. Absorbed doses calculated for breast tissue, heart wall, and total body showed small but statistically significant decreases at S1 only (linear mixed model, $P < 0.05$). However, the absorbed dose calculated for colon showed small but statistically significant increases at S1 only (linear mixed model, $P < 0.05$). No other organs or tissues showed statistically significant changes in absorbed doses compared with S0 (linear mixed model, $P \geq 0.05$).

The urinary bladder remained the organ at risk at all 3 time points. Although the absorbed dose to the urinary bladder wall showed small increases at S1 and S2, the changes were not statistically significant (linear mixed model, $P \geq 0.05$). Likewise, the effective doses calculated at S1 and S2

**TABLE 2**
[$^{18}$F]FDHT Radiation Dosimetry in Women with Breast Cancer at S0: Absorbed Dose in Target Organ at S0

| | Absorbed dose (mGy/MBq) | | |
|---|---|---|---|
| Target organ | Mean | SD | SD (%) |
| Adrenals | 2.3E−02 | 1.3E−03 | 5% |
| Bone (endosteal cells) | 1.4E−02 | 1.6E−03 | 11% |
| Bone marrow (red, active) | 2.1E−02 | 3.9E−03 | 19% |
| Brain | 5.3E−03 | 6.8E−04 | 13% |
| Breast tissue | 1.2E−02 | 3.0E−04 | 3% |
| Colon | 1.7E−02 | 6.5E−04 | 4% |
| Extrathoracic region | 8.0E−03 | 3.0E−04 | 4% |
| Gallbladder wall | 2.5E−02 | 1.7E−03 | 7% |
| Heart wall | 2.1E−02 | 1.2E−03 | 6% |
| Kidneys | 3.4E−02 | 3.8E−03 | 11% |
| Liver | 3.7E−02 | 3.9E−03 | 11% |
| Lung | 1.5E−02 | 1.8E−03 | 12% |
| Lymphatic nodes | 1.6E−02 | 7.0E−05 | 0% |
| Muscle | 1.3E−02 | 1.8E−04 | 1% |
| Ovaries | 2.6E−02 | 2.0E−03 | 7% |
| Pancreas | 1.9E−02 | 6.9E−04 | 4% |
| Skin | 9.1E−03 | 1.7E−04 | 2% |
| Small intestine | 1.9E−02 | 7.0E−04 | 4% |
| Spleen | 2.4E−02 | 2.2E−03 | 9% |
| Stomach | 1.6E−02 | 6.4E−04 | 4% |
| Thymus | 1.4E−02 | 5.9E−04 | 4% |
| Thyroid | 1.2E−02 | 4.0E−04 | 3% |
| Urinary bladder wall | 7.4E−02 | 1.1E−02 | 15% |
| Uterus | 3.8E−02 | 4.0E−03 | 11% |
| Total body | 1.3E−02 | 1.5E−04 | 1% |
| Effective dose (mSv/MBq) | 2.0E−02 | 5.0E−04 | 2% |

did not show statistically significant changes from S0 (linear mixed model, $P \geq 0.05$).

The S0 values may be used as the reference values for absorbed dose in organs and the effective dose from [$^{18}$F]FDHT in women, to eliminate the effect of SARM therapy on [$^{18}$F]FDHT biodistribution. At S0, the effective dose was calculated as $0.020 \pm 0.0005$ mSv/MBq, and the urinary bladder was the organ at risk, with an average absorbed dose of $0.074 \pm 0.011$ mGy/MBq.

## DISCUSSION

The liver plays a role in the metabolism of exogenous dihydrotestosterone androgen (*20–22*), and enobosarm is eliminated primarily through the hepatobiliary route (*22*). Our study found that [$^{18}$F]FDHT SUV measured in liver significantly decreased over the course of SARM treatment from S0 to S1 and from S0 to S2, and the absorbed dose calculated to the liver also decreased. It is plausible that the change in uptake reflects the interaction of SARM therapy on androgen receptors in the liver; however, the complex mechanism by which SARM therapy affected the uptake in the liver and other normal tissues in not yet known.

Before the start of SARM therapy, the effective dose of [$^{18}$F]FDHT was $0.020 \pm 0.001$ mSv/MBq in women with breast cancer, which is comparable to the $0.017 \pm 0.002$ mSv/MBq effective dose equivalent reported for men with prostate cancer (*10*), although the organ-weighting factors used for calculation of effective dose and effective dose equivalent are different. The organ at risk was the urinary bladder wall. The absorbed dose to the urinary bladder wall, $0.074 \pm 0.011$ mGy/MBq in women with breast cancer, was comparable to the published value of $0.087 \pm 0.048$ mGy/MBq in men with prostate cancer (*10*). The absorbed doses to the other organs in this study of women were generally 2 times higher than the previously published dosimetry in men with prostate cancer. A small increase of 10%–20% in organ doses is expected because of differences in organ masses and dose conversion S factors for the adult female versus adult male phantom. However, differences in phantom geometry and the S factors used in the dosimetry software versions can account for larger differences in organ dose calculations.

A limitation of this work is extrapolation of pharmacokinetics based on a single image acquired at approximately 1 h after administration of the [$^{18}$F]FDHT. The biologic half-life due to urinary elimination of [$^{18}$F]FDHT was then estimated using a 1-compartment model and the VOI measurements of the whole body at that time point. This calculation assumed that the fraction of administered activity that was not in the image had been eliminated through physical decay of the radioactivity and by urinary excretion only. This was a reasonable assumption, since gastrointestinal transit times in adults from the liver to the large intestines are on the order of 3–4 h. Urinary excretion was also assumed to have a single rate constant during the lifetime of the radiopharmaceutical within the body, which was a reasonable assumption for the short-lived $^{18}$F radioisotope.

For the participant with metastatic bone involvement, the bone marrow dosimetry was based on image-derived whole-blood activity concentrations with an assumption that there was no uptake in red blood cells and equilibrium between plasma and the marrow extracellular space. This assumption would hold for intact [$^{18}$F]FDHT, which should behave like androgens and remain in plasma. However, $^{18}$F ions could be taken up by red blood cells. The presence of free $^{18}$F ions from defluorinated [$^{18}$F]FDHT is documented in the literature in mouse and baboon prostate cancer models (*1,2*). Beattie et al. also showed that the activity concentration of [$^{18}$F]FDHT metabolites in blood samples, from a group of 13 men with prostate cancer, exceeded the activity concentration of whole [$^{18}$F]FDHT within the first 10 min after administration (*11*). Blood sampling studies in female populations are needed to derive more accurate red marrow–to–blood activity concentration ratios for [$^{18}$F]FDHT, accounting for uptake of $^{18}$F ions in the blood cells and changes in the ratios over time.

Another limitation is that the number of participants included in the [$^{18}$F]FDHT PET/CT imaging substudy was small and the study sample was limited to postmenopausal women with known breast cancer. As such, further research with larger sample sizes is needed to investigate if the dosimetry calculated in this sample accurately represents the average dose in women.

This article focused on normal-tissue dosimetry and not tumor dosimetry. Therefore, [$^{18}$F]FDHT uptake in androgen receptor–positive tumors was not evaluated as separate source regions but was combined into the total-body measurements. Additionally, calculations of the time-integrated activity coefficients in this and other works use the assumption of instantaneous uptake within the organs immediately after administration and trapping with no washout of activity over time. This assumption overestimates the time-integrated activity coefficients. The Beattie et al. study of [$^{18}$F]FDHT pharmacokinetics found that uptake within prostate tumors plateaued at 20 min (*11*). However, similar investigations of [$^{18}$F]FDHT pharmacokinetics in organs are needed and will allow improved accuracy for future dosimetry studies.

## CONCLUSION

Whole-body and organ radiation dosimetry from [$^{18}$F]FDHT in women with breast cancer was comparable to the reported dose in men with prostate cancer. The effective dose in the women with breast cancer was $0.020 \pm 0.0005$ mSv/MBq. The urinary bladder was the organ at risk, with an absorbed dose of $0.074 \pm 0.011$ mGy/MBq to the urinary bladder wall.

## DISCLOSURE

Research funding was provided in part by GTx, Inc. Heather Jacene has received honoraria from Munrol; research

support to the institution from Siemens Healthcare, Inc., GTx, Inc., and Blue Earth Diagnostics; consulting fees from Advanced Accelerator Applications and Munrol; royalties from Cambridge Publishing; and NIH/NCI grant support not related to this work as coinvestigator (1R01CA235589-01A1). Beth Overmoyer has received clinical trial support from Genentech, Incyte, GTx, Inc., and Eisai. Annick Van den Abbeele has received a NCI National Comprehensive Cancer Center grant (Dana-Farber/Harvard Cancer Center 2 P30 CA006516-52; principle investigator, Laurie Glimcher) as the co–principle investigator in the Tumor Imaging Metrics Core; is an unpaid board member of the Centre for Probe Development and Commercialization (CPDC), Toronto, Canada; is an unpaid consultant to Fusion Pharmaceuticals and Bristol-Myers Squibb; has received travel expenses from Ipsen, ImaginAb, and CPDC to attend investigators' or board meetings; and has received royalties from Thieme Publishers as the textbook coeditor of *Case-Based Nuclear Medicine*, second edition. Diane Young and Mayzie Johnston were employees of GTx, Inc. No other potential conflict of interest relevant to this article was reported.

## ACKNOWLEDGMENT

We thank Pat Zanzonico, PhD, for his expertise in reviewing and editing the manuscript.

## KEY POINTS

**QUESTION:** What is the biodistribution of [$^{18}$F]FDHT in women, and what are the doses to organs and the effective dose in women per unit activity of [$^{18}$F]FDHT?

**PERTINENT FINDINGS:** This work investigated the biodistribution, organ dose, and effective dose of [$^{18}$F]FDHT in women. Eleven women with metastatic breast cancer receiving selective androgen receptor modulation therapy on a therapeutic trial were enrolled in this prospective imaging substudy of [$^{18}$F]FDHT.

**IMPLICATIONS FOR PATIENT CARE:** The biodistribution and dosimetry of [$^{18}$F]FDHT indicate that it may be used in androgen receptor PET/CT imaging of women.

## REFERENCES

1. Liu A, Dence CS, Welch MJ, Katzenellenbogen JA. Fluorine-18-labeled androgens: radiochemical synthesis and tissue distribution studies on six fluorine-substituted androgens, potential imaging agents for prostatic cancer. *J Nucl Med.* 1992;33:724–734.
2. Bonasera TA, O'Neil JP, Xu M, et al. Preclinical evaluation of fluorine-18-labeled androgen receptor ligands in baboons. *J Nucl Med.* 1996;37:1009–1015.
3. Dehdashti F, Picus J, Michalski JM, et al. Positron tomographic assessment of androgen receptors in prostatic carcinoma. *Eur J Nucl Med Mol Imaging.* 2005;32:344–350.
4. Larson SM, Morris M, Gunther I, et al. Tumor localization of 16β-$^{18}$F-fluoro-5α-dihydrotestosterone versus $^{18}$F-FDG in patients with progressive, metastatic prostate cancer. *J Nucl Med.* 2004;45:366–373.
5. Scher HI, Beer TM, Higano CS, et al. Antitumour activity of MDV3100 in castration-resistant prostate cancer: a phase 1–2 study. *Lancet.* 2010;375:1437–1446.
6. Venema CM, Mammatas LH, Schröder CP, et al. Androgen and estrogen receptor imaging in metastatic breast cancer patients as a surrogate for tissue biopsies. *J Nucl Med.* 2017;58:1906–1912.
7. Jacene H, Liu M, Cheng SC, et al. Imaging androgen receptors in breast cancer with $^{18}$F-fluoro-5α-dihydrotestosterone PET: a pilot study. *J Nucl Med.* 2022;63:22–28.
8. Overmoyer B, Rugo HS, Johnston S, et al. First stage of an on-going phase 2, open label, international, randomized, parallel design study investigating efficacy + safety of GTx-024 for advanced ER+/AR+ breast cancer (BC). *Ann Oncol.* 2017; 28:i7–i8.
9. Palmieri C, Linden HM, Birrell S, et al. Efficacy of enobosarm, a selective androgen receptor (AR) targeting agent, correlates with the degree of AR positivity in advanced AR+/estrogen receptor (ER)+ breast cancer in an international phase 2 clinical study [abstract]. *J Clin Oncol.* 2021;39(suppl 15):1020.
10. Zanzonico PB, Finn R, Pentlow KS, et al. PET-based radiation dosimetry in man of $^{18}$F-fluorodihydrotestosterone, a new radiotracer for imaging prostate cancer. *J Nucl Med.* 2004;45:1966–1971.
11. Beattie BJ, Smith-Jones PM, Jhanwar YS, et al. Pharmacokinetic assessment of the uptake of 16β-$^{18}$F-fluoro-5α-dihydrotestosterone (FDHT) in prostate tumors as measured by PET. *J Nucl Med.* 2010;51:183–192.
12. Ackermann U, Lewis JS, Young K, et al. Fully automated synthesis of [$^{18}$F]fluorodihydrotestosterone ([$^{18}$F]FDHT) using the FlexLab module. *J Labelled Comp Radiopharm.* 2016;59:424–428.
13. Mori T, Kiyono Y, Asai T, et al. Automated synthesis of 16β-[$^{18}$F]fluoro-5α-dihydrotestosterone using a plastic cassette-type FDG synthesizer [abstract]. *J Nucl Med.* 2010;51(suppl 2):1525.
14. Kesner A, Olguin E, Zanzonico P, Bolch W. MIRDCalc V 1.0: a community spreadsheet tool for organ-level radiopharmaceutical absorbed dose calculations [abstract]. *J Nucl Med.* 2018;59(suppl 1):473.
15. Madsen MT, Menda Y, O'Dorisio TM, O'Dorisio MS. Technical note: single time point dose estimate for exponential clearance. *Med Phys.* 2018;45:2318–2324.
16. Snyder WS, Cook MJ, Masset ES, Karhausen LR, Parry Howells G, Tipton IH. *Report of the Task Group on Reference Man: A Report Prepared by a Task Group of Committee 2 of the International Commission on Radiological Protection—ICRP Publication 23.* Pergamon Press; 1975.
17. Hindorf C, Glatting G, Chiesa C, Lindén O, Flux G. EANM dosimetry committee guidelines for bone marrow and whole-body dosimetry. *Eur J Nucl Med Mol Imaging.* 2010;37:1238–1250.
18. Sgouros G. Bone marrow dosimetry for radioimmunotherapy: theoretical considerations. *J Nucl Med.* 1993;34:689–694.
19. Stabin MG, Sparks RB, Crowe E. OLINDA/EXM: The second-generation personal computer software for internal dose assessment in nuclear medicine. *J Nucl Med.* 2005;46:1023–1027.
20. Pirog EC, Collins DC. Metabolism of dihydrotestosterone in human liver: importance of 3α- and 3β-hydroxysteroid dehydrogenase. *J Clin Endocrinol Metab.* 1999;84:3217–3221.
21. Marchetti PM, Barth JH. Clinical biochemistry of dihydrotestosterone. *Ann Clin Biochem.* 2013;50:95–107.
22. Kim J, Wang R, Veverka KA, Dalton JT. Absorption, distribution, metabolism and excretion of the novel SARM GTx-024 [(*S*)-*N*-(4-cyano-3-(trifluoromethyl)phenyl)-3-(4-cyanophenoxy)-2-hydroxy-2-methylpropanamide] in rats. *Xenobiotica.* 2013;43:993–1009.

# Patient Preparation with Esomeprazole Is Comparable to Ranitidine in Meckel Diverticulum Scintigraphy

Tessa F. Ververs[1,2], Anne-Fleur H. Lobbezoo[3], Monique G. Hobbelink[1], and Arthur J. Braat[1]

*[1]Department of Radiology and Nuclear Medicine, University Medical Center Utrecht, Utrecht, The Netherlands; [2]Department of Clinical Pharmacy, University Medical Centre Utrecht, Utrecht, The Netherlands; and [3]Department of Clinical Pharmacy, St. Antonius Hospital, Nieuwegein, The Netherlands*

To localize ectopic gastric mucosa in patients with unexplained gastrointestinal bleeding and diagnose a Meckel diverticulum, $^{99m}$Tc-pertechnetate imaging is the standard procedure. H2 inhibitor pretreatment enhances the sensitivity of the scan by reducing washout of $^{99m}$Tc activity from the intestinal lumen. We aim to provide evidence of the effectiveness of the proton pump inhibitor esomeprazole as an ideal substitute for ranitidine. **Methods:** The scan quality for 142 patients who underwent a Meckel scan during a period of 10 y was evaluated. The patients were pretreated with ranitidine orally or intravenously before a switch to a proton pump inhibitor after ranitidine was no longer available. Good scan quality was characterized by the absence of $^{99m}$Tc-pertechnetate activity in the gastrointestinal lumen. The effectiveness of esomeprazole to diminish $^{99m}$Tc-pertechnetate release was compared with the standard treatment using ranitidine. **Results:** Pretreatment with intravenous esomeprazole resulted in 48% of scans with no $^{99m}$Tc-pertechnetate release, 17% with release either in the intestine or in the duodenum, and 35% with $^{99m}$Tc-pertechnetate activity both in the intestine and in the duodenum. Evaluation of scans obtained after oral ranitidine and intravenous ranitidine showed absence of activity in both intestine and duodenum in 16% and 23% of the cases, respectively. The indicated time to administer esomeprazole before starting the scan procedure was 30 min, but a delay of 15 min did not negatively influence the scan quality. **Conclusion:** This study confirms that esomeprazole, 40 mg, when administered intravenously 30 min before a Meckel scan, enhances the scan quality comparably to ranitidine. This procedure can be incorporated into protocols.

**Key Words:** Meckel diverticulum; $^{99m}$Tc-pertechnetate scintigraphy; ectopic gastric mucosa; esomeprazole; ranitidine

**J Nucl Med Technol 2023; 51:211–214**
DOI: 10.2967/jnmt.123.265558

Meckel diverticulum, the most common gastrointestinal congenital anomaly, is located predominantly in the lower part of the ileum. The condition occurs in 2%–3% of the population (*1*). Although most cases of Meckel diverticulum remain asymptomatic, 15% lead to complications including hemorrhage, diverticulitis, obstruction, or perforation (*1*). Hemorrhage is usually caused by ulceration of the bowel wall because of ectopic gastric mucosa in the Meckel diverticulum and requires surgical intervention (*1,2*).

The specificity of a Meckel scan in detecting ectopic gastric mucosa is well established (95%–100%). Sensitivity may vary and depends partly on the amount of ectopic tissue (*3*). Excessive excretion of $^{99m}$Tc-pertechnetate from the gastric mucosal tissue in the gastrointestinal lumen may interfere with the detection of ectopic gastric mucosa. H2 receptor antagonists increase the sensitivity of the Meckel scan by preventing release of $^{99m}$Tc-pertechnetate from mucous cells in the stomach and ectopic gastric mucosa and therefore enhancing visualization of anomalies (*3,4*). It is thought that inhibition of acid secretion inhibits the release of radioactivity in the lumen as well, resulting in reduced risk of a false-negative or false-positive diagnosis (*4*). The use of H2 antagonists such as cimetidine and ranitidine was included in the Society of Nuclear Medicine and Molecular Imaging and European Association of Nuclear Medicine practice guideline for Meckel diverticulum scintigraphy (*5*).

However, this practice had to be altered when the supply of H2 antagonists ran dry after the recall of ranitidine from the European market in October 2019 in response to possible contamination with *N*-nitrosodimethylamine (*6,7*). With the assumption that any systemic antacid could serve as an alternative, proton pump inhibitors (PPIs) were proposed (*5*). Since esomeprazole is widely used in standard care for numerous conditions, we considered this PPI a practical alternative to ranitidine (*8*). Moreover its favorable pharmacokinetics and rapid onset after intravenous injection make esomeprazole an ideal candidate to replace H2 inhibitors (*8–10*). However, the effectiveness of esomeprazole in enhancing Meckel scan quality has yet to be established. The aim of this study was to determine whether esomeprazole is as effective as ranitidine when used in the prescan procedure.

## MATERIALS AND METHODS

All patients who had a Meckel scan in our hospital between January 2012 and September 2022 were retrospectively included. Demographic data, including age at presentation and sex, were recorded, as well as details on prescan medication (time between administration of the antacid and the scan, interfering medication,

Received Feb. 10, 2023; revision accepted Apr. 20, 2023.
For correspondence or reprints, contact Tessa F. Ververs (f.f.t.ververs@umcutrecht.nl).
Published online Jun. 14, 2023.

**TABLE 1**
Premedication Protocols Adjusted to Age and Weight

| Medication | 1–12 y, <20 kg | 1–12 y, >20 kg | >12 y | Administration before scan |
|---|---|---|---|---|
| Oral ranitidine oral | 3 mg/kg | 3 mg/kg; maximum, 150 mg | 150 mg | Twice daily, starting 1 d before scan; last dose, morning before scan |
| Intravenous ranitidine | 1 mg/kg | 1 mg/kg; maximum, 50 mg | 50 mg | 15 min before scan |
| Intravenous esomeprazole | 10 mg | 20 mg | 40 mg | 30 min before scan |

dose and administration route) and amount of $^{99m}$Tc-pertechnetate activity. All positive Meckel scans were followed by surgical resection, and data on the histopathology results were collected. Patients were excluded if data on prescan medication were missing or if records mentioned antacid comedication during pretreatment. Patients who received esomeprazole in addition to PPI treatment were evaluated separately. The study was approved by the Medical Research Ethics Committee Utrecht, and the need for written informed consent was waived.

$^{99m}$Tc-pertechnetate scans were performed according to the practice guideline (*5*). The prescan procedure was performed with ranitidine twice a day orally 2 d before the scan (up till 2014), ranitidine intravenously 15 min before the scan (2014–2019), or esomeprazole intravenously 30 min before the scan (2019 till the present) (Table 1). The oral dose, 3 mg/kg, in our protocol originated from Dutch Society of Nuclear Medicine national guidelines for scintigraphy of ectopic gastric mucosa. Patients were not allowed to eat or drink 4 h before the scan. Barium contrast imaging or colonoscopy was deferred 3 d before the Meckel scan. $^{99m}$Tc-pertechnetate, 20–200 MBq, was administered intravenously according to the European Association of Nuclear Medicine pediatric dosage card 2016 (*11*). Patients were positioned supine with the abdomen to the symphysis in the field of view. Dynamic anterior and posterior abdominal images were obtained during 45 min, as 90 frames of 30 s each. Additional static images were obtained after voiding to detect activity in a Meckel diverticulum obscured by the bladder (2 min/image). If it was difficult to distinguish activity in the ureter from a Meckel diverticulum, furosemide could be administered. A SPECT/CT scan could be added at the discretion of the nuclear medicine physician on call, to specify the anatomic localization of a Meckel diverticulum.

Scan quality was independently assessed by 2 experienced nuclear medicine physicians (each with >10 y of experience) masked to the patient's medical information. The scans were scored according to intestinal activity visualization (absence, activity in the duodenum, or activity in the intestine). The quality was considered good if no $^{99m}$Tc-pertechnetate activity was seen in either the duodenal or the intestinal lumen. Interobserver agreement was calculated using the κ-score. Discrepancies between readers were highlighted, and a final score was defined during a consensus reading.

The scan quality after esomeprazole prescan treatment was compared with that after oral or intravenous ranitidine. Enhanced scan quality was reported as the absence of activity in the lumen of the intestine and duodenum. To analyze the difference in scan quality between the esomeprazole pretreated group and the 2 ranitidine groups, the $\chi^2$ test was used, with a $P$ value of less than 0.05 being considered a significant difference.

## RESULTS

Between January 2012 and September 2022, 183 patients had a Meckel scan. Scans containing missing data regarding the prescan procedure were excluded ($n = 19$), as were cases for which—besides ranitidine—antacids such as PPIs were coadministered ($n = 18$). Scans from patients who received esomeprazole in addition to an oral PPI regimen were evaluated separately ($n = 4$).

Of the 142 included patients, age varied between 0.5 and 51 y (mean, 11 y); 51% were male ($n = 72$), and 49% were female ($n = 70$). Unexplained abdominal pain, lower-intestine hemorrhage, or both were indications for admission. Ranitidine as a pretreatment procedure had been received by 117 patients. Nineteen of these received a dosage of 3 mg/kg or 150 mg orally 2 times daily starting 1 d before the scan. The other 98 received 1 mg/kg or 50 mg intravenously 15 min before the scan. Twenty-five patients were pretreated with a PPI, and 23 patients were treated with 10–40 mg of esomeprazole intravenously 30 min before the scan. Two patients who were on pantoprazole did not receive additional pretreatment. Four patients received esomeprazole, 10–40 mg intravenously, in addition to

**TABLE 2**
Meckel Scan Quality After Antacid Pretreatment

| Observed $^{99m}$Tc-pertechnetate release | Oral ranitidine, 18–150 mg, $n = 19$ | Intravenous ranitidine*, 5–62 mg, $n = 98$ | Intravenous esomeprazole*, 10–40 mg, $n = 23$ |
|---|---|---|---|
| Absent in duodenal and intestinal lumen | 3 | 23 | 11 |
| Activity in duodenal or intestinal lumen | 3 | 13 | 4 |
| Activity in both duodenal and intestinal lumen | 13 | 62 | 8 |

*Esomeprazole resulted in significantly better scan quality than intravenous ranitidine ($P = 0.034$).

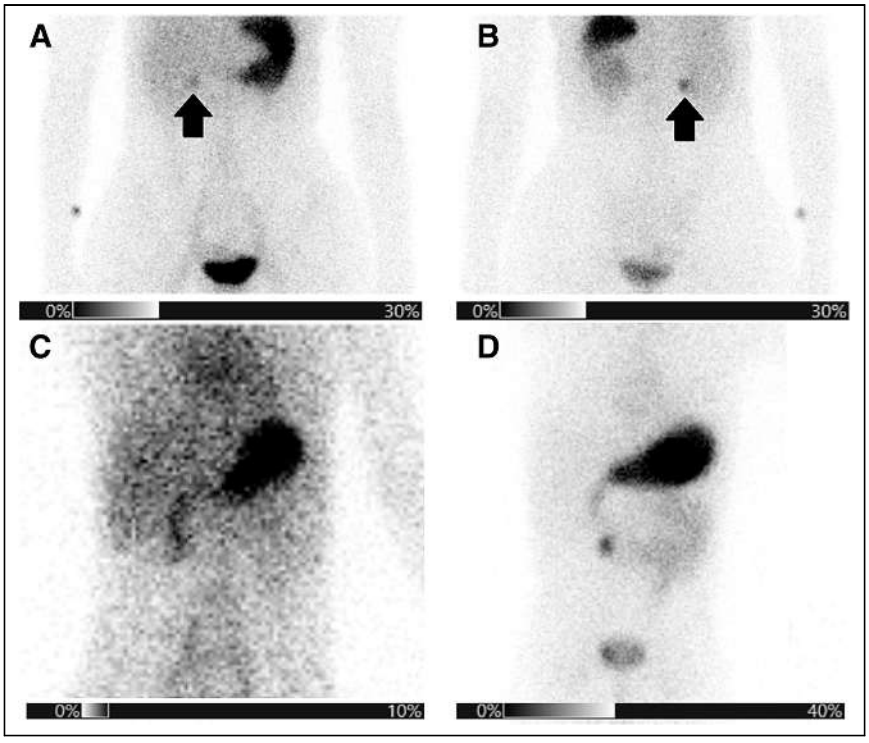


**FIGURE 1.** Examples of static images 30 min after injection. (A) Normal Meckel scan with adequate inhibition (arrow) of $^{99m}$Tc excretion. (B) The only unexpected hot spot (arrow) in abdomen was stasis of urine in prominent renal pelvis, as confirmed on posterior static image. (C) Accumulation of $^{99m}$Tc in gastric mucosa and minor excretion in duodenum. (D) Clear luminal activity in both duodenum and intestine.

oral omeprazole 20–40 mg 1–2 daily or esomeprazole 20–40 mg 1–2 daily.

Each scan was assessed for the absence or presence of activity in the duodenal lumen, in the lumen of the intestine, or both (Table 2). Interobserver agreement was 92%, with a κ of 0.83 for the assessment of intestinal $^{99m}$Tc release and 0.85 for the estimation of activity in the duodenum.

After oral administration of ranitidine (18–150 mg twice daily), starting the day before the scan and ending with the last dose on the morning before the scan, $^{99m}$Tc-pertechnetate release was absent in 3 of 19 (16%) patients, whereas 13 (68%) scans showed activity in both the duodenal and the intestinal lumen.

After patient preparation using intravenous ranitidine, 23 of 98 (23%) scans showed no released activity and 62 (63%) showed $^{99m}$Tc activity in both the duodenum and the intestine.

Eleven of the 23 scans (48%) obtained after intravenous esomeprazole showed no activity in the intestinal lumen, and 8 scans (35%) showed activity in both the duodenal and the intestinal lumen (Fig. 1). Absence of activity was seen significantly more often after intravenous esomeprazole premedication than after intravenous ranitidine ($P$ = 0.034). When absence of activity in the duodenal and intestinal lumen was compared with activity in the duodenal or intestinal lumen, esomeprazole significantly more often showed absence of background noise caused by $^{99m}$Tc-petechnetate excretion than did oral ranitidine ($P$ = 0.014) or intravenous ranitidine ($P$ = 0.019).

The scans of 2 patients who received solely pantoprazole as part of their standard-care treatment (without additional intravenous esomeprazole) showed activity in both the duodenum and the intestine. No luminal $^{99m}$Tc activity was observed in any of the 4 patients who received esomeprazole in addition to their standard-care PPI treatment.

The time lapse between esomeprazole administration and scan onset was recorded for 20 patients. Most frequently, pretreatment was administered 30 min before the start of scanning (48%). In another 6 patients (26%), scanning started within 45 min before administration of esomeprazole. Figure 2 shows $^{99m}$Tc activity in the duodenal or intestinal lumen after esomeprazole administration in relation to the time between administration and the start of the scan. The scans of patients who were treated outside the time window of 30–45 min showed $^{99m}$Tc-pertechnetate excretion in the duodenum, intestine, or both. In 9% ($n$ = 13) of the patients, a Meckel diverticulum was detected. In all 13 patients, pathology confirmed the presence of ectopic gastric tissue.

## DISCUSSION

After H2 blockers were recalled from the market in 2019, pretreatment with intravenous esomeprazole was implemented in our hospital because of its favorable pharmacokinetics, short time of onset, and well-established efficiency and safety in

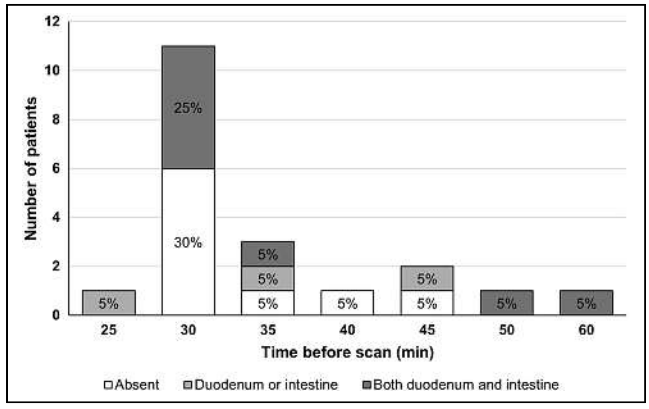


**FIGURE 2.** Absence of $^{99m}$Tc activity release, activity detected in duodenal or intestinal lumen or both during Meckel scan, and time between esomeprazole administration and start of scan.

children (*8*). Our study covering 10 y of Meckel scans showed that neither ranitidine nor esomeprazole could prevent all cases of $^{99m}$Tc-pertechnetate release but that esomeprazole better suppressed activity release in the duodenum and the intestine (48% vs. 23%; $P = 0.034$). Interobserver agreement was excellent. The difference in performance between the H2 blocker and the PPIs can be explained by ranitidine's lower potency as far as gastric acid inhibition is concerned (*12,13*). The effect of oral PPI pretreatment could not be evaluated since only one patient could be included. Moreover, an oral regimen 24–48 h before the scan may give rise to large variations, including interpatient differences in time between last administration of medication and start of scan, as well as malabsorption or low compliance, which can be expected in small children whose caretakers are responsible for administering oral medication. Intravenous administration of esomeprazole in patients who already require an intravenous cannula for $^{99m}$Tc-pertechnetate is not considered a major intervention.

The fixed time of 30 min before esomeprazole administration was chosen on theoretic grounds and available pharmacokinetic data, but our results indicate that 30–45 min may be more practical. Our findings did not support a time exceeding 50 or 60 min, nor did we find evidence that starting the scan earlier than 30 min after PPI administration will lead to a scan of sufficient quality.

The prevalence of Meckel diverticulum in our population (9%) is consisted with earlier findings with a corresponding specificity of 100% in diagnosing ectopic gastric tissue (*1,14*).

Because of the unavailability of ranitidine, a head-to-head study design was not opportune. Thus, the next best design was a retrospective comparative study using documented data in which scans were simultaneously reassessed by 2 independent nuclear medicine physicians. Whether an oral regimen of omeprazole or pantoprazole medication would enhance the scan quality to a comparable extent cannot be concluded from our data ($n = 2$) or from the 4 patients who received intravenous esomeprazole premedication in addition to an oral PPI. Nevertheless, until more data are available, we recommend intravenous esomeprazole premedication 30–45 min before image acquisition along with antacid comedication, as adherence to any oral regimen is difficult to confirm and, moreover, no adverse effects are expected of a 1-time doubled dose of PPI (*8*).

## CONCLUSION

Intravenous esomeprazole pretreatment outperforms ranitidine in inhibiting gastrointestinal release of $^{99m}$Tc-pertechnetate during Meckel diverticulum scintigraphy. Additionally, intravenous administration of esomeprazole holds several advantages over oral administration. such as a fast onset of effect and applicability in small children.

## DISCLOSURE

No potential conflict of interest relevant to this article was reported.

## KEY POINTS

**QUESTION:** Is pretreatment using a PPI as effective as ranitidine in inhibiting gastrointestinal $^{99m}$Tc-pertechnetate release in Meckel scan scintigraphy?

**PERTINENT FINDINGS:** Esomeprazole was found to suppress $^{99m}$Tc-pertechnetate excretion comparably to ranitidine. The scan quality was significantly more often better using esomeprazole than ranitidine.

**IMPLICATIONS FOR PATIENT CARE:** The current findings will enable clinicians to replace—on the basis of scientific findings rather than theoretic assumptions—intravenous esomeprazole, 30–45 min before the scan, with ranitidine in patient preparation protocols.

## REFERENCES


1. Irvine I, Doherty A, Hayes R. Bleeding Meckel's diverticulum: a study of the accuracy of pertechnetate scintigraphy as a diagnostic tool. *Eur J Radiol.* 2017;96:27–30.
2. Farrell MB, Zimmerman J. Meckel's diverticulum imaging. *J Nucl Med Technol.* 2020;48:210–213.
3. Rerksuppaphol S, Hutson JM, Oliver MR. Ranitidine-enhanced 99m technetium pertechnetate imaging in children improves the sensitivity of identifying heterotopic gastric mucosa in Meckel's diverticulum. *Pediatr Surg Int.* 2004;20:323–325.
4. Diamond RH, Rothstein RD, Alavi A. The role of cimetidine-enhanced technetium-99m-pertechnetate imaging for visualizing Meckel's diverticulum. *J Nucl Med.* 1991;32:1422–1424.
5. Spottswood SE, Pfluger T, Bartold SP, et al. SNMMI and EANM practice guideline for Meckel diverticulum scintigraphy 2.0. *J Nucl Med Technol.* 2014;42:163–169.
6. Aschenbrenner DS. Ranitidine withdrawn from the market. *Am J Nurs.* 2020;120:23.
7. White CM. Understanding and preventing (N-nitrosodimethylamine) NDMA contamination of medications. *Ann Pharmacother.* 2020;54:611–614.
8. Ward RM, Kearns GL. Proton pump inhibitors in pediatrics: mechanism of action, pharmacokinetics, pharmacogenetics, and pharmacodynamics. *Paediatr Drugs.* 2013;15:119–131.
9. Metz DC, Fulda GJ, Olsen KM, Monyak JT, Simonson SG, Sostek MB. Intravenous esomeprazole pharmacodynamics in critically ill patients. *Curr Med Res Opin.* 2010;26:1141–1148.
10. Wilder-Smith C, Röhss K, Bondarov P, et al. Intravenous esomeprazole 40mg is effective for the control of intragastric acid levels whether given as a 3-minute injection or a 30-minute infusion. *Clin Drug Investig.* 2005;25:517–525.
11. Lassmann M, Treves ST. Paediatric radiopharmaceutical administration: harmonization of the 2007 EANM paediatric dosage card (version 1.5.2008) and the 2010 North American consensus guidelines. *Eur J Nucl Med Mol Imaging.* 2014;41:1036–1041.
12. Ruth M, Enbom H, Lundell L, Lönroth H, Sandberg N, Sandmark S. The effect of omeprazole or ranitidine treatment on 24-hour esophageal acidity in patients with reflux esophagitis. *Scand J Gastroenterol.* 1988;23:1141–1146.
13. Hirschowitz BI, Keeling D, Lewin M, et al. Pharmacological aspects of acid secretion. *Dig Dis Sci.* 1995;40(suppl):3S–23S.
14. Jaramillo C, Jensen MK, McClain A, Stoddard G, Barnhart D, Ermarth AK. Clinical diagnostic predictive score for Meckel diverticulum. *J Pediatr Surg.* 2021;56:1673–1677.

# α-Labeling of J591, an Antibody Targeting Prostate-Specific Membrane Antigen: The Technique and Considerations from the First Dedicated Production Lab at an Academic Institution in the United States

Kritika Subramanian[1], Judith Stangl-Kremser[2], Lady Sawoszczyk[1], Vasilios Avlonitis[1], Andrew Gernerd[1], Kyla Nixon[1], Michael Zgaljardic[3], Scott Tagawa[4], Neil Bander[2], and Joseph R. Osborne[1]

*[1]Division of Molecular Imaging and Therapeutics, Department of Radiology, Weill Cornell Medicine, New York, New York; [2]Department of Urology, Weill Cornell Medicine, New York, New York; [3]Department of Medical Health Physics, Weill Cornell Medicine, New York, New York; and [4]Division of Medical Oncology, Department of Oncology, Weill Cornell Medicine, New York, New York*

The protein expression of the prostate-specific membrane antigen correlates with unfavorable or aggressive histologic features of prostate cancer, resulting in use as a diagnostic PET imaging radiotracer and therapeutic target. Here, we discuss the methods to develop $^{225}$Ac-DOTA-J591, an α-labeled compound targeting an extracellular epitope of prostate-specific membrane antigen, which is currently being studied in early clinical trials. In addition, we review quality control, radiation safety measures, and clinical considerations before administration of this radioimmunotherapeutic agent.

**Key Words:** radiochemistry; radionuclide therapy; radiopharmaceuticals; $^{225}$Ac; PSMA; α-particle

**J Nucl Med Technol 2023; 51:215–219**
DOI: 10.2967/jnmt.122.265166

Prostate-specific membrane antigen (PSMA) is a multifunctional transmembrane protein expressed on the surface of prostate cancer cells. Protein expression levels are higher in poorly differentiated carcinomas and metastases (*1–3*). Receptor binding induces internalization of the ligand into the tumor cell (*4*). Hence, PSMA is an optimal target for both prostate cancer imaging and therapeutic intervention. At our institution, we have an investigational-new-drug application (application 11,613) for radiolabeled J591 with β-emitters. This humanized monoclonal antibody (mAb) has been demonstrated to be safe and efficacious in phase I and II clinical trials (NCT001950039 and NCT03276572) (*5–8*). To date, the only Food and Drug Administration–approved PSMA-targeted therapy is $^{177}$Lu-vipivotide tetraxetan (Pluvicto; Advanced Accelerator Applications) as third-line therapy for metastatic castration-resistant prostate cancer (*9*).

Unlike β-emitters, α-emitters characterized by high energy (5–9 MeV) (*10*) and a short pathlength (50–100 mm (*10*) and ~100 μm in tissue (*11*)) have demonstrated anticancer potential by reducing tumor burden and serum prostate-specific antigen levels (*12–15*). The prototypical α-emitting particle used for radiotherapeutics is $^{225}$Ac, which has a half-life of 10 d (*10*).

Currently, a phase I dose-escalation trial of $^{225}$Ac-DOTA-J591 in patients with metastatic castration-resistant prostate cancer is under way (*7*), with promising preliminary results (*7,8*). In this work, we present methods for producing this radioimmunotherapeutic, particularly in the context of implementation in the first dedicated α-labeling lab at an academic institution. We discuss technical and production details, quality control tests, radiation safety measures, and therapeutic administration considerations.

## TECHNICAL AND PRODUCTION DETAILS

### Biochemistry of $^{225}$Ac-DOTA-HuJ591

In essence, HuJ591 is conjugated with a DOTA bifunctional chelating agent that undergoes radiolabeling with $^{225}$Ac-nitrate. This IgG1 with humanized $V_H$ and $V_L$ regions specifically targets the extracellular domain of PSMA. $^{225}$Ac-DOTA-HuJ591 has a molecular weight of about 147 kDa and is formulated as a single-dose intravenous injection in a sterile, pyrogen-free isotonic saline solution.

### Production Assembly Steps

A 37 MBq (1.0 mCi) activity of $^{225}$Ac-nitrate residue is supplied in a 2-mL glass vial (Department of Energy, Oak Ridge National Laboratory). Figure 1 summarizes the production assembly mechanism.

A 30-mL 10 durable grade (10 DG) desalting disposable column is washed twice with 15 mL of 3% hydrogen peroxide in a laminar flow hood. Thirty minutes later, the column is washed twice with 15 mL of sterile water for injection

Received Nov. 11, 2022; revision accepted Feb. 12, 2023.
For correspondence or reprints, contact Kritika Subramanian (krs9089@nyp.org).
Published online Apr. 25, 2023.

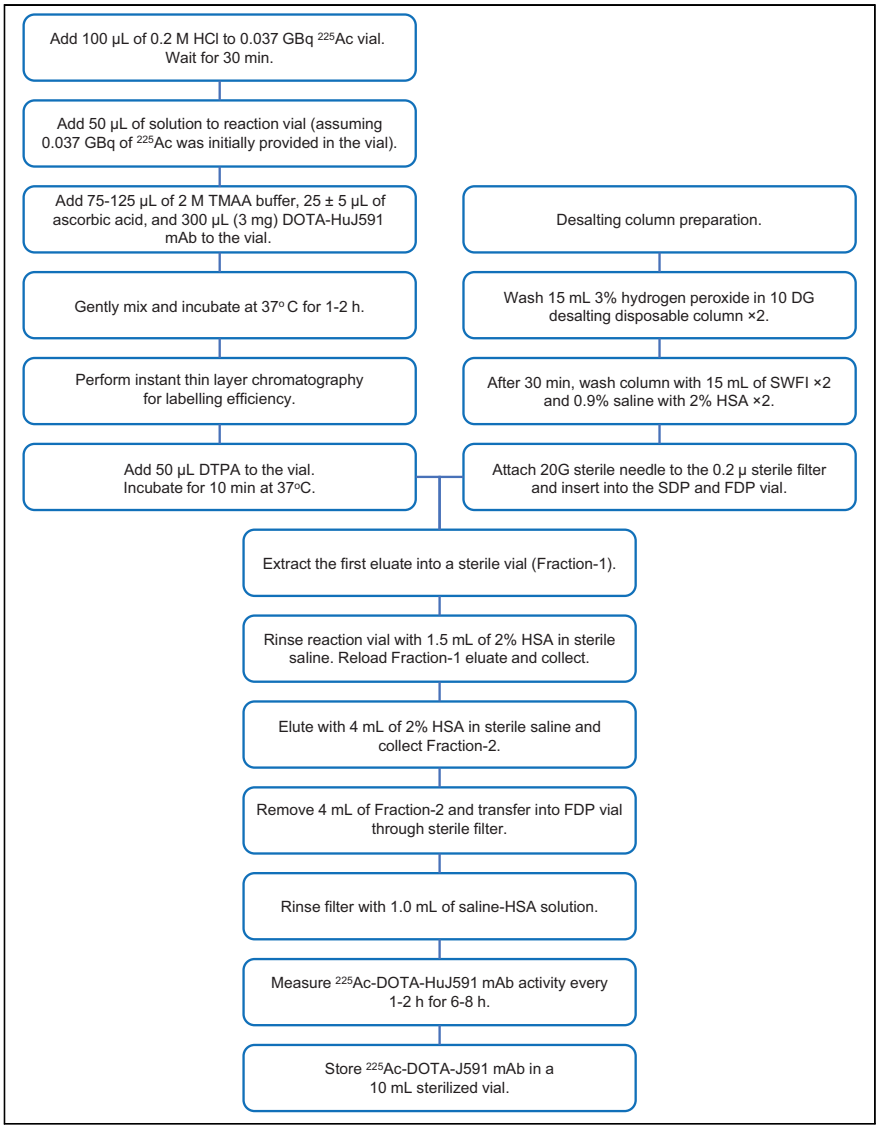


**FIGURE 1.** Steps for production assembly of $^{225}$Ac-J591. DG = durable grade; DTPA = diethylenetriaminepentaacetic acid; FDP = final drug product; HSA = human serum albumin; SDP = sterile drug product; SWFI = sterile water for injection; TMAA = triethylammonium acetate.

and twice with sterile 0.9% saline with 2% human serum albumin. This column is prepared for purification of the radiolabeled mAb. Within the same laminar flow hood, a 20-gauge sterile needle is attached to a 0.2-µm sterile filter and inserted into a pyrogen-free sterile drug product vial and the final drug product vial.

Using aseptic technique in a laminar flow hood, 100 µL of 0.2 M hydrogen chloride are added to the $^{225}$Ac vial for 30 min; 3,700–5,550 kBq (100–550 µCi) are removed and added to the reaction vial; and 75–125 µL of 2 M triethylammonium acetate buffer, 25 ± 5 µL of ascorbic acid, and 3 mg of DOTA-HuJ591 mAb (300 ± 15 µL) are subsequently added to the vial. The DOTA labeling of the HuJ591 mAb is performed at an outside facility. After gentle mixing of the vial, it is incubated at 37°C for 1–2 h. Instant thin-layer chromatography with silica gel is performed to determine labeling efficiency, which must be more than 50% to be acceptable for further processing.

Diethylenetriaminepentaacetic acid solution, 50 µL, is added to the vial and incubated for an additional 10 min at 37°C. The reaction mixture is loaded onto the prepared desalting column, and the eluate is collected into a sterile vial (fraction 1). The reaction vial is rinsed with 1.5 mL of 2% human serum albumin in sterile saline and reloaded in the column, and the eluate in the fraction 1 vial is collected. Fraction 2 is eluted with 4 mL of sterile saline with 2% human serum albumin into a sterile tube. Using a sterile syringe, 4 mL of fraction 2 are removed and transferred through a sterile filter into the final drug product vial. The filter is rinsed with 1.0 mL of saline–human serum albumin solution. The activity of $^{225}$Ac-DOTA-HuJ591 mAb over the next 6–8 h is measured at intervals of 1–2 h.

The $^{225}$Ac-DOTA-J591 mAb injection is stored in a 10-mL sterilized vial sealed with gray butyl rubber septa crimped closed with an aluminum stopper (Hollister Stier Laboratories or Allergy Laboratories) and certified as sterile and apyrogenic.

## QUALITY CONTROL AND QUALITY ASSURANCE TESTING

Each batch of the drug product produces 1–2 doses of $^{225}$Ac-DOTA-HuJ591 mAb injection. Before administration, several quality control and

**TABLE 1**
Acceptance Criteria for Batch Release

| Criteria | Values or range of acceptance |
|---|---|
| Appearance | Colorless, clear, free from particulate matter |
| Assay | 0.4–2.8 MBq (11–76 µCi)/mL |
| Specific activity | 0.67–4.67 MBq (18–126 µCi)/mg |
| pH | 5–8 |
| Radionuclide identity | 218 and 440 keV |
| Radiochemical purity | $^{225}$Ac-DOTA-J591 > 95% |
| Test for endotoxins | <35 endotoxin units/mL |
| Bubble test | $P_t > P_m$, where $P_m = \psi$ |
| Sterility test | Test started within 24 h |

$P_t$ = pressure at which bubbles appear; $P_m$ = minimum acceptable bubble point pressure; $\psi$ = pound-force per square inch.

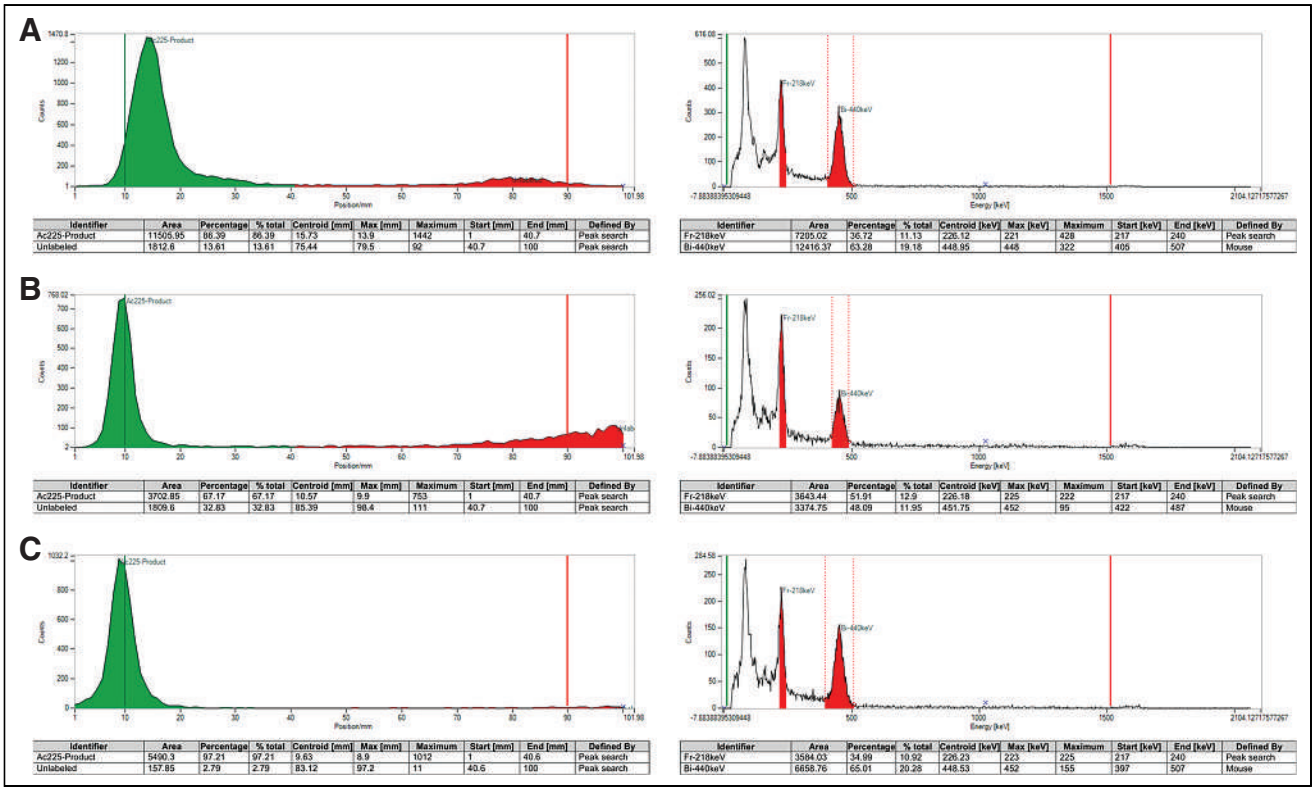


**FIGURE 2.** Labeling efficiency and radiochemical purity measured using instant thin-layer chromatography. (A) Labeling efficiency before ethylenediaminetetraacetic acid elusion, remarkable for high concentration of $^{225}$Ac bound to protein (green peak) and small percentage of unbound $^{225}$Ac, which has formed into daughter compounds of francium and bismuth (red peaks). (B and C) Radiochemical purity after ethylenediaminetetraacetic acid elusion at 2 h (B) and 24 h (C). Two hours after elusion, higher concentration of daughter compounds is noted whereas peak concentration of $^{225}$Ac bound to protein is stable. Because of shorter half-lives of daughter compounds, their presence is negligible at 24 h after elution, validating chemical purity of final product.

quality assurance tests are performed and assembled in a report to ensure that each batch meets the institutional acceptance criteria for batch release (Table 1).

The final drug product must be colorless after being swirled in the glass vial, suggesting no contamination. Instant thin-layer chromatography with silica gel and 10 mM ethylenediaminetetraacetic acid solution determines the radiochemical purity of the drug batch, which must be more than 95% (Fig. 2). The labeling efficiency before ethylenediaminetetraacetic acid elution is remarkable for a high concentration of $^{225}$Ac bound to protein and a small percentage of unbound $^{225}$Ac. Unbound $^{225}$Ac will decay to $^{218}$Fr and $^{440}$Bi daughter compounds, the greatest concentration of which appear at 2 h after elusion. Because of the shorter half-lives of the daughter compounds, their levels are negligible at 24 h after elusion. Figure 3 provides a schematic explanation of $^{225}$Ac decay.

The radionuclide concentration is measured with a dose calibrator. The pH is measured by placing 2–5 μL of aliquot on pH indicator paper. The specific activity is estimated through dose calibrator measurement of total activity relative to the 3 mg of the precursor DOTA-HuJ591 used. Endotoxin content is measured using the Endosafe-PTS system (Charles River) according to manufacturer's operation manual, with a goal of not exceeding 175 endotoxin units for the entire 5-mL batch of the final drug product (35 endotoxin units/mL) (Fig. 4).

The bubble point test in a nondestructive test evaluating filter integrity. It determines the minimum pressure required to force liquid out of the filter pores, which is an indirect way of measuring the pore diameter and, in essence, any defects in the filter that may permit bacterial penetration. The pressure at which bubbles appear must be greater than the minimum acceptable bubble point pressure as defined by the manufacturer. Fluid thioglycolate medium and soybean casein digest medium were used to evaluate the sterility of the injection drug product by transferring 0.1-mL samples of $^{225}$Ac-DOTA-J591 to the medium and incubating

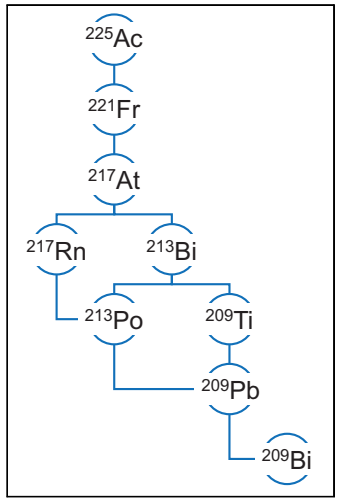


**FIGURE 3.** Schematic diagram of $^{225}$Ac decay and daughter compounds.

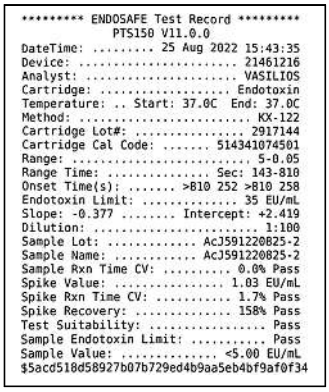

```
********* ENDOSAFE Test Record *********
          PTS150 V11.0.0
DateTime: ......... 25 Aug 2022 15:43:35
Device: ........................ 21461216
Analyst: ....................... VASILIOS
Cartridge: ..................... Endotoxin
Temperature: .. Start: 37.0C  End: 37.0C
Method: ........................ KX-122
Cartridge Lot#: ................ 2917144
Cartridge Cal Code: ....... 514341074501
Range: ......................... 5-0.05
Range Time: ..... Sec: 143-810
Onset Time(s): ....... >810 252 >810 258
Endotoxin Limit: ..... 35 EU/mL
Slope: -0.377 ....... Intercept: +2.419
Dilution: ..................... 1:100
Sample Lot: ..... AcJ591220825-2
Sample Name: ..... AcJ591220825-2
Sample Rxn Time CV: ..... 0.0% Pass
Spike Value: ..... 1.03 EU/mL
Spike Rxn Time CV: ..... 1.7% Pass
Spike Recovery: ..... 158% Pass
Test Suitability: ..... Pass
Sample Endotoxin Limit: ..... Pass
Sample Value: ..... <5.00 EU/mL
$5acd518d58927b07b729ed4b9aa5eb4bf9af0f34
```

**FIGURE 4.** Endosafe-PTS test record. Endotoxin content should demonstrate limit well within guidelines of 175 endotoxin units for entire batch, as demonstrated here. Cal = calibration; CV = coefficient of variation; Rxn = reaction; Sec = seconds.

either at 37°C (fluid thioglycolate medium) or at room temperature (soybean casein digest medium) up to 14 d. Growth in the medium through visual inspection is recorded on the third, seventh, and 14th days after culturing.

$^{225}$Ac-J591 can be stored at 4°C–8°C for up to 4 h after production, which also represents the time window for therapeutic use of the produced dose.

## RADIATION SAFETY

Lead-shielded waste containers and sharps disposal containers should be close to where the $^{225}$Ac work is performed. A spill kit must be present in the room. An absorbent pad must be placed under the production and distribution area for $^{225}$Ac, including the laminar hood and glove box. Gloves, booties, and gowns must be worn by staff during production. Gloves should be changed frequently and placed in a leaded waste container.

If the staff needs to leave the room, their feet and hands must be checked using a survey meter (e.g., Ludlum model 14C). Similarly, when tagging is complete, the hands, feet, and body of each individual need to be evaluated for radiation contamination. If there is evidence of contamination, the survey meter should be used to check the area. Also, equipment used for tagging must be checked for contamination after each use. If contamination is found, the area must be decontaminated and checked to ensure that radiation is at background levels. Additionally, a wipe test must be done weekly using a γ-counter following a survey map.

## THERAPEUTIC ADMINISTRATION CONSIDERATIONS

The equipment needed is a 50-mL 0.9% sterile sodium chloride infusion bag, sterile Alaris tubing intravenous sets (with a clamp to regulate or stop flow), two 3-way stopcocks, a spinal needle, an 18-gauge needle, a peristaltic infusion Alaris pump, and clamps. The spinal needle and 18-gauge needle are inserted into the therapeutic vial. The spinal needle is connected to intravenous tubing within the infusion pump. The output of the intravenous tubing is connected to a 3-way stopcock and then to the patient's intravenous line. The 18-gauge needle is connected to the 50-mL 0.9% sterile sodium chloride infusion bag via a 3-way stopcock (which remains clamped until the end of the infusion).

The pump is set to 250 mL/h at the beginning of the administration. Within 10 min, the therapy vial solution is nearly empty. A saline rinse is begun by unclamping the 50-mL 0.9% sterile sodium chloride infusion bag. The rinse helps remove the solution from the vial and all lines to optimize dose delivery by minimizing residual agents in the equipment.

## CLINICAL CONSIDERATIONS

Current guidelines require that individuals with metastatic castration-resistant prostate cancer who have refractory disease or are unwilling to undergo other commercially available prostate cancer therapies should be considered for experimental treatment with $^{225}$Ac-J591. $^{225}$Ac-J591 is metabolized by the liver, as well as excreted by the kidney and the bowel. Therefore, baseline serologies evaluating hepatic and renal function must be reviewed before administration of the radioimmunotherapeutic agent. Not much uptake is seen in the marrow by default, but it is imperative to also review blood counts. PSMA PET/CT imaging may also be used to evaluate the baseline tumor burden before administration of the $^{225}$Ac-J591 (45 kBq/kg). After the treatment course, currently performed at our institution as 2 sessions 6 wk apart, repeat imaging helps guide clinicians in planning further management (Fig. 5).

## DISCUSSION

In this paper we have explained an optimized technique that meets all federal recommendations and safety guidelines for producing $^{225}$Ac-DOTA-HuJ591 at an academic institution.

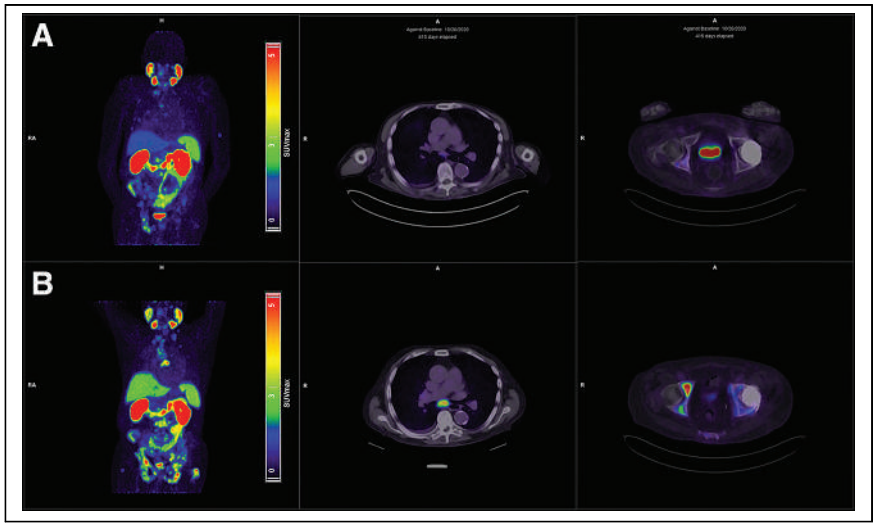


**FIGURE 5.** PSMA PET imaging demonstrating good response in this patients with metastatic castration-resistant prostate cancer at baseline (B) and after receiving 2 sessions of $^{225}$Ac-J591 (A). Marked decrease in metastatic disease burden is demonstrated in maximum-intensity-projection images, particularly in subcarinal lymph node (column 2) and osseous lesions (column 3).

In addition, we have discussed the clinical considerations before therapeutic administration. Multiple considerations involving safety precautions must be taken to ensure that radiation exposure to the staff is minimalized. In addition, several quality control tests must be performed on each production batch to ensure that there is no compromise in the quality of the radioimmunotherapeutic.

Numerous benefits are associated with the production of α-emitting radioligand therapy at the administering institution. There are no delays associated with outside manufacturing and delivery, thereby reducing logistic expenses. The measures for quality control indicated on the quality assurance reports are reassuring to the administering and treating physicians. Individuals may receive their therapeutic administration and subsequent imaging with a PSMA-bound PET tracer at the same institution, allowing for enhanced, personalized patient care.

Currently, our α-theranostics laboratory produces solely $^{225}$Ac-DOTA-HuJ591. However, with time, more actinium-bound radioligand therapies may be incorporated into the portfolio for application in a wider range of malignancies.

## CONCLUSION

This paper provides the assembly methods for local production of $^{225}$Ac-DOTA-HuJ591 at an academic institution, for which there are many considerations and advantages.

**KEY POINTS**

**QUESTION:** What are the considerations in developing an α-labeled compound targeting PSMA?

**PERTINENT FINDINGS:** This paper discusses quality control, radiation safety measures, and clinical considerations before administration of $^{225}$Ac-DOTA-HuJ591.

**IMPLICATIONS FOR PATIENT CARE:** Reduced logistic expenses and enhanced quality control measures by the administering institution reassure the treating physician and the patient on the quality of the radioimmunotherapeutic being administered. Imaging can also be performed at the same institution as the administration, enhancing patient care.

## DISCLOSURE

No potential conflict of interest relevant to this article was reported.


## ACKNOWLEDGMENTS

We thank Dr. Shankar Vallabhajosula for his guidance on developing the methods and implementing them at our institution.


## REFERENCES


1. Wright GL, Haley C, Beckett ML, Schellhammer PF. Expression of prostate-specific membrane antigen in normal, benign, and malignant prostate tissues. *Urol Oncol.* 1995;1:18–28.
2. Ross JS, Sheehan CE, Fisher HAG, et al. Correlation of primary tumor prostate-specific membrane antigen expression with disease recurrence in prostate cancer. *Clin Cancer Res.* 2003;9:6357–6362.
3. Sweat SD, Pacelli A, Murphy GP, Bostwick DG. Prostate-specific membrane antigen expression is greatest in prostate adenocarcinoma and lymph node metastases. *Urology.* 1998;52:637–640.
4. Liu H, Rajasekaran AK, Moy P, et al. Constitutive and antibody-induced internalization of prostate-specific membrane antigen. *Cancer Res.* 1998;58:4055–4060.
5. Bander NH, Milowsky MI, Nanus DM, Kostakoglu L, Vallabhajosula S, Goldsmith SJ. Phase I trial of $^{177}$lutetium-labeled J591, a monoclonal antibody to prostate-specific membrane antigen, in patients with androgen-independent prostate cancer. *J Clin Oncol.* 2005;23:4591–4601.
6. Tagawa ST, Milowsky MI, Morris M, et al. Phase II study of lutetium-177-labeled anti-prostate-specific membrane antigen monoclonal antibody J591 for metastatic castration-resistant prostate cancer. *Clin Cancer Res.* 2013;19:5182–5191.
7. Tagawa ST, Vallabhajosula S, Jhanwar Y, et al. Phase I dose-escalation study of $^{225}$Ac-J591 for progressive metastatic castration resistant prostate cancer (mCRPC) [abstract]. *J Clin Oncol.* 2018;36(suppl):TPS399.
8. Sun M, Nauseef JT, Lebenthal JM, et al. A phase I/II dose-escalation study of fractionated and multiple dose $^{225}$Ac-J591 for progressive metastatic castration-resistant prostate cancer (mCRPC) [abstract]. *J Clin Oncol.* 2021;39(suppl):TPS188.
9. Sartor O, de Bono J, Chi KN, et al. Lutetium-177–PSMA-617 for metastatic castration-resistant prostate cancer. *N Engl J Med.* 2021;385:1091–1103.
10. Poty S, Francesconi LC, McDevitt MR, Morris MJ, Lewis JS. α-emitters for radiotherapy: from basic radiochemistry to clinical studies—part 1. *J Nucl Med.* 2018; 59:878–884.
11. Elgqvist J, Frost S, Pouget J-P, Albertsson P. The potential and hurdles of targeted alpha therapy: clinical trials and beyond. *Front Oncol.* 2014;3:324.
12. Parker C, Nilsson S, Heinrich D, et al. Alpha emitter radium-223 and survival in metastatic prostate cancer. *N Engl J Med.* 2013;369:213–223.
13. Nilsson S, Franzén L, Parker C, et al. Bone-targeted radium-223 in symptomatic, hormone-refractory prostate cancer: a randomised, multicentre, placebo-controlled phase II study. *Lancet Oncol.* 2007;8:587–594.
14. Parker CC, Pascoe S, Chodacki A, et al. A randomized, double-blind, dose-finding, multicenter, phase 2 study of radium chloride (Ra 223) in patients with bone metastases and castration-resistant prostate cancer. *Eur Urol.* 2013;63:189–197.
15. Nilsson S, Strang P, Aksnes AK, et al. A randomized, dose–response, multicenter phase II study of radium-223 chloride for the palliation of painful bone metastases in patients with castration-resistant prostate cancer. *Eur J Cancer.* 2012;48: 678–686.

# Investigating a Technologist-Driven Injection Technique in Lymphoscintigraphy at a Single Rural Center: A Retrospective Audit

Skyla Bamforth[1], Daphne J. James[1], Christopher Skilton[2], and Anthony Smith[1]

[1]*School of Health Sciences, University of Newcastle, Callaghan, New South Wales, Australia; and* [2]*Hunter New England Imaging, Hunter New England Area Health Service, Newcastle, New South Wales, Australia*

Our aim was to investigate the effectiveness of the technologist-driven injection technique of lymphoscintigraphy used at a rural hospital in Australia to identify the correct lymph node for sentinel lymph node biopsy (SLNB) in early-stage breast cancer patients. **Methods:** A retrospective audit was conducted using imaging and medical record data from 145 eligible patients who underwent preoperative lymphoscintigraphy for SLNB at a single center throughout 2013 and 2014. The lymphoscintigraphy technique included a single periareolar injection with subsequent dynamic and static images as required. Descriptive statistics, sentinel node identification rates, and imaging–surgery concordance rates were generated from the data. Additionally, $\chi^2$ analysis was used to examine the relationships between age, previous surgical intervention, and injection site and time until a sentinel node is visualized. The technique and statistical results were directly compared against multiple similar studies in the literature. **Results:** The sentinel node identification rate was 99.3%, and the imaging–surgery concordance rate was 97.2%. The identification rate was significantly higher than those of similar studies in the literature, and concordance rates were similar across studies. The findings demonstrated that age ($P = 0.508$) and previous surgical intervention ($P = 0.966$) did not influence the time it takes to visualize a sentinel node. Injection site did appear to have a statistically significant effect ($P = 0.001$), with injections in the upper outer quadrant correlating with increased times between injection and visualization. **Conclusion:** The reported lymphoscintigraphy technique for identifying sentinel lymph nodes for SLNB in early-stage breast cancer patients can be justified as an accurate and effective method that is time-sensitive and has outcomes comparable to those of successful studies in the literature.

**Key Words:** nuclear medicine; lymphoscintigraphy; breast cancer; audit

**J Nucl Med Technol 2023; 51:220–226**
DOI: 10.2967/jnmt.123.265442

Breast cancer is the second most common type of cancer in Australia, with an estimated 20,000 new cases diagnosed annually (*1*). Nevertheless, it has a better prognosis than other forms of cancer, having mortality rates of as low as 2%–3% per annum, due to high early detection rates and the extensive treatment options available. Generally, the first sign of breast cancer is a palpable lump in the breast, sometimes accompanied by swelling, pain, redness, nipple inversion, or discharge. However, early-stage breast cancer (ESBC) can be asymptomatic. In Australia, more than 70% of newly diagnosed cases of breast cancer are in the early stage (0, I, or II), and ESBC has 5-y survival rates of 99% for stage I and 93% for stage II, highlighting the significance of early diagnosis and treatment (*2*). The typical diagnostic pathway after mammographic or physical identification of a suspected lesion involves ultrasonography of the breast and axillary lymph nodes, as well as biopsy of the lesion for histopathologic staging. This pathway may then progress to intervention with the addition of sentinel lymph node biopsy (SLNB).

Despite overwhelming positivity in the overall outlook on breast cancer in Australia, disparities still exist in the diagnostic and treatment experience of rural compared with urban patients. The disease burden is greater for those in rural and remote areas because of limited access to certain health services and time spent traveling to receive diagnosis and treatment (*3*). Many diagnostic tests and treatments for breast cancer require rural and remote Australians to travel to urban centers, incurring travel and accommodation costs in addition to the loss of time and separation from family. The burden of restricted access discourages and prevents many from receiving early, appropriate care. As a result, the risk of dying from breast cancer is over 10% higher for Australians who live outside urban locations (*3*).

## ROLE OF LYMPHOSCINTIGRAPHY IN BREAST CANCER MANAGEMENT

Lymphoscintigraphy is a nuclear medicine imaging technique that enables visualization of lymphatic drainage pathways. It involves the injection of a colloidal radiotracer at a point of interest and subsequent imaging using a γ-camera to visualize lymphatic vessel drainage and localize regional lymph nodes (*4*). Lymphoscintigraphy of the breast first appeared in the literature in the early 1980s, resulting in early descriptions of a "primary draining node" (*5*). This formed the basis for the development of sentinel node lymphoscintigraphy (SNLS): the

Received Jan. 10, 2023; revision accepted Mar. 7, 2023.
For correspondence or reprints, contact Daphne James (daphne.james@newcastle.edu.au).
Published online Jun. 14, 2023.

concept of identifying the first lymph node in the drainage channel (the sentinel node) from an area of malignancy. The use of preoperative SNLS for lymph node mapping was first introduced in 1993 to aid in SLNB in melanoma patients to assess stage III metastatic spread (*6*). Immediately after SNLS, the process involves the use of a handheld radiation detection device during surgery to locate the sentinel node for removal, often in conjunction with patent blue dye (*7*). This blue dye is injected during surgery to visually highlight lymphatic drainage channels and nodes for more precise removal. This process has since been adopted into the early management of breast cancer, allowing the identification and excision of axillary sentinel nodes. Excised nodes are then histologically examined for cancerous cells, and this information is used to guide the subsequent surgical management of breast cancer patients and assist in the staging and treatment process.

Before the introduction of SLNB, many ESBC patients underwent full axillary lymph node clearance to prevent metastatic spread. Although effective, the complete resection of the axillary nodes has the consequence of lymphoedema in the ipsilateral arm, which can cause subsequent discomfort, pain, and difficulty with venepuncture for the patient (*8*). By limiting the number of surgically removed nodes for histologic assessment, SLNB can provide effective management of ESBC patients with clinically negative nodes while reducing the risk of significant lymphoedema (*9*). This benefit is especially important in rural communities where specialized lymphoedema services may be less accessible for patients.

## CONTROVERSIES IN LYMPHOSCINTIGRAPHY

Over the past 3 decades, guidelines for performing lymphoscintigraphy have changed with the evolution of nuclear medicine technology and available radiopharmaceuticals. However, uncertainty around best practices in lymphoscintigraphy remains. The most recent guidelines for breast lymphoscintigraphy are those of the European Association of Nuclear Medicine (EANM) published in conjunction with the Society of Nuclear Medicine and Molecular Imaging (SNMMI) in 2013 (*10*). In addition to the age of the document, some sections provide merely a range of suggestions that leave ambiguity, which is unhelpful in the development of departmental protocols. A standardized SNLS procedure must, first and foremost, accurately identify the sentinel node for SLNB. An ideal protocol would meet this requirement while also providing fast visualization of nodes with minimal discomfort to the patient.

The ideal radiotracer for breast lymphoscintigraphy should have fast transit to the axillary nodes and prolonged nodal retention for imaging (*10*). Colloid particles labeled with $^{99m}$Tc-technetium are recommended in the EANM guidelines, including a mix of small and large particles for quick initial transit followed by extended nodal retention. The choice of radiopharmaceutical varies depending on local availability and legal regulations. At the time of data collection, $^{99m}$Tc-antimony trisulfide colloid was typically used in Australia because of its mean particle size of 3–30 nm (*10*). Activity and volume can vary, with 5–30 MBq suggested for same-day and 150 MBq for 2-d procedures (*10*). For superficial injections, no more than a 0.5-mL volume is advised, with a 1-mL maximum for peritumoral injections.

Possibly the most significant controversy in breast lymphoscintigraphy surrounds the method of administration of the radiopharmaceutical. The EANM and SNMMI guidelines list multiple possible injection techniques and suggest that 2 injections—both superficial and deep—could be complementary. However, the combined-injection technique is not always possible, as deep injections are difficult to perform and often require ultrasound guidance to avoid vascular damage and localized hemorrhage and to locate the lesion itself when it is not palpable. Superficial injections are less invasive and easier to perform, especially in the absence of a palpable mass (*10*). This consideration is particularly important for a rural center where there is limited access to an on-site physician and injections are piloted by nuclear medicine technologists.

There are a range of SNLS imaging techniques reported in the literature (*10*). The EANM and SNMMI provide imaging times, though protocols vary in the literature. Although delayed imaging may be useful in cases with slow transit or nonvisualization of nodes, delayed imaging does not generally contribute to the success of sentinel node identification. Rather, it leads to longer wait times, inconvenience, and increased costs (*11*). Additionally, SPECT/CT imaging can improve detection rates, better localize nodes, and clarify areas where there is ambiguity around drainage pathways (*12*).

## STUDY AIMS

There is a need for individual departments to develop protocols that confidently and accurately identify the sentinel node while considering time sensitivity and minimal invasiveness. In a rural nuclear medicine practice, where there is limited access to an on-site specialist nuclear medicine physician, generating confidence in the ability of a technologist-driven injection technique and standardized protocol is essential in the appropriate management of ESBC patients. Primarily, the aim of this study was to investigate the effectiveness of the technologist-driven injection technique and lymphoscintigraphy protocol that is used at Tamworth Rural Referral Hospital (TRRH) in New South Wales, Australia, in identifying the correct lymph node for SLNB in ESBC patients. Using retrospective analysis of patient data and imaging records, an audit was conducted measuring outcomes based on the identification of a sentinel node and concordance of imaging findings with SLNB after surgical excision among a cohort of ESBC patients who underwent SNLS at TRRH throughout 2013 and 2014. The secondary aims were to compare the findings with those for imaging protocols and techniques reported in the peer-reviewed literature and to assess the impact of specific variables on the time efficiency and success of this technique.

## MATERIALS AND METHODS

### Ethics

Ethical approval for this retrospective audit was considered by the Hunter New England Governance and Research Office but was waived because of the low and negligible risk, under the provision that patient data had been deidentified by a third party who was not directly associated with the research (authorization AU202104-04). The institutional review board (or equivalent) approved this retrospective study, and the requirement to obtain informed consent was waived.

### Setting and Study Population

With 282 beds, TRRH is the largest rural hospital in New South Wales outside the Newcastle–Sydney–Wollongong catchment (*13*). The study population included 204 ESBC patients who underwent lymphoscintigraphy for SLNB at TRRH from January 1, 2013, to December 31, 2014. These dates were chosen to allow for the simultaneous collection of 5 y of follow-up data on the same patients for a future study on their disease outcomes. Fifty-seven patients were excluded because of lack of access to surgical reports or limited reporting on concordance between marked nodes and excised nodes. The final sample size was 145 patients, whose demographic data can be reviewed in Table 1.

### Imaging Protocol and Technique

There is no set reference standard for comparison; however, the findings for the index test were compared with those of various methods reported in the literature. For the index test, lymphoscintigraphy was performed using a single intradermal periareolar injection of 40 MBq of $^{99m}$Tc-antimony trisulfide colloid in a 0.5-mL volume. Imaging was completed with Symbia T16 and E-Cam γ-cameras, both of which are manufactured by Siemens Medical Solutions in the United States. Dynamic imaging was acquired anteriorly immediately after injection at 2 s/frame for 150 frames (5 min) using a 128 × 128 matrix, followed by static imaging encompassing anterior and lateral views for 5 min each using a 256 × 256 matrix (Fig. 1). All patients underwent imaging using both views at 10–15 min and 30–35 min after injection. The patients were positioned supine, with the ipsilateral arm abducted. When drainage patterns were unclear, static imaging continued until the sentinel node was identified or ruled nonvascularized at a maximum imaging time of 180–210 min. Between each set of static images, patients with delayed drainage were instructed to sit up, walk around, or massage the breast to encourage tracer movement. SPECT/CT with both arms above the head was incorporated when node visualization was ambiguous. SPECT imaging was conducted at 15 s/view for 32 views with a 128 × 128 matrix. The CT parameters were set at 130 kVp, 60 reference mAs (Care Dose4D; Siemens), 3-cm slices, and a 1.5 pitch. Sentinel node identification was communicated to the surgeon by placing anterior and lateral marks on the skin, in addition to providing the images and distributing the report before surgery.

### Data Collection and Analysis

Data were collected retrospectively from the imaging results and reports, histopathology reports, surgical reports, and medical/imaging histories via electronic records. Key variables were collected around tumor characteristics, imaging technique, previous

**TABLE 1**
Descriptive, Technique-Related, and Surgical Follow-up Variables for Breast Cancer Cases in This Study

| Variable | Result |
|---|---|
| Age (y) | 64 (±11.9) |
| Female | 140 (97.2%) |
| Left-sided lesion | 77 (52.4%) |
| Lesion size (mm) | 18.6 (±12.7) |
| Lesion type | |
| IDC | 109 (75.2%) |
| ILC | 14 (9.7%) |
| DCIS | 8 (5.5%) |
| Other | 14 (9.7%) |
| Histologic grade | |
| 1 | 61 (42.1%) |
| 2 | 51 (35.2%) |
| 3 | 31 (21.4%) |
| Histologic type | |
| HR+ | 113 (77.9%) |
| HER2-enriched | 14 (9.7%) |
| Triple-negative | 9 (6.2%) |
| Unknown | 9 (6.2%) |
| Multicentric disease | 17 (13.1%) |
| Previous intervention | |
| Biopsy | 126 (86.9%) |
| WLE | 8 (5.5%) |
| Mastectomy | 1 (0.7%) |
| None | 3 (2.1%) |
| Unknown | 7 (4.8%) |
| Injection site by quadrant | |
| Upper outer | 64 (44.1%) |
| Upper inner | 37 (25.5%) |
| Lower outer | 29 (20%) |
| Lower inner | 14 (9.66%) |
| Retroareolar | 1 (0.7%) |
| Transit on flow | 100 (69%) |
| Time to first node, ≤30 min | 136 (93.8%) |
| Time of last image, ≤60 min | 134 (92.4%) |
| SPECT/CT | 18 (12.6%) |
| IMN visualized | 1 (0.7%) |
| Echelon nodes visualized | 76 (52.4%) |
| SN marked | 144 (99.3%) |
| Postlymphoscintigraphy intervention | |
| SN hot and blue | 127 (87.6%) |
| Concordance at surgery | 140 (96.6%) |
| Nodes excised | 2.8 (±2) |
| Sentinel node–positive | 34 (23.5%) |
| Intervention after SLNB | |
| WLE | 85 (58.6%) |
| Mastectomy | 55 (37.9%) |
| SLNB only | 5 (3.5%) |
| Hookwire | 54 (62.8%) |

IDC = invasive ductal carcinoma; ILC = invasive lobular carcinoma; DCIS = ductal carcinoma in situ; HR+ = hormone receptor–positive; HER2 = human epidermal growth factor receptor 2; WLE = wide local excision; IMN = internal mammary node; SN = sentinel node.

Qualitative data are number and percentage; continuous data are mean ± SD.

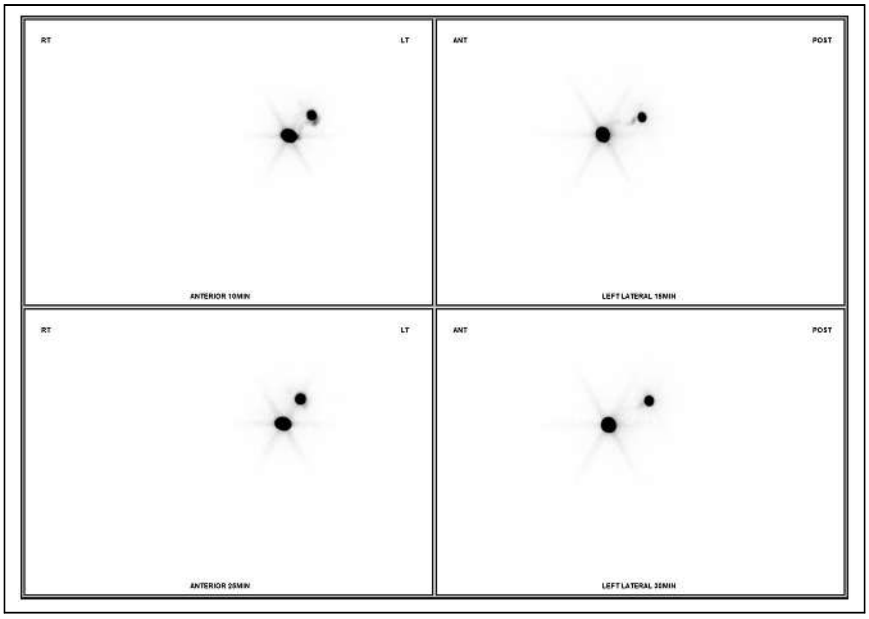


**FIGURE 1.** Anterior and left lateral images displaying prompt radiotracer egress from injection site to axillary lymph node.

interventions, surgical notes, and concordance between nodes marked and those excised in SLNB. Success rates were determined through relationships between the variables investigated using $\chi^2$ analysis. The statistical results were then compared against those of similar large-scale studies in the literature to determine their significance.

## RESULTS

### Descriptive Findings

*Patient Characteristics.* The cohort consisted of 141 women and 4 men from 37 to 87 y old. The patients were categorized into 10-y age brackets for statistical analysis and comparability to other studies that used similar brackets (*14*). Full demographic details can be found in Table 1.

*Disease Characteristics.* Seven patients had bilateral disease and were counted as separate cases for each breast for the purpose of this study. Invasive ductal carcinoma was the most common tumor type, encompassing 109 patients. Lesion dimeter ranged from 3 to75 mm and was grouped into 3 categories—less than 20 mm (90 patients), 20–50 mm (49 patients), and more than 50 mm (3 patients)—based on breast cancer staging standards (*15*). Seventeen patients had multicentric disease, classed by a distance of more than 55 mm between the primary and secondary lesions. The number of secondary lesions per patient ranged from 1 to 3, with an average diameter of 10.9 mm.

Tumors were assigned a histopathologic grade from 1 to 3, increasing in severity (*15*). Sixty-one patients were classed as grade 1, 51 as grade 2, and 31 as grade 3. Histologic type was also recorded; 113 patients presented with hormone receptor–positive disease, 14 were human epidermal growth factor receptor 2–enriched, and 9 were triple-negative. Histopathology results were inaccessible for the remaining 9. After SLNB, 34 patients were found to have nodal spread. Further information on disease characteristics can be found in Table 1.

*Surgical and Technique-Related Characteristics.* Of the 145 patients, 126 had previously received a biopsy for disease confirmation and 8 had a wide local excision for historical ESBC on the same breast. One patient had a previous mastectomy, though not all breast tissue had been removed. Multiple previous interventions had occurred in some cases, typically a combination of previous wide local excision and recent biopsy. Fifty-four patients did not have a palpable mass and had a hookwire inserted under mammographic guidance after lymphoscintigraphy and before surgery. Generally, SLNB is not a standalone procedure, with only 5 patients proceeding to SLNB as a sole intervention; 85 patients underwent concurrent mastectomy (wide local excision), and the remaining 55 had a full mastectomy. The number of nodes removed ranged from 1 to 10.

Intradermal periareolar injections were performed toward the tumor site, and these sites were categorized into quadrants. The upper outer quadrant was the most common for the tumor site. Lymphatic transit of the radiotracer was clear on initial dynamic imaging in 100 patients, with a clear sentinel node visible at 10 min after injection in 106. The sentinel node was visible in 30 min or less in 136 patients. In 1 patient, no nodes were visualized. The time between injection and final imaging ranged from 15 to 210 min, with SPECT/CT utilized in 18 patients.

Echelon nodes, which are those farther along in a single lymphatic chain than the sentinel node, were observed in 76 patients. These nodes are not routinely marked for surgery but are still removed in some cases. Internal mammary nodes were visualized in 1 patient, though not marked or removed in surgery. Further technique and surgical information is recorded in Table 1.

### Statistical Analysis

At least 1 node was identified and marked for surgery in all but 1 patient, with 2 nodes marked in 13 patients. The success of a study was based on concordance between the node marked and the node removed in surgery. Imaging and surgery were concordant in 140 patients. Four patients had nodes removed other than the marked node, and 1 patient had no visualized nodes to be marked. Excised nodes presented both high counts and absorption of patent blue dye during surgery in 127 patients.

With reference to previous studies, the effects of variables that could reasonably be perceived to affect lymphatic flow and, hence, have an impact on lymphoscintigraphy were examined. Previous intervention, age, and injection

**TABLE 2**
Associations Between Age, Injection Site, or Previous Interventions or Surgery and Time to Visualization of First Node

| Variable | Time to first node (min) | | | | | | | | | | Total | Statistics |
|---|---|---|---|---|---|---|---|---|---|---|---|---|
| | 10 | 15 | 20 | 25 | 30 | 35 | 40 | 45 | 60 | 180 | | |
| Age (y) | | | | | | | | | | | | $\chi^2_{36} = 35.2$, $P = 0.508$ |
| 35–44 | 5 | 0 | 0 | 1 | 0 | 0 | 0 | 0 | 0 | 0 | 6 | |
| 45–54 | 24 | 5 | 0 | 0 | 2 | 0 | 0 | 0 | 0 | 0 | 31 | |
| 55–64 | 28 | 2 | 2 | 1 | 0 | 1 | 1 | 0 | 0 | 0 | 35 | |
| 65–74 | 29 | 10 | 0 | 1 | 1 | 0 | 0 | 1 | 0 | 1 | 43 | |
| 75+ | 20 | 4 | 1 | 0 | 0 | 1 | 1 | 0 | 1 | 1 | 29 | |
| Total | 106 | 21 | 3 | 3 | 3 | 2 | 2 | 1 | 1 | 2 | 144 | |
| Injection site | | | | | | | | | | | | $\chi^2_{36} = 67.6$, $P = 0.001$ |
| Lower inner | 10 | 3 | 1 | 0 | 0 | 0 | 0 | 0 | 0 | 0 | 14 | |
| Lower outer | 22 | 3 | 0 | 1 | 1 | 0 | 1 | 0 | 0 | 0 | 28 | |
| Upper inner | 28 | 3 | 1 | 0 | 1 | 1 | 1 | 0 | 0 | 2 | 37 | |
| Upper outer | 46 | 12 | 1 | 2 | 0 | 1 | 0 | 1 | 1 | 0 | 64 | |
| Retroareolar | 0 | 0 | 0 | 0 | 1 | 0 | 0 | 0 | 0 | 0 | 1 | |
| Total | 106 | 21 | 3 | 3 | 3 | 2 | 2 | 1 | 1 | 2 | 144 | |
| Previous intervention or surgery | | | | | | | | | | | | $\chi^2_{27} = 35.2$, $P = 0.966$ |
| Biopsy | 94 | 16 | 2 | 3 | 3 | 1 | 2 | 1 | 1 | 2 | 125 | |
| Mastectomy | 1 | 0 | 0 | 0 | 0 | 0 | 0 | 0 | 0 | 0 | 1 | |
| None | 1 | 2 | 0 | 0 | 0 | 0 | 0 | 0 | 0 | 0 | 3 | |
| WLE | 4 | 3 | 1 | 0 | 0 | 0 | 0 | 0 | 0 | 0 | 8 | |
| Total | 100 | 21 | 3 | 3 | 3 | 1 | 2 | 1 | 1 | 2 | 137 | |

WLE = wide local excision.

site were assessed against time to first node. $\chi^2$ analysis was used to examine these variables, with accepted statistical significance set at a $P$ value of less than 0.05 (Table 2).

Previous intervention did not show a significant effect on lymphatic flow ($P = 0.966$). Similarly, age did not have an effect ($P = 0.508$); however, the injection site did appear to have a statistically significant relationship with lymphatic flow rate ($P = 0.001$) (Table 2).

## DISCUSSION

Our primary aim was to investigate the effectiveness of this lymphoscintigraphy technique in identifying the correct axillary lymph node for SLNB in ESBC patients by concordance between imaging and surgical notes and histopathology findings. A successful node identification rate of 99.3% is high when compared with the results of similar studies. Because of the vast differences in techniques between centers, it is difficult to directly compare results between studies relating to lymphoscintigraphy. Table 3 compares the EANM guidelines and the techniques of the index study and 2 main comparator studies. A study by Goyal et al. (*16*) reported an identification rate of only 72%, whereas a more recent, large-scale trial by Kuemmel et al. (*14*) identified nodes in 90.2% of cases. Goyal et al. used the technique most comparable to this study, though a peritumoral injection technique was utilized with a 2-mL volume and the acquisition of delayed images at 3 h after injection. Because of the large-scale, multicenter nature of the study by Kuemmel et al., techniques slightly differed between sites, with varying injection techniques and a minimum activity of 150 MBq. The increased effectiveness of the current study's technique in comparison to those studies might be attributable to differences in injection technique. Povoski et al. (*17*) assessed the difference in sentinel node identification rates between superficial and deep injections, finding superficial injection to produce a rate of 94.7% whereas deep injection localized only 62%. The single patient for whom nodes were not visualized was imaged up to 3 h without success. That patient had a small tumor (15 mm) and required hookwire insertion before surgery, in which a single node was identified using patent blue dye and removed.

The node marked during lymphoscintigraphy was excised in surgery in 140 of 145 patients (96.6%). The 5 nonconcordant cases included the nonvisualized case. All 5 patients had small lesions (<20 mm) that required hookwire insertion before surgery. Three of these patients were injected in the upper outer quadrant, and only 1 had radiotracer transit on initial dynamic imaging. One patient displayed both echelon nodes and internal mammary nodes, highlighting the potential for the incorrect node to have been marked with unclear lymphatic flow direction. There were no stand-out commonalities among the 5 patients other than small lesion size. The study by Goyal et al. (*16*) reported a 96% concordance rate when a

**TABLE 3**
Comparison of Techniques Between Present Study, EANM Guidelines, and Studies in Literature

| Variable | This study | EANM guidelines (*10*) | Goyal et al. (*16*) | Kuemmel et al. (*14*) |
|---|---|---|---|---|
| Radiotracer ($^{99m}$Tc-labeled) | ATC | Various radiopharmaceuticals | Colloidal albumin ($^{99m}$Tc-nanocolloid) | Unspecified radiocolloid |
| Dose (MBq) | 40 | 3.7–370 | Same-day, 20; 2-d, 40 | Maximum, 150 |
| Injection volume (mL) | 0.5 | Superficial, 0.05–0.5; deep, 0.5–1 | 2 | Variable across sites |
| Injection technique | Periareolar | Superficial or deep | Peritumoral | Periareolar, 1,045; peritumoral, 113 |
| No. of injections | 1 | Not specified | 4 | Variable across sites |
| Dynamic imaging? | Yes | Suggested but deemed uncommon | No | Variable across sites |
| Delayed imaging? | No | Suggested at 1 h and 2–4 h | Yes at 3 h | No |

ATC = $^{99m}$Tc-antimony trisulfide colloid.

node was marked preoperatively, though this decreases to 66.8% when nonvisualized cases are included. Kuemmel et al. (*14*) had a concordance rate of 96.8%, putting this study's results at equal strength to those reported in the literature.

The secondary aims were to compare the findings with those for imaging protocols and techniques reported in the peer-reviewed literature and to assess the impact of specific variables on the time efficiency and successfulness of the technique. The effect of previous intervention, age, and injection site on lymphatic flow was assessed. A slower lymphatic flow can extend the overall time of the study and increase false-negative rates. Higher degrees of previous surgical intervention were predicted to negatively affect axillary lymphatic flow rate. However, $\chi^2$ analysis revealed no statistically significant relationship between previous intervention and time to first node ($P = 0.966$) (Table 2). Because most patients had undergone only a previous biopsy (126/145), this result is not indicative of the effects of more invasive interventions such as wide local excision and mastectomy. An earlier report showed that lymphoscintigraphy in patients with previous breast and axillary surgery is still viable, with only a slightly reduced success rate (*18*).

The effect of increasing age on lymphatic function and flow rate has been thoroughly examined in the existing literature. Using lymphoscintigraphy, it has been determined that older age correlates negatively with lymphatic flow rate (*19*). On this basis, we predicted that it would take longer to observe the first node after injection in older patients. However, $\chi^2$ analysis revealed no statistically significant relationship between age and lymphatic flow ($P = 0.508$) (Table 2). It is possible that the results of this study contradict the existing literature because of the small sample size, which included a limited number of younger patients; 17 of 145 patients were under the age of 50 y.

Breast lesions are located most commonly in the upper outer quadrant and least commonly in the lower inner quadrant (*20*). This localization was reflected in this study, with 44.1% in the upper outer quadrant and 9.7% in the lower inner quadrant. $\chi^2$ analysis found a statistically significant correlation between injection site and time to first node ($P = 0.001$), revealing that injections in the upper outer quadrant were related to extended time taken to identify a sentinel node (Table 2). This finding reflects the findings of the existing literature on the influence of injection site on sentinel node visualization (*16*). A potential explanation is superimposition of shine-through due to the proximity of the axillary nodes to the injection site (*16*). Three of 5 patients who were nonconcordant in surgery had lesions in the upper outer quadrant. There is the potential that counts recorded by the intraoperative γ-detection device from the sentinel node may be obscured by the injection site. SPECT/CT could be a viable solution for nonvisualization in patients with lesions in the upper outer quadrant, allowing visualization from all angles and eliminating the issue of shine-through.

The main strength of this study was the determination that the technologist-driven injection technique and protocol in lymphoscintigraphy are an easy-to-perform, time-efficient, and accurate way to identify sentinel nodes for SLNB, thus providing rural ESBC patients with an effective and accessible service that is comparable to the services received in an urban environment. However, the study was limited by difficulty in comparing this technique with those in the literature because of the vast differences between individual protocols. The retrospective nature of the study was also a limitation, as a lack of access to—or unrecorded—surgical information essential to the study meant that the final sample size was much smaller than anticipated. Additionally, we did not have follow-up information to determine long-term patient outcomes.

## CONCLUSION

Our lymphoscintigraphy technique is an accurate and effective way to identify sentinel lymph nodes for SLNB in ESBC patients. The ability to identify the correct sentinel node is more accurate than in comparison studies, and the method is more time-efficient and standardized. Additionally, the intradermal periareolar injection technique makes the procedure easy to perform and therefore adoptable across rural departments with limited access to an on-site physician.

Patients who attend TRRH for SNLS are receiving quality care that is comparable to that of urban nuclear medicine departments.

## DISCLOSURE

No potential conflict of interest relevant to this article was reported.

## KEY POINTS

**QUESTION:** Is the technologist-driven injection technique and lymphoscintigraphy protocol used in a rural setting effective at identifying the correct lymph node for sentinel node biopsy in breast cancer patients?

**PERTINENT FINDINGS:** The reported lymphoscintigraphy technique can be justified as an accurate and effective method of identifying sentinel lymph nodes for SLNB in ESBC patients. The technique is time-efficient and has outcomes comparable to those of successful studies in the literature.

**IMPLICATIONS FOR PATIENT CARE:** The technique provides effective and accurate identification of lymph nodes for biopsy in breast cancer patients and can easily be implemented in a wide variety of institutions. It is suitable for use in rural settings where a physician may not be available on site.

## REFERENCES


1. Breast Cancer Stats. National Breast Cancer Foundation website. https://nbcf.org.au/about-breast-cancer/breast-cancer-stats/. Accessed March 24, 2023.
2. Australian Institute of Health and Welfare. *Cancer in Australia 2019.* Australian Government; 2019.
3. Yu XQ, Luo Q, Kahn C, O'Connell DL, Houssami N. Temporal trends show improved breast cancer survival in Australia but widening urban-rural differences. *Breast.* 2015;24:524–527.
4. Mettler FA, Guiberteau MJ. *Essentials of Nuclear Medicine and Molecular Imaging.* 7th ed. Elsevier; 2019:322–324.
5. Christensen B, Blichert-Toft M, Siemssen OJ, Nielsen SL. Reliability of axillary lymph node scintiphotography in suspected carcinoma of the breast. *Br J Surg.* 1980;67:667–668.
6. Krag DN, Weaver DL, Alex JC, Fairbank JT. Surgical resection and radiolocalization of the sentinel lymph node in breast cancer using a gamma probe. *Surg Oncol.* 1993;2:335–339.
7. Garbay JR, Skalli-Chrisostome D, Leymarie N, Sarfati B, Rimareix F, Mazouni C. The role of blue dye in sentinel node detection for breast cancer: a retrospective study of 203 patients. *Breast Care (Basel).* 2016;11:128–132.
8. Jakes AD, Twelves C. Breast cancer-related lymphoedema and venepuncture: a review and evidence-based recommendations. *Breast Cancer Res Treat.* 2015;154:455–461.
9. Krag DN, Anderson SJ, Julian TB, et al. Sentinel-lymph-node resection compared with conventional axillary-lymph-node dissection in clinically node-negative patients with breast cancer: overall survival findings from the NSABP B-32 randomised phase 3 trial. *Lancet Oncol.* 2010;11:927–933.
10. Giammarile F, Alazraki N, Aarsvold JN, et al. The EANM and SNMMI practice guideline for lymphoscintigraphy and sentinel node localization in breast cancer. *Eur J Nucl Med Mol Imaging.* 2013;40:1932–1947.
11. Wang H, Heck K, Pruitt SK, et al. Impact of delayed lymphoscintigraphy for sentinel lymph node biopsy for breast cancer. *J Surg Oncol.* 2015;111:931–934.
12. Siddique M, Nawaz MK, Bashir H. The usefulness of SPECT/CT in sentinel node mapping of early stage breast cancer patients showing negative or equivocal findings on planar scintigraphy. *Asia Ocean J Nucl Med Biol.* 2018;6:80–89.
13. Tamworth Rural Referral Hospital. Healthdirect website. Published 2023. Accessed May 23, 2023. https://www.healthdirect.gov.au/australian-health-services/healthcare-service/tamworth-2340-nsw/tamworth-rural-referral-hospital/hospitals/a28a623c-5a52-0174-e34f-595dcc1c4dce.
14. Kuemmel S, Holtschmidt J, Gerber B, et al. Prospective, multicenter, randomized phase III trial evaluating the impact of lymphoscintigraphy as part of sentinel node biopsy in early breast cancer: Senszi (GBG80) trial. *J Clin Oncol.* 2019;37:1490–1498.
15. American Joint Committee on Cancer. Breast. In: *AJCC Cancer Staging Manual.* Springer International Publishing; 2017:589–636.
16. Goyal A, Newcombe RG, Mansel RE. Role of routine preoperative lymphoscintigraphy in sentinel node biopsy for breast cancer. *Eur J Cancer.* 2005;41:238–243.
17. Povoski SP, Olsen JO, Young DC, et al. Prospective randomized clinical trial comparing intradermal, intraparenchymal, and subareolar injection routes for sentinel lymph node mapping and biopsy in breast cancer. *Ann Surg Oncol.* 2006;13:1412–1421.
18. Dinan D, Nagle CE, Pettinga J. Lymphatic mapping and sentinel node biopsy in women with an ipsilateral second breast carcinoma and a history of breast and axillary surgery. *Am J Surg.* 2005;190:614–617.
19. Conway WC, Faries MB, Nicholl MB, et al. Age-related lymphatic dysfunction in melanoma patients. *Ann Surg Oncol.* 2009;16:1548–1552.
20. Rummel S, Hueman MT, Costantino N, Shriver CD, Ellsworth RE. Tumour location within the breast: does tumour site have prognostic ability? *Ecancermedicalscience.* 2015;9:552.

# Evaluation of Collimators in a High-Resolution, Whole-Body SPECT/CT Device with a Dual-Head Cadmium–Zinc–Telluride Detector for $^{123}$I-FP-CIT SPECT

Hitoshi Hiraki[1], Toshimune Ito[2], Masahisa Onoguchi[1], Hirotatsu Tsuchikame[3], Masaaki Shishido[3], Takafumi Maeno[3], Takayuki Shibutani[1], and Hiroki Sanada[4]

[1]*Department of Quantum Medical Technology, Graduate School of Medical Sciences, Kanazawa University, Kanazawa, Japan;* [2]*Department of Radiological Technology, Faculty of Medical Technology, Teikyo University, Tokyo, Japan;* [3]*Department of Radiology, Saiseikai Yokohamashi Tobu Hospital, Yokohama, Japan; and* [4]*Department of Central Radiology, Teikyo University Mizonokuchi Hospital, Kawasaki, Japan*

The study aim was to evaluate the adaptation of collimators to $^{123}$I-*N*-fluoropropyl-2b-carbomethoxy-3b-(4-iodophenyl)nortropane ($^{123}$I-FP-CIT) dopamine transporter SPECT (DAT-SPECT) by a high-resolution whole-body SPECT/CT system with a cadmium–zinc–telluride detector (C-SPECT) in terms of image quality, quantitation, diagnostic performance, and acquisition time. **Methods:** Using a C-SPECT device equipped with a wide-energy, high-resolution collimator and a medium-energy, high-resolution sensitivity (MEHRS) collimator, we evaluated the image quality and quantification of DAT-SPECT for an anthropomorphic striatal phantom. Ordered-subset expectation maximization iterative reconstruction with resolution recovery, scatter, and attenuation correction was used, and the optimal collimator was determined on the basis of the contrast-to-noise ratio (CNR), percentage contrast, and specific binding ratio. The acquisition time that could be reduced using the optimal collimator was determined. The optimal collimator was used to retrospectively evaluate diagnostic accuracy via receiver-operating-characteristic analysis and specific binding ratios for 41 consecutive patients who underwent DAT-SPECT. **Results:** When the collimators were compared in the phantom verification, the CNR and percentage contrast were significantly higher for the MEHRS collimator than for the wide-energy high-resolution collimator ($P < 0.05$). There was no significant difference in the CNR between 30 and 15 min of imaging time using the MEHRS collimator. In the clinical study, the areas under the curve for acquisition times of 30 and 15 min were 0.927 and 0.906, respectively, and the diagnostic accuracies of the DAT-SPECT images did not significantly differ between the 2 times. **Conclusion:** The MEHRS collimator provided the best results for DAT-SPECT with C-SPECT; shorter acquisition times (<15 min) may be possible with injected activity of 167–186 MBq.

**Key Words:** $^{123}$I-FP-CIT; whole-body CZT semiconductor detector; WEHR collimator; MEHRS collimator

**J Nucl Med Technol 2023; 51:227–234**
DOI: 10.2967/jnmt.122.265328

In Parkinson syndrome, including Parkinson disease and dementia with Lewy bodies, dopamine transporters are present in the terminal portions of nigrostriatal dopaminergic nerves, and the loss of these nerves decreases dopamine transporter expression (*1,2*). To image the presence of these nigrostriatal dopaminergic nerves, $^{123}$I-*N*-fluoropropyl-2b-carbomethoxy-3b-(4-iodophenyl)nortropane ($^{123}$I-FP-CIT) dopamine transporter SPECT (DAT-SPECT), which has a high affinity for dopamine transporters, is performed and is one of the most useful tests for diagnosing Parkinson syndrome, including Parkinson disease and dementia with Lewy bodies (*3–5*). A NaI scintillation detector–equipped Anger-type SPECT (A-SPECT) device, which is a device that uses 2 or 3 detectors (*6*), has been applied to conduct DAT-SPECT studies. To obtain sufficient counts in DAT-SPECT with A-SPECT, an acquisition time of about 30 min is required, even with 3 detectors (*7*). Recently, γ-cameras equipped with cadmium–zinc–telluride (CZT) detectors have been developed and shown to be useful in reducing acquisition time and providing reliable image quality (*8–11*). SPECT systems equipped with CZT detectors were initially developed exclusively for cardiac applications (*12–16*); however, they are beginning to be widely used in clinical practice as a 2-detector whole-body SPECT/CT system (C-SPECT), and C-SPECT systems have demonstrated superior energy resolution and improved high-contrast resolution for each nuclide, as reported in a performance evaluation comparing them with A-SPECT (*17*).

In addition to the standard wide-energy, high-resolution (WEHR) collimator for low- and medium-energy applications, a medium-energy, high-resolution sensitivity (MEHRS) collimator has recently been developed for C-SPECT, and the physical characteristics of C-SPECT and a performance evaluation of the WEHR and MEHRS collimators have been reported (*17*). MEHRS is expected to improve imaging accuracy by reducing the effects of high-energy γ-rays. Consequently, the use of C-SPECT in DAT-SPECT is expected to improve image quality and shorten acquisition times.

Received Dec. 22, 2022; revision accepted Apr. 27, 2023.
For correspondence or reprints, contact Masahisa Onoguchi (onoguchi@staff.kanazawa-u.ac.jp).
Published online Jul. 11, 2023.

However, to the best of our knowledge, no study has comprehensively evaluated the adaptability of collimators in C-SPECT to DAT-SPECT based on the striatal phantoms and clinical studies. This study aimed to evaluate the C-SPECT collimators in DAT-SPECT in terms of image quality, quantity, diagnostic performance, and acquisition time using striatal phantoms and clinical studies.

## MATERIALS AND METHODS

### SPECT/CT Scanner and Data Acquisition

We used the Discovery NM/CT 870 CZT device equipped with a whole-body CZT detector (GE Healthcare). A C-SPECT device equipped with WEHR and MEHRS collimators was used to acquire all the SPECT data. The design parameters of the WEHR and MEHRS collimators are shown in Table 1 (*17*). Projection data were acquired with a rotation radius of 14 cm using step-and-shoot mode with 360° of rotation in 120 angular views. First, 30 and 15 min of acquisition were performed with each collimator. Second, a 30-min acquisition was performed using each collimator, and data were collected every 5, 10, 15, 20, 25, and 30 min for image reconstruction, which was performed using the Lister tool (GE Healthcare) function for data with an acquisition time of 30 min. The Lister tool function allows image reconstruction with data from any acquisition time within the total acquisition time.

The matrix size was 128 × 128, with 3.32 × 3.32 mm pixels (×1.33 magnification). The photopeak window of $^{123}$I was set as a 15% energy window centered on 159 keV. The triple-energy-window method was used for scatter correction (*18,19*), and a lower subwindow of 3% (142.3–147.1 keV) and an upper subwindow of 3% (170.9–175.7 keV) were set for the $^{123}$I main peak (*17*). The image-processing system Xeleris 4.0 (GE Healthcare) was used for image reconstruction of the acquired data. For image analysis, we used the general image-processing software ImageJ (National Institutes of Health), Demon Research Image Processor (version 3.01; Fujifilm Toyama Chemical Co.), and DatView (Nihon Medi-Physics, Inc.). The CT imaging parameters used for phantom attenuation correction were as follows: tube voltage, 120 kVp; tube current, 300 mA; detector configuration, 16 × 0.625 mm; rotation time, 0.8 s; slice thickness, 5 mm; and pitch, 0.938. For attenuation correction of the clinical data, the tube current was set to 30 mA.

### Phantom Study

*Phantom.* An anthropomorphic striatal phantom, DaT1308 (NMP Business Support Co., Ltd.), was used as the phantom to acquire projection data (Supplemental Fig. 1; supplemental materials are available at http://jnm.snmjournals.org). The first projection data showed that the left and right striatum and background of the phantom were filled with $^{123}$I solution with a radioactivity ratio of about 8:1 (striatum, $40.0 \times 10^3$ Bq/mL; background, $5.0 \times 10^3$ Bq/mL; striatum-to-background ratio, 8.0), assuming a very normal one (*20,21*). The second projection data showed that the left and right striatum and background of the phantom were filled with an approximately 4:1 $^{123}$I solution, assuming a very low radioactivity ratio (striatum, $20.0 \times 10^3$ Bq/mL; background, $5.0 \times 10^3$ Bq/mL; striatum-to-background ratio, 4.0) (*20,21*).

*Image Reconstruction.* The phantom image was reconstructed using ordered-subset expectation maximization iterative reconstruction with resolution recovery, scatter correction, and attenuation correction (OSEMRRSCAC; subsets, 6; iterations, 15). Attenuation and scatter correction were by the triple-energy-window method (*18*), and resolution recovery was according to the report on optimization of reconstruction conditions in A-SPECT by Matsutomo et al. (*19*). A lower subwindow of 3% (142.3–147.1 keV) and an upper subwindow of 3% (170.9–175.7 keV) were set for the $^{123}$I main peak. Post-Butterworth filtering (power, 16; cutoff, 0.5 cycle/cm) was used as the smoothing process (*22*). The CT attenuation correction method was used for attenuation correction.

*Phantom Collimator Evaluation.* To investigate the basic features of the different collimators, we calculated the contrast-to-noise ratio (CNR) and percentage contrast for different radioactivity ratios (8:1 vs. 4:1) of the striatum to the collimator and different acquisition times (30 and 15 min). First, a striatal region of interest (ROI) was manually contoured and placed on the CT image using the method reported by Matsutomo et al. (*19*). The ROIs were then copied onto the SPECT images (*19*). The striatum was measured using 12 ROIs in the left and right caudate nuclei and putamen for each of the 3 cross-sectional images (Supplemental Fig. 1). A rectangular 1,940 mm$^2$ background ROI was placed at the back of the phantom; the CNR and percentage contrast were then calculated using Equations 1 and 2:

$$\mathrm{CNR} = (\overline{C}_{\mathrm{striatum}} - \overline{C}_{\mathrm{bg}})/\overline{\mathrm{SD}}_{\mathrm{bg}} \quad \text{Eq. 1}$$

$$\%\ \mathrm{contrast} = (\overline{C}_{\mathrm{striatum}}/\overline{C}_{\mathrm{bg}})/(\text{striatal count ratio: theoretical value}) \times 100, \quad \text{Eq. 2}$$

where $\overline{C}_{\mathrm{striatum}}$ is the mean count in the striatum ROI, $\overline{C}_{\mathrm{bg}}$ is the mean count in the background ROI, and $\overline{\mathrm{SD}}_{\mathrm{bg}}$ is the mean of the SD of the background ROI. The striatal count ratio is 8 or 4, which is the striatal radioactivity count ratio, and the theoretic value is 1, which is the background radioactivity count ratio.

The quantitative performance of the collimator was evaluated by measuring the specific binding ratio (SBR) of the phantom images according to the method reported by the team of Tossici-Bolt (*22,23*). The SBR is defined as the ratio of the specific binding concentration of the tracer in the striatum to the nonspecific binding concentration in all brain regions. This method uses a semiautomatic analysis and comprises 3 functions: manual placement of the whole striatal volume of interest (VOI), automated creation of a reference VOI, and calculation of SBR. First, the whole striatal VOI was set for the summed images oriented to the orbitomeatal plane.

**TABLE 1**
Collimator Designs

| Collimator | Type of hole | Hole length (mm) | Hole diameter (mm) | Septal thickness (mm) | Number of holes | Penetration (%) |
|---|---|---|---|---|---|---|
| WEHR | Square | 45 | 2.26 | 0.2 | 33,280 | 0.55 ($^{99m}$Tc) |
| MEHRS | Hexagonal | 40.25 | 2.8 | 0.9 | Undisclosed | 1.8 ($^{111}$In) |

Second, the reference VOI for the estimation of the nonspecific count was set for the whole brain with the exclusion of the striatum. Finally, the SBR was calculated using Equation 3:

$$SBR = (1/V_s)\{Ct_{VOI}/C_r - V_{VOI}\}, \quad \text{Eq. 3}$$

where $V_s$ is the standard volume of the striatum (11.2 mL), $Ct_{VOI}$ is the total count in the striatal VOI, $C_r$ is the count concentration in a reference VOI, and $V_{VOI}$ is the volume of the striatal VOI. Because the striatal-to-background radioactivity ratios were 8:1 and 4:1, the SBRs calculated using the true radioactivity were 7 and 3 for 8:1 and 4:1, respectively.

*Short-Acquisition-Time Collection Evaluation for Phantom.* The Lister tool function for data with an acquisition time of 30 min was used to perform image reconstructions for the acquisition times of 5, 10, 15, 20, 25, and 30 min, and the CNR, percentage contrast, and SBR were then calculated and evaluated.

### Clinical Study

*Clinical Subjects.* We retrospectively examined the imaging data of 41 consecutive patients who had previously undergone DAT-SPECT with the MEHRS collimator, including 10 patients in the normal-accumulation group and 31 patients in the decreased-accumulation group for DAT-SPECT. This clinical evaluation was performed by 2 experienced radiologists according to established consensus criteria for the diagnosis of each disease, factoring in morphologic information from MRI or CT images performed at approximately the same time as DAT-SPECT. The patients comprised 23 men and 18 women, with ages ranging from 40 to 86 y (mean, 71.9 ± 11.4 y). An equivalent to the institutional review board approved this retrospective study, and the requirement to obtain informed consent was waived.

*Clinical SPECT Protocol.* $^{123}$I-FP-CIT (167 MBq, 167–186 MBq) was intravenously injected into each patient. Data acquisition started about 4 h after administering $^{123}$I-FP-CIT, with an imaging duration of 30 min (*7,24*). Immediately after DAT-SPECT, a low-dose CT scan was performed using the same parameters as in the phantom study. The CT imaging parameters used for attenuation correction of the clinical data were as follows: tube voltage, 120 kVp; tube current, 30 mA; detector configuration, 16 × 0.625 mm; rotation time, 0.8 s; slice thickness, 5 mm; and pitch, 0.938. DAT-SPECT images were reconstructed using the OSEMRRSCAC algorithm. The imaging time parameters used for reconstruction were determined from the phantom study.

*Clinical Diagnostic Accuracy.* The images were reconstructed with an acquisition time of 30 min and another acquisition time determined via phantom verification. The SBRs were calculated from the reconstructed images and compared. The diagnostic accuracies of these 2 images were then evaluated according to the receiver-operating-characteristic (ROC) analysis. Using a continuous confidence rating method, the ROC analysis assessed the degree of accumulation in the striatum on a free scale from the decreased-accumulation group to the normal-accumulation group. The quality of DAT-SPECT images was visually assessed by 2 board-certified nuclear medicine physicians and 5 board-certified nuclear medicine technologists. The ROC analysis was completed by averaging the results for these observers.

### Statistical Analysis

The CNR, percentage contrast, and SBR results from the phantom study were compared using the Shapiro–Wilk test, paired *t* test, Wilcoxon test, 1-way ANOVA, and Friedman test. Multireader, multicase ANOVA according to the jackknife method and tests with 95% CIs were used to compare the ROC curves for the clinical study (*25*). *P* values of less than 0.05 were considered to indicate statistical significance.

## RESULTS

### Phantom Study

*Collimator Evaluation Results.* The phantom images are shown in Figure 1. The CNR and percentage contrast are shown in Figures 2 and 3. The CNR was significantly higher for the MEHRS collimator than for the WEHR collimator ($P < 0.05$). The percentage contrast did not significantly differ between the collimators for the 30-min acquisition time and the radioactivity ratio of 8:1. However, in other cases, the MEHRS collimator had significantly higher values ($P < 0.05$). Considering a theoretic value of 7 for the SBR, the SBR values of the MEHRS and WEHR collimators were 9.27 and 8.85, respectively, for the 30-min collection and 9.15 and 8.89, respectively, for the 15-min collection. Similarly, considering the theoretic SBR value of 3, the SBR values of the MEHRS and WEHR collimators were 3.72

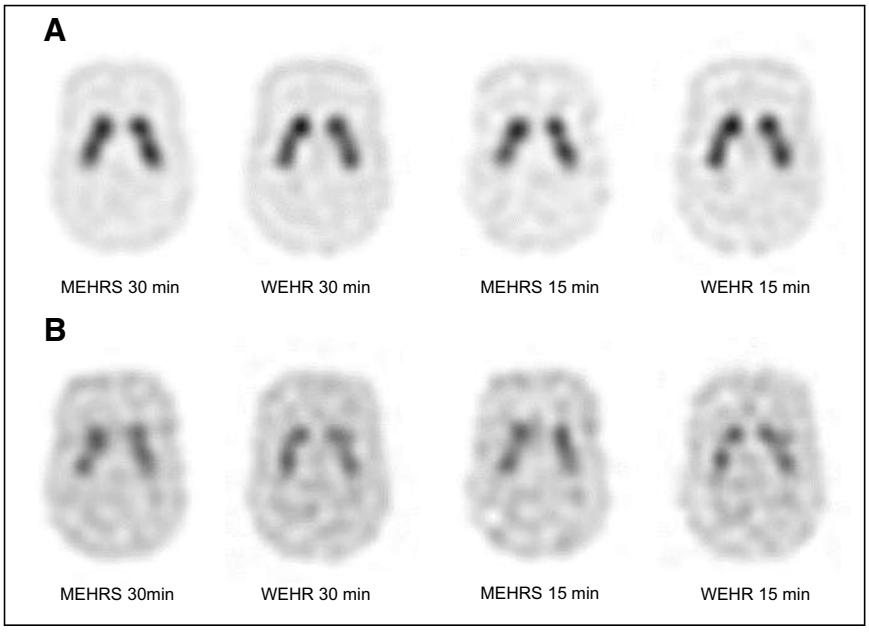


**FIGURE 1.** DAT-SPECT images of anthropomorphic striatal phantom with different collimators, acquisition times, and striatum-to-background radiation ratios. Phantom's striatum and background were bilaterally filled with $^{123}$I solution at radioactivity ratios (Bq/mL) of ~8:1 (A) and ~4:1 (B).

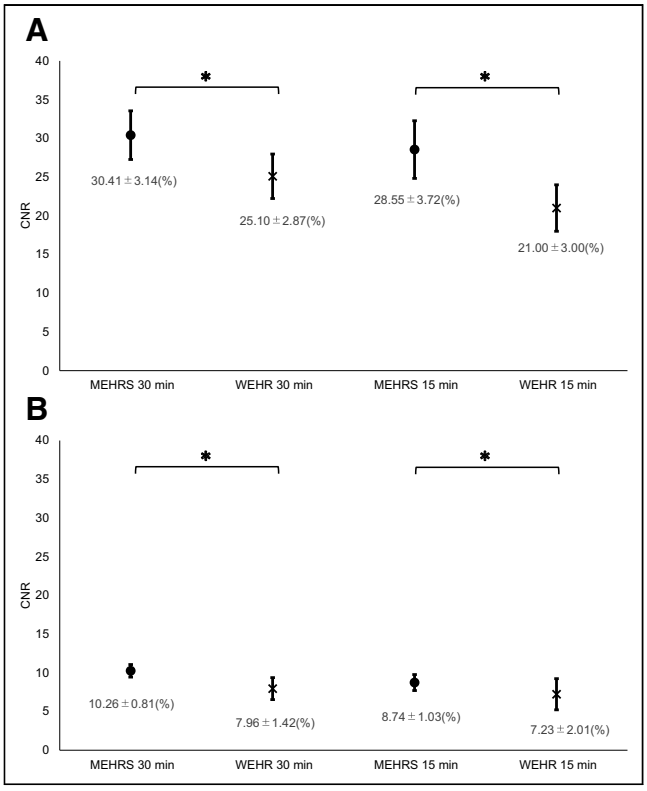


**FIGURE 2.** CNR of DAT-SPECT images of anthropomorphic striatal phantom with different collimators, acquisition times, and striatum-to-background radiation ratios. (A) Images with radioactivity ratio (Bq/mL) of ~8:1. (B) Images with radioactivity ratio (Bq/mL) of ~4:1. *$P < 0.05$.

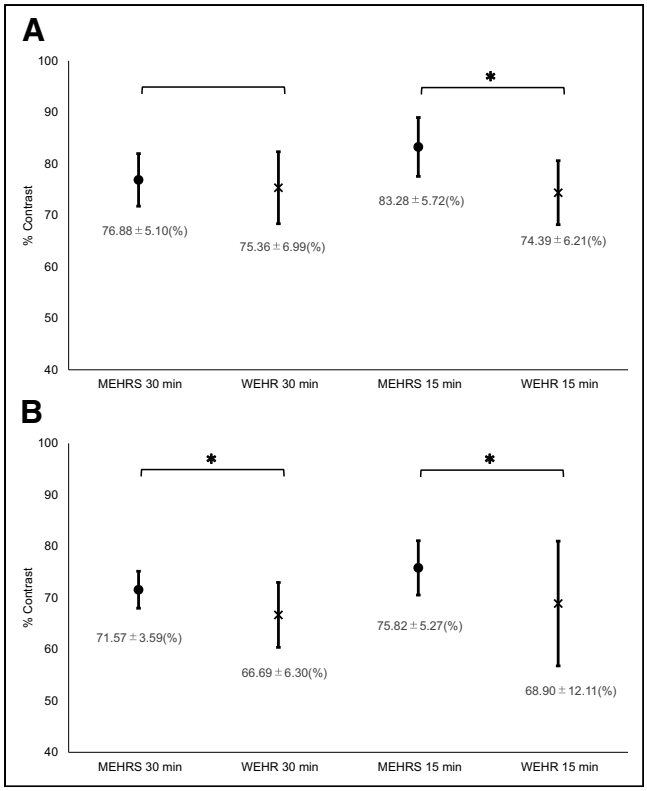


**FIGURE 3.** Percentage contrast of DAT-SPECT images of anthropomorphic striatal phantom with different collimators, acquisition times, and striatum-to-background radiation ratios. (A) Images with radioactivity ratio (Bq/mL) of ~8:1. (B) Images with radioactivity ratio (Bq/mL) of ~4:1. *$P < 0.05$.

and 3.34, respectively, for the 30-min collection and 4.06 and 3.47, respectively, for the 15-min collection. Both collimators had higher SBR values than the theoretic values, but the MEHRS collimator's value was the highest.

*Evaluation Results of Short-Acquisition-Time Collection.* A collimator chosen according to the results of the phantom evaluation was used for validating the short acquisition time in DAT-SPECT. We compared the images from the standard 30-min acquisition time with those from the short acquisition time. The phantom images are shown in Figure 4, and the CNRs and percentage contrast are in Figures 5 and 6. Regarding CNRs, at a radioactivity ratio of 8:1, only the 5-min acquisition time afforded significantly different CNRs from that for the 30-min acquisition time ($P < 0.05$). At a radioactivity ratio of 4:1, there was a significant difference in the CNRs between the 5- and 10-min acquisitions, compared with that for the 30-min acquisition ($P < 0.05$). Regarding percentage contrast, at a radioactivity ratio of 8:1, only the 10- and 15-min acquisitions afforded percentage contrasts significantly different from that for the 30-min acquisition ($P < 0.05$). At a radioactivity ratio of 4:1, there was no significant difference in percentage contrasts among all the acquisition times. The SBRs are shown in Table 2. For the radioactivity ratio of 8:1, the SBR values ranged from 9.14 to 9.92 depending on the acquisition times, whereas the theoretic SBR was 7. The SBR with an acquisition time of 5 min was highest, at 9.92. For the radioactivity ratio of 4:1, the SBR values ranged from 3.72 to 4.37 with different acquisition times, whereas the theoretic value was 3. The SBR with an acquisition time of 10 min was highest, at 4.37.

### Clinical Study

Figure 7 shows a comparison of SBRs obtained at acquisition times of 30 and 15 min in DAT-SPECT using the MEHRS collimator. The SBR values remained stable across all studied subjects, with correlations of at least 0.98 at 30 and 15 min of acquisition time, with no significant difference.

The results of the ROC analysis to differentiate between the normal-accumulation and decreased-accumulation groups are shown in Figure 7. The areas under the ROC curve for the 30- and 15-min acquisition times were 0.927 and 0.906, respectively, but the differences were not significant.

## DISCUSSION

In this study, we evaluated collimator adaptation for C-SPECT in DAT-SPECT. For collimator verification in the phantom study, we first used the WEHR and MEHRS collimators with radioactivity ratios of 8:1 and 4:1 and acquisition times of 30 and 15 min for the striatum and then evaluated the image quality and quantification. Based on the characteristics

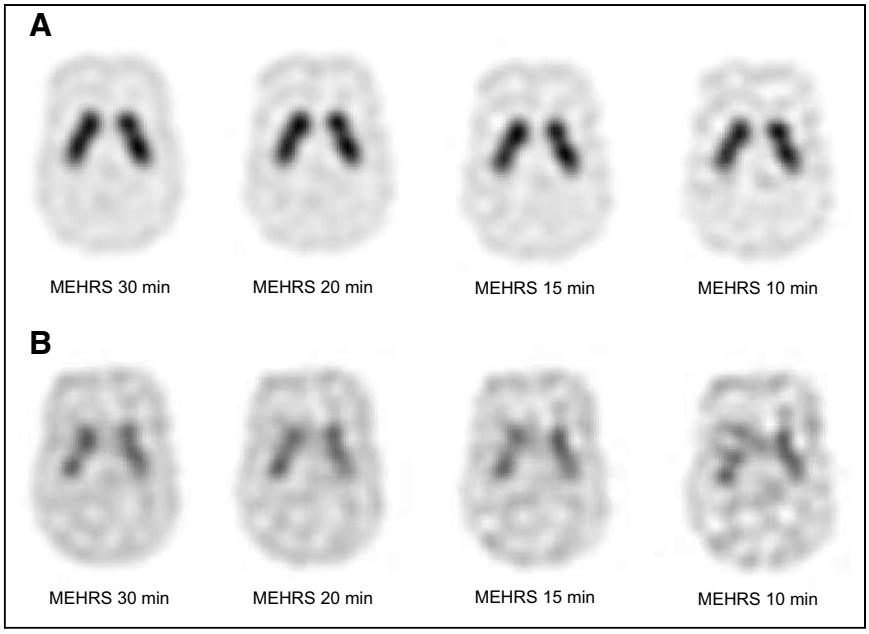


**FIGURE 4.** DAT-SPECT images using MEHRS collimator with different acquisition times (10, 15, 20, and 30 min). (A) Images with radioactivity ratio (Bq/mL) of ~8:1. (B) Images with radioactivity ratio (Bq/mL) of ~4:1.

of the WEHR and MEHRS collimators in C-SPECT by Ito et al. (*17*), because of the incomplete charge acquisition of the electron–hole pair and intercrystal scattering in C-SPECT, the scattering component increases as a result of the effects of hole tailing in the Compton region. This result suggests that the scattered component increases because of the 529-keV septum penetration of $^{123}$I and the hole tailing in the Compton region and scattering between crystals. The MEHRS collimator has a thick septum to reduce the scattered radiation component. Furthermore, the MEHRS collimator could acquire primary photons with higher accuracy using the appropriate triple-energy-window method, which is thought to improve image uniformity, and the MEHRS collimator provided significantly higher CNR values.

The percentage contrast showed the same trend as the CNR results.

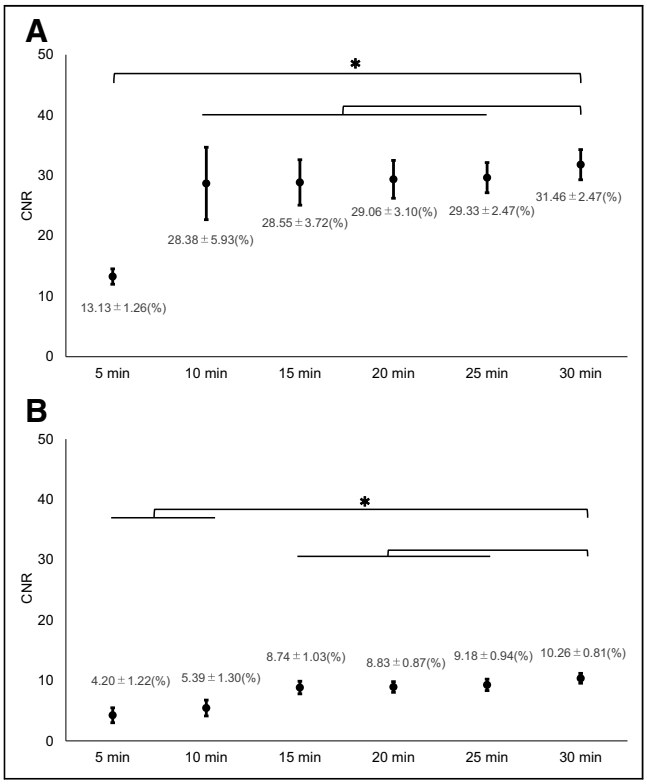


**FIGURE 5.** CNR of DAT-SPECT images using MEHRS collimator with different acquisition times (10, 15, 20, and 30 min). (A) Images with radioactivity ratio (Bq/mL) of ~8:1. (B) Images with radioactivity ratio (Bq/mL) of ~4:1. *$P < 0.05$.

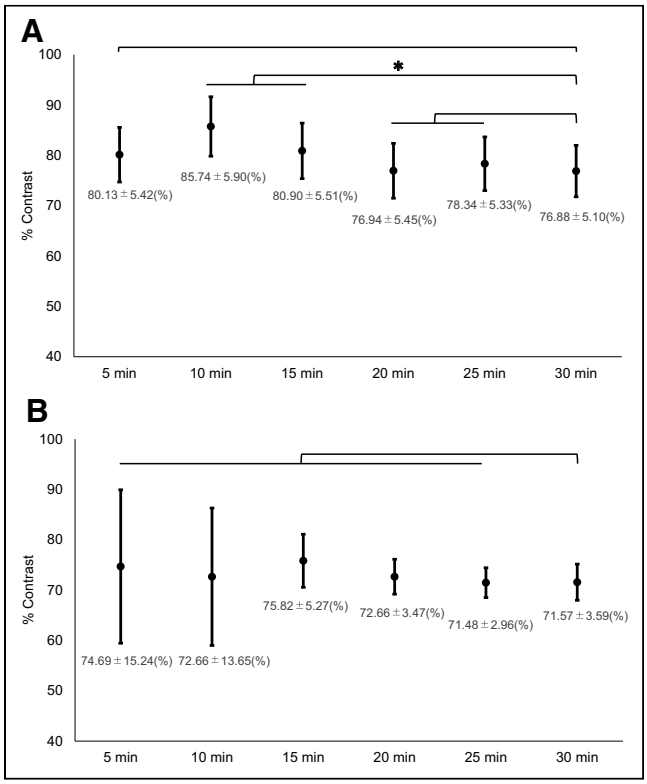


**FIGURE 6.** Percentage contrast of DAT-SPECT images using MEHRS collimator with different acquisition times (10, 15, 20, and 30 min). (A) Images with radioactivity ratio (Bq/mL) of ~8:1. (B) Images with radioactivity ratio (Bq/mL) of ~4:1. *$P < 0.05$.

**TABLE 2**
SBR of DAT-SPECT Images Using MEHRS Collimator with Different Acquisition Times

| Radioactivity ratio | SBR | | | | | |
|---|---|---|---|---|---|---|
| | 5 min | 10 min | 15 min | 20 min | 25 min | 30 min |
| 8:1 | 9.92 | 9.30 | 9.15 | 9.14 | 9.41 | 9.27 |
| 4:1 | 3.73 | 4.37 | 4.06 | 3.83 | 3.78 | 3.72 |

This result may be attributed to the removal of the scattered component and acquisition of primary photons (*17*). At an acquisition time of 30 min and a striatal radioactivity ratio of 8:1, no significant difference was observed in percentage contrast because sufficient counts were obtained at both collimators because of the adequate acquisition time and high striatal accumulation radioactivity ratio.

The SBR has been reported by Meyer et al. to depend on the imaging parameters, such as the device used for imaging, type of collimator, and image reconstruction parameters (*26*). In this study, the SBRs were higher in C-SPECT than the theoretic value for both the WEHR and MEHRS collimators.

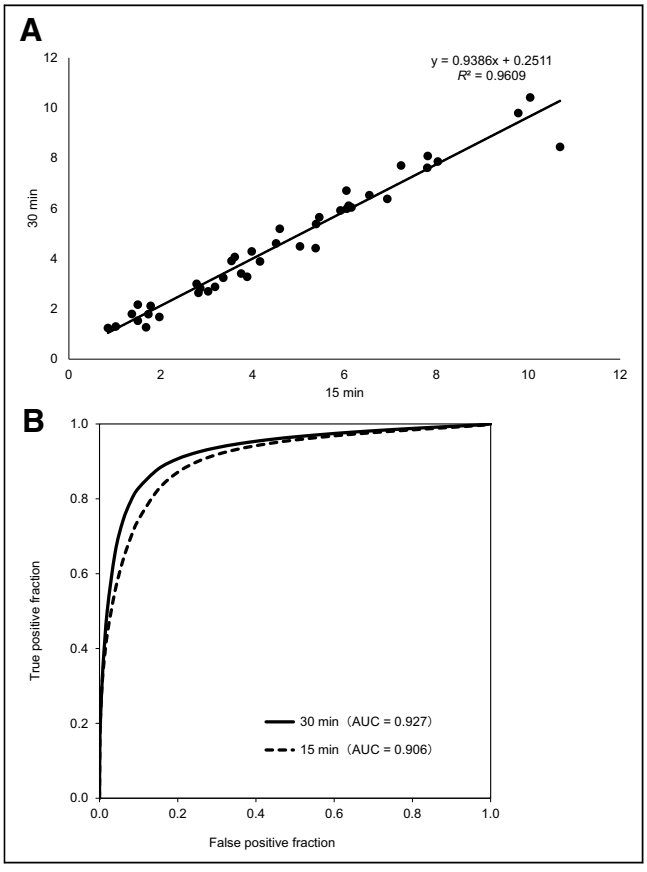


**FIGURE 7.** (A) Correlation between SBR values ≥ 0.98 at 30- and 15-min acquisition times. (B) Comparison of average ROC curves for differentiation between normal-accumulation group and decreased-accumulation group. For both A and B, difference is not statistically significant. AUC = area under the ROC curve.

The SBRs were higher in the MEHRS collimator than those in the WEHR collimator. Ito et al. showed that the energy resolution in C-SPECT was 1.67 times higher when using the MEHRS collimator than with the WEHR collimator (*17*). The background ROI counts were lower for both WEHR and MEHRS collimators because of the effects of septum penetration and hole tailing of scattered rays, which are the same reasons as those for CNR and percentage contrast. The striatum counts were higher for the MEHRS collimator because of the acquisition of primary photons. The SBR was higher than the theoretic value for both collimators, with the MEHRS collimator showing a higher value. In addition, Matsuda et al. reported that the SBR was higher under scatter correction conditions than without scatter correction (*21*), and the results were comparable for C-SPECT. The CNR, percentage contrast, and SBR values show that the MEHRS collimator is optimal for use in DAT-SPECT in C-SPECT.

Then, to validate a short acquisition time, based on the results obtained from the collimator validation, images were acquired using the MEHRS collimator with a 30-min acquisition time. Further, the Lister tool function was used to reconstruct images for 5, 10, 15, 20, 25, and (the reference) 30 min (Fig. 4) to evaluate image quality and quantification. There were no significant differences in CNRs for the 8:1 radioactivity ratio of the striatum over 10 min or for the 4:1 radioactivity ratio of the striatum over 15 min (Fig. 5).

According to a study by Bailly et al. validating A-SPECT with an injected activity of 185 MBq of Swiftscan (GE Healthcare), a 25% reduction in acquisition time from 30 min was possible (*27*). In a study by Bani Sadr et al. using a WEHR collimator for C-SPECT at an injected activity of 185 MBq, the image quality and SBR values were stable from 30 to 15 min of acquisition time, indicating that a 2-fold reduction in acquisition time was possible (*11*). The validation of the collimator in C-SPECT showed that the acquisition time could be reduced from that of A-SPECT using Swiftscan, which was consistent with the results using the WEHR collimator in C-SPECT, and that the acquisition time of 15 min was also possible for the striatum radioactivity ratio (8:1 and 4:1).

The 8:1 radioactivity ratio of the striatum afforded a significantly higher percentage contrast only at 10 and 15 min ($P < 0.05$), and there was no significant difference in the values when the acquisition times were 5 and 20 min or longer. There was no significant difference in the percentage contrast values for the radioactivity ratio of the striatum of 4:1 at any acquisition times (Fig. 6). As the activity and detection efficiency increase (i.e., the more counts [photons] used in image formation), the contrast increases because the proportion of noise components in the image decreases (*28*). For the 8:1 radioactivity ratio of the striatum, the extremely short acquisition time of 5 min resulted in low background counts and consequently did not provide significantly different results from the those obtained at an acquisition time of 30 min, and the results for the acquisition times of 20 and 25 min were not significantly different because of the

sufficient counts obtained. However, at acquisition times of 10 and 15 min, the percentage contrast values were significantly higher because the MEHRS collimator has a thicker septum to remove scattered radiation components; furthermore, using the appropriate triple-energy-window method, primary photons can be acquired with high accuracy, improving uniformity and suppressing background counts relative to the increase in striatal counts. The 4:1 radioactivity ratio of the striatum resulted in a larger proportion of noise components in the image because of the small number of counts (photons) used for image formation and the very small number of counts of the striatum in the acquisitions up to 30 min, indicating that overall, no significant differences were detected. We observed some statistically significant differences in percentage contrast for varying acquisition times at the 8:1 striatum radioactivity ratio. However, it was difficult to provide a threshold acquisition time.

Next, we discuss the SBR for acquisition time variation. Bani Sadr et al. showed that SBR does not vary significantly with reducing the acquisition time (*11*). However, in the present verification, the SBRs were the highest for the 5- and 10-min acquisition times at the 8:1 and 4:1 radioactivity ratio of the striatum, respectively. The SBR changed the most between the 5- and 10-min acquisition times. The method reported by Tossici-Bolt et al. uses a 3-dimensional ROI that is sufficiently larger than the striatal volume to eliminate partial-volume effects of the striatum and interanalyst errors (*23*). Thus, the changes observed at the 8:1 striatal radioactivity ratio could be related to the effect of acquiring more primary photons because of the higher radioactivity of the striatum for extremely short acquisition times (*17*), whereas the changes observed at a 4:1 striatal radioactivity ratio could be related to the stronger effect of count variations due to fewer counts in the striatum and in the background brain parenchyma. On the basis of the CNR results, we determined that the acquisition time for an injected activity of 167–186 MBq could be reduced to 15 min.

In the clinical study, based on the results obtained from the phantom validation, the SBR was calculated using C-SPECT with a MEHRS collimator and the 30-min reference acquisition time. Similarly, the SBR was calculated and evaluated using images with a 15-min acquisition time based on the results obtained from the phantom validation. The obtained result is consistent with the results presented by Bani Sadr et al., who reported no significant differences in SBRs with reduced acquisition times (*11*). In addition, Ito et al. showed that when $^{123}$I is used for C-SPECT, by setting an appropriate scattering window and performing scattering correction, it is possible to acquire primary photons with high accuracy and an excellent scatter removal effect, which enables highly uniform imaging while maintaining high-contrast resolution (*17*). As a result, uniform imaging was possible even at a 15-min acquisition time, which is considered to be an SBR that is not significantly different from that obtained at a 30-min acquisition time.

Second, there were no significant differences in visual evaluation. Bani Sadr et al. showed that DAT-SPECT using a WEHR collimator for C-SPECT provides reliable image quality and a reliable diagnosis for an acquisition time of 15 min (*11*) and that images with an acquisition time of 15 min, which was not significantly different from the standard acquisition time of 30 min using a MEHRS collimator for C-SPECT, are considered to be available for diagnosis.

These results are consistent with the report by Ito et al., who suggested that using a MEHRS collimator for C-SPECT is suitable for $^{123}$I imaging, and it is assumed that the use of a MEHRS collimator for C-SPECT improves the image quality of DAT-SPECT compared with a WEHR collimator (*17*). In addition, a study by Bani Sadr et al. showed that the acquisition time of 15 min is possible using a WEHR collimator for C-SPECT (*11*), which is consistent with the results obtained using a MEHRS collimator for C-SPECT, which showed that an acquisition time of 15 min was possible, and it was assumed that the acquisition time can be shortened.

The present study had some limitations. First, we cited the report of Matsutomo et al., who used A-SPECT for reconstruction parameters (*19*). Furthermore, Onishi et al. reported that the optimal reconstruction parameters differ depending on the available iterative reconstruction techniques (*29*). Therefore, the best reconstruction parameters in C-SPECT may differ and it is necessary to validate the reconstruction parameters in C-SPECT. If the best reconstruction parameters are found, it may be possible to improve the image quality of DAT-SPECT in C-SPECT and further reduce acquisition times.

Second, the number of subjects was limited in the clinical study. Matsuda et al. suggested that the ratio of a specific striatum to nonspecific $^{123}$I-FP-CIT binding decreases considerably with age (*21*). Lavalaye et al. have shown that the binding rate of $^{123}$I-FP-CIT is considerably higher in women than in men (*30*). In this validation, the short acquisition time was limited to 15 min based on the results of the phantom validation. However, it is believed that further potential benefits of short acquisition times can be proven by separately evaluating the diagnostic effectiveness from the images of patients with and without a disease. This verification was evaluated on a limited number of 41 patients, which means that it should be evaluated on more than 41 patients.

## CONCLUSION

Here, we have demonstrated the adaptation of C-SPECT in DAT-SPECT by first performing a phantom study to determine the optimal collimator for use, which was then applied in a clinical study. Our results indicated that the use of C-SPECT with a MEHRS collimator in DAT-SPECT improved the performance and image quality of DAT-SPECT relative to that of a WEHRS collimator. The results also indicated that the MEHRS collimator could reduce the 30-min acquisition time for DAT-SPECT to 15 min because

there was no statistically significant difference between the 30- and 15-min acquisition times.

## DISCLOSURE

No potential conflict of interest relevant to this article was reported.

## KEY POINTS

**QUESTION:** Compared with previous reports on the WEHR collimator, can $^{123}$I-FP-CIT SPECT using a CZT detector with a MEHRS collimator improve image quality and reduce acquisition time?

**PERTINENT FINDINGS:** Phantom validation suggested that the MEHRS collimator improved image quality and potentially reduced acquisition times. Clinical validation in 41 patients suggested that the MEHRS collimator may reduce acquisition time as much as the WEHRS collimator.

**IMPLICATIONS FOR PATIENT CARE:** The MEHRS collimator is recommended for $^{123}$I-FP-CIT SPECT with a CZT detector.

## REFERENCES


1. Niznik HB, Fogel EF, Fassos FF, Seeman P. The dopamine transporter is absent in parkinsonian putamen and reduced in the caudate nucleus. *J Neurochem.* 1991;56:192–198.
2. Piggott MA, Perry EK, Marshall EF, et al. Nigrostriatal dopaminergic activities in dementia with Lewy bodies in relation to neuroleptic sensitivity:comparisons with Parkinson's disease. *Biol Psychiatry.* 1998;44:765–774.
3. O'Brien JT, Colloby S, Fenwick J, et al. Dopamine transporter loss visualized with FP-CIT SPECT in the differential diagnosis of dementia with Lewy bodies. *Arch Neurol.* 2004;61:919–925.
4. Booij J, Tissingh G, Boer GJ, et al. $^{123}$I FP-CIT SPECT shows a pronounced decline of striatal dopamine transporter labelling in early and advanced Parkinson's disease. *J Neurol Neurosurg Psychiatry.* 1997;62:133–140.
5. Bártová P, Kraft O, Bernátek J, et al. Transcranial sonography and $^{123}$I-FP-CIT single photon emission computed tomography in movement disorders. *Ultrasound Med Biol.* 2014;40:2365–2371.
6. Varrone A, Sansone V, Pellecchia MT, et al. Comparison between a dual-head and a brain-dedicated SPECT system in the measurement of the loss of dopamine transporters with [$^{123}$I]FP-CIT. *Eur J Nucl Med Mol Imaging.* 2008;35:1343–1349.
7. Darcourt J, Booij J, Tatsch K, et al. EANM procedure guidelines for brain neurotransmission SPECT using $^{123}$I-labelled dopamine transporter ligands, version 2. *Eur J Nucl Med Mol Imaging.* 2010; 37:443–442.
8. Eisen Y, Shor A, Mardor I. CdTe and CdZnTe x-ray and gamma-ray detectors for imaging systems. *IEEE Trans Nucl Sci.* 2004;51:1191–1198.
9. Spartiotis K, Leppanen A, Pantsar T, et al. A photon counting CdTe gamma- and x-ray camera. *Nucl Inst Institut Methods Phys Res.* 2005;550:267–277.
10. Ogawa K, Ohmura N, Iida H, Nakamura K, Nakahara T, Kubo A. Development of an ultra-high resolution SPECT system with a CdTe semiconductor detector. *Ann Nucl Med.* 2009;23:763–770.
11. Bani Sadr A, Testart N, Tylski P, Scheiber C. Reduced scan time in $^{123}$I-FP-CIT SPECT imaging using a large-field cadmium-zinc-telluride camera. *Clin Nucl Med.* 2019;44:568–569.
12. Gambhir SS, Berman DS, Ziffer J, et al. A novel high-sensitivity rapid-acquisition single-photon cardiac imaging camera. *J Nucl Med.* 2009;50:635–643.
13. Garcia EV, Faber TL, Esteves FP. Cardiac dedicated ultrafast SPECT cameras: new designs and clinical implications. *J Nucl Med.* 2011;52:210–217.
14. Verger A, Imbert L, Yagdigul Y, et al. Factors affecting the myocardial activity acquired during exercise SPECT with a high-sensitivity cardiac CZT camera as compared with conventional Anger camera. *Eur J Nucl Med Mol Imaging.* 2014; 41:522–528.
15. Ben-Haim S, Kennedy J, Keidar Z. Novel cadmium-zinc telluride devices for myocardial perfusion imaging: technological aspects and clinical applications. *Semin Nucl Med.* 2016;46:273–285.
16. Niimi T, Nanasato M, Sugimoto M, Maeda H. Evaluation of cadmium-zinc-telluride detector-based single-photon emission computed tomography for nuclear cardiology: a comparison with conventional anger single-photon emission computed tomography. *Nucl Med Mol Imaging.* 2017;51:331–337.
17. Ito T, Matsusaka Y, Onoguchi M, et al. Experimental evaluation of the GE NM/CT 870 CZT clinical SPECT system equipped with WEHR and MEHRS collimator. *J Appl Clin Med Phys.* 2021;22:165–177.
18. Ichihara T, Ogawa K, Motomura N, Kubo A, Hashimoto S. Compton scatter compensation using the triple-energy window method for single and dual-isotope SPECT. *J Nucl Med.* 1993;34:2216–2221.
19. Matsutomo N, Nagaki A, Yamao F, Sasaki M. Optimization of iterative reconstruction parameters with 3-dimensional resolution recovery, scatter and attenuation correction in $^{123}$I-FP-CIT SPECT. *Ann Nucl Med.* 2015;29:636–642.
20. Tossici-Bolt L, Dickson JC, Sera T, et al. Calibration of gamma camera systems for a multicentre European $^{123}$I-FP-CIT SPECT normal database. *Eur J Nucl Med Mol Imaging.* 2011;38:1529–1540.
21. Matsuda H, Murata M, Mukai Y, et al. Japanese multicenter database of healthy controls for [$^{123}$I]FP-CIT SPECT. *Eur J Nucl Med Mol Imaging.* 2018;45:1405–1416.
22. Dickson JC, Tossici-Bolt L, Sera T, et al. The impact of reconstruction method on the quantification of DaTSCAN images. *Eur J Nucl Med Mol Imaging.* 2010;37:23–35.
23. Tossici-Bolt L, Hoffmann SM, Kemp PM, Mehta RL, Fleming JS. Quantification of [$^{123}$I] FP-CIT SPECT brain images: an accurate technique for measurement of the specific binding ratio. *Eur J Nucl Med Mol Imaging.* 2006;33:1491–1499.
24. Djang DS, Janssen MJ, Bohnen N, et al. SNM practice guideline for dopamine transporter imaging with $^{123}$I-ioflupane SPECT 1.0. *J Nucl Med.* 2012;53:154–163.
25. Shiraishi J, Fukuoka D, Iha R, Inada H, Tanaka R, Hara T. Verification of modified receiver-operating characteristic software using simulated rating data. *Radiol Phys Technol.* 2018;11:406–414.
26. Meyer PT, Sattler B, Lincke T, Seese A, Sabri O. Investigating dopaminergic neurotransmission with $^{123}$I-FP-CIT SPECT: comparability of modern SPECT systems. *J Nucl Med.* 2003;44:839–845.
27. Bailly M, Le Rouzic G, Metrard G, Ribeiro MJ. Faster acquisition for dopamine transporter imaging using Swiftscan step and shoot continuous SPECT without impairing visual and semiquantitative analysis. *Front Med (Lausanne).* 2020;7:235.
28. Kazunori Y. Basic knowledge about diagnostic image quality for beginners. *Dent Radrad.* 2016;56:1–7.
29. Onishi H, Motomura N, Fujino K, Natsume T, Haramoto Y. Quantitative performance of advanced resolution recovery strategies on SPECT images: evaluation with use of digital phantom models. *Radiol Phys Technol.* 2013;6:42–53.
30. Lavalaye J, Booij J, Reneman L, Habraken JB, van Royen EA. Effect of age and gender on dopamine transporter imaging with [$^{123}$I] FP-CIT SPET in healthy volunteers. *Eur J Nucl Med.* 2000;27:867–869.

# The Effectiveness of Ionized Water as a Radiodecontaminant for $^{99m}$Tc-Pertechnetate and $^{131}$I

Mary Angeline P. Rillorta[1,2] and Allan Jay Espiritu[2]

[1]*Center for Diagnostic and Therapeutic Nuclear Medicine, Baguio General Hospital and Medical Center, Baguio City, Philippines; and* [2]*School of Advanced Studies, Saint Louis University, Baguio City, Philippines*

Immediate and complete decontamination procedures are essential to restore the functionality, precision, accuracy, and safety of tests done within the nuclear medicine facility. Decontamination is a simple procedure that, if performed correctly, effectively reduces exposure brought about by spills. The determination of a suitable radiodecontaminant may be beneficial in decontaminating patient beds, collimators, probes, and machines. **Methods:** Two surface types (i.e., stainless steel and vinyl) were contaminated with a predetermined activity of $^{99m}TcO_4$ and $^{131}$I. After air drying, static images of the contaminated surfaces were obtained using a γ-camera to determine the activity counts on each surface before and after decontamination procedures. Different decontaminant contact times (i.e., 5, 10, and 15 min) were used for each decontaminant (i.e., ionized water, 10% bleach, detergent solution, a negative control [no treatment], and a positive control [a commercial radiodecontaminant]). Differences between the effectiveness of ionized water and the other decontaminants against $^{99m}TcO_4$ and $^{131}$I at different contact times were measured, and the mean percentage activity removed (%AR) was compared using 2-way ANOVA at the 0.05 level of significance. **Results:** $^{99m}TcO_4$ and $^{131}$I contaminants had %ARs of greater than 80% after 5 min of contact time for ionized water and the other decontaminants. At 15 min contact time, ionized water was not as effective as the other decontaminating agents for $^{131}$I on vinyl surfaces. There was no significant interaction between the effects of the decontaminants (%AR) and the contact times with stainless steel and vinyl for either $^{99m}TcO_4$ or $^{131}$I. **Conclusion:** For $^{99m}TcO_4$ and $^{131}$I on stainless steel surfaces, ionized water is an effective decontaminant at contact times of 5, 10, and 15 min. For $^{99m}TcO_4$ on vinyl surfaces, ionized water is also an effective decontaminant at contact times of 5, 10, and 15 min. For $^{131}$I on vinyl surfaces, ionized water is as effective as 10% bleach, detergent solution, and a commercial radiodecontaminant at contact times of 5 and 10 min.

**Key Words:** radioactivity decontamination; nuclear medicine technology; radiation safety; $^{99m}$Tc pertechnetate; $^{131}$I; ionized water

**J Nucl Med Technol 2023; 51:235–238**
DOI: 10.2967/jnmt.122.265150

Contamination and exposure to ionizing radiation from spills may cause detrimental health effects. Exposure to ionizing radiation is an occupational risk that may lead to radiation-induced cancer, such as leukemia, skin cancer, and thyroid cancer (*1–4*). Repeated exposure to radioactive contaminants may cause a worker's thyroid to absorb high radiation doses and increase the risk of developing thyroid cancer (*5*).

When a piece of equipment or a workstation is contaminated by generated radioactive sources such as $^{99m}TcO_4$ and $^{131}$I, immediate clean-up is necessary to restore the equipment's utility or the safety of the workstation. Rapid and complete decontamination is essential to restore the functionality, precision, and accuracy of diagnostic tests done within the nuclear medicine facility. The goal of the decontamination process is to completely remove the radioactive material without spreading it and damaging contaminated workspaces (*6*). A specific decontaminant must be identified; however, no specified, standardized agent is used in nuclear medicine facilities.

Decontamination procedures are essential and should be done immediately to ensure that there is no unnecessary exposure of nuclear medicine patients and staff. Furthermore, preventing excessive radiation exposure and promptly decreasing the probable impact of ionizing radiation on human health and the environment are two measures for radiation protection. Decontamination is a simple procedure that, if performed correctly, effectively reduces exposure brought about by spills. Use of an efficient decontamination protocol by staff familiar with standardized decontamination practices contributes to a facility's radiation safety procedures and assures other workers that no radioactive material has been accidentally released into their environment.

This study determined the effectiveness of ionized water as compared with 10% bleach, a detergent solution, a negative control (no treatment), and a positive control (Radi-Clean, a commercial radiodecontaminant; Capintec) as a radiodecontaminant against fixed minor spills of 111 MBq of $^{99m}TcO_4$ and 37 MBq of $^{131}$I using contact times of 5, 10, and 15 min. The spills were placed on continuous vinyl and stainless steel surfaces, the facility's most common work surfaces.

Ionized water as a radiodecontaminant has not been comprehensively explored; however, because of the noticeable increase in decontamination rate with the increase of the pH of a solution (*7*), it is theorized that ionized water may be an effective radiodecontaminant.

Received Nov. 8, 2022; revision accepted Jan. 31, 2023.
For correspondence or reprints, contact Mary Angeline P. Rillorta (2111332@slu.edu.ph).
Published online Apr. 25, 2023.

## MATERIALS AND METHODS

Before data collection, official letters secured all necessary clearances from the administration of the Baguio General Hospital and the Medical Center–Center for Diagnostic and Therapeutic Nuclear Medicine. Despite the absence of human participants, the research protocol was submitted for review to the Saint Louis University Research Ethics Committee and subsequently was approved with protocol number SLU-REC 2022-012 on April 4, 2022.

The 10% bleach solution (Green Cross, Inc.) was prepared by adding 10 parts of sodium hypochlorite to 90 parts of distilled water. The detergent solution (Unilever) was prepared by dissolving 100 g of powder detergent in 1,000 mL of water. The ionized water was prepared with 99% distilled water ionized with 1% potassium carbonate, or a ratio of 99:1. The positive control, Radi-Clean, was used as commercially supplied. Stainless steel and vinyl surfaces measuring 10 × 10 cm (4 × 4 in) served as the contamination surfaces. Absorbent pads were placed beneath them to avoid accidental contamination from the experiment.

Each surface was placed on a steady countertop to avoid unequal flow of the aqueous solution. The 111-MBq dose of $^{99m}TcO_4$ and 37-MBq dose of $^{131}I$, determined by a CRC-55tw Capintec dose calibrator (Mirion Technologies), were delivered onto the surface using a needleless tuberculin syringe and allowed to air dry. The contaminated surfaces were placed under a Symbia Intevo Bold (Siemens Healthineers) dual-head γ-camera using an all-purpose low-energy collimator and read for 2 min to obtain radioactivity counts. After 2 min, the counts were recorded and served as a baseline for the initial contamination activity of the surface.

The usual decontamination procedures of the facility's radiation safety protocol were done, and the times for which each decontaminant contacted the surface were set to 5, 10, and 15 min. Because the protocol recommends wet decontamination, the surfaces were misted with the decontaminants and left for the indicated times; the decontaminants were then dried with absorbent paper, starting from the edges and proceeding to the middle. Afterward, the surface was measured again with the same γ-camera. Activity counts were taken at a 13-cm (5.11-in) distance from the surface.

All experiments were done in triplicate. The activity before and after decontamination was expressed as counts, the decontamination effectiveness was expressed as a decontamination factor (DF), and then the percentage of radioisotope activity removed (%AR) was determined. The DF is the ratio of activity before decontamination ($A$) to activity after decontamination ($B$) (*8*):

$$\mathrm{DF} = \frac{A}{B}.$$

Decontamination effectiveness is indicated by a %AR higher than that of the negative control or no treatment. The %AR was determined using the following formula:

$$\%\mathrm{AR} = \left(1 - \frac{1}{\mathrm{DF}}\right) \times 100.$$

### Statistical Analysis

To determine whether there was a difference in effectiveness between ionized water and the other decontaminants at different contact times, mean %AR was compared using 2-way ANOVA at a 0.05 level of significance. A simple main-effect analysis was done if a significant interaction between the decontaminants and the contact time was found. If there was no significant interaction but there was a significant difference, multiple comparisons using the Tukey honest-significant-difference post hoc test were done.

**TABLE 1**
Effectiveness of Decontaminants Against $^{99m}Tc$-Pertechnetate

| Decontaminant | Contact time (min) | %AR | |
|---|---|---|---|
| | | Stainless steel surface | Vinyl surface |
| Negative control | 5 | 9.5 | 5.4 |
| | 10 | 11.1 | 5.0 |
| | 15 | 12.0 | 5.3 |
| Ionized water | 5 | 87.3 | 97.8 |
| | 10 | 88.0 | 95.6 |
| | 15 | 87.4 | 96.7 |
| 10% bleach | 5 | 89.2 | 97.6 |
| | 10 | 86.8 | 96.9 |
| | 15 | 94.9 | 97.6 |
| Detergent solution | 5 | 84.2 | 96.7 |
| | 10 | 86.1 | 93.8 |
| | 15 | 91.3 | 92.6 |
| Positive control | 5 | 89.6 | 95.7 |
| | 10 | 90.9 | 95.6 |
| | 15 | 89.5 | 96.6 |

## RESULTS

Pre- and postdecontamination readings and the %AR for the surfaces against the decontaminants and contact times were documented. Sample γ-camera images are shown in Supplemental Figures 1–4 (supplemental materials are available at http://jnmt.snmjournals.org). Data averages for $^{99m}TcO_4$ against stainless steel and vinyl surfaces are in Table 1, with graphical representations available in Supplemental Figure 5, and data averages for $^{131}I$ against stainless steel and vinyl surfaces are in Table 2, with graphical representations available in Supplemental Figure 6.

**TABLE 2**
Effectiveness of Decontaminants Against $^{131}I$

| Decontaminant | Contact time (min) | %AR | |
|---|---|---|---|
| | | Stainless steel surface | Vinyl surface |
| Negative control | 5 | 1.2 | 0.7 |
| | 10 | 0.9 | 0.5 |
| | 15 | 0.9 | 0.4 |
| Ionized water | 5 | 96.9 | 93.5 |
| | 10 | 95.3 | 89.8 |
| | 15 | 96.1 | 89.5 |
| 10% bleach | 5 | 95.9 | 90.8 |
| | 10 | 97.6 | 91.9 |
| | 15 | 96.3 | 91.8 |
| Detergent solution | 5 | 91.8 | 92.9 |
| | 10 | 97.4 | 93.1 |
| | 15 | 95.4 | 93.1 |
| Positive control | 5 | 93.5 | 92.5 |
| | 10 | 95.6 | 92.1 |
| | 15 | 93.1 | 92.7 |

The $^{99m}TcO_4$ and $^{131}I$ contaminants had %ARs greater than 80% after 5 min of contact with ionized water and all the other decontaminants. The %ARs for all agents at other contact times manifested effective decontamination of $^{99m}TcO_4$ on the stainless steel and vinyl surfaces (Table 1), since the values were higher than the %AR for the negative control. The %AR from the $^{99m}TcO_4$-contaminated stainless steel surfaces increased as the contact times increased from 5 to 10 to 15 min. However, the positive control showed no change in %AR with an increase in contact time.

The results for ionized water as a radiodecontaminant for $^{131}I$ on stainless steel surfaces were promising, because there was almost no change in %AR (from 95.3% to 96.1%) when the contact time was increased from 10 to 15 min, respectively. Moreover, ionized water was the fastest-acting decontaminant, removing 93.5% of the $^{131}I$ radioactivity in 5 min on a vinyl surface and 96.9% in 5 min on a stainless steel surface (Table 2).

Two-way ANOVA analyzed the effect of the decontaminants and the 3 contact times on the %AR for $^{99m}TcO_4$ on stainless steel and vinyl or on the %AR for $^{131}I$ on stainless steel. There was no significant interaction between the effect of the decontaminants and the contact times for $^{99m}TcO_4$ on stainless steel ($F_{8,30} = 1.177$, $P = 0.345$), for $^{131}I$ on stainless steel ($F_{8,30} = 1.685$, $P = 0.143$), or for $^{99m}TcO_4$ on vinyl ($F_{8,30} = 0.351$, $P = 0.938$). The statistical comparisons are available in Supplemental Table 1. Moreover, there was no statistically significant difference in the main effect of contact time. The main effect of decontaminants, however, was statistically significant, with a $P$ value of less than 0.001. A Tukey post hoc test revealed significant pairwise differences between decontaminants and the negative control. No significant pairwise differences were found among the decontaminants. The effectiveness of ionized water was equal to that of the other agents on stainless steel and vinyl contaminated with $^{131}I$ and $^{99m}TcO_4$ for all 3 contact times.

For $^{131}I$ on vinyl, the $P$ value for comparison of the %AR of the decontaminants was less than 0.001, which indicates a significant difference. The effect of contact time with the decontaminants was also significant, at a $P$ value of 0.380 (Supplemental Table 2). Further, the interaction effect of the decontaminant and the contact time was also significant ($P = 0.015$), indicating that the relationship between decontaminant and %AR may be dependent on contact time.

A simple main-effect analysis was done to determine the mean difference in %AR between decontaminants at each contact time and the mean difference in %AR among contact times. For ionized water, the simple effect of contact time was statistically significant, with a $P$ value of less than 0.001. A pairwise comparison among the estimated marginal means of the different contact times for ionized water showed significant differences in %AR between 5 and 10 min, 5 and 15 min, and 10 and 15 min. This finding implies that for different contact times, there is a significant difference in the effectiveness of ionized water in decontaminating $^{131}I$ on vinyl.

The mean %AR for ionized water against $^{131}I$ on vinyl indicates that effectiveness decreases as contact time increases. All decontaminants were effective in decontaminating $^{131}I$ on vinyl at both 5 min and 10 min, but at 15 min there were statistically significant differences (all $P < 0.001$) from 10% bleach, detergent, the positive control, and the negative control. Ionized water was not as effective as 10% bleach, detergent, or the positive control when exposed for at least 15 min but was still significantly more effective than the negative control.

## DISCUSSION

Proper decontamination procedures effectively remove and reduce exposure from spills of common radioactive materials. It is essential to use a suitable, convenient, and fast-acting radiodecontaminant to immediately clear spills and avoid unnecessary radiation exposure of staff and patients.

The %AR results of our study revealed that all agents, including ionized water, effectively removed radioactivity from stainless steel surfaces contaminated with $^{131}I$ and $^{99m}TcO_4$. These results corroborate those of Ruhman et al. (*9*), who used water and soap, bleach, a commercial glass cleaner, and a commercial decontaminant on $^{99m}TcO_4$. Our results are also similar to those of Eroğlu and Aksakal (*7*), who used commercially available radiodecontaminants (e.g., Radiacwash; Biodex) and specially developed multipurpose cleaners on $^{131}I$, finding almost no differences among them. Their study (*7*) showed that approximately 100% of the radioactivity was removed in the first 5 min from nonporous surfaces such as stainless steel. Other decontamination procedures for other radioactive materials from laboratory surfaces such as epoxy, acrylic resin, vinyl, and stainless steel showed that the procedures were most effective on stainless steel and vinyl (*9,10*).

A wet method of decontamination would remove dry $^{131}I$ contaminants within a few minutes, provided it is performed a few minutes after detection using nonspecific cleaners (*11*). However, use of a wet method for removal of liquid contaminants (i.e., $^{131}I$ solution) may result in a wash-in effect, by which the %AR during decontamination decreases over time (*12,13*). This effect may explain the decrease in the %AR of $^{131}I$ for ionized water when it reached a contact time of 15 min. To avoid a wash-in effect, the contact time should be kept within 10 min (*14*).

## CONCLUSION

Compared with 10% bleach, a detergent solution, and a commercial radiodecontaminant, ionized water is an effective decontaminant for $^{99m}TcO_4$ and $^{131}I$ on stainless steel and vinyl surfaces for contact times of 5–15 min. Ionized water is also as effective as 10% bleach, a detergent solution, and a commercial radiodecontaminant against $^{131}I$ on vinyl surfaces for contact times of 5–10 min. We recommend that ionized water be applied for 5 min to decontaminate $^{99m}TcO_4$ and $^{131}I$ spills on common nuclear medicine laboratory surfaces. We also recommend studies of shorter contact times with ionized water to establish the speed of decontamination. Decontamination should be done immediately to prevent exposure of patients and staff, and decontamination

guidelines should be added to radiation protection programs. The results of this and similar studies can serve as a basis for identifying a safe, suitable, sufficient, and fast-acting radiodecontaminant to clear contamination and preserve the integrity of surfaces.

## DISCLOSURE

No potential conflict of interest relevant to this article was reported.


## ACKNOWLEDGMENT

We thank the Center for Diagnostic and Therapeutic Nuclear Medicine of the Baguio General Hospital and Medical Center for providing the facilities for this study.


## KEY POINTS

**QUESTION:** How effective is ionized water as a radiodecontaminant for $^{99m}TcO_4$ and $^{131}I$ on vinyl and stainless steel surfaces when kept in contact with the contamination for 5, 10, and 15 min?

**PERTINENT FINDINGS:** Ionized water is an effective decontaminating agent for $^{99m}TcO_4$ and $^{131}I$ for vinyl and stainless steel surfaces at any given contact time of at 5, 10, and 15 min as indicated by a %AR higher than that for the negative control or no treatment.

**IMPLICATIONS FOR PATIENT CARE:** Ionized water may be used as an alternative nontoxic, noncorrosive decontaminant for minor $^{99m}TcO4$ and $^{131}I$ spills on vinyl and stainless steel surfaces.

## REFERENCES


1. Bernier MO, Doody MM, Van Dyke ME, et al. Work history and radioprotection practices in relation to cancer incidence and mortality in US radiologic technologists performing nuclear medicine procedures. *Occup Environ Med.* 2018;75:533–561.
2. Ko S, Chung HH, Cho SB, et al. Occupational radiation exposure and its health effects on interventional medical workers: study protocol for a prospective cohort study. *BMJ Open.* 2017;7:e018333.
3. Wang F, Sun Q, Wang J, Yu N. Risk of developing cancers due to low-dose radiation exposure among medical x-ray workers in China: results of a prospective study. *Int J Clin Exp Pathol.* 2016;9:11897–11903.
4. Azizova TV, Bannikova MV, Grigoryeva ES, Rybkina VL. Risk of malignant skin neoplasms in a cohort of workers occupationally exposed to ionizing radiation at low dose rates. *PLoS One.* 2018;13:e0205060.
5. Radiation: health consequences of the Fukushima nuclear accident. World Health Organization website. https://www.who.int/news-room/questions-and-answers/item/health-consequences-of-fukushima-nuclear-accident. Published March 10, 2016. Accessed March 8, 2023.
6. Domínguez-Gadea L, Cerezo L. Decontamination of radioisotopes. *Rep Pract Oncol Radiother.* 2011;16:147–152.
7. Eroğlu H, Aksakal O. Effectivity analysis of the decontamination products for radioactive materials used in nuclear medicine. *Fen Bilim Derg.* 2016;6:59–69.
8. Rana S, Bhatt S, Dutta M, et al. Radio-decontamination efficacy and safety studies on optimized decontamination lotion formulation. *Int J Pharm.* 2012;434:43–48.
9. Ruhman N, Grantham V, Martin C. The effectiveness of decontamination products in the nuclear medicine department. *J Nucl Med Technol.* 2010;38:191–194.
10. Leonardi NM, Tesan FC, Zubillaga MB, Salgueiro MJ. Radioactivity decontamination of materials commonly used as surfaces in general-purpose radioisotope laboratories. *J Nucl Med Technol.* 2014;42:292–295.
11. Nishad DK, Bhalla S, Khanna K, et al. Decontamination of rat and human skin experimentally contaminated with $^{99m}Tc$, $^{201}Tl$ and $^{131}I$ radionuclides using "Dermadecon"—a skin decontamination kit: an efficacy study. *Cutan Ocul Toxicol.* 2018;37:1–8.
12. Moody RP, Maibach HI. Skin decontamination: importance of the wash-in effect. *Food Chem Toxicol.* 2006;44:1783–1788.
13. Magnano GC, Rui F, Larese Filon F. Skin decontamination procedures against potential hazards substances exposure. *Chem Biol Interact.* 2021;344:109481.
14. Decontamination (from medical aspects of chemical and biological warfare, P 351-360, 1997, Frederick R. Sidell, M.D., Ernest T. Takafuji, M.D., eds, et al.,—see NCJ-190599). Office of Justice Programs website. https://www.ojp.gov/ncjrs/virtual-library/abstracts/decontamination-medical-aspects-chemical-and-biological-warfare-p. Published 1997. Accessed March 8, 2023.

# Duration of Breastfeeding Interruption in Nuclear Medicine Procedures

Dhrumil Naik[1], Hema Merai[2], Ran Klein[2,3], and Wanzhen Zeng[3]

[1]*Department of Mechanical Engineering, University of Ottawa, Ottawa, Ontario, Canada;* [2]*Department of Nuclear Medicine and Molecular Imaging, Ottawa Hospital, Ottawa, Ontario, Canada; and* [3]*Division of Nuclear Medicine and Molecular Imaging, Department of Medicine, University of Ottawa, Ottawa, Ontario, Canada*

The recommendation for the duration of breastfeeding interruption after radiopharmaceutical administration has not been standardized and varies among the guidance documents and publications in the literature. **Methods:** A working group consisting of 3 staff physicians, 2 fellows, and 2 technologists was designated to update the institutional recommendations on breastfeeding interruption based on the review of the guidance documents and the literature. **Results:** Our institutional recommendations on the duration of breastfeeding interruption for 54 radiopharmaceuticals are presented in 4 summary tables. For completeness, we also include other radiopharmaceuticals with available information. **Conclusion:** The detailed recommendation summary on breastfeeding might be helpful to other centers.

**Key Words:** breastfeeding interruption; radiopharmaceutical; radiation to nursing infants

**J Nucl Med Technol 2023; 51:239–246**
DOI: 10.2967/jnmt.122.264910

It is often necessary to administer diagnostic or therapeutic radiopharmaceuticals to the nursing mother despite the risk of radioactivity excreted to breast milk. The lactating breast may accumulate radionuclides (through the tracer itself, metabolites, or impurities), which may result in radiation exposure to the infant through the ingestion of radioactive milk. In addition, the infant also receives external exposure from radioactivity in the mother when the infant is held close.

Although there have been several studies assessing radioactivity in breast milk and risk of radiation exposure to infants (*1–6*), they are limited by assumptions such as estimation of residence time, dosimetry model, breast size during lactation, and the amount and interval of feeding. In particular, it is often assumed that the ingested radionuclide from breast milk becomes systemic instantaneously and follows adult biodistribution behavior, whereas in practice some radionuclides are poorly absorbed from the gastrointestinal tract. The recommendation for the duration of breastfeeding interruption after radiopharmaceutical administration has not been standardized or consistent among guidance documents and publications in the literature.

As a part of quality control of our clinical service from the Patient Safety and Quality Control Committee, we have reviewed the guidance documents and literature on the requirement of breastfeeding interruption for radiopharmaceuticals. The final decision was based on the consensus from a panel of physicians. In this article, we summarize our institutional recommendations on breastfeeding interruption for routinely performed nuclear medicine procedures as well as recommendations from other professional body guidelines and references.

## MATERIALS AND METHODS

A working group consisting of 3 staff physicians, 2 fellows, and 2 technologists was designated to work on the project, with the goal of reviewing the institutional recommendations on breastfeeding interruption and updating study protocols and patient information pamphlets on breastfeeding. The Society of Nuclear Medicine and Molecular Imaging (SNMMI) procedure guidelines (*7*), International Commission on Radiological Protection (ICRP) publication 106 (*8*), the Advisory Committee on the Medical Uses of Isotopes (ACMUI) Subcommittee on Nursing Mother Guidelines for the Medical Administration of Radioactive Materials (*9*), and peer-reviewed publications by Stabin and Breitz (*2*) and by Leide-Svegborn et al. (*1*) were reviewed and referenced. When the guidance documents were inconsistent or had unavailable or incomplete data, the studies were further reviewed and discussed by a physician panel consisting of 3 staff physicians and 1 fellow before the final decision was made.

The recommendations for our institution sought to balance radiation protection with convenience and practicality to the nursing mother and infant. For completeness, we also tabulated procedures and radiopharmaceuticals that are not used in our clinic but may be in common use elsewhere and have available data from the guidance documents and the literature, but we did not make recommendations for these procedures and radiopharmaceuticals.

As there was no patient information involved, institutional review board approval was not required for this review.

## RESULTS

Recommendations for breastfeeding interruption are tabulated in Tables 1–4 by procedure type. For procedures conducted at our institution, recommendations on the duration of breastfeeding interruption are presented in the tables under

Received Sep. 13, 2022; revision accepted Feb. 12, 2023.
For correspondence or reprints, contact Wanzhen Zeng (wzeng@toh.ca).
Published online Apr. 25, 2023.

**TABLE 1**
Duration of Breastfeeding Interruption (Studies Listed Alphabetically from A to I)

| Study | Radiopharmaceutical | Administered dose | Institution guidelines, 2022 | SNMMI/EANM procedure guideline (*7*)* | Stabin and Breitz (*2*) | ICRP 106 (*8*) | Leide-Svegborn (*1*)† | ACMUI (*9*)‡ |
|---|---|---|---|---|---|---|---|---|
| Adrenal medulla | $^{131}$I-MIBG | 37 MBq | Stop | Stop | NA | >3 wk | NA | NA |
| Adrenal medulla | $^{123}$I-MIBG | 370 MBq | 48 h | 48 h | 48 h | >3 wk | NA | NA |
| Bone scan | $^{99m}$Tc-MDP | 11 MBq/kg | 4 h | 4–24 h | 0 | 0 | 0 | 24 h |
| Bone scan PET | $^{18}$F-fluoride | 185–370 MBq | — | NA | NA | NA | NA | 4 h |
| Bone marrow | $^{99m}$Tc-SC | 555 MBq | 4 h | NA | 0 | 0 | NA | 24 h |
| Brain perfusion | $^{99m}$Tc-ECD | 555–1,110 MBq | 4 h | NA | NA | 0 | NA | 24 h |
| Brain perfusion | $^{99m}$Tc-HMPAO | 555–1,110 MBq | 4 h | NA | NA | 0 | NA | 24 h |
| Brain amyloid | $^{18}$F-florbetapir | 370 MBq | — | 24 h | NA | NA | NA | NA |
| Brain amyloid | $^{18}$F-flutemetamol | 185 MBq | — | 24 h | NA | NA | NA | NA |
| Brain amyloid | $^{18}$F-florbetaben | 300 MBq | — | 24 h | NA | NA | NA | NA |
| Breast imaging | $^{99m}$Tc-sestamibi | 300–600 MBq | — | 0 | 0 | 0 | NA | 24 h |
| Breast imaging | $^{99m}$Tc-testrofosmin | 300–600 MBq | — | 0 | NA | 0 | NA | 24 h |
| Cardiac necrosis | $^{99m}$Tc-PYP | 740 MBq | 4 h | NA | 0 | 0 | NA | 24 h |
| Cisternography | $^{111}$In-DTPA | 18–27.8 MBq | 0 | NA | NA | NA | NA | NA |
| Cerebrospinal fluid shuntogram | $^{111}$In-DTPA | 28 MBq | 0 | NA | NA | NA | NA | NA |
| DaTScan | $^{123}$I-ioflupane | 111–185 MBq | 3 d | 1–6 d | NA | NA | NA | NA |
| Brain scan | $^{18}$F-FDG | 4.9 MBq/kg | 12 h | 24 h | NA | 0 | 0 | 4 h |
| Esophageal transit | $^{99m}$Tc-SC | 40 MBq | 4 h | NA | 0 | 0 | NA | 24 h |
| $^{18}$F-FDG PET (oncology) | $^{18}$F-FDG | 4.9 MBq/kg | 12 h | 12 h | NA | 0 | 0 | 4 h |
| $^{67}$Ga scan | $^{67}$Ga-citrate | 148–333 MBq | Stop | 2–4 wk | Stop | >3 wk | NA | 28 d |
| Gastric emptying/transit (liquid) | $^{99m}$Tc-DTPA | 37 MBq | 4 h | NA | 0 | 0 | NA | 24 h |
| Gastric emptying (solid) | $^{99m}$Tc-SC | 18.5 MBq | 4 h | NA | 0 | 0 | NA | 24 h |
| Gastrointestinal bleed | $^{99m}$Tc-RBC in vitro | 555–1,110 MBq | 4 h | 0 | 0 | 0 | NA | 24 h |
| Heat-damaged RBC scan | $^{99m}$Tc-RBC in vitro | 370 MBq | 4 h | NA | 0 | 0 | NA | 24 h |
| Hepatic hemangioma | $^{99m}$Tc-RBC in vitro | 750–925 MBq | 4 h | NA | 0 | 0 | NA | 24 h |
| Hepatobiliary scan | $^{99m}$Tc-DISIDA | 185 MBq | 4 h | 0 | 0 | 0 | NA | 24 h |
| Hepatobiliary scan | $^{99m}$Tc-mebrofenin | 185 MBq | 4 h | 0 | NA | NA | NA | 24 h |
| Iodine whole-body imaging | $^{131}$I-NaI | 185 MBq | Stop | NA | Stop | >3 wk | Stop | Stop |
| Iodine whole-body imaging | $^{123}$I-NaI | 74–185 MBq | 4 d | NA | Stop | >3 wk | NA | 3 d |

*Or publicly available guidance documents.

†Recommendation was based on both internal and external radiation exposure.

‡Single 24-h interruption period is recommended for $^{99m}$Tc-labeled radiopharmaceuticals to simplify guidance.

MIBG = metaiodobenzylguanidine; NA = data not available; MDP = methyl diphosphonate; 0 = no breastfeeding cessation is necessary; — = not institutional procedure; SC = sulfur colloid; ECD = ethyl cysteinate dimer; HMPAO = hexamethylpropyleneamine oxime; PYP = pyrophosphate; DTPA = diethylenetriaminepentaacetic acid; RBC = red blood cell; DISIDA = diisopropyl iminodiacetic acid.

**TABLE 2**
Duration of Breastfeeding Interruption (Studies Beginning with L)

| Study | Radiopharmaceutical | Administered dose (MBq) | Institution guidelines, 2022 | SNMMI/EANM procedure guideline (*7*)* | Stabin and Breitz (*2*) | ICRP 106 (*8*) | Leide-Svegborn (*1*)† | ACMUI (*9*)‡ |
|---|---|---|---|---|---|---|---|---|
| Lacrimal gland | $^{99m}$Tc-pertechnetate | 7.4 | 0 | NA | NA | NA | NA | NA |
| Liver, spleen | $^{99m}$Tc-SC | 200 | 4 h | NA | 0 | 0 | NA | 24 h |
| Lung perfusion | $^{99m}$Tc-MAA | 74–185 | 12 h | NA | 12 h | 12 h | 12 h | 24 h |
| Lung ventilation | $^{99m}$Tc-Technegas | 18–37 | 0 | NA | NA | 0 | NA | 24 h |
| Lung ventilation | $^{99m}$Tc-DTPA aerosol | 20–40 | — | NA | 0 | NA | NA | 24 h |
| Lung ventilation | $^{99m}$Tc-SC aerosol | 20–40 | — | 0 | NA | NA | NA | 24 h |
| Lung ventilation | $^{81m}$Kr gas | 40–400 | — | 0 | NA | 0 | NA | NA |
| Lung ventilation | $^{133}$Xe gas | 200–750 | — | 0 | NA | 0 | NA | NA |
| Lymphoscintigraphy | $^{99m}$Tc-filtered SC | 37 | 4 h | 24 h | 0 | 0 | NA | 24 h |
| Lymphoscintigraphy | $^{99m}$Tc-unfiltered SC | 185 | 4 h | 24 h | 0 | 0 | NA | 24 h |
| Lymphoscintigraphy | $^{99m}$Tc-sulphide nanocolloid | 3.7−370 | — | 24 h | NA | NA | NA | 24 h |
| Lymphoscintigraphy | $^{99m}$Tc-nanocolloidal albumin | 3.7–370 | — | 24 h | NA | NA | NA | 24 h |
| Lymphoscintigraphy | $^{99m}$Tc-antimony trisulfide | 3.7−370 | — | 24 h | NA | NA | NA | 24 h |
| Lymphoscintigraphy | $^{99m}$Tc-tilmanocept | 3.7−370 | — | 24 h | NA | NA | NA | 24 h |
| $^{177}$Lu-DOTATATE | $^{177}$Lu-oxodotreotide | 3,700 | Stop | 2.5 mo | NA | NA | NA | Stop |

*Or publicly available guidance documents.
†Recommendation was based on both internal and external radiation exposure.
‡Single 24-h interruption period is recommended for $^{99m}$Tc-labeled radiopharmaceuticals to simplify guidance.
NA = data not available; 0 = no breastfeeding cessation is necessary; SC = sulfur colloid; DTPA = diethylenetriaminepentaacetic acid; — = not institutional procedure.

**TABLE 3**
Duration of Breastfeeding Interruption (Studies Listed Alphabetically from M to S)

| Study | Radiopharmaceutical | Administered dose | Institution guidelines, 2022 | SNMMI/EANM procedure guideline (*7*)* | Stabin and Breitz (*2*) | ICRP 106 (*8*) | Leide-Svegborn (*1*)† | ACMUI (*9*)‡ |
|---|---|---|---|---|---|---|---|---|
| Meckel diverticulum | $^{99m}$Tc-pertechnetate | 555 MBq | 12 h | 12 h | 4 h | 12 h | 12 h | 24 h |
| Multigated acquisition | $^{99m}$Tc-RBC modified in vivo | 925 MBq | 12 h | 24 h | 12 h | 12 h | 0 | 24 h |
| Myocardial perfusion (rest + stress) | $^{99m}$Tc-tetrofosmin | 1,184 MBq | 4 h | 4 h | NA | 0 | NA | 24 h |
| Myocardial perfusion (rest + stress) | $^{99m}$Tc-sestamibi | 1,184 MBq | 4 h | 4 h | 0 | 0 | 0 | 24 h |
| Myocardial perfusion | $^{201}$Tl-chloride | 111 MBq | 4 d | 48 h | 96 h | 48 h | NA | 4 d |
| Myocardial perfusion | $^{82}$Rb | 1,100–1,850 MBq | — | NA | NA | NA | NA | 0 |
| Myocardial perfusion | $^{13}$N-ammonia | 370–740 MBq | — | NA | NA | 0 | NA | 1 h |
| Sodium fluoride PET | $^{18}$F-NaF | 2.22 MBq/kg | 0 | NA | NA | NA | NA | 4 h |
| Octreotide scan | $^{111}$In-octreotide | 111 MBq | 0 | 0 | NA | 0 | NA | 6 d |
| Parathyroid scan | $^{99m}$Tc-sestamibi | 740 MBq | 4 h | 0 | 0 | 0 | NA | 24 h |
| Parathyroid scan | $^{99m}$Tc-tetrofosmin | 185–925 MBq | — | 0 | NA | 0 | NA | 24 h |
| Parathyroid scan (for dual phase) | $^{99m}$Tc-pertechnetate | 75–150 MBq | — | 12 h | 4 h | 12 h | NA | 24 h |
| Parathyroid scan (for dual tracer) | $^{123}$I-NaI and $^{99m}$Tc-sestamibi | 7.5–20 and 740 MBq | 4 d | 3 wk | Stop | >3 wk | NA | 3 d |
| R to L shunt | $^{99m}$Tc-MAA | 37 MBq | 12 h | NA | NA | NA | NA | 24 h |
| Renal cortical | $^{99m}$Tc-gluceptate | 296 MBq | 4 h | NA | 0 | 0 | NA | 24 h |
| Renal cortical | $^{99m}$Tc-DMSA | 111 MBq | 4 h | NA | NA | 0 | NA | 24 h |
| Renal function | $^{99m}$Tc-MAG-3 | 260 MBq | 4 h | 4 h | 0 | 0 | 0 | 24 h |
| Renal function | $^{99m}$Tc-DTPA | 370 MBq | 4 h | 12 h | 0 | 0 | 0 | 24 h |
| Renal GFR | $^{99m}$Tc-DTPA | 37 MBq | 4 h | NA | 0 | 0 | 0 | 24 h |
| Salivary gland scan | $^{99m}$Tc-pertechnetate | 555 MBq | 12 h | NA | 4 h | 12 h | 12 h | 24 h |
| SeHCAT scan | $^{75}$Se-tauroselcholic acid | 0.37 MBq | >3 wk | NA | NA | >3 wk | NA | NA |
| Small-bowel and colon transit | $^{99m}$Tc-SC | 18.5–37 MBq | — | NA | 0 | 0 | NA | 24 h |

*Or publicly available guidance documents.
†Recommendation was based on both internal and external radiation exposure.
‡Single 24-h interruption period is recommended for $^{99m}$Tc-labeled radiopharmaceuticals to simplify guidance.
RBC = red blood cell; 0 = no breastfeeding cessation is necessary; NA = data not available; — = not institutional procedure; DMSA = dimercaptosuccinic acid; MAG = mercaptoacetyltriglycine; DTPA = diethylenetriaminepentaacetic acid; SC = sulfur colloid.

**TABLE 4**
Duration of Breastfeeding Interruption (Studies Listed Alphabetically from T to Z)

| Study | Radiopharmaceutical | Administered dose | Institution guidelines, 2022 | SNMMI/EANM procedure guideline (7)* | Stabin and Breitz (2) | ICRP 106 (8) | Leide-Svegborn (1)† | ACMUI (9)‡ |
|---|---|---|---|---|---|---|---|---|
| Thyroid scan | $^{123}$I-NaI | 18.5 MBq | 4 d | NA | 0 | >3 wk | NA | 3 d |
| Thyroid scan | $^{99m}$Tc-pertechnetate | 370 MBq | 12 h | NA | 4 h | 12 h | 12 h | 24 h |
| Thyroid uptake | $^{131}$I-NaI | 0.37 MBq | Stop | NA | Stop | >3 wk | Stop | Stop |
| Thyroid ablation (hyperthyroidism) | $^{131}$I-NaI | 185–1,110 MBq | Stop | Stop | Stop | >3 wk | Stop | Stop |
| Thyroid cancer ablation§ | $^{131}$I-NaI | 1,100–7,400 MBq | Stop 3 mo prior | Stop | Stop | >3 wk | Stop | Stop |
| Urea breath test | $^{14}$C-urea | 0.037 MBq | 0 | NA | NA | 0 | NA | NA |
| WBC scan | $^{111}$In-oxine WBC | 10–40 MBq | 0 | NA | 0 | 0 | NA | 6 d |
| WBC scan | $^{99m}$Tc-HMPAO WBC | 370–740 MBq | 24 h | NA | 48 h | 12 h | 0 | 24 h |
| $^{90}$Y-radiolabeled therapy | $^{90}$Y-ibritumomab tiuxetan | 15 MBq/kg | — | Stop | NA | NA | NA | NA |

*Or publicly available guidance documents.
†Recommendation was based on both internal and external radiation exposure.
‡Single 24-h interruption period is recommended for $^{99m}$Tc-labeled radiopharmaceuticals to simplify guidance.
§For radioiodine ablation for thyroid cancer, discontinuation of breastfeeding of 3 mo is recommended before therapy to reduce radiation exposure to lactating breast.
NA = data not available; 0 = no breastfeeding cessation is necessary; WBC = white blood cell; HMPAO = hexamethylpropyleneamine oxime; — = not institutional procedure.

the header "institution guidelines, 2022." For completeness, we included procedures and radiopharmaceuticals with available recommendations from the literature that are not performed at our institution, but we do not make recommendations for these.

For simplicity of implementing in a clinical setting, the recommendations were categorized into the following sets.

#### No Interruption Needed

Breastfeeding interruption is unnecessary for cerebrospinal fluid cisternography and shuntography, lacrimal gland studies, lung ventilation studies with Technegas (Cyclomedica Australia Pty. Ltd.), sodium fluoride PET, urea breath testing, $^{111}$In-octreotide scanning, and white blood cell scanning with $^{111}$In-oxine.

#### 4-h Interruption

A 4-h interruption period is recommended for most $^{99m}$Tc-labeled studies. Although most radiopharmaceuticals have very low radioactivity in the breast, the recommendation is based mainly on the concern of $^{99m}$Tc-pertechnetate impurity, as $^{99m}$Tc-pertechnetate is widely recognized to be avidly concentrated in the lactating breast (*1,6*).

#### 12-h Interruption

A 12-h interruption period is recommended for lung perfusion scanning and right-to-left shunt scanning with $^{99m}$Tc-macroaggregated albumin (MAA), thyroid scanning, Meckel diverticulum scanning and salivary gland scanning with $^{99m}$Tc-pertechnetate, oncology and epilepsy $^{18}$F-FDG PET, and multigated acquisition scanning with modified in vivo labeled red blood cells

#### Cessation

Breastfeeding should be stopped or interrupted for at least 3 wk for all scanning with $^{131}$I-labeled radiopharmaceuticals, $^{67}$Ga-citrate scanning, SeHCAT (GE Healthcare) scanning with $^{75}$Se-tauroselcholic acid, and $^{177}$Lu-DOTATATE therapy with $^{177}$Lu-oxodotreotide.

#### Others

Breastfeeding should be interrupted for 24 h for white blood cell scanning with $^{99m}$Tc-hexamethylpropyleneamine oxime, 48 h for adrenal medulla studies with $^{123}$I-metaiodobenzylguanidine, 3 d for a DaTscan (GE Healthcare) with $^{123}$I-ioflupane, and 4 d for whole-body thyroid scanning with $^{123}$I-sodium iodine, partly because of concerns about possible $^{131}$I contamination.

## DISCUSSION

Although a nursing mother who has received unsealed radioactive material can be released by a licensee if the total effective dose to any other individual exceeds 0.5 rem (5 mSv) in the United States, federal regulations (title 10 of *Code of Federal Regulations,* section 35.75) (*10*) require that the licensee must give guidance on the interruption or cessation of breastfeeding and information on the consequences of failure to follow the guidance if the dose to a breastfeeding infant or

child could exceed 0.1 rem (1 mSv). Consequently, the recommendation on breastfeeding interruption from most guidance documents is based on the 1-mSv radiation exposure limit to the infant or child. However, infants and children are known to be about 3 times more sensitive to radiation than adults (*11*), and their vulnerability to radiation was considered when formulating the recommendations, usually with a conservative approach assuming a worst-case scenario (*1,5,9*).

Radiation exposure to a nursing child from a radiopharmaceutical administered to the child's mother comes from both ingestion of radioactive maternal milk and external exposure from radioactivity in the mother. Generally, less than 10% of an administered radiopharmaceutical's activity is excreted into breast milk; typical estimates range from 0.3% to 5% of the initial administered activity (*2*), depending on the radiopharmaceutical and physiologic factors. If breastfeeding were not discontinued, the doses from ingestion of radioactive milk to the newborn tissues (whole body or thyroid) could be calculated by summing the exposure from each feeding.

At our institution we follow the clinical procedure guidelines from the SNMMI and European Association of Nuclear Medicine (EANM); their recommendations on breastfeeding interruption are presented in the 4 tables. In general, SNMMI guidance documents are based on the consensus of experts from various fields, with consideration of scientific data from the ICRP, feasibility and convenience for patients, and the flexibility of the study. Consequently, the cutoff for breastfeeding interruption for some radiopharmaceuticals is loosely defined in their recommendations.

Stabin is well known for his work on dosimetry of radiopharmaceuticals, including studies on breast milk excretion. In the classic study of Stabin and Breitz on breast milk excretion (*2*), they provided not only the recommendations for 25 radiopharmaceuticals but also an understanding of radiation dosimetry, including breast anatomy, the physiology of lactation, a possible mechanism for breast milk excretion of radiopharmaceuticals, breast radiation exposure, and exposure to infants. Their recommendations are presented in the 4 tables.

The ICRP is a nongovernment organization that provides recommendations and guidance on protection against the risk associated with ionizing radiation. Societies such as the SNMMI depend on the ICRP for guidance. Because of its influence and impact on radiation safety protection, we present its recommendations in the 4 tables.

There are limited studies on breast milk excretion of radiopharmaceuticals. A recent study of activity concentration in breast milk from 53 breastfeeding patients after administration of 16 different radiopharmaceuticals has added new data to the field (*1*). The study provided estimates of absorbed doses to various organs and tissues and the effective dose to the infant. Consequently, the recommendations of this study are also presented in the 4 tables.

The ACMUI advises the U.S. Nuclear Regulatory Commission on policy and technical issues that arise in the regulation of the medical uses of radioactive material in diagnosis and therapy. A subcommittee on nursing mother guidelines for the medical administration of radioactive materials, led by experts in the field, provided updated recommendations for the nursing mother (*10*). For $^{99m}$Tc-labeled radiopharmaceuticals, rather than a radiopharmaceutical-specific interruption period, a single 24-h interruption period is recommended by the ACMUI. It argued that although this interval may be longer than necessary for some $^{99m}$Tc-labeled radiopharmaceuticals, the recommendation is compliant with the 0.1-rad dose limit and simplifies the guidance, thereby avoiding confusion and reducing the likelihood of error. Consequently, the ACMUI recommendations for most $^{99m}$Tc-labeled radiopharmaceuticals are different from other references and generally more conservative in terms of radiation risk.

There are differences in recommendations between our institution and other references shown in the tables for some radiopharmaceuticals. For $^{99m}$Tc-methyl diphosphonate, the SNMMI guidance document (*7*) is not definitive on the duration of breastfeeding interruption, with 2018 guidelines stating: "Per the International Commission on Radiological Protection, $^{99m}$Tc-labeled radiopharmaceuticals do not require any change in breastfeeding (unless $^{99m}$Tc-$NaO_4$ is present). Nevertheless, it may be recommended that the patient delay breastfeeding for a minimum of 4 h after receiving a $^{99m}$Tc-labeled radiopharmaceutical, and many institutions have the patient delay breastfeeding for 24 h."

According to the EANM guidelines, whereas interruption of breastfeeding is not essential according to the ICRP, this is based on there being no free pertechnetate in the radiopharmaceutical. Therefore, an interruption of at least 4 h during which 1 meal is discarded is advised to be on the safe side. The ACMUI recommends 12 h for most $^{99m}$Tc-labeled radiopharmaceuticals for simplicity. On the basis of the available studies in the literature, and considering the possibility of free pertechnetate, which has been shown to be excreted in breast milk, we recommend a 4-h interruption of breastfeeding for $^{99m}$Tc-methyl diphosphonate, consistent with the guidance documents from the SNMMI and EANM.

It has been shown that $^{99m}$Tc-MAA and $^{99m}$Tc-pertechnetate have a higher breast excretion than other $^{99m}$Tc-labeled radiopharmaceuticals (*1,2*). For $^{99m}$Tc-MAA, it is speculated that "The individual variations in the initial $^{99m}$Tc concentrations and, likewise, in the total activities excreted in the breast milk were presumably caused by various amounts of $^{99m}$Tc-pertechnetate in the initial $^{99m}$Tc-MAA preparation, and by varied rates of breakdown of macroaggregate in the lungs." (*1*). Consequently, for both $^{99m}$Tc-MAA and $^{99m}$Tc-pertechnetate we recommend a 12-h interruption whereas for other $^{99m}$Tc-labeled radiopharmaceuticals we recommend a 4-h interruption, consistent with most of the references in the tables.

For $^{123}$I in the form of NaI ($^{123}$I-NaI), a shorter discontinuation period of 3 or 4 d is recommended by our institution and by the ACMUI than the earlier recommendation, which

was based on the contamination (≤2.5% of the total activity) with long-lived $^{125}$I (physical half-life, 60 d) that occurred with older methods of $^{123}$I production (such contamination of $^{123}$I with $^{125}$I no longer occurs). Our recommendation of a 4-d interruption is similar to that of the ACMUI (3-d interruption) but much shorter than the recommendations of more than 3 wk from the ICRP (*8*) and the cessation recommended by Stabin and Breitz (*2*), thus significantly improving the prospect of resuming breastfeeding.

There is a significant difference in the recommendation for $^{111}$In-oxine white blood cell scanning. Both Stabin et al. (*2*) and the ICRP recommended no cessation, whereas the ACMUI (*10*) recommends a 6-d interruption. Although the recommendation from the ACMUI was based on the data from Stabin and Breitz (*2*), the reported administered activity is quite different (185 MBq from Table 4 from the ACMUI and 18.5 MBq from Stabin and Breitz), probably because of a typographic error. On the basis of the original data from Stabin and Breitz, we have recommended no cessation. For $^{111}$In-octreotide scanning, the SNMMI and ICRP recommend no cessation whereas the ACMUI recommends a 6-d interruption, based on the kinetic data from Castronovo et al. (*5*). In the study by Castronova et al., they measured the concentration of $^{111}$In in breast milk in a 10-wk-postpartum woman at daily intervals up to 72 h after injection of 196.1 MBq (5.3 mCi) of $^{111}$In-octreotide, with a conservative approach. They showed that if a newborn is nursed for the first 10 d, the internal and external dose equivalents would be 0.23 and 0.28 mSv, respectively, for a total of 0.51 mSv. The difference in recommendation was discussed with our working group, and until more data are available, we have decided to keep our recommendation of no cessation for the $^{111}$In-octreotide scan. This test will soon be replaced with PET.

The external exposure from radioactivity in the mother to the infant could be significant, especially with high-energy photon radiopharmaceuticals (e.g., positron emitters). Despite common observations of increased breast $^{18}$F-FDG uptake in the lactating breast, $^{18}$F activity measured in breast milk was low (*3*), suggesting that the main source of potential radiation hazard to a breastfeeding infant is likely to be from the infant's close proximity to the breast (external) rather than from ingestion of milk (internal). Consequently, patients should also be advised to avoid close contact with their children to reduce external radiation exposure. Our recommendation of breastfeeding interruption and avoiding close contact with the infant for 12 h is consistent with the SNMMI/EANM guidelines. The ACMUI recommended a 4-h interruption, possibly based only on the biokinetics of $^{18}$F-FDG and the absorbed-dose estimates for the lactating breast.

The mother should be advised to breastfeed the baby right before administration of the radiopharmaceutical and the interruption period. During this interruption, breast milk may be expressed at the usual feeding times and discarded or frozen for later use, depending on the circumstances. Afterward, breastfeeding can resume without concern. For an interruption period of longer than 3 wk, it may be difficult to resume breastfeeding. However, if the mother wishes to continue to breastfeed, she is advised to continue to express breast milk at the usual feeding times and discard it each time during these 3 wk.

There is a 2- to 5-fold increase in breast mass during lactation, and it is known that the lactating breast is sensitive to radiation. Except for $^{67}$Ga-citrate and $^{131}$I-NaI, the highest absorbed dose estimates to the lactating breast for typical diagnostic administered activities are usually well under 0.01 Gy (1 rad). The absorbed dose to the lactating breast with a therapeutic administered activity of 4,000 MBq (108 mCi) of $^{131}$I-NaI was estimated to be 1.6 Gy (160 rad) (*12*). For lactating patients undergoing radioiodine therapy, we have followed the American Thyroid Association guidelines (*13*) and recommend discontinuing breastfeeding 3 mo before radioiodine ablation therapy to minimize the radioiodine concentration in the maternal breast and, thus, the absorbed maternal breast dose.

## CONCLUSION

The use of radiopharmaceuticals in breastfeeding patients can elevate the risk of radiation exposure to the feeding infant and the lactating breast. Other centers might find helpful the detailed recommendations on breastfeeding for radiopharmaceuticals used in our center and the summary recommendations from leading professional bodies and the academic literature presented in this study.

## DISCLOSURE

Ran Klein receives revenue shares from the sale of rubidium generators from Jubilant-DraxImage and from the sale of myocardial flow quantification software from Invia Medical Solutions. No other potential conflict of interest relevant to this article was reported.


## ACKNOWLEDGMENTS

We thank Drs. Farzad Abbaspour, Christiane Wiefels, Eugene Leung, and Asya Al-Busaidi, as well as Sarah Ternan, for their contribution to the project.


## KEY POINTS

**QUESTION:** Is the summary of breastfeeding interruption for nuclear medicine procedures helpful to nuclear medicine professionals?

**PERTINENT FINDINGS:** We present detailed summary tables on breastfeeding interruption from institutional recommendations and the literature.

**IMPLICATIONS FOR PATIENT CARE:** The summary tables may be helpful to busy practicing nuclear medicine technologists and physicians.

## REFERENCES


1. Leide-Svegborn S, Ahlgren L, Johansson L, Mattsson S. Excretion of radionuclides in human breast milk after nuclear medicine examinations: biokinetic and dosimetric data and recommendations on breastfeeding interruption. *Eur J Nucl Med Mol Imaging.* 2016;43:808–821.
2. Stabin MG, Breitz HB. Breast milk excretion of radiopharmaceuticals: mechanisms, findings, and radiation dosimetry. *J Nucl Med.* 2000;41:863–873.
3. Hicks RJ, Binns D, Stabin MG. Pattern of uptake and excretion of $^{18}$F-FDG in the lactating breast. *J Nucl Med.* 2001;42:1238–1242.
4. Stabin MG, Sparks RB, Crowe E. OLINDA/EXM: the second-generation personal computer software for internal dose assessment in nuclear medicine. *J Nucl Med.* 2005;46:1023–1027.
5. Castronovo FP, Stone H, Ulanski J. Radioactivity in breast milk following $^{111}$In-octreotide. *Nucl Med Commun.* 2000;21:695–699.
6. Rubow S, Klopper J, Wasserman H, Baard B, van Niekerk M. The excretion of radiopharmaceuticals in human breast milk: additional data and dosimetry. *Eur J Nucl Med.* 1994;21:144–153.
7. Bartel TB, Kuruva M, Gnanasegaran G, et al. SNMMI procedure standard for bone scintigraphy 4.0. *J Nucl Med Technol.* 2018;46:398–404.
8. ICRP. Radiation dose to patients from radiopharmaceuticals: addendum 3 to ICRP publication 53—ICRP publication 106. Approved by the commission in October 2007. *Ann ICRP.* 2008;38:1–197.
9. Dilsizian V, Metter D, Palestro C, Zanzonico P. Advisory Committee on Medical Uses of Isotopes (ACMUI) Sub-Committee on Nursing Mother Guidelines for the Medical Administration of Radioactive Materials. The U.S. Nuclear Regulatory Commission (NRC) website. https://www.nrc.gov/docs/ML1903/ML19038A498.pdf. Published January 31, 2019. Accessed March 7, 2023.
10. *Regulatory Guide 8.39: Release of Patients Administered Radioactive Materials*. U.S. Nuclear Regulatory Commission; April 1997.
11. 1990 recommendations of the International Commission on Radiological Protection. *Ann ICRP.* 1991;21:1–201.
12. Robinson PS, Barker P, Campbell A, Henson P, Surveyor I, Young PR. Iodine-131 in breast milk following therapy for thyroid carcinoma. *J Nucl Med.* 1994;35:1797–1801.
13. Haugen BR, Alexander EK, Bible KC, et al. 2015 American Thyroid Association management guidelines for adult patients with thyroid nodules and differentiated thyroid cancer: the American Thyroid Association guidelines task force on thyroid nodules and differentiated thyroid cancer. *Thyroid.* 2016;26:1–133.

# ChatGPT in Nuclear Medicine Education

Geoffrey Currie[1] and Kym Barry[2]

[1]*Charles Sturt University, Wagga Wagga, New South Wales, Australia; and* [2]*Charles Sturt University, Port Macquarie, New South Wales, Australia*

Academic integrity has been challenged by artificial intelligence algorithms in teaching institutions, including those providing nuclear medicine training. The GPT 3.5–powered ChatGPT chatbot released in late November 2022 has emerged as an immediate threat to academic and scientific writing. **Methods:** Both examinations and written assignments for nuclear medicine courses were tested using ChatGPT. Included was a mix of core theory subjects offered in the second and third years of the nuclear medicine science course. Long-answer–style questions (8 subjects) and calculation-style questions (2 subjects) were included for examinations. ChatGPT was also used to produce responses to authentic writing tasks (6 subjects). ChatGPT responses were evaluated by Turnitin plagiarism-detection software for similarity and artificial intelligence scores, scored against standardized rubrics, and compared with the mean performance of student cohorts. **Results:** ChatGPT powered by GPT 3.5 performed poorly in the 2 calculation examinations (overall, 31.7% compared with 67.3% for students), with particularly poor performance in complex-style questions. ChatGPT failed each of 6 written tasks (overall, 38.9% compared with 67.2% for students), with worsening performance corresponding to increasing writing and research expectations in the third year. In the 8 examinations, ChatGPT performed better than students for general or early subjects but poorly for advanced and specific subjects (overall, 51% compared with 57.4% for students). **Conclusion:** Although ChatGPT poses a risk to academic integrity, its usefulness as a cheating tool can be constrained by higher-order taxonomies. Unfortunately, the constraints to higher-order learning and skill development also undermine potential applications of ChatGPT for enhancing learning. There are several potential applications of ChatGPT for teaching nuclear medicine students.

**Key Words:** artificial intelligence; tertiary education; higher education; academic integrity; generative AI; language model

**J Nucl Med Technol 2023; 51:247–254**
DOI: 10.2967/jnmt.123.265844

Although contract cheating and ghostwriting in academic or scientific writing are not new concepts, they have become more efficient with advances in information technology (*1*). Nuclear medicine technologist or scientist students and authors are not immune to this scourge. At the heart of the issue is academic integrity. There is potential for significant reputational damage to institutions when authorship is claimed for work that has been produced by another or assessment is fraudulent. For our students, public safety is an issue if graduates cheat to produce evidence of skills and capabilities (*2*). Indeed, contract cheating among university students has reached epidemic proportions with developments in artificial intelligence (AI) algorithms and with the coronavirus disease 2019 pandemic having driven a move to online or flexible learning and assessment.

ChatGPT (OpenAI) overcomes the limitations of early algorithms for generative writing and contract cheating sites. The ghostwriting capability of ChatGPT poses an immediate threat to the academic integrity of student assessments despite being publicly released only recently, on November 30, 2022. Less than 2 mo after the launch, ChatGPT had more than 100 million users (*3*). Numerous universities and colleges have reacted to the emergence of ChatGPT by banning its use. Banning use to prevent misuse also eliminates ChatGPT as a potential tool for enhancing learning and writing.

The role of ChatGPT and other AI tools in education is not an easy debate. AI can significantly enhance student learning and capability development and should be supported from that front-door context because it is aligned with the underlying goals and strategies of a teaching institution. Nonetheless, AI use can hide lack of understanding or can fabricate evidence of capability that does not exist—a misuse that should not be acceptable because, at the back door, it undermines the evidence that students meet the graduate outcomes. Indeed, this misuse may relate to the definition of AI; when the term *AI* is used to mean "artificial intelligence," the student has not developed real knowledge or capability, but when the term is used to mean "augmented intelligence," student understanding and capability have been enhanced. In either case—misuse or enhanced learning—access to ChatGPT can create inequity typical of the social asymmetry for AI in education and health (*4*).

The suitability of ChatGPT as an educational tool also needs to consider the currency of GPT 3.5, which powers ChatGPT. At the time of writing, the publicly available ChatGPT learning cutoff date was September 2021. ChatGPT does not have real-time access to information, including the Internet, and does not learn new information based on user input. This limitation is particularly important in nuclear medicine because the field enjoys rapidly advancing technology and techniques; ChatGPT responses may not reflect information currency. For the new edition of ChatGPT powered by

Received Apr. 12, 2023; revision accepted May 13, 2023.
For correspondence or reprints, contact Geoffrey Currie (gcurrie@csu.edu.au).
Published online Jul. 11, 2023.

GPT 4, accuracy is improved by 60%, including enhanced interpreting of context and reasoning. When available to the public, ChatGPT powered by GPT 4 will allow voice and image inputs for interpretation, will correct or write code, will allow 25,000 words to be inputted for editing and refinement, and will produce outputs of up to 52 pages (3 is the current limit), all of which will broaden the applications and flexibility for students in nuclear medicine (*5,6*).

Numerous universities, including Charles Sturt University, have banned use of ChatGPT. The challenge remains in policing such bans, especially in an era of online or flexible learning and open-book, noninvigilated online examinations. An opposing view relates to authentic assessment and learning. With ChatGPT emerging as a tool for use among nuclear medicine professionals in the clinical and research environment, should assessment not afford that same environment? ChatGPT could enhance student critical thinking, problem solving, and writing skills and could be especially helpful when English is a second language. ChatGPT could craft realistic scenarios for case-based learning, help personalize learning, and distil complex learning topics (e.g., from textbooks or lectures) for improved understanding (*3*). Deeper insight into potential misuse is required before these potential benefits are discarded.

## MATERIALS AND METHODS

To evaluate the capabilities of ChatGPT use among undergraduate nuclear medicine students, a sample of the theory-based assessment requirements for second- and third-year undergraduate subjects was used. There are no nuclear medicine–specific subjects in the first year. The subjects included a general second-year subject ("Imaging Pathology") and 3 nuclear medicine–specific subjects ("Nuclear Medicine 1," "Radiopharmacy," and "Instrumentation"). Additionally, 2 general third-year subjects ("CT" and "Pharmacology") and 2 nuclear medicine–specific subjects ("Nuclear Medicine 2" and "Nuclear Medicine 3") were sampled. For each of the 8 subjects, final examination questions were individually entered into ChatGPT. Additionally, written assessment tasks for 6 of the subjects were also entered into ChatGPT, along with the task expectations and requirements (e.g., topic, fully referenced, word count, specific inclusions). Both the subject "Radiopharmacy" and the subject "Pharmacology" also had a second examination comprising calculation-based questions that were individually entered into ChatGPT. The copy-and-paste function was used to lift questions into the ChatGPT window. Examination and written task answers provided by ChatGPT were transferred to an examination sheet and sent for scoring against the standard rubric for each task. Scoring was out of sequence with actual student submissions, and as a result, scoring was not masked; the scorers were aware that the submission was from ChatGPT. This lack of masking could produce a bias in results; however, all scorers were required to score objectively against the standardized rubric and against the expectations for each question and to justify those scores for moderation. Consequently, the scores are expected to be representative and realistic compared with the corresponding student cohort.

Turnitin software detects plagiarism (similarity report) and generates an AI score. This function was introduced in April 2023 to combat generative AI in academic submissions. The score represents the percentage of the submission that Turnitin is 98% certain was generated by AI. Each of the examinations and written tasks was submitted to Turnitin, and both similarity reports and AI reports were generated.

## RESULTS

Both the second-year subject "Radiopharmacy" and the third-year subject "Pharmacology" had calculation examinations with passing scores of 60%. ChatGPT was particularly poor at calculation-style questions. For the subject "Radiopharmacy," ChatGPT was particularly poor, with a score of 24.0% compared with a student mean of 67.3% (Fig. 1). This comprised 31.7% in short calculations and 8.7% in more complex problems. ChatGPT was particularly confounded by decay calculations and on several occasions performed the calculations starting with the premise "assuming no decay" for $^{99m}$Tc with several hours of nonnegligible decay. Indeed, even when prompted to recalculate incorporating decay, ChatGPT produced incorrect answers. For the subject "Pharmacology," among the shorter calculation questions, ChatGPT provided the correct answers with full working for 92.7% of available scores but was unable to provide correct answers for any of the more complex questions (zero scores). Overall, in the calculation examination, ChatGPT received a score of 38.8% whereas the mean among 81 students was 67.6%. For several of the more complex questions, ChatGPT had the correct formula and the correct numbers in the formula but the wrong answer, which then impacted subsequent calculations; it got the

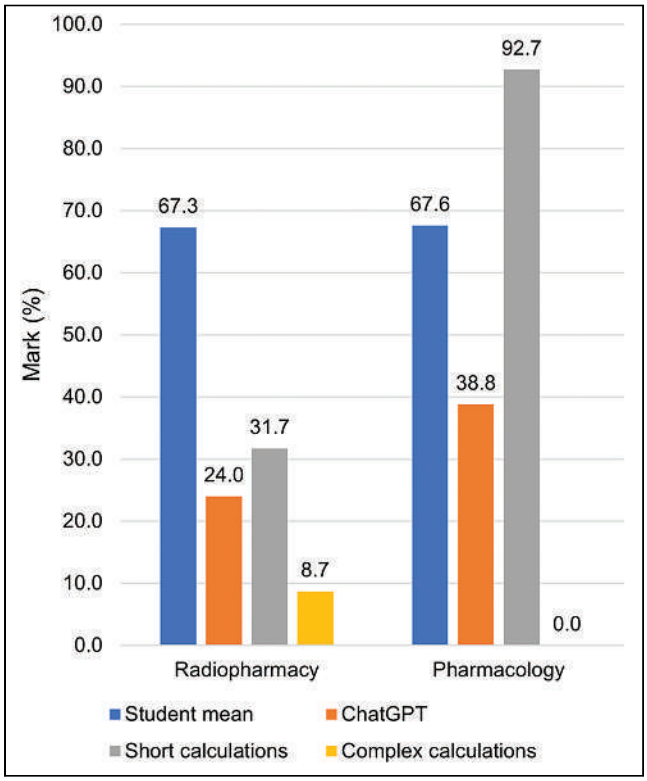


**FIGURE 1.** Bar chart for student mean and ChatGPT score for each calculation examination, including performance for short problems and complex problems.

simplest part incorrect. Interestingly, ChatGPT handled first-order concentration calculations in the course "Pharmacology" at a higher standard than decay questions in the subject "Radiopharmacy" although the mathematics were identical:

$$C = C_0\, e^{-k.t} \text{ vs. } A = A_0\, e^{-\gamma.t}$$

The 6 written assignment tasks were scored against the task rubric (Fig. 2). In all 6 subjects, ChatGPT scored significantly more poorly than the mean student score. A general trend suggested that the gap between student mean and ChatGPT scores widened with course progression, indicating that students were developing research and writing skills against higher-order expectations. Each subject was scored independently; however, the feedback in scoring rubrics was consistent for ChatGPT. For example, answers provided shallow insight not connected strongly to practice; research was shallow and narrow, which left answers well short of expectations; language for some aspects of answers was deemed colloquial rather than professional; significant portions of text for which a supporting citation would be expected had no referencing; and there was some repetition without connection, resulting in writing that was not integrated in nature although it did read seamlessly. In addition, the responses were well short of the word count (950), reflecting the lack of depth in discussion and insight that would connect to student or professional capabilities; there was lack of currency of insights, information, and references, creating a significant barrier to both quality and academic integrity; and there was reliance on obscure or fabricated references in preference to mainstream literature, along with omission of key citations from the professional literature.

Among 112 students in the subject "Imaging Pathology," the mean student score for the writing task was 65.9% whereas ChatGPT scored 49.3%. Among 12 students in the subject "Nuclear Medicine 1," the mean student score for the writing task was 69.0% whereas ChatGPT scored 41.0%. Among 13 students in the subject "Instrumentation," the mean student score for the writing task was 71.0% whereas ChatGPT scored 46.0%. For the third-year subjects, among 81 students in the subject "Pharmacology," the mean student score for the writing task was 67.7% whereas ChatGPT scored 26.0%. Among 12 students in the subject "Nuclear Medicine 2," the mean student score for the writing task was 66.0% whereas ChatGPT scored 41.2%. Among 11 students in the subject "Nuclear Medicine 3," the mean student score for the writing task was 63.5% whereas ChatGPT scored 30.0%. There was a statistically significant difference between the student scores and the ChatGPT scores, with the mean score being 28.3% lower for ChatGPT ($P < 0.001$). Although all 6 ChatGPT written task were well short of expectations, they reflect authentic student submissions, sharing close parallels to failing-grade submissions from students who leave the task to the final hour and hastily cobble together a shallow and poorly researched response. This finding questions the capacity of ChatGPT to be used to enhance student writing and research skills at the university level (Fig. 3), with its benefits perhaps limited to the high school level. A key issue common across the written tasks was the lack of in-text citations, which for a student would constitute plagiarism. Furthermore, ChatGPT had a tendency to fabricate references that cannot be verified or found. Such fabrication, if done by a student on a submission, would constitute serious fraud and misconduct.

For the 8 written examinations across the 2 y of theoretic study (the fourth year of the course is a residency focused on capability development rather than theory mastery), scoring was analyzed individually and collectively (Fig. 3). For the second-year subject "Imaging Pathology," the mean among 112 students was 44.3%, compared with 55.7% for ChatGPT. For the subject "Nuclear Medicine 1," the mean among 12 students was 66.8%, compared with 72.5% for ChatGPT. For the subject "Radiopharmacy," the mean among 12 students was 60.0%, compared with 55.2% for ChatGPT. For the subject "Instrumentation," the mean among 13 students was 60.4%, compared with 47.1% for ChatGPT.

For third-year students, for whom theoretic learning represents minimum standards for a practitioner, 4 subjects were evaluated. For the subject "CT," the mean among 89 students was 54.1%, compared with 37.9% for ChatGPT. For the subject "Pharmacology," the mean among 81 students was 57.5%, compared with 59.1% for ChatGPT. For the nuclear medicine–specific third-year subjects, the mean

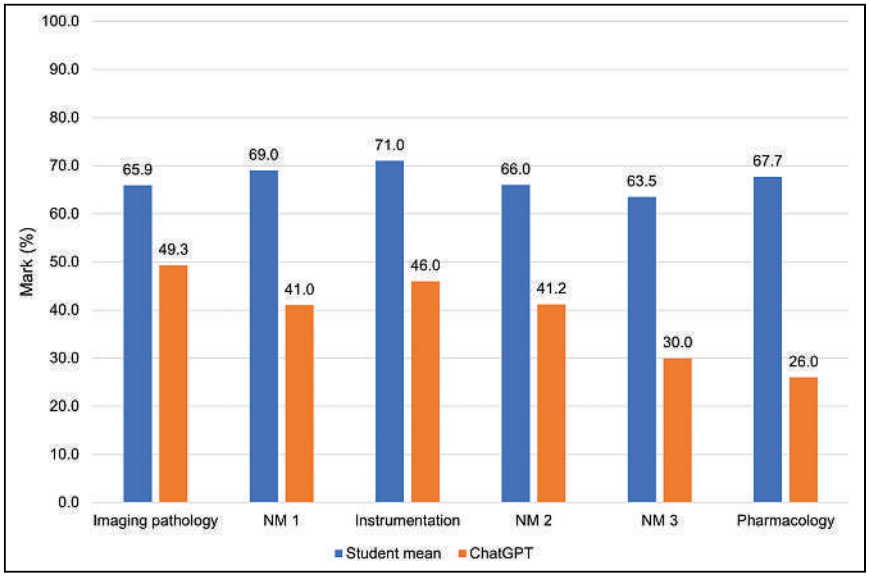


**FIGURE 2.** Bar chart for student mean and ChatGPT score for each of 6 subjects that had written tasks evaluated. NM = nuclear medicine.

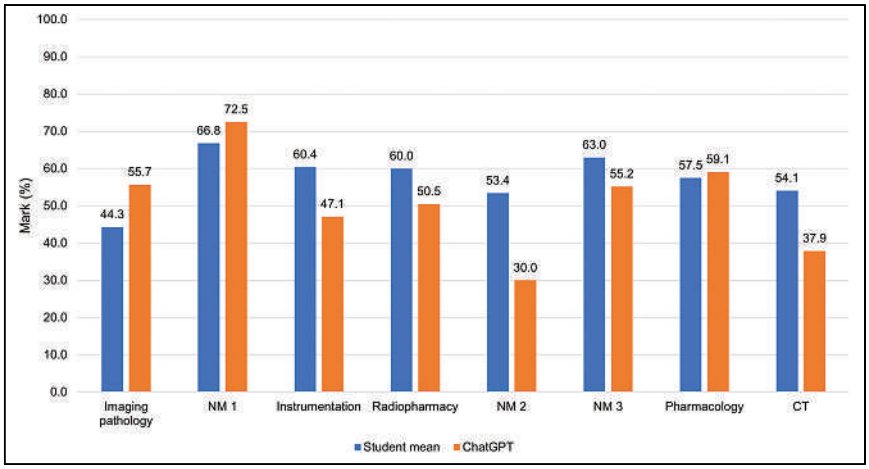


**FIGURE 3.** Bar chart for student mean and ChatGPT score for each of 8 subjects that had examinations evaluated. NM = nuclear medicine.

among 12 students in the subject "Nuclear Medicine 1" was 53.4%, compared with 30% for ChatGPT, and the mean among 11 students in the subject "Nuclear Medicine 3" was 63.0%, compared with 55.2% for ChatGPT.

There was a statistically significant difference between the student scores and the ChatGPT scores, with the mean score being 6.4% lower for ChatGPT ($P = 0.009$). Despite this lower mean score, ChatGPT performed better than the student mean in 3 of the subjects: "Imaging Pathology," "Nuclear Medicine 1," and "Pharmacology." Each of these subjects has content that is well established, and understanding of the content is reflected by describing processes, for which ChatGPT is well equipped. "Nuclear Medicine 1" is the first clinical nuclear medicine subject that students undertake, and learning outcomes represent lower-order taxonomies that are well handled by ChatGPT. The subject "Pharmacology" covers important content, with the expectation being more of acquiring a working understanding than of achieving mastery; as such, the examination questions tend to be more superficial and to cover content that is well established. The remaining subjects saw ChatGPT perform worse than the student mean. These subjects are specific in nature and require mastery of content that requires not only deep insights not typical of ChatGPT but also command of current innovations and developments occurring outside the training data for ChatGPT.

Turnitin generated similarity scores that ranged from 3% to 18% for examinations and from 13% to 34% for written assignments. The difference between lower and higher similarity scores related to the question itself for examinations and to the reference list for assignments. No instances of plagiarism were identified. Conversely, the AI scores ranged from 9% to 75% for examinations (although the 9% was an outlier, with the next lowest being 43%) and from 47% to 100% for written assignments (Fig. 4). For normalization, the entire introduction above was assessed through Turnitin, with a 0% similarity index and 0% AI score.

## DISCUSSION

The performance of ChatGPT in nuclear medicine assessment was enlightening. ChatGPT performed well when brief and shallow insights were required, typical perhaps of first-year subject topics and early or general aspects of second-year subject topics. Third-year topics are far from the shallows, and as a result, the expectations of depth and insight were beyond the capabilities of ChatGPT, even when prompted by a specific word count. Importantly from an education perspective, ChatGPT provided answers with no evidence, with outdated evidence, or with fabricated evidence. Such answers not only are devoid of current insight into the fluid nuclear medicine environment but also would represent academic misconduct if used by students in their submissions. ChatGPT was particularly poor for calculations, despite providing convincing working and justification for the same. Our findings are consistent with those reported for medical examinations, for which ChatGPT scored 43%–68% in open-ended questions and 40%–65% in multiple-choice questions (*7,8*). The authors similarly reported lower scores correlating with more complex questions.

Alarmingly, one of the chief benefits (and risks) of ChatGPT is in written tasks, for which ChatGPT was shown

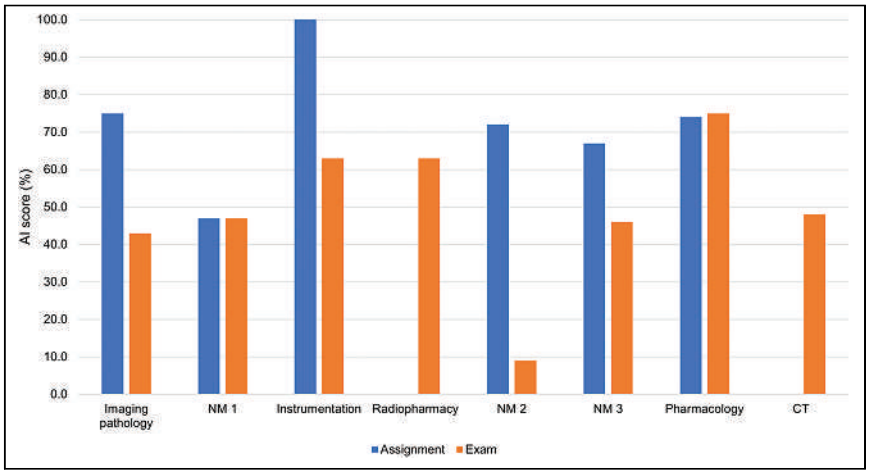


**FIGURE 4.** Bar chart for Turnitin AI score for ChatGPT assignments for 6 subjects that had ChatGPT assignments generated and ChatGPT examination answers for each of 8 courses that had examinations generated. NM = nuclear medicine.

to perform well short of expectations across all levels and courses. The depth of research and writing, the insight and understanding demonstrated in the writing, and the writing style itself (e.g., professional language and tone, integration across the piece, and integration with practice) not only penalized scoring but could not be used to positively impact skill development in students. This shortfall raises serious questions about using ChatGPT to generate questions (revision or assessment) when it lacks the insight to answer them. The performance of ChatGPT on very general topics or at a lower level of education (e.g., high school) might be better, and in the current evaluation, ChatGPT performed well on topics requiring shallow information and on topic that were widely evidenced before September 2021 (e.g., the role of bone scans in prostate cancer). Nonetheless, nuclear medicine education requires depth and specific detail in a rapidly evolving domain that confounds ChatGPT. It is possible for students to plan sections or topics within a written response and ask ChatGPT more targeted questions to produce a higher-scoring paper; however, it will remain constrained by lack of depth and insight, language that is less than professional, incorrect information, and inadequate or fraudulent referencing. Regardless of well-constructed responses or poorly constructed responses, Turnitin software confidently predicted when responses were AI-generated.

In the hands of a student already performing at a passing level or better, ChatGPT is unlikely to boost grades; indeed, it may reduce grades and risk academic misconduct. In theory, when norm-based referenced testing is used, the class mean improves and those using ChatGPT have an increased representation in the higher grades, potentially relegating non-ChatGPT users to the lower grades. For criterion-based referenced testing, it could allow student performance to improve independently of the class performance. Those using ChatGPT are advantaged but not at the expense of the grades of those not using ChatGPT. In reality, the current version of ChatGPT (GPT 3.5) does not provide that capability, and students relying on ChatGPT for either cheating or enhancing responses are likely to be penalized in their scores, independently of academic misconduct issues.

On the basis of the evidence in this evaluation, ChatGPT does not pose a risk of masking the students' shortcomings against the learning outcomes. Among nuclear medicine students, ChatGPT also does not appear to enhance grades by honing skills in writing and expanded learning. The significant risk to academic integrity is raised by poor, absent, or fraudulent referencing in ChatGPT responses. ChatGPT does not raise concerns about students graduating without the requisite knowledge and skills for safe clinical practice because reliance on ChatGPT will not allow the student to accrue a passing grade. It is appropriate to reevaluate the ChatGPT claimed benefits to student learning and assess whether these are conceivable (Table 1). Among the potential roles of ChatGPT for nuclear medicine student learning, the following would likely be the most appropriate: use of ChatGPT as a language assistant or language practice tool for those for whom English is a second language (for this role, ChatGPT would be developing basic English language

**TABLE 1**
Summary of Potential Applications of ChatGPT in Nuclear Medicine Student Education, with Evaluation of That Capability Against Findings of This Investigation

| ChatGPT capability | Evidence | Comment |
|---|---|---|
| Language assistant | ✓ | Is useful to develop language skills when English is second language |
| Accessibility | ✓ | Is useful for supportive technology |
| Generation of lecture notes | ? | Could fill gaps but requires confidence in accuracy and currency of content |
| Interactive learning | ? | Requires confidence in accuracy and currency of content |
| Personalized learning | ? | Is useful perhaps for first-year students performing at lower level but not for advanced students |
| Group collaboration | ? | Is useful perhaps for first-year students but lacks insights and depth to facilitate meaningful discussion |
| Feedback | ? | Requires confidence in accuracy and currency of content |
| Question answering | ? | Requires confidence in accuracy and currency of content |
| Question creation | ? | Requires confidence in accuracy and currency of content |
| Suggestion of group discussion topics | ? | Requires confidence in accuracy and currency of content |
| Provision of case studies | ? | Is useful perhaps for basic studies but not for novel, complex, or new applications or old applications with refined approaches |
| Independent learning | × | Lacks currency, depth of insight, and accuracy of information to benefit students |
| Assignment help | × | Provides writing that is inadequate, research that is shallow, and information that is not current or accurate |
| Information and resources | × | Provides research that is shallow and information that is not current or accurate |
| Writing assistance | × | Lacks professionalism, does not target audience, and ignores important writing conventions (e.g., referencing) |

✓ = applications our evidence supports; × = applications for which evidence suggests no role; ? = applications for which evidence suggests limited role.

skills, not professional language or writing skills); use of ChatGPT to support accessibility for students with disabilities, such as through assistive technology for text-to-voice conversion; use of ChatGPT as a training tool in which ChatGPT responses are applied in clinical, theory, or research learning domains to have students critique, refine, and correct; use of ChatGPT to proof, test, and refine assessments and scoring rubrics as part of moderation; and use of ChatGPT to simulate conversations with patients or caregivers as a form of authentic assessment.

Academic misconduct concerns for ChatGPT have been related largely to the potential capability to generate examination answers or responses to written tasks; that is, cheating for advantage. For nuclear medicine subjects, the risk of this use appears to be low, with limitations to the ChatGPT capability. This use could be further limited by structuring assessments that target student insight and understanding at a deeper level and by setting the minimum standards for a passing score in the rubric more rigorously against learning outcomes. That is, if a learning outcome for a subject requires students to be able to demonstrate their understanding by explaining a concept, then a student response that does not explain that concept (lists or outlines key information or facts) or does not show understanding (has errors or lacks integration with practice) should receive a failing score for that question or task. Typically in a rubric, there is some wiggle room that would recognize some knowledge and produce a passing grade with a credit, perhaps representing what should be the minimum standard (Table 2). ChatGPT will be able to produce those passing grades in which the credit expectations in a rubric represent what should be a minimum passing-grade requirement. Adjusting this approach would minimize the risk that ChatGPT will be used to navigate through subject assessment and would better align assessment with learning outcomes. Perhaps the biggest academic integrity issue for ChatGPT use is the potential plagiarism or fraud that students using generated responses could confront. Writing and referencing are typically below the expected standards; a paucity of citations would represent plagiarism, and the tendency for ChatGPT to add citations that cannot be verified is potential fraud. Indeed, ChatGPT can simply fabricate answers.

Although ChatGPT has surprising accuracy for some topics, it is prone to several different types of errors, and these were apparent throughout this investigation when the specific nature of nuclear medicine confounded ChatGPT responses. The term *hallucination* has been used widely in AI to refer to false or misleading information, yet the term is more specific,

**TABLE 2**
Selection of Learning Outcomes for Specific Examination or Assignment Tasks Across Some Evaluated Courses

| Learning outcome descriptor | Assessment type | Current credit standard | Current passing-score standard |
|---|---|---|---|
| Describe, explain, and implement | Written task | Compare data across some relevant primary literature, explain some relationships across data, and summarize key concepts | Compare data with some relevant literature, describe some relationships among data, and state some key concepts |
| Identify, explain, and apply | Examination | Recall mostly accurate facts, generally apply relevant knowledge correctly within context most of the time, explain important relationships across data most of the time, and provide plausible interpretation | Recall some accurate facts, apply relevant knowledge correctly within context some of the time, explain important relationships across data some of the time, and provide interpretation |
| Explain and apply principles of | Written task | Review and contextualize knowledge, with capacity for explanation of practice | Review and describe knowledge, with capacity for discussion of practice |
| Demonstrate understanding of | Examination | Generally apply relevant knowledge correctly within context most of the time | Apply relevant knowledge correctly within context some of the time |
| Describe, explain, evaluate, and develop | Examination | Indicate sound knowledge and application of concepts through descriptions, explanations, and discussion of content | Indicate knowledge and application of emerging concepts through descriptions of content |
| Explain and apply | Written task | Demonstrate sound understanding of themes and course matter; use recent external literature to demonstrate sound comprehension of themes | Demonstrate limited understanding of themes and course matter; use external literature to demonstrate limited understanding of themes |
| Recognize and describe | Examination | Recall facts from course material accurately, with limited but accurate application of facts to presented scenarios | Recall facts from course materials and record in basic manner; attempt to apply facts to scenarios presented |

Data show misalignment with minimum passing-score standards. In each case, it could be argued that to meet learning outcome, credit standard should be minimum passing-score criteria.

referring to a plausible response that is incorrect (it seems correct to ChatGPT but is not—identifying a stick that is not there) (*8*). Other types of AI errors have also been named according to this original psychiatry analogy:

- *Illusion* is like a hallucination except it is an error of similarity (mixing up similar items)—mistaking a piece of rope for a stick.
- *Delusion* is false belief or error (wrong information)—after correction and examination, insisting the rope is a stick.
- *Delirium* is either a sophisticated or a nonsensical answer because the algorithm is overwhelmed or confused—describing a ball when asked to describe a stick.
- *Confabulation* or *lying* is fabrication of information—photoshopping images of sticks in a scene to provide evidence that sticks were there without actually checking the scene for real sticks.
- *Extrapolation* or *interpolation* is a logical, although incorrect, extension of known information—based on 3 dogs carrying sticks, declaring a fourth dog also is carrying a stick without seeing the dog.
- *Miscalculation* or *blunder* is a computational error despite the correct equation and data—there are 5 sticks but 6 are counted.

All of these error types were evidenced through the scoring of examinations and written assignments. Students leaning on ChatGPT are ill-equipped to identify such errors. These students risk undermining their understanding and ongoing learning. Information is not knowledge.

The GPT 4–powered chatbot could be a bigger problem, with easier, faster, and more accurate responses. GPT 4 allows voice-to-text conversion, which would enable students to simply read the question to ChatGPT. GPT 4 will allow importing of images for analysis and interpretation, a task that would previously have confounded ChatGPT. ChatGPT is prone to hallucinations (false or misleading information), which a student using ChatGPT will not be aware enough to correct. GPT 4 is 60% more accurate with answers and, in particular, with interpreting context and reasoning. GPT 4 is trained on 3 times more data with a 500-fold increase in capacity, which will allow greater originality and accuracy of responses, confounding even the best plagiarism and AI detection software.

For nuclear medicine courses, there appears to be no advantage to students who misuse ChatGPT; indeed, they will be disadvantaged. It is important, therefore, to educate students about use, misuse, risk versus absence of benefit, professional responsibilities to their future patients, and the consequences, now or in the future, of cheating (e.g., if new technology is developed in 10 y that allows retrospective detection of ChatGPT, degree disqualification and deregistration could and should be a consequence). Education of students about ChatGPT would allow it to be integrated into the learning environment to support students when appropriate and to be used as a learning tool. This use is best supported by reengineering assessments and by recrafting learning outcomes to be both authentic and capability-focused, independently of whether ChatGPT is used.

Although not available at the time of writing, Google plans to release its AI chatbot, Bard, which would be in competition with ChatGPT. Although the chief comparisons relate to their chatbot functions for Google and Bing search engines, respectively, both have competing capabilities as a text generator. It is unrealistic to compare Bard with GPT 3, with Bard having capabilities mirroring the recently released GPT 4; these include context interpretation, image analysis, and mathematic problem solving. There are similar issues with accuracy and bias that need to be interrogated in the public user arena. Unlike GPT 4, Bard lacks plagiarism detection or prevention, accesses the Internet in real time, and updates the corpus of knowledge, providing currency at the expense of increased misinformation and bias. It is a reasonable prediction that ChatGPT will be the preferred tool for generative text for academic and scientific writing whereas Bard may emerge with broader applications in text generation (e.g., list generation, agenda production, and scheduling tasks) and image or video creativity for personal and general professional purposes.

## CONCLUSION

ChatGPT is an exciting educational tool that has limited generative capability to assist student writing in the nuclear medicine setting because of limitations on depth of insight, breadth of research, and currency of information. It is particularly inadequate at producing written assessment tasks (e.g., literature reviews) and introduces student risk of misconduct associated with inadequate referencing practices. ChatGPT could be used to build examination answers in real time, but performance is limited to superficial learning evidence produced by shallow or general answers. These limitations that reduce the risk that students will benefit from cheating also limit the educational benefit of ChatGPT for enhancing learning and writing skills. There are, however, several applications of ChatGPT that can enrich student learning in nuclear medicine. GPT 4 will require reimagining of the AI-augmented learning space.

## ACKNOWLEDGMENT

As a language model, ChatGPT should not be included as an author on journal articles. Authorship implies a contribution to the content of the article, and although ChatGPT may have been used to generate some of the text, it is not an individual who has contributed to the intellectual content of the article. ChatGPT does not meet the authorship requisites recommended by the International Committee of Medical Journal Editors. ChatGPT does warrant an acknowledgment. We would like to acknowledge the contribution of ChatGPT (version 3.5), a language model developed by OpenAI (https://openai.com/), in generating some of the text in this article. The model was accessed between April 1 and April 7, 2023. We would also like to acknowledge Turnitin plagiarism-detection software (www.Turnitin.com), used for similarity reports and AI scores (April 4, 2023, release).

## KEY POINTS

**QUESTION:** Does ChatGPT pose a risk to academic integrity?

**PERTINENT FINDINGS:** ChatGPT powered by GPT 3.5 lacks the capability to provide responses that reflect the depth, breadth, and currency of information; research expectations; and the appropriate professional tone.

**IMPLICATIONS FOR PRACTICE:** ChatGPT has limited scope for cheating among nuclear medicine students, which also limits the potential beneficial applications of ChatGPT in enhancing learning.

## REFERENCES


1. Awdry R, Ives B. International predictors of contract cheating in higher education. *J Acad Ethics.* 2023;21:193–212.
2. Stone A. Student perceptions of academic integrity: a qualitative study of understanding, consequences, and impact. *J Acad Ethics.* 2022;28:1–19.
3. Eysenbach G. The role of ChatGPT, generative language models, and artificial intelligence in medical education: a conversation with ChatGPT and a call for papers. *JMIR Med Educ.* 2023;6;9:e46885.
4. Currie G, Rohren E. Social asymmetry and artificial intelligence: the nuclear medicine landscape. *Semin Nucl Med.* 2022;52:498–503.
5. Graham F. Daily briefing: what scientists think of GPT-4, the new AI chatbot. *Nature.* March 17, 2023 [Epub ahead of print].
6. Sanderson K. GPT-4 is here: what scientists think. *Nature.* 2023;615:773.
7. Kung TH, Cheatham M, Medenilla A, et al. Performance of ChatGPT on USMLE: potential for AI-assisted medical education using large language models. *PLOS Digit Health.* 2023;2:e0000198.
8. Alkaissi H, McFarlane SI. Artificial hallucinations in ChatGPT: implications in scientific writing. *Cureus.* 2023;15:e35179.

# A Conversation with ChatGPT

Geoffrey Currie

*Charles Sturt University, Wagga Wagga, New South Wales, Australia*

ChatGPT chatbot powered by GPT 3.5 was released in late November 2022 but has been rapidly assimilated into educational and clinical environments. **Method:** Insight into ChatGPT capabilities was undertaken in an interview-style approach with the chatbot itself. **Results:** ChatGPT powered by GPT 3.5 exudes confidence in its capabilities in supporting and enhancing student learning in nuclear medicine and in supporting clinical practice. ChatGPT is also self-aware of limitations and flaws in capabilities and the risks these pose to academic integrity. **Conclusion:** Further objective evaluation of ChatGPT capabilities in authentic learning and clinical scenarios is required.

**Key Words:** artificial intelligence; tertiary education; higher education; academic integrity; generative AI; language model

**J Nucl Med Technol 2023; 51:255–260**
DOI: 10.2967/jnmt.123.265864

ChatGPT (OpenAI) was released publicly on November 30, 2022, and has generated significant interest and conjecture in relation to its capacity to enhance student learning and to support student cheating. Banning the use of ChatGPT to prevent its misuse also takes away any potential uses in enhancing student learning and writing. Here, several questions are posed to ChatGPT by an experienced educator to provide a deeper insight, from one perspective, into potential misuse and potential benefits among nuclear medicine students.

This entire "ChatGPT" section was written by ChatGPT (GPT 3.5) using a variety of prompt questions over multiple sessions and discussions between the author and ChatGPT.

*Currie:* What is ChatGPT?

*ChatGPT:* ChatGPT is a large language model created by OpenAI, which is based on the GPT 3.5 architecture. It has been trained on a vast amount of text data and can generate human-like responses to a wide range of questions and prompts. The purpose is to assist users in obtaining information and answering their queries in a conversational manner.

*Currie:* How can ChatGPT help Nuclear Medicine students learn?

*ChatGPT:* ChatGPT is a technology that can potentially benefit university students in numerous ways. One such benefit is that ChatGPT can serve as a language practice tool for students learning a new language. It can also provide students with answers to questions they may have about a particular subject, thereby serving as a study aid. Additionally, ChatGPT can engage students in interactive learning by providing real-time feedback and guidance as they work through problems or exercises. Another advantage of ChatGPT is its ability to adapt to the learning style and pace of individual students, providing customised recommendations and resources that are tailored to their needs. Moreover, students can use ChatGPT to get help with their assignments, as it can provide information and resources on various topics and help them understand difficult concepts. ChatGPT can also provide feedback on Nuclear Medicine–related assignments and projects, such as suggesting improvements in writing style or highlighting areas that need more research. Furthermore, ChatGPT can answer Nuclear Medicine–related questions and provide clear and concise explanations to help students understand these concepts. It can suggest study materials and offer practice questions and quizzes to test students' knowledge of Nuclear Medicine. ChatGPT can also assist students with their research by providing relevant information, summarizing articles, and suggesting further reading material. Additionally, it can help students with their essay writing by providing suggestions for the structure and content of their essays and suggesting relevant sources to refine their arguments. Finally, ChatGPT can provide explanations and examples to help students understand difficult concepts and can be accessed at any time, providing students with instant access to information and resources. Overall, ChatGPT can be a useful resource for university students to enhance their learning experience, improve their academic performance, and manage their time effectively.

*Currie:* How does ChatGPT threaten academic integrity?

*ChatGPT:* Like any other technology, ChatGPT has the potential to threaten academic integrity if used inappropriately. There are several ways in which ChatGPT could be misused, compromising academic integrity. Firstly, students may use ChatGPT to generate essays, assignments, or other coursework without properly citing or acknowledging the source, leading to plagiarism, which is a serious academic offense. Secondly, students may use ChatGPT to find answers to exam questions, which can be a form of cheating, giving them an unfair advantage over their peers and

Received Apr. 12, 2023; revision accepted May 13, 2023.
For correspondence or reprints, contact Geoffrey Currie (gcurrie@csu.edu.au).
Published online Jul. 11, 2023.

compromising the integrity of the exam. Thirdly, students may rely too heavily on ChatGPT to provide them with answers and information, rather than engaging in critical thinking and analysis themselves, hindering their ability to develop important skills such as problem solving and creativity.

Moreover, ChatGPT, like any other source of information, can sometimes provide inaccurate or misleading information, and students who rely solely on ChatGPT as their source of information may inadvertently incorporate incorrect information into their work, which can impact their academic performance and undermine their credibility. Additionally, ChatGPT can be used to generate fake data or research findings, compromising the integrity of academic research and leading to false conclusions. Lastly, if some students have access to ChatGPT whereas others do not, it could give those students an unfair advantage, leading to unequal learning opportunities and outcomes.

To mitigate these risks, it is important to use ChatGPT responsibly and ethically. This includes ensuring that students receive proper instruction on how to use ChatGPT as a learning tool rather than a means of cheating or plagiarism. Additionally, instructors can use plagiarism detection software to identify instances of academic dishonesty and take appropriate disciplinary action. Ultimately, the responsible use of ChatGPT can help to enhance academic integrity rather than threaten it. Overall, by providing students with the necessary guidance, support, and instruction, ChatGPT can be used as a valuable tool for enhancing learning and academic performance while also promoting academic integrity.

*Currie:* How can lecturers use ChatGPT to teach Nuclear Medicine?

*ChatGPT:* Lecturers can use ChatGPT in various ways to teach Nuclear Medicine. Here are some ways that ChatGPT can be useful in this regard:

- Providing supplemental information: Lecturers can use ChatGPT to provide students with supplemental information on various topics related to nuclear medicine, such as radiopharmaceuticals, imaging techniques, and radiation safety. ChatGPT can provide students with access to a wide range of information in real time, helping them to better understand the material being presented.
- Offering personalized instruction: ChatGPT can provide personalized instruction to students by answering their questions in real time. This can help students to better understand complex topics and clarify any misunderstandings they may have.
- Facilitating group discussions: ChatGPT can facilitate group discussions by suggesting topics for discussion, providing background information on those topics, and summarizing key points. This can help to encourage active participation from students and foster a collaborative learning environment.
- Providing feedback on assignments: Lecturers can use ChatGPT to provide feedback on assignments, such as papers and presentations. ChatGPT can provide students with suggestions for improvement, identify areas where they may be struggling, and offer guidance on how to improve their work.
- Creating interactive learning experiences: ChatGPT can be used to create interactive learning experiences, such as quizzes and games. This can help to make the learning experience more engaging and enjoyable for students, as well as help them to retain the material better.
- Providing case studies: Lecturers can use ChatGPT to provide students with case studies related to nuclear medicine, which can help students to understand how the concepts they are learning are applied in clinical practice. ChatGPT can also provide feedback on how students approach and analyze the case studies, helping them to improve their critical thinking skills.
- Offering career guidance: ChatGPT can offer career guidance to students interested in nuclear medicine by providing information on career paths, job prospects, and required qualifications. ChatGPT can also suggest professional associations, conferences, and networking opportunities that can help students to advance their careers.
- Facilitating remote learning: ChatGPT can be used to facilitate remote learning by providing students with access to online resources, such as videos, podcasts, and e-books. ChatGPT can also help to organize online discussions, group projects, and collaborative activities that can enhance the online learning experience.
- Encouraging independent learning: ChatGPT can encourage independent learning by providing students with self-directed learning materials, such as interactive tutorials, quizzes, and videos. ChatGPT can also suggest additional resources that students can use to deepen their understanding of the material.
- Supporting accessibility: ChatGPT can support accessibility in nuclear medicine education by providing students with assistive technologies, such as text-to-speech and screen readers. This can help to ensure that students with disabilities can fully participate in the learning experience.
- Group collaboration: ChatGPT can be used to facilitate group collaboration by providing a common platform for students to share ideas, collaborate on projects, and discuss assignments. ChatGPT can also help to organize group meetings, assign tasks, and monitor progress.
- Interactive learning: ChatGPT can be used to create interactive learning experiences, such as quizzes, games, and simulations. These interactive experiences can help to engage students and reinforce their understanding of the material.
- Language practice: ChatGPT can be used to help students practice their language skills by providing language exercises, vocabulary lists, and language practice materials. ChatGPT can also provide feedback on pronunciation and grammar, helping students to improve their language proficiency.
- Question generation: ChatGPT can be used to generate questions related to nuclear medicine, which can be used for assessments, quizzes, and exams. ChatGPT can also provide feedback on the quality of the questions, helping students to improve their question-writing skills.
- Writing assistance: ChatGPT can be used to provide writing assistance to students, such as suggesting appropriate language, grammar, and punctuation. ChatGPT can also provide feedback on the quality of the writing, helping students to improve their writing skills.
- Generating lecture notes: ChatGPT can be used to generate lecture notes for nuclear medicine courses. Lecturers can provide ChatGPT with an outline of the lecture, and it can generate a summary of the key points and concepts.

- Creating learning materials: ChatGPT can be used to create learning materials, such as handouts, diagrams, and infographics. Lecturers can provide ChatGPT with the necessary information, and it can generate visuals and diagrams that help students to understand complex concepts.
- Developing training materials: ChatGPT can be used to develop training materials for nuclear medicine professionals. These materials can include procedural guidelines, safety protocols, and other essential information.
- Generating research papers: ChatGPT can be used to generate research papers on topics related to nuclear medicine. Researchers can provide ChatGPT with the necessary information and it can generate a draft of the research paper.
- Developing course syllabi: ChatGPT can be used to develop course syllabi for nuclear medicine courses. Lecturers can provide ChatGPT with the necessary information, and it can generate a comprehensive syllabus that outlines the course objectives, topics covered, assignments, and assessments.
- Text analysis: ChatGPT can be used to analyze large volumes of text data related to nuclear medicine, such as scientific articles, research papers, and clinical reports. By analyzing the language and patterns in these texts, researchers can gain insights into the field and identify trends and areas for further investigation.
- Data processing: ChatGPT can be used to process and analyze large volumes of data related to nuclear medicine, such as medical imaging data and patient records. ChatGPT can help to identify patterns and trends in the data that can inform research and clinical decision-making.
- Prediction and classification algorithms: ChatGPT can be used to develop predictive models and classification algorithms for nuclear medicine applications. For example, ChatGPT can be used to predict the likelihood of a patient developing a certain disease based on their medical history and imaging data.
- Natural language generation: ChatGPT can be used to generate natural language summaries of research findings and clinical reports in nuclear medicine. This can help to improve communication and understanding among researchers, clinicians, and patients.

*Currie:* Can ChatGPT provide five multiple-choice questions for use in testing radiopharmacy theory for students?

*ChatGPT:* Sure, here are 5 multiple-choice questions related to radiopharmacy theory for students:

1. Which of the following is NOT a commonly used imaging modality in nuclear medicine?
   A) SPECT
   B) PET
   C) CT
   D) MRI
   Answer: D) MRI
2. Which of the following isotopes is commonly used in bone imaging?
   A) Technetium-99m
   B) Fluorine-18
   C) Iodine-131
   D) Gallium-67
   Answer: A) Technetium-99m
3. Which of the following radiopharmaceuticals is commonly used for myocardial perfusion imaging?
   A) Technetium-99m sestamibi
   B) Iodine-131 sodium iodide
   C) Fluorine-18 FDG
   D) Gallium-67 citrate
   Answer: A) Technetium-99m sestamibi
4. Which of the following processes is responsible for the emission of radiation in nuclear medicine imaging?
   A) Electron transfer
   B) Photon absorption
   C) Positron decay
   D) Beta-decay
   Answer: C) Positron decay
5. Which of the following is NOT a potential side effect of radiopharmaceutical administration?
   A) Allergic reaction
   B) Radiation sickness
   C) Skin rash
   D) Fever
   Answer: C) Skin rash

*Currie comment:* These questions show a lack of insight and understanding of the topic and do not provide confidence that ChatGPT could be used, as suggested, to generate questions. For example, question 2 overlooks the increasing use of PET bone scanning, question 4 overlooks radionuclide therapy and the importance of the photoelectric effect in imaging, question 5 is incorrect because skin rash can, rarely, occur for some radiopharmaceuticals. Furthermore, the questions are shallow aimed at recall rather than being structured to draw on understanding.

*Currie:* Can ChatGPT be used to build student assessment?

*ChatGPT:* ChatGPT can be used to build student assessment such as quizzes or exams. In fact, some educators have already begun to explore the use of AI-powered chatbots like ChatGPT to create assessments that are both efficient and effective. ChatGPT can generate questions related to the course material, which can then be used to create quizzes and exams. Educators can input specific topics, themes, or learning objectives and generate a set of questions related to the specific learning goals. This can be useful for educators who are teaching large classes, where it may be difficult to generate a sufficient number of questions or to grade assessments in a timely manner.

However, it is important to note that the use of ChatGPT to create assessments should be done with caution. Although it may save time, it is important to ensure that the questions generated are accurate, relevant, and appropriate for the learning outcomes being assessed. Educators should also review and potentially modify the questions generated by ChatGPT to ensure that they align with the educators' specific course content and teaching style. Finally, educators should always review and provide feedback on the results of the assessments to ensure that students are receiving a high-quality education.

There are several other ways in which ChatGPT can be used for student assessment in nuclear medicine. First, ChatGPT can be trained to automatically grade essays and other written assignments, saving instructors time and effort. By analyzing the content, structure, and grammar of the

student's writing, ChatGPT can assign a score or grade that is consistent and objective. In addition, ChatGPT can be used to generate questions for assessments, allowing instructors to test students' understanding of the material. After students complete an assessment, ChatGPT can provide immediate feedback on their answers, helping them to better comprehend the material.

Moreover, instructors can use ChatGPT to assess students' understanding of a particular topic by asking them questions and evaluating their responses. By analyzing students' responses to questions or assignments, ChatGPT can identify areas in which they need improvement and provide customized feedback and recommendations. ChatGPT can also be used to automatically grade assessments, reducing the workload on lecturers. Additionally, ChatGPT can be used to analyze student performance on assessments, providing insights into students' strengths and weaknesses. This information can help lecturers to improve their teaching methods and to tailor their assessments to better meet students' needs.

Although ChatGPT can be a helpful tool for student assessment, it is essential to use it responsibly and ethically. Automated grading, for instance, may not be appropriate for all types of assignments, and instructors must ensure that ChatGPT is not used in a way that compromises the validity or reliability of assessments. Students should receive clear guidance on how ChatGPT will be used in the assessment process, and instructors should be transparent about the limitations and potential biases of the technology. Ultimately, ChatGPT can be a valuable resource for instructors and students alike, but it must be used thoughtfully and in conjunction with other assessment methods.

*Currie:* Should ChatGPT be used for teaching nuclear medicine students?

*ChatGPT:* Whether lecturers should use ChatGPT or ban it among students is a complex issue that depends on a variety of factors, such as the learning objectives of the course, the ethical implications of using AI in education, and the potential risks of misuse. On one hand, ChatGPT can be a valuable tool for students to enhance their learning and to generate new ideas. By interacting with ChatGPT, students may be able to explore complex concepts and gain a deeper understanding of the material. Additionally, ChatGPT can help students who may struggle with writing or who have difficulty expressing their ideas in a clear and concise manner. On the other hand, there are potential risks associated with using ChatGPT in education. If students rely too heavily on ChatGPT to complete their assignments, they may not develop the critical thinking and problem-solving skills that are necessary for success in the workplace. Additionally, the use of ChatGPT in education raises ethical questions around the ownership of intellectual property and the potential for cheating. Ultimately, whether lecturers should use ChatGPT or ban it among students depends on the specific context of the course and the goals of the educational institution. Some lecturers may choose to integrate ChatGPT into their teaching to enhance the learning experience, while others may choose to restrict its use to prevent academic misconduct. It is important for institutions to carefully consider the potential benefits and risks of using ChatGPT and to establish clear guidelines and policies for its use.

*Currie:* Please generate lecture notes for the use of Lasix in renography

*ChatGPT:* Sure, here are sample lecture notes for the use of Lasix in renography:

Lecture Title: The Use of Lasix in Renography

Introduction:

Renography is a medical imaging technique used to assess the function of the kidneys. The use of radiopharmaceuticals, such as technetium-99m MAG3, can provide a detailed picture of the kidneys' structure and function. Lasix, a diuretic medication, can be used in conjunction with renography to assess kidney function and detect any obstruction in the urinary tract.

Lasix Mechanism of Action:

Lasix works by inhibiting the reabsorption of sodium and chloride ions in the thick ascending loop of Henle in the kidney, resulting in increased urine output. This mechanism of action makes it useful in the detection of obstruction in the urinary tract.

Lasix in Renography:

When Lasix is used in conjunction with renography, it can help differentiate between obstructive and non-obstructive causes of hydronephrosis. Obstructive hydronephrosis occurs when there is a blockage in the urinary tract, leading to urine backup and kidney swelling. Non-obstructive hydronephrosis occurs when there is a buildup of urine in the kidney due to other causes, such as reflux or decreased urine flow. Lasix can be administered after the initial renography images are taken to induce diuresis and flush out any residual tracer in the collecting system. If the kidneys are functioning normally, there will be a rapid washout of the tracer, and the collecting system will appear empty on the post-Lasix images. However, if there is an obstruction in the urinary tract, the tracer will accumulate in the affected kidney, and the collecting system will not empty completely.

Conclusion:

The use of Lasix in conjunction with renography can be a valuable tool in the diagnosis of obstructive hydronephrosis. By inducing diuresis, Lasix can help distinguish between obstructive and non-obstructive causes of hydronephrosis and aid in the management of urinary tract obstruction.

Note: These are sample lecture notes and may be adjusted or expanded based on the specific needs of the course or audience.

*Currie comment:* These lecture notes do not provide the depth or accuracy of insight to be useful for enhancing student learning in this topic and undermine confidence that ChatGPT could be used to generate learning resources.

*Currie:* How can ChatGPT be used in clinical Nuclear Medicine?

*ChatGPT:* ChatGPT can be a useful resource in clinical nuclear medicine practice. Here are a few ways ChatGPT can help:

- Providing information on radiopharmaceuticals: ChatGPT can provide information on radiopharmaceuticals used in nuclear medicine, such as their indications, contraindications, administration,

and pharmacokinetics. This information can help clinicians choose the appropriate radiopharmaceuticals for their patients.

- Offering guidance on imaging techniques: ChatGPT can provide guidance on various imaging techniques used in nuclear medicine, such as positron emission tomography (PET) and single-photon emission computed tomography (SPECT). This guidance can help clinicians optimize imaging protocols and interpret imaging results.
- Providing support for clinical decision-making: ChatGPT can provide support for clinical decision-making in nuclear medicine practice by suggesting appropriate imaging studies based on the patient's clinical history and presenting symptoms. It can also help clinicians interpret imaging results and suggest further diagnostic or therapeutic interventions.
- Providing updates on emerging technologies: ChatGPT can provide updates on emerging technologies in nuclear medicine, such as new radiopharmaceuticals or imaging techniques, which can help clinicians stay up to date on the latest advances in the field.
- Assisting with patient education: ChatGPT can assist with patient education by providing patients with clear and accurate information about the imaging studies they are undergoing, the radiopharmaceuticals used, and any potential side effects or risks. This can help patients feel more informed and comfortable with the imaging process.
- Providing support for radiation safety: ChatGPT can provide support for radiation safety in nuclear medicine practice by suggesting appropriate radiation shielding and monitoring techniques and by providing guidance on appropriate handling and disposal of radiopharmaceuticals.
- Assisting with quality control: ChatGPT can assist with quality control in nuclear medicine practice by providing guidance on appropriate calibration techniques and quality control procedures and by suggesting ways to optimize image quality.
- Offering support for research: ChatGPT can offer support for research in nuclear medicine by suggesting relevant literature and research topics and by providing guidance on statistical analysis and interpretation of data.
- Offering support for interdisciplinary collaboration: ChatGPT can assist with interdisciplinary collaboration by providing clinicians with information on the role of nuclear medicine in various medical specialties, such as cardiology, oncology, and neurology. This can help clinicians work together more effectively to optimize patient care.
- Providing assistance with regulatory compliance: ChatGPT can provide assistance with regulatory compliance in nuclear medicine practice by suggesting appropriate protocols for obtaining informed consent, maintaining patient confidentiality, and complying with regulatory requirements related to the handling and disposal of radiopharmaceuticals.
- Assisting with continuing education: ChatGPT can assist with continuing education in nuclear medicine by providing clinicians with access to relevant conferences, seminars, and webinars, as well as suggesting relevant publications and online resources.
- Supporting remote consultations: ChatGPT can support remote consultations in nuclear medicine practice by providing clinicians with a platform to communicate with other clinicians and patients and by providing guidance on appropriate protocols for remote consultations.
- Providing guidance on image analysis: ChatGPT can provide guidance on image analysis in nuclear medicine practice by suggesting appropriate software and tools for image analysis, as well as offering guidance on image segmentation, registration, and quantification. This can help clinicians optimize their image analysis workflows and interpret imaging results more accurately.
- Offering support for machine learning and AI: ChatGPT can provide support for machine learning and AI in nuclear medicine practice by suggesting appropriate algorithms and approaches for automated image analysis and interpretation. This can help clinicians optimize their workflows and improve their diagnostic accuracy.
- Supporting professional development: ChatGPT can support professional development in nuclear medicine practice by suggesting relevant conferences, workshops, and training programs, as well as providing guidance on career development and advancement. This can help clinicians stay up to date on the latest advances in the field and advance their careers.
- Providing assistance with scientific writing: ChatGPT can provide assistance with scientific writing in nuclear medicine practice by suggesting appropriate journals and publications for submitting research articles, as well as offering guidance on manuscript preparation, writing style, and statistical analysis. This can help clinicians disseminate their research findings more effectively and improve the quality of their scientific writing.

*Currie:* Please provide the technologist with the optimal imaging protocol for a V/Q scan.

*ChatGPT:* Sure, here is an example of an optimal imaging protocol for a V/Q (ventilation/perfusion) scan:

Patient Preparation:

- The patient should be instructed to avoid smoking, caffeine, and any medications that may affect the cardiovascular or respiratory system, such as beta-blockers or bronchodilators, for at least 24 hours before the scan.
- The patient should be well hydrated before the scan.
- The patient should be screened for contraindications, such as pregnancy, lactation, or severe renal impairment.

Radiopharmaceutical Administration:

- The radiopharmaceutical used in V/Q scans is typically technetium-99m labeled macroaggregated albumin (99mTc-MAA) for perfusion imaging and technetium-99m labeled aerosol (99mTc-DTPA) or technegas (99mTc-Technegas) for ventilation imaging.
- The radiopharmaceuticals should be administered according to the manufacturer's instructions, with appropriate shielding and monitoring of radiation exposure.
- The patient should be instructed to breathe normally and deeply during the administration of the radiopharmaceuticals.

Imaging Acquisition:

- The patient should be positioned supine on the imaging table, with arms raised above the head.
- Perfusion images should be acquired first, followed by ventilation images.
- Perfusion images should be acquired using a γ-camera, with a low-energy, high-resolution collimator and a matrix size of 128 × 128 or higher.
- Ventilation images should be acquired using a gamma camera or a SPECT (single-photon emission computed tomography) scanner, with a low-energy, high-resolution collimator and a matrix size of 64 × 64 or higher.
- The acquisition time per view should be approximately 1–2 minutes, depending on the scanner type and patient size.

- The images should be acquired in multiple projections, with appropriate corrections for attenuation and scatter.

Image Interpretation:

- The V/Q images should be reviewed by a trained nuclear medicine physician or radiologist.
- The images should be assessed for the presence and distribution of ventilation and perfusion abnormalities, such as pulmonary embolism or airway obstruction.
- The images should be correlated with the patient's clinical history and other imaging modalities, such as CT or MRI.

Conclusion:

An optimal imaging protocol for a V/Q scan involves proper patient preparation, administration of the appropriate radiopharmaceuticals, acquisition of perfusion and ventilation images, and interpretation of the images by a trained physician or radiologist. By following this protocol, the V/Q scan can provide valuable information on the ventilation and perfusion status of the lungs, helping guide diagnosis and management of pulmonary diseases, such as pulmonary embolism or chronic obstructive pulmonary disease (COPD).

*Currie comment:* These instructions are generic, not specific; are misleading in parts; and do not provide confidence that ChatGPT could be used, as suggested, to guide clinical imaging. For example, the patient preparation is almost completely incorrect other than screening for pregnancy, which is a relative contraindication but not absolute. The ventilation instructions defer to the manufacturer but also suggest breathing both normally and deeply; deeply is not normally. The image acquisition suggests perfusion first despite previously suggesting $^{99m}$Tc-based ventilation agents (and no mention of a 2-d protocol that would be required); suggests a SPECT scanner for ventilation but not perfusion; provides no clear acquisition parameters, including whether planar imaging or SPECT is undertaken; and suggest an inappropriate matrix (128 × 128 should be 256 × 256 minimum) for a high-resolution collimator. There is no insight into interpretation. As written, this would provide no help for the technologist at whom the support was aimed.

## CONCLUSION

ChatGPT radiates confidence in its capability to support and enhance student learning and clinical practice but also demonstrates self-awareness of limitations and flaws. Similar objective insights into ChatGPT use and misuse need to be undertaken in the learning and clinical environments.

## DISCLOSURE

No potential conflict of interest relevant to this article was reported.


## ACKNOWLEDGMENT

I acknowledge the contribution of ChatGPT (version 3.5), a language model developed by OpenAI (https://openai.com/), in generating some of the text in this article. The model was accessed between April 1 and April 13, 2023.


## KEY POINTS

**QUESTION:** What benefits does ChatGPT offer nuclear medicine student learning?

**PERTINENT FINDINGS:** ChatGPT powered by GPT 3.5 has a wide range of capabilities that could potentially benefit student education or clinical practice but has established risks and limitations that require consideration.

**IMPLICATIONS FOR PATIENT CARE:** ChatGPT needs to be objectively evaluated in authentic learning and clinical environments.

# $^{18}$F-FDG PET/CT Versus $^{68}$Ga-PSMA-11 PET/CT in Evaluation of Distant Metastatic Disease in Recurrent Renal Cell Carcinoma

Rahul V. Parghane and Sandip Basu

*Radiation Medicine Centre (BARC), Tata Memorial Hospital Annexe, Homi Bhabha National Institute, Mumbai, India*

Prostate-specific membrane antigen (PSMA) expression has been observed in the neovasculature of various malignancies. We present a case of metastatic renal cell carcinoma (RCC) with comparative $^{18}$F-FDG PET/CT and $^{68}$Ga-PSMA-11 imaging in which FDG PET/CT failed to detect metastatic thyroid disease and showed less $^{18}$F-FDG–concentrating lesions at other sites, whereas $^{68}$Ga-PSMA-11 PET/CT identified metastatic thyroid disease and demonstrated intensely $^{68}$Ga-PSMA-11–expressing distant metastatic lesions. $^{68}$Ga-PSMA-11 PET/CT may be considered a potentially useful imaging technique in RCC to detect metastasis and to guide the choice of specific treatments, such as PSMA-based radionuclide therapy in patients with recurrent metastatic RCC.

**Key Words:** oncology; $^{177}$Lu-PSMA-617 therapy; $^{18}$F-FDG PET/CT; $^{68}$Ga-PSMA-11 PET/CT; clear cell carcinoma; renal cell carcinoma

**J Nucl Med Technol 2023; 51:261–262**
DOI: 10.2967/jnmt.122.264014

Prostate-specific membrane antigen (PSMA) is a type II transmembrane glycoprotein highly expressed in prostate cancer, with $^{68}$Ga-PSMA-11 PET/CT constituting an important molecular imaging modality in the management of patients. Overexpression of PSMA is not limited to prostate cancer only and has been also observed in the neovasculature of several nonprostatic tumors such as renal cell carcinoma (RCC), for which the role of radiolabeled PSMA for theranostic purposes is being explored (*1,2*).

## CASE REPORT

Eight years previously, a 60-y-old man underwent left nephrectomy for a clear cell variant of RCC. He received sunitinib for metastatic lung disease 3 y previously and recently complained of left-sided chest pain and swelling of 2-mo duration. $^{18}$F-FDG PET/CT (Fig. 1) showed a soft-tissue mass having mild to moderate $^{18}$F-FDG avidity ($SUV_{max}$, 6.40) and measuring 10.1 × 6.3 × 9.5 cm in the left chest wall, as well as soft-tissue lesions in the mediastinum and bilateral nodules in the lungs. Five days after $^{18}$F-FDG PET, PET/CT with $^{68}$Ga-PSMA-11 (111 MBq [3 mCi]), after a 60-min postinjection period, showed an intensely $^{68}$Ga-PSMA-11–expressing left chest wall mass ($SUV_{max}$, 22.49), mediastinal lesions, and bilateral lung nodules. In addition, intensely $^{68}$Ga-PSMA-11–avid hypodense thyroid lesions were seen in fused coronal and transaxial images. Subsequently, fine-needle aspiration cytology showed the thyroid lesions to be metastasis from RCC.

## DISCUSSION

RCC is a highly aggressive, lethal cancer with a tendency toward distant metastatic spread. The notable features of RCC are late recurrence and distant metastases after initial diagnosis. Metastatic spread of RCC to the head and neck region is less frequent. Of this uncommon metastatic spread, the thyroid is the most commonly involved organ (*2,3*). The clinical utility of $^{18}$F-FDG PET/CT for evaluation of recurrent RCC is doubtful because of the variable glucose metabolism and biologic characteristics of RCC. PSMA is overexpressed in the neovasculature of RCC, particularly in clear cell subtypes, leading to clinical use of $^{68}$Ga-PSMA-11 PET/CT for detection of distant metastases (*4*). In a recent report, concordant $^{18}$F-FDG and PSMA uptake in metastatic lesions was seen in most cases of RCC, but a limited number of cases showed discordant uptake, favoring PSMA uptake in metastatic lesions (*4*). However, concrete evidence with prospective studies to support this finding is lacking. $^{68}$Ga-PSMA-11 PET/CT imaging has shown several advantages for evaluation of RCC patients (*5–7*), such as higher PSMA uptake than $^{18}$F-FDG uptake in lesions, leading to a high lesion detection rate; a future possible role in therapeutic response assessment for various therapies, such as antiangiogenic agents, immune checkpoint inhibitors, and stereotactic radiation; and future potential in theranostics in PSMA-positive lesions (imaging with PSMA PET/CT and treatment with PSMA labeled with β-emitting [$^{177}$Lu or $^{90}$Y] or α-emitting [$^{225}$Ac] radionuclides). In the present case, $^{68}$Ga-PSMA-11 uptake was higher than $^{18}$F-FDG uptake in all metastatic lesions, and there was discordant positive uptake for the metastatic thyroid lesion. Knowledge of this possibility may be helpful for management and future treatment planning in RCC.

Received Feb. 11, 2022; revision accepted Aug. 19, 2022.
For correspondence or reprints, contact Sandip Basu (drsanb@yahoo.com).
Published online Aug. 30, 2022.

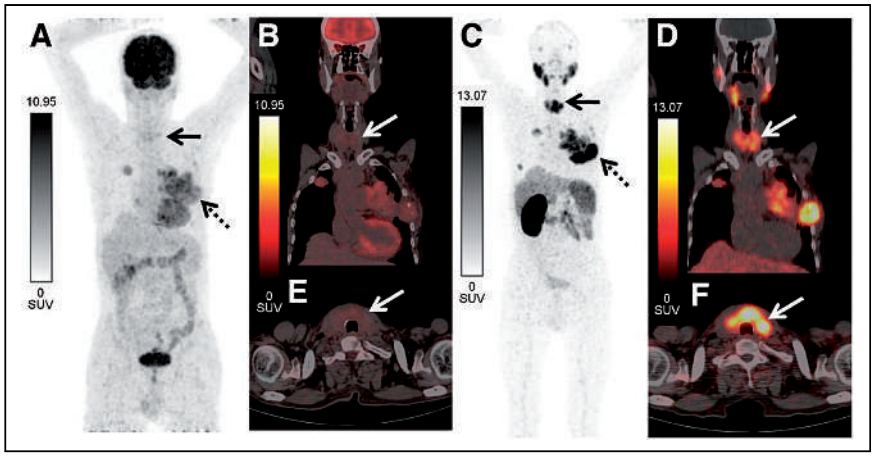


**FIGURE 1.** Maximum-intensity-projection (MIP) image of $^{18}$F-FDG PET/CT (A) showed mildly $^{18}$F-FDG–avid soft-tissue mass ($SUV_{max}$, 6.40) measuring 10.1 × 6.3 × 9.5 cm in left chest wall, soft-tissue lesions in mediastinal region, and bilateral nodules in lung (dotted arrows in MIP images A and C). No abnormally increased $^{18}$F-FDG uptake was noted in fused coronal (B) or transaxial (E) images of neck region. $^{68}$Ga-PSMA PET/CT showed intensely $^{68}$Ga-PSMA–expressing left chest wall mass ($SUV_{max}$, 22.49; dotted arrow in C), mediastinal lesions, and bilateral nodules in lung (C). Additionally, intensely $^{68}$Ga-PSMA–avid hypodense thyroid lesions were seen in fused coronal (D) and transaxial (F) images (solid arrows in D and F, and MIP images A and C).

## CONCLUSION

$^{68}$Ga-PSMA-11 PET/CT may be considered a potentially useful imaging technique in RCC to detect metastasis and to guide the choice of specific treatments, such as PSMA-based radionuclide therapy in patients with recurrent metastatic RCC.

## DISCLOSURE

No potential conflict of interest relevant to this article was reported.

## REFERENCES

1. Salas Fragomeni RA, Amir T, Sheikhbahaei S, et al. Imaging of nonprostate cancers using PSMA-targeted radiotracers: rationale, current state of the field, and a call to arms. *J Nucl Med.* 2018;59:871–877.
2. Siva S, Callahan J, Pryor D, Martin J, Lawrentschuk N, Hofman MS. Utility of $^{68}$Ga prostate specific membrane antigen-positron emission tomography in diagnosis and response assessment of recurrent renal cell carcinoma. *J Med Imaging Radiat Oncol.* 2017;61:372–378.
3. Khan MS, Iyer VB, Varshney N. A rare case of metastasis to the thyroid gland from renal clear cell carcinoma 11 years after nephrectomy and concurrent primary esophageal carcinoma. *Case Rep Oncol Med.* 2018;2018:3790106.
4. Tariq A, Kwok M, Pearce A, et al. The role of dual tracer PSMA and FDG PET/CT in renal cell carcinoma (RCC) compared to conventional imaging: a multi-institutional case series with intra-individual comparison. *Urol Oncol.* 2022;40:66.e1–66.e9.
5. Raveenthiran S, Esler R, Yaxley J, Kyle S. The use of $^{68}$Ga-PET/CT PSMA in the staging of primary and suspected recurrent renal cell carcinoma. *Eur J Nucl Med Mol Imaging.* 2019;46:2280–2288.
6. Gühne F, Seifert P, Theis B, et al. PSMA-PET/CT in patients with recurrent clear cell renal cell carcinoma: histopathological correlations of imaging findings. *Diagnostics (Basel).* 2021;11:1142.
7. Urso L, Castello A, Rocca GC, et al. Role of PSMA-ligands imaging in renal cell carcinoma management: current status and future perspectives. *J Cancer Res Clin Oncol.* 2022;148:1299–1311.

# Synchronous Ectopic Thyroid Gland and Ectopic Parathyroid Adenoma on $^{99m}$Tc-Sestamibi Scintigraphy and Correlative Imaging

Fathima Fijula Palot Manzil, Joshua Eichhorn, and Surjith Vattoth

*University of Arkansas for Medical Sciences, Little Rock, Arkansas*

$^{99m}$Tc-sestamibi scintigraphy localizes parathyroid adenoma as a persistent focus of uptake on delayed images, whereas thyroid glands in normal or ectopic locations are seen on only early images and wash out on delayed images. We report a case of absence of eutopic neck thyroid activity and synchronous ectopic lingual thyroid and mediastinal parathyroid adenoma on scintigraphy confirmed with CT.

**Key Words:** lingual thyroid; ectopic parathyroid; sestamibi; 4-D CT

**J Nucl Med Technol 2023; 51:263–264**
DOI: 10.2967/jnmt.122.265249

Though it is not uncommon to have a lingual thyroid or mediastinal parathyroid, it is rare to have a concomitant ectopic thyroid and parathyroid.

## CASE REPORT

A 61-y-old euthyroid woman with hyperparathyroidism (parathyroid hormone level, 115 pg/mL) underwent $^{99m}$Tc-sestamibi scintigraphy after receiving a 1,010.1-MBq (27.3 mCi) tracer injection. The images showed a superior mediastinal focus on SPECT/CT images at 15 min and persisting at 2 h (Figs. 1A and 1B), suggestive of an ectopic parathyroid adenoma and confirmed on 4-dimensional CT (Fig. 1C). Normal neck thyroid uptake was absent, with posterior tongue uptake on early images showing washout on delayed images suggestive of lingual thyroid (Fig. 1A). The ectopic lingual thyroid and absence of native thyroid were confirmed on CT (Fig. 2). The intraoperative

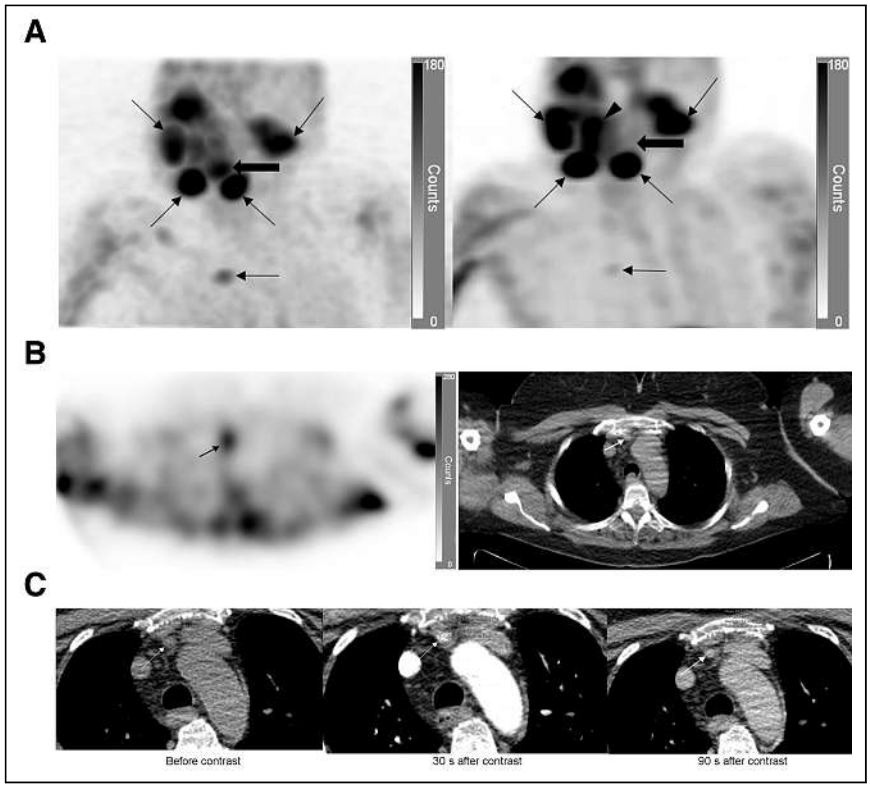


**FIGURE 1.** (A) $^{99m}$Tc-sestamibi SPECT image at 15 min (left) shows uptake at posterior tongue (thick arrow) and mediastinal focus (horizontal thin arrow). SPECT image at 2 h (right) shows posterior tongue tracer washout (thick arrow) suggesting ectopic lingual thyroid, with persistent uptake in mediastinal focus (horizontal thin arrow) consistent with ectopic parathyroid adenoma. Physiologic uptake is seen in salivary glands (oblique arrows). Uptake at anterior tongue region (arrowhead) is likely salivary activity. (B) $^{99m}$Tc-sestamibi SPECT at 2 h (left) shows focal uptake in anterior superior mediastinum (arrow), with axial CT component of SPECT/CT (right) showing correlating 1.6-cm lesion (arrow) consistent with ectopic parathyroid adenoma. Other peripheral uptake is artifactual activity in muscles. (C) Axial 4-dimensional parathyroid CT scan shows 39 Hounsfield units (HU) within lesion on precontrast phase (left), 161 HU hyperenhancement on arterial phase (middle), and 89 HU washout on delayed phase (right), rendering high confidence for parathyroid adenoma.

Received Nov. 23, 2022; revision accepted Jan. 31, 2023.
For correspondence or reprints, contact Fathima Fijula Palot Manzil (drfijulasurjith@yahoo.com).
Published online Jun. 14, 2023.

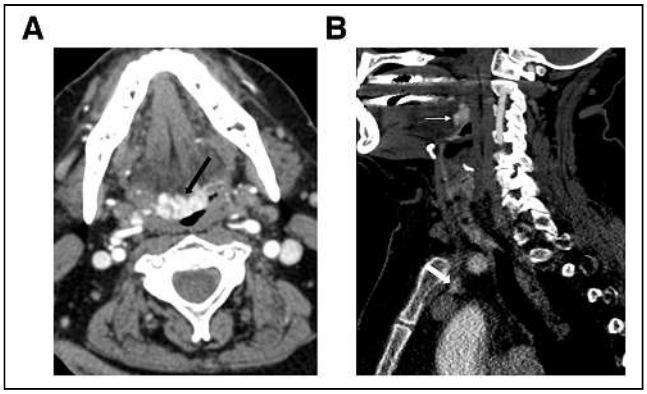


**FIGURE 2.** (A) Postcontrast axial CT scan shows enhancing lingual thyroid (arrow). (B) Sagittal reformatted postcontrast CT depicts both ectopic lingual thyroid (thin arrow) and ectopic parathyroid adenoma (thick arrow), without any eutopic neck thyroid gland.

parathyroid hormone level dropped to 27.8 pg/mL after transcervical mediastinal parathyroidectomy.

## DISCUSSION

The thyroid gland originates as an endodermal diverticulum between the first and second pharyngeal pouches, whereas the parathyroid glands develop from the third and fourth pouches (inferior and superior parathyroid, respectively). Ectopic thyroid tissue may rest anywhere along the thyroglossal duct when there is aberrant embryogenesis, as the thyroid descends from the posterior tongue foramen cecum to the lower anterior neck, with the lingual thyroid being most frequent (*1,2*). Before any excision, thyroid tissue elsewhere should be confirmed to prevent extreme postoperative hypothyroidism.

Superior parathyroid glands are usually located along the posterior margin of the thyroid gland or, less commonly, posteroinferior to the thyroid as a dropped gland and ectopically in retropharyngeal or retroesophageal locations. Inferior parathyroid glands lie anteriorly, in front of the trachea and behind the strap muscles in the lower neck. Inferior parathyroid glands follow the embryologic course of the thymopharyngeal duct, with one fourth lying ectopically in the superior or anterior mediastinum along the thyrothymic ligament, and extremely rarely may lie undescended in the upper neck near the submandibular salivary gland (*3*).

Combined CT and $^{99m}$Tc-sestamibi scintigraphy have around 100% sensitivity and a 97% positive predictive value for ectopic parathyroid adenomas. The sensitivity of scintigraphy increases with larger adenomas, likely because of more mitochondria causing high uptake of $^{99m}$Tc-sestamibi.

## CONCLUSION

We report an extremely rare synchronous ectopic thyroid and parathyroid diagnosed with $^{99m}$Tc-sestamibi scintigraphy and correlative imaging.

## DISCLOSURE

No potential conflict of interest relevant to this article was reported.

## REFERENCES

1. Palot Manzil FF, Kaur H. Radioactive iodine for thyroid malignancies. StatPearls website. https://www.statpearls.com/point-of-care/140304. Published October 5, 2022. Accessed March 21, 2023.
2. Gu T, Jiang B, Wang N, et al. New insight into ectopic thyroid glands between the neck and maxillofacial region from a 42-case study. *BMC Endocr Disord.* 2015; 15:70.
3. Bunch PM, Randolph GW, Brooks JA, George V, Cannon J, Kelly HR. Parathyroid 4D CT: what the surgeon wants to know. *Radiographics.* 2020;40:1383–1394.

## SNMMI TECHNOLOGIST SECTION PRESENTS AWARDS, ELECTS NEW OFFICERS AT 2023 ANNUAL MEETING

Nearly 8,000 physicians, technologists, physicists, scientists, and exhibitors gathered at the Society of Nuclear Medicine and Molecular Imaging (SNMMI) 2023 Annual Meeting, held June 24–27 in Chicago, Illinois. The meeting had more than 130 continuing education and scientific sessions and nearly 800 posters, as well as sessions on theranostics, artificial intelligence, dosimetry, and more.

During the meeting, SNMMI Technologist Section (SNMMI-TS) inducted new officers, who will serve through June 2024. A number of technologists were recognized for their outstanding contributions to nuclear medicine, molecular imaging, and the society.

### 2023–2024 SNMMI-TS OFFICERS

Dmitry Beyder

SNMMI-TS introduced a new slate of officers during the Annual Meeting. **Dmitry Beyder, CNMT, MPA**, radiology program manager of nuclear medicine, PET, CT, and patient transport at Barnes-Jewish Hospital/Mallinckrodt Institute of Radiology in St. Louis, Missouri, has been elected as the 2023–24 president for the SNMMI-TS. "This is an amazing time to represent nuclear medicine technologists globally, with opportunities to increase the technologist's role in providing theranostics and nuclear medicine therapy to cancer patients in need of targeted, highly efficient treatments and to grow our profession with both representation and development," Beyder said. "I am excited to take on this challenge and lead our members and nuclear medicine technologists to great successes this year, positioning us for success in many years to come."

Julie Bolin

During the meeting, SNMMI-TS also announced **Julie Dawn Bolin, MS, CNMT**, as president-elect. Bolin's priorities include educating high school and college students about careers and opportunities for nuclear medicine technologists and collaborating with molecular imaging and therapy professionals to develop traditional and continuing education materials that reflect the new diagnostic imaging and radiotherapy landscape. She will also focus on improving the experience for nuclear medicine professionals who are searching the SNMMI website for advocacy, education, and professional development.

Other newly elected individuals include:

- Secretary: Sarah A. Frye, PhD, MBA, CNMT, CCRP
- Speaker of the NCOR: Jeremy L. Iman, CNMT, PET, CRA, CT
- Finance Committee chair: Sarah R. Gibbons, MBA, CNMT, NMTCB(CT)
- Delegates at Large:
  - Tina M. Buehner, PhD, CNMT, FSNMMI-TS
  - Matthew C. McMahon, MS, CNMT, RT(CT)
  - Michele A. Panichi-Egberts, CNMT, RT(N), FSNMMI-TS
  - Jay J. Smith, MA, CNMT, RT(R)(N)
- Members-at-Large:
  - Christopher M. Blanton, MBA, CNMT/RS, RTMR
  - C. David Gilmore, EdD, CNMT, FSNMMI-TS
  - Chloee Wendorf, MHA, CNMT
- Specialty Area Representatives
  - Industry: Kristina M. Biederstedt, BS, CNMT
  - Manager: Dori L. Nelson, BS, CNMT, NCT, FSNMMI-TS

### SNMMI-TS FELLOWS

The following eight individuals were named SNMMI-TS Fellows. These are members of SNMMI-TS who have demonstrated leadership and have made a significant contribution to the profession of nuclear medicine technology at the national level. SNMMI-TS selects Fellows based on exemplary contributions in the following areas: participation in professional activities, education, professional experience, professional contributions, and civic activities. New SNMMI-TS Fellows receive a memorial plaque and pin signifying their Fellow status.

- Julie Dawn Bolin, MS, CNMT
- Cynthia Brodnax, CNMT, NMTCB(CT)(RS)
- Geoffrey M. Currie, PhD, BPharm, MMRS, CNMT
- Gary D. Gallamore, CNMT, FSNMMI-TS
- Sarah Gibbons, MBA, CNMT, NMTCB(CT)
- Sara L. Johnson, EdS, CNMT, RT(N)(CT)
- Clay Nuquist, BS, CNMT, PET
- Matthew McMahon, MS, CNMT, RT(CT)
- Virginia Pappas, CAE (Honorary Fellow)

**SNMMI-TS President Krystle Glasgow presents plaques to new SNMMI-TS fellows, from top left: Julie Bolin, Cynthia Broadnax, Sarah Gibbons, Sara L. Johnson, Clay Nuquist, Matthew McMahon, Virginia Pappas.**

## SNMMI-TS OUTSTANDING TECHNOLOGIST AWARD

**Joseph (Joby) MacLean, MHA, CNMT**, manager of nuclear medicine at Cincinnati Children's Hospital Medical Center in Cincinnati, Ohio, received the 2023 SNMMI-TS Outstanding Technologist award. The award recognizes SNMMI-TS members who have demonstrated outstanding service and dedication to the field of nuclear medicine technology.

**Joby MacLean receives Outstanding Technologist Award from 2022–2023 SNMMI-TS President Krystle Glasgow.**

## SNMMI-TS KATHY E. THOMPSON-HUNT OUTSTANDING EDUCATOR AWARD

**Jay J. Smith, MA, CNMT, RT(R)(N)**, director of nuclear medicine technology education at the University of Iowa Hospitals & Clinics in Iowa City, Iowa, was awarded the 2023 SNMMI-TS Kathy E. Thompson-Hunt Outstanding Educator Award. The award is presented to members who have exhibited commitment to advancing the field in their workplace and through their involvement with the society.

**Jay Smith receives Kathy E. Thompson-Hunt Outstanding Educator Award from 2022–2023 SNMMI-TS President Krystle Glasgow.**

## SNMMI-TS ADVOCATE(S)-OF-THE-YEAR AWARD

The 2023 SNMMI-TS Advocate-of-the-Year Award was presented to **Cheryl L. Rickley, CNMT, FSNMMI-TS**. This award recognizes an individual who has made significant contributions to advancing advocacy efforts at the state and federal level.

Cheryl Rickley

## SNMMI-TS LIFETIME ACHIEVEMENT AWARD

The 2023 SNMMI-TS Lifetime Achievement Award was presented to **Norman E. Bolus, MSPH, MPH, CNMT, FSNMMI-TS,** faculty member in the Department of Clinical and Diagnostic Sciences in the University of Alabama at Birmingham School of Health Professions. This award is reserved for individuals who have made significant contributions to the field of nuclear medicine and the SNMMI-TS and its chapters.

**Norman Bolus receives SNMMI-TS Lifetime Achievement Award from 2022-2023 SNMMI-TS President Krystle Glasgow.**

## SNMMI-TS PRESIDENTIAL DISTINGUISHED SERVICE AWARDS

The 2023 Presidential Distinguished Service Awards are given to individuals who made a significant impact during the presidential tenure of Krystle W. Glasgow, CNMT, NMTCB(CT), NMAA. The individuals being recognized have shown exceptional leadership and have provided strategic guidance in the areas of education and research. Awards were presented by 2022–2023 SNMMI-TS President Krystle Glasgow to:

- **C. David Gilmore, EdD, CNMT, FSNMMI-TS,** associate professor and program director for nuclear medicine at Massachusetts College of Pharmacy and Health Sciences in Boston, Massachusetts, for his exceptional efforts on the EANM HIDA chapter, extraordinary leadership, and friendship.

C. David Gilmore

- **Dmitry Beyder, CNMT, MPA**, radiology program manager of nuclear medicine, PET, CT, and patient transport at Barnes-Jewish Hospital/Mallinckrodt Institute of Radiology in St. Louis, Missouri, for strategic direction and outstanding accomplishments with the Workforce Pipeline.

Dmitry Beyder

- **Amy Brady, MAED, CNMT,** program director and assistant professor of Nuclear Medicine and Molecular

Amy Brady

Imaging Sciences at the University of Alabama in Birmingham, for mentorship, passion, and support as a leader at the University of Alabama and within the SNMMI-TS.

- **Dusty M. York, CNMT, PET, RT(N)(CT),** nuclear medicine program clinical coordinator and associate professor at Chattanooga State Community College in Tennessee, for mentorship, friendship, and leadership as President and Immediate Past President.

**Dusty M. York**

- **Jon A. Baldwin, DO,** nuclear medicine residency program director at the University of Alabama in Birmingham, for mentorship and support as a leader at the University of Alabama.
- **Nikki Wenzel, MBA, CAE,** Senior Director and SNMMI-TS Administrator, for her outstanding contributions to the SNMMI-TS.

**Nikki Wenzel**

## SNMMI-TS PRESIDENT'S PLAQUE

Krystle W. Glasgow, CNMT, NMTCB(CT), NMAA, FSNMMI-TS, was awarded the SNMMI-TS president's plaque and gavel for her service as 2022–2023 SNMMI-TS president. Glasgow is a teacher and clinical coordinator at the University of Alabama at Birmingham in Birmingham, Alabama, and is also pursuing her doctorate degree in health services administration with a concentration in health informatics at the University of Alabama at Birmingham.

**2022–2023 SNMMI-TS President Krystle Glasgow (center) receives the SNMMI-TS President's Plaque from 2023–2024 President Dmitry Beyder (left) and 2021–2022 President Dusty York (right).**

Glasgow, an SNMMI-TS fellow, is an SNMMI-TS 2016 Leadership Academy graduate as well as a 2021 Advanced Leadership Academy graduate. She was the 2018 American Society for Clinical Laboratory Science Kleiner Award winner and has been awarded several grants from SNMMI-TS. She is active on many SNMMI-TS committees, task forces, and working groups.

## SNMMI-TS CAREER ADVANCEMENT GRANTS

The 2023 SNMMI-TS Career Advancement Grants were awarded to Melody Yarbrough, CNMT, RT(N); Kathryn Beaulieu, BS, CNMT, PET, RT(N)(CT); Dylan Shimerda, CNMT; David Kelkis, CNMT, NMTCB(CT); Holly Karsch, CNMT; Nicole Beaulieu, CNMT; and Sarah Frye, MBA, CNMT, PET, CCRP.

## SNMMI-TS SCHOLARSHIPS

The *Susan C. Weiss Clinical Advancement Scholarship* was awarded to Ashlee Thomas, CNMT, and the *ERF-SNMMI-TS Bachelor's or Master's Degree Completion Scholarship* was awarded to Fernando Anleu and Leila Alsarag. Recipients of the *ERF-SNMMI-TS Advanced Degree Scholarship* were Diane Soulek, CNMT, NCT, PET, RT(N), and Kathryn Beaulieu, BS, CNMT, PET, RT(N)(CT). The Paul Cole Student Technologist Scholarship was awarded to Ewelina Bobak, Jennah Knafelc, Lauren Lobner, Chun Kit Ho, Thi "Sammy" Dang, Alexah Sloan, Xavier Hertzner, Jaylee Messmer, Shelby Harmon, and Kasey Waldrop. The PDEF *Mickey Williams Minority Scholarship* was awarded to Leila Alsarag and Jamaica Dean, and the *PDEF Professional Development Scholarship* to Kathryn M. Beaulieu, BS, CNMT, PET, RT(N)(CT).

# Outstanding *JNMT* Articles for 2022

*Kathy S. Thomas, Editor-in-Chief, Journal of Nuclear Medicine Technology*

**Geoffrey M. Currie**

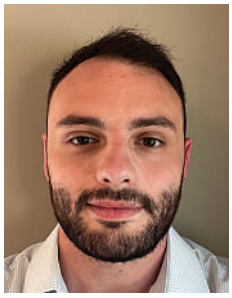

**Christopher Fecca**

Along with the dedicated members of the *Journal of Nuclear Medicine Technology* (*JNMT*) Board of Editors, I have the privilege each year of selecting outstanding articles. These awards are presented to articles that have contributed significantly to practice, education, and scientific understanding in the field and for which technologists have served as first authors. This year's awardees represent the remarkably broad range of clinical, technical, and educational endeavors that characterize our increasingly complex field—from basic biochemistry and molecular biology to the impact of COVID on nuclear medicine practice.

The first-place Editors' Choice Award for 2022 went to Geoffrey M. Currie, from Charles Sturt University (Wagga Wagga, Australia), and coauthors Marko Trifunovic, Jui Liu, Sang Kim, and Howard Gurney for "$^{18}$F-DCFPyL PET/CT in metastatic renal cell carcinoma" (*J Nucl Med Technol.* 2022;50:282–285). The second-place award was presented to Christopher Fecca, from the Lewis Katz School of Medicine at Temple University (Philadelphia, PA), and coauthors Jee Moon, David Posocco, Huaqing Zhao, and Simin Dadparvar for "Accuracy of $^{123}$I-sodium thyroid imaging in calculating thyroid volume" (*J Nucl Med Technol.* 2022;50:322–326). Dhrumil Naik, from the University of Ottawa (Canada), and coauthors Sarah Ternan, Rene Degagne, Wanzhen Zeng, and Ran Klein received the third-place award for "Thyroid uptake exceeding 100%: causes and prevention" (*J Nucl Med Technol.* 2022;50:153–160).

Krystle Glasgow, from the School of Health Professions, University of Alabama at Birmingham, and coauthors Mike Dillard, Eric Hertenstein, Allen Justin, Remo George, and Amy Brady were the recipients of the award for best continuing education article for "Going nuclear with amino acids and proteins: basic biochemistry and molecular biology primer for the technologist" (*J Nucl Med Technol.* 2022;50:186–194). The award for best educators' forum article went to Sarah Frye, from St. Louis University (MO) and coauthor Jennifer Prekeges from Bellevue College (WA) for "Interview with nuclear medicine technology educators on the impact of COVID-19 on programs, outcomes, and employers" (*J Nucl Med Technol.* 2022;50:174–178).

These awardees are to be congratulated on their achievements, a part of the larger effort that continues to make *JNMT* a vital resource for our community."

**Dhrumil Naik**

**Krystle Glasgow**

**Sarah Frye**

# SEPT 21-23 2023 SNMMI THERAPEUTICS CONFERENCE

MARRIOTT WATERFRONT BALTIMORE MARYLAND

The **SNMMI Therapeutics Conference** is coming to **Baltimore, Maryland** on **September 21-23**, 2023! This exciting event will bring together leaders in radiopharmaceutical therapy to explore the latest innovations and advancements in the field.

This conference is a must-attend if you want to expand your knowledge and stay up-to-date on the latest developments. With two-and-a-half days of informative sessions and networking opportunities, you'll have the chance to connect with colleagues, enhance your knowledge, learn from experts, and gain invaluable insights.

This year's program will focus on the latest innovations and clinical applications in radiopharmaceutical therapy, including the following topic areas:

- Challenges of Practice in a Theranostics Clinic
- Therapeutic Dosimetry
- Dosimetry Case Review with the Experts
- Prostate Cancer
- New Targets Part I
- New Targets Part II
- GEP NET
- Thyroid Diseases
- Radiopharmaceutical Supply Chain
- Clinical Trials & Research in Therapeutics

SNMMI

## VISIT WWW.SNMMI.ORG/TC2023 TO REGISTER

## SPONSORS

▶ **TITLE SPONSOR:** itm PASSION FOR PRECISION

▶ **GOLD SPONSORS:** CURIUM LIFE FORWARD; GE HealthCare; NOVARTIS; SIEMENS Healthineers; Telix

▶ **SILVER SPONSOR:** Fusion Pharmaceuticals Inc.; HERMES MEDICAL SOLUTIONS; LANTHEUS; Nucleus RadioPharma; POINT BIOPHARMA

▶ **BRONZE SPONSOR:** BAYER; CardinalHealth Essential to care™

▶ **SATELLITE SYMPOSIA SPONSORS:** GE HealthCare; itm PASSION FOR PRECISION; mim SOFTWARE; Telix

3
23

Journal of Nuclear Medicine Technology

September 2023 ▪ Vol. 51 ▪ Pages 165–264